Ecology-based bed protection of offshore wind turbines

K.W. Buijs

Ecology-based bed protection
of offshore wind turbines

by

K.W. Buijs
(1543571)

in partial fulfilment of the requirements for the degree of

Master of Science
in Civil Engineering

at the Delft University of Technology,
to be defended publicly on Wednesday July 1, 2015 at 16:00

**Section of Coastal Engineering
Faculty of Civil Engineering and Geosciences**

June 2015

Graduation Committee
Prof. dr. Ir. W.S.J. Uijttewaal	Environmental Fluid Mechanics	Delft University of Technology
Prof. dr. J.H. Slinger	Coastal&Environmental Science	Delft University of Technology
Ir. J.P. van den Bos	Hydraulic Engineering	Delft University of Technology
	Coastal Engineer	Boskalis, Hydronamic
Drs. A. Hermans	Environmental Engineer	Boskalis, Hydronamic
J. Brocklehurst B.Sc, MIEMA	Environmental Engineer	Boskalis, Hydronamic

An electronic version of this thesis is available at: http://repository.tudelft.nl/.

PREFACE

The thesis is conducted as the last part of the Master in Hydraulic Engineering at Delft University of Technology. The research is carried out in cooperation with Boskalis. The topic of this thesis is 'Ecology-based bed protection of offshore wind turbines'.

I would like to thank my entire graduation committee for their wise input and good guidance. Prof. dr. ir. W.S.J. Uijttewaal for keeping me on track, prof. dr. J.H. Slinger for her inspiring talks, ir. J.P. van den Bos for his substantive support, and J. Brocklehurst B.Sc, MIEMA for the environmental discussions. I also would like to thank my daily supervisor in the beginning of this thesis, Annemiek Hermans, for overloading me with ecological knowledge which was really needed at that stage of the research and also for all her enthusiasm.

This thesis would not have been possible without the support of others. First of all I would like to thank Stefan Aarninkhof for providing me the opportunity to conduct my thesis at Boskalis. It has been a very pleasant working environment.

Furthermore I would like to thank Joop Coolen and Babeth van der Weide from Imaris for their ecological vision. Also the ecological input of Luca van Duren and the technical feedback of Tim Raaijmakers of Deltares are appreciated. From the section geosciences at TU Delft I would like to thank Ellen Meijvogel-de Koning for helping me with the CT scans and Joost van Meel for providing me insight in the imaging analysis technique.

Second-last I would like to thank my Boskalis colleagues including the student interns for the nice atmosphere, the helpful discussions, the joyful time, and for all the sporting events.

Finally I would like to thank my family for their care throughout my education and my friends for all their support.

Wieger Buijs
Delft, May 2015

ABSTRACT

The offshore wind industry is a growing market in Europe due to the sustainable energy targets of European Union. In the coming years the Dutch government will invest in offshore wind farms at the North Sea. For a contractor like Boskalis the inclusion of favorable ecological conditions in designs is a unique selling point and can help to win tenders to build offshore wind farms and acquire projects. This was the starting point of this thesis.

The thesis is split up in two parts. The first part is an extensive literature study and searches for opportunities and influencing parameters to provide favorable ecological conditions for marine life. The second part of the thesis will explore one opportunity in detail, which can be included in bed protection design of offshore wind farms.

The research question is formulated as follows:

"How can technical aspects of bed protection designs of offshore wind turbines be altered to provide favorable ecological conditions for marine life?"

Part I: Literature review and parameter study
In the first part of the thesis interviews with ecologists are conducted to gain knowledge about ecological systems, and to explore the social acceptability besides the motivation to win tenders. The ecologists don't support installations of offshore wind farms, because it is not natural and anthropogenic interferences are in principal not good. However, in the past a significant part of the North Sea floor consisted of hard substrate, but due to trawling activities by humans this hard substrate is removed. Nowadays the North Sea floor consists of sand. By placing stones for the bed protection of offshore wind farms, hard substrate will be added which was present in the past. So, the hard substrate balance will more or less be restored. Furthermore, offshore wind turbines will be built, so then it is better to build them properly and in consultation with the environment.

In the extensive literature study a technical analysis and an ecological analysis are conducted. During this literature study the context and scope of this research are defined. The scope is set to the bed protection of one offshore wind turbine. The technical analysis resulted in the structure, failure mechanisms, and design calculations of the bed protection. The ecological analysis focuses on the two key species, and biodiversity in general. The key species are the European lobsters and the European cod. The outcome of the literature study is a list of controllable parameters for functional requirements. This is a list with potential parameters in combining favorable ecological conditions and technical requirements. From this list the *pore-size distribution* is chosen to investigate in further detail. The pore-size distribution includes the cavity sizes and openings in which species can find shelter. The parameter study and selection of the parameter *pore-size distribution* is the outcome of the first part of this thesis.

<u>Part II: Model and interpretation</u>
The second part of the thesis focuses on the pore-size distribution and the pore openings, derived from a stone-size distribution. Furthermore, it focuses on the ecological interpretation of the derived distributions.

First of all models are designed and evaluated to crack this problem. The chosen models are an analytical model of spheres and an experimental model. The analytical model of spheres is based on geometry and is derived to give indications and to validate the results of experimental model.

The analytical model provides results to describe the pore size and the pore openings of uniform spheres. The pore-size distribution of multi-sized spheres could not be derived. However, the pore-opening distribution of multi-sized spheres is derived. The results of this distribution are approximated with a curve fit of a normal distribution. The mean of the pore-opening distribution (μ) and the standard deviation (σ) of this approximation are formulated below:

$$\mu = (1.57 * \phi - 0.267\,) * D50 * \left(-0.152 * \frac{D85}{D15} + 1.23\right) \qquad [m]$$

$$\sigma = (0.148 * \phi - 0.0223) * D50 \qquad [m]$$

In which:
Φ	: porosity	[-]
D50	: median sphere diameter (of mass distribution)	[m]
D85/D15	: sphere grading (of mass distribution)	[-]

The experimental model is executed with a medical CT scanner and imaging software. First, a test scan is made to identify the possibilities and limits of this method. Secondly, a validation scan is made of glass balls to explore the errors and the accuracy of the medical CT scanner and the imaging software. The results of the validation scan are compared with the analytical results. Both models showed the same result.

Therefore, an experimental program is designed and 8 scans are performed on stones (quarry material). The sieve curve of the stones is in advance specified and manufactured. The derived formula that describes the pore-size distribution, after analyzing the scans with the imaging program and post-processing of the data, is formulated below:

$$f\,(x, P_{80}, m, F) = 1 - e^{\ln(0.2) * \left(\frac{x-F}{P_{80}}\right)^m} \qquad [m] \qquad for\ x > F$$

With
$$P_{80} = \left(-2.13 * \phi * \frac{D85}{D15} + 13.2\right) * \frac{D50}{25}$$
$$m = \left(-0.533 * \phi * \frac{D85}{D15} + 2.29\right)$$
$$F = (27.5 * \phi - 3.35) * \frac{D50}{25}$$

In which:
D50	: median stone diameter (of mass distribution)	[m]
D85/D15	: stone grading (of mass distribution)	[-]

The number of pores found during the same analyses can be described with two formulas.

$$Number\ of\ pores = 1.81 * \left(\frac{D85}{D15}stone\right)^{0.25} * \frac{V*(1-\phi)}{D50^3} \qquad [-]$$

$$Number\ of\ pores = 0.737 * number\ of\ stones \qquad [-]$$

In which:
V : volume of the bed protection [m]

Both formulas contain an acceptable error. The disadvantage of the last formula, that describes the number of pores, is that the number of stones has to be calculated first.

The pore openings are also investigated during the same experiment. However, the constriction-size distribution is not derived using the experimental model. Most of the constrictions are connected using this model. Therefore, a few constrictions are manually investigated and the results could not falsify the analytical results.
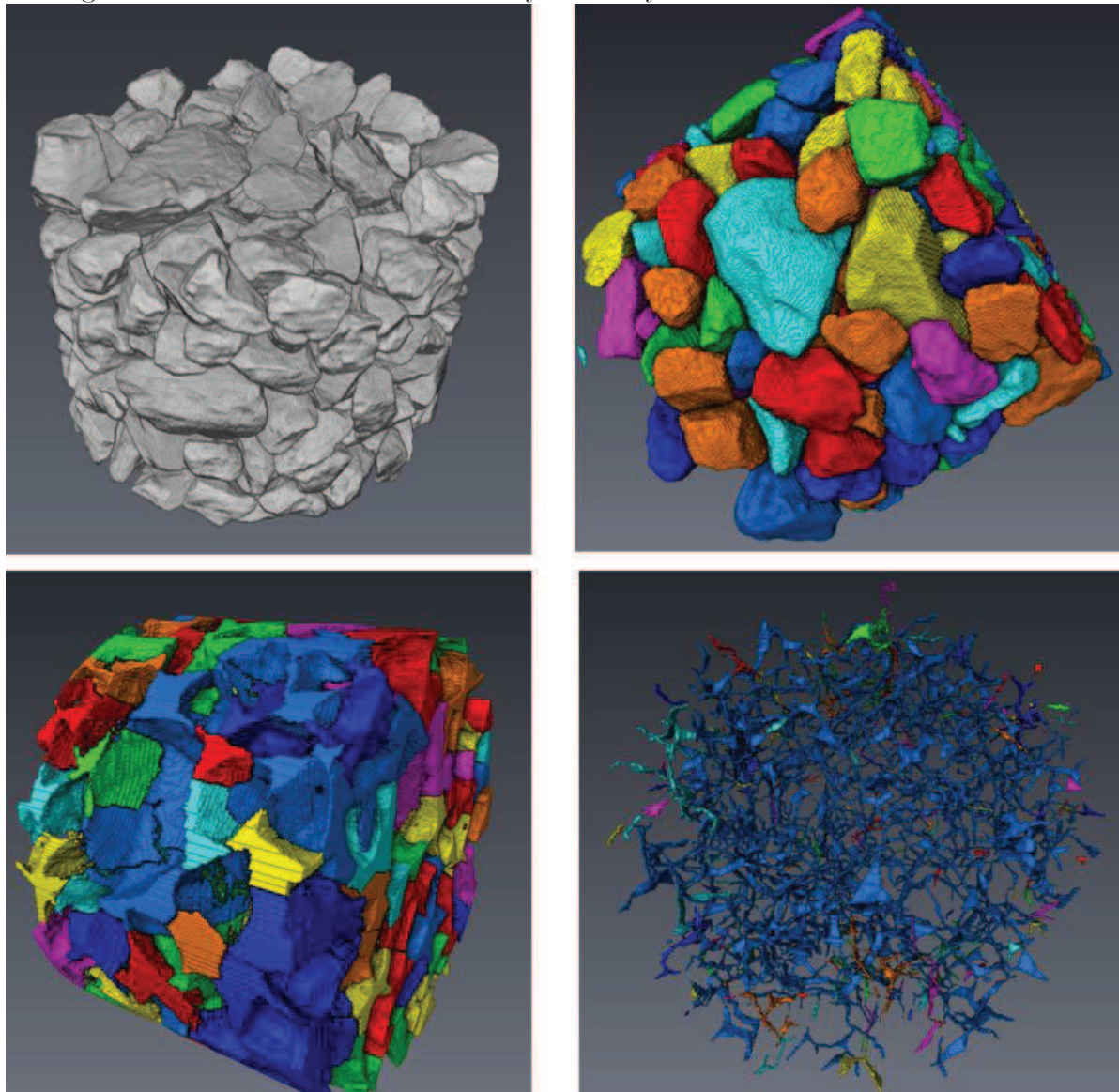
(upper left): stones after scanning, (upper right): stones after scanning and labeling, (lower left): pores after scanning and labeling, (lower right): openings between the pores after scanning and labeling.

The derived formulas for the pore-size distribution and the pore opening distribution are applied on a brief case study of a bed protection of an offshore wind turbine. In this calculation example, the pore sizes are compared with the preferred pore sizes for the lobster. Targeted pore sizes can be created by applying another grading width, other stone sizes, or changing the porosity. In this way the bed protection could be adapted to the preferences of the lobster.

The research question is answered within the scope of this research: the *pore-size distribution* is one of the technical aspects found, which can be included and altered in bed protection designs to provide favorable ecological conditions for marine life. The pore-size distribution has until now not been included in bed protection designs, while, in fact, it is always installed. This distribution can be derived, and future bed protections can be designed based on favorable cavity sizes for species, as well as technical stability. This holds for the *constriction-size distribution*.

The main recommendation for the industry is:
- The pore-size distribution can be included in future designs to estimate the impact of the structure on the species. Moreover, designs of civil rock works can be based on the preferred pore sizes for native species. This fits perfectly in the philosophy of Building with Nature.

The four main recommendation for further research are:
- Testing this principle with an ecological pilot.
- Scanning and analyzing more samples to make the formula statistical more reliable.
- Further development of the experimental model. Extra properties of the pores, such as the shape, can be derived and included in the model.
- Adding more species by describing the limiting conditions of these species in a matrix.

TABLE OF CONTENTS

ACRONYMS

OWF	Offshore Wind Farm
EMFs	Electromagnetic Fields
CT	Computed Tomography
OWEZ	Offshore Windpark Egmond aan Zee
KC	Keulegan-Carpenter
ROV	Remotely Operated Vehicle
HGI	Habitat Suitability Index
CL	Carapace Length

LIST OF SYMBOLS

a	Wave amplitude	[m]
A	amplitude of orbital movement at the bed	[m]
Blc	Blockiness	[-]
C_i	Coefficients	[-]
CL	Carapace length	[cm]
d	Stone size	[m]
D	Monopile diameter	[m]
D	Diameter of sphere	[m]
D_v	Constriction-size diameter	[m]
D15	Sieve size when 15% of mass is passed	[m]
D50	Median sieve diameter of mass curve	[m]
D85	Sieve size when 85% of mass is passed	[m]
Dn50	Median grain diameter of weight	[m]
e	Pore number	[-]
f	Frequency	[years^{-1}]
f_c	Friction coefficient of the bed due to currents	[-]
f_w	Friction coefficient of the bed due to waves	[-]
F	Force	[N]
F	Coefficient of Rosin Rammler	[-]
g	Acceleration of gravity	[m/s^2]
h	Water depth	[m]
H	Wave height	[m]
h_s	Scour depth	[m]
k	Wave number	[m^{-1}]
k	Number of adjacent spheres	[-]
K	Constant	[-]
K	Factor for shape, angle of attack, and velocity	[-]
KC	Keulegan-Carpenter	[-]
L	Wave length	[m]
L_s	Radial distance to edge of the scour hole	[m]
LT	Length to thickness ratio	[-]
m	Coefficient for waves	[-]
m	Shape coefficient of Rosin Rammler	[-]
m_i	Mass of stone with dimension i	[kg]
n	Number of sphere sizes	[-]
P	Probability of failure	[-]
P80	Slope coefficient of Rosin Rammler	[-]
r	Pore radius	[m]
Re	Reynolds number	[-]
S	Sediment transport per unit width	[m^2/s]
S	equilibrium scour depth	[m]

S_v	Area of constriction	[m^2]
T	Wave period	[s]
T	Lifetime	[years]
u	Particle velocity in x direction	[m/s]
u_*	Shear velocity	[m/s]
u_c	Critical velocity	[m/s]
$u_{w,max}$	Maximum near bed velocity	[m/s]
v	Kinematic velocity	[m^2/s]
w	Particle velocity in z direction	[m/s]
W_{50}	Weight of equivalent cube of D_{n50}	[kg]
z	Interesting depth	[m]
z_b	position of the bed level	[m]
α	Angle of corner between spheres	[°]
α	amplification factor	[-]
β	Angle of corner between spheres	[°]
β	Angle between the current and the waves	[°]
γ	Angle of corner between spheres	[°]
δ	Angle of corner between spheres	[°]
Δ	Relative density	[-]
Δp	Probability density	[-]
$ρ_w$	Density of water	[kg/m^3]
$ρ_s$	Density of stones	[kg/m^3]
$τ_c$	Bed shear stress due to flow	[N/m^2]
$τ_w$	Bed shear stress due to waves	[N/m^2]
$τ_b$	Actual bed shear stress	[N/m^2]
φ	Angle of repose	[°]
φ	Porosity	[-]
Ψ	Shields parameter	[-]
ω	Wave frequency	[s^{-1}]

1. INTRODUCTION

The Dutch government has embraced a target of 14% sustainable energy production in 2020 in the energy agreement (Rijksoverheid, 2014). Nowadays only 4% is generated from sustainable sources. One of the measures to achieve this goal is an increase in wind energy. The current production of wind energy is already a significant share of the total sustainable energy. The Netherlands is very flat and windy and therefore there is a lot of potential to generate more wind energy. The generation of wind energy is envisaged to occur both on land and at sea.

There are two offshore wind farms in front of the Dutch coast in the North Sea, three offshore wind farms are under construction, and the minister of Economic Affairs announced that there will be built another five offshore wind farms in the Dutch North Sea (Kamp & Schultz van Haegen, 26 september 2014). This study is part of the growing offshore wind energy generation.

To win tenders and acquire projects, contractors of offshore wind farms try to provide unique selling points in comparison to competitors. An example of a unique selling point is the ability to include favorable ecological conditions into the design. If a contractor has a better understanding of the impact on the environment during the installation phase and the total lifetime of the civil structure, he can gain a competitive advantage during scoring procedures. The (brand) image of the client and corporate responsibility of the contractor is of great importance, so often a 'green solution' is preferred when economically feasible.

At the moment civil structures and favorable ecological conditions are two separate topics and are rarely combined in research. The civil structures have to fulfill only technical requirements. A good example of this is the reinforcement of the dike sections in the Oosterschelde. The foreshore was strengthened with too fine gravel. It served the practical/technical application of prevention of erosion due to strong currents, but lobsters cannot survive in this environment (Omroep Zeeland, 2014). On the other hand, ecological reefs are designed and applied, which have no technical application.

The Minister of Infrastructure and Environment has announced that the foreshore strengthening of the dike section in the Oosterschelde gets an extra ecological covered layer (Omroep Zeeland, 2014). An integral mindset and good engineering could prevent these types of mistakes.
An integral approach is already tested in pilots of the rich dike, for example the water retaining pools (Deltares, WINN, & RWS, 2010).
Another example is the integral approach for coastal protections; artificial reefs that stimulate biodiversity (ecology), reduce wave height (technical function), and are attractive for scuba divers (recreational). Unfortunately the experiment for a multifunctional artificial reef in the North sea has not taken place.

In Singapore, the Building with Nature program has adopted a pilot for a multifunctional coastal protection scheme. The integral design should prevent extreme coastal erosion, strengthen the biodiversity, enhance the potential for recreation, and taking housing development into account (EcoShape, 2014).
The above provided examples of integral approach for coastal structures do not include offshore wind turbines.

Waves and currents cause extra turbulence around the foundation pile of a wind turbine, which results in scour of the seabed. Scour holes are not desirable because they have a negative effect on/affect the foundations in the seabed (negatively), and thus the stability of wind turbines. The current method to deal with scour is by placing a bed protection around the piles or by driving the monopile deeper into the ground and omit the bed protection (Raaijmakers, Joon, Segeren, & Meijers, 2014). The common method to install a bed protection is by placing stones. Until now the bed protections of offshore wind turbines are designed to fulfill only technical requirements, while at other places in the sea ecological stimulating measures, such as artificial reefs, are attempted for fish stock enhancement and fishery management (Fabi, 2011). These ecological stimulating measures don't have a technical function and are only build for stimulating biodiversity (Ecomare, 2014).

Multi-purpose offshore platforms are researched in the innovative Mermaid project. Brainstorm impressions are sketched below, see Figure 1-1 (Coastal energy and environment, 2014) (Mermaid, 2012).

Figure 1-1: Out of the box sketch of an ecological friendly monopile (left) and a multi-purpose offshore wind farm.

The focus of this study lies on the protection of the foundation of the wind turbines and tries to have an integral approach by combining favorable ecological conditions and technical requirements. It is an interdisciplinary topic, as the bed protection will not only be elaborated from a technical point of view, but also from ecological perspective.

1.1   OBJECTIVE

The aim of this research is to continue with the integral mindset and apply this approach to the bed protection of offshore wind turbines. To accomplish this aim the problem description and research goal are formulated in this section.

In 2006 the Offshore Wind farm Egmond aan Zee (OWEZ) was put into operation. From that moment on an extensive environmental impact monitoring program started. The impact on a large number of faunal groups has been studied. The short-term results (two years) show the following (Lindeboom, Kouwenhoven, Bergman, & Bouma, 2011):

- no significant effects on the benthos in the sandy area between the turbines;
- new species and new fauna communities;
  (due to the new hard substratum of the monopiles and the scour protection)
- no impact on the bivalve recruitment;
- new type of habitat with a higher biodiversity of benthic organism;
- a possible increased use of the area by the benthos , fish, marine mammals and some bird species; and
- a possible decreased use of the area by several other birds species.

Overall, the OWEZ wind farm acts as a new type of habitat with a higher biodiversity of benthic organisms, a possible increased use of the area by the benthos, fish, marine mammals and some bird species and a decreased used by several other bird species (Lindeboom, Kouwenhoven, Bergman, & Bouma, 2011). The explanation of the monitored phenomenon is very important. When the driving mechanisms of the ecological impacts are made clear, the ecological changes due to future offshore wind farms can more accurately be predicted. Also some desired ecological effects can be stimulated by adjustments in design.

Technical feasibility will always be the dominant factor in the design and construction, but research can help to see if ecological boundaries/principles in the design can increase the positive aspects of the observed ecology (add targeted extra ecological value). Extra requirements (seen from ecological point of view) for the bed protection in the design phase can stimulate the enhancement of the biodiversity and/or increase settlement potential. This thesis is searching, with the future developments of offshore wind parks in front of the Dutch coast in mind, if adjustments/innovations in the design- and construction approach of the bed protection, can lead to a more integrated solution of building offshore wind farms.

1.2   MOTIVATION & SOCIAL ACCEPTABILITY

This thesis is conducted in cooperation with the contractor Boskalis. To strengthen the position in the offshore wind market and to win tenders, unique selling points are essential for Boskalis. To include favorable ecological conditions into the design of the bed protection of wind turbines can be such a unique selling point. This was the proposition for Boskalis and motivation for the author to start this research.

To support this interpretation interviews are conducted with ecologists. The marine biology expert Joop Coolen said: "The installation of offshore wind farms is not natural and anthropogenic interferences are in principal not good. However, in the past a significant part of the North Sea floor consisted of hard substrate, but due to trawling activities by humans this hard substrate is removed. Nowadays the North Sea floor consists of sand. B dumping stones for the bed protection of offshore wind farms hard substrate will be added which was present in the past. So the hard substrate balance will more or less be restored. Furthermore, offshore wind turbines will be built, so then it is better to build them properly and in consultation with the environment". The other ecologists agreed on the last comment: "If it has to be built, build it properly".

Overall, the motivation of this thesis is (brand) image of the clients, the corporate responsibility of the contractor, the historical hard substrate conditions of the North Sea, and the conception of the ecologists.

1.3   APPROACH

This thesis is not a predefined path that can be walked. Because of the interdisciplinary topic and the background of the author the thesis is split in two parts, see Figure 1-2.

Part I: Parameter study
The first part of this thesis is a literature study, aiming to find controllable parameters for functional requirements. First of all an ecological analysis and a technical analysis will be conducted:

- The ecological analysis results in parameters for favorable ecological conditions;
- The technical analysis results in parameters for technical requirements.

In totality, this results in a list of context-defined parameters. The list of context-defined parameters will be reduced to only the matching parameters. For example: color is a parameter which is of influence for favorable ecological conditions, but is not a parameter which is of influence for the technical requirements. Therefore color is a context-defined parameter, but is not a matching parameter and will be not be studied in further detail.

The aim is to find controllable parameters for functional requirements, for which a selection of matching parameters will be made. Not all the matching parameters are controllable parameters. An example of a matching parameter which is not a controllable parameter, is salinity. Salinity determines the stability of the bed protection (technical requirements) as well as the habitat preferences of the species (favorable ecological conditions). However, significant salinity differences are not controllable in the North Sea.

An example of a matching <u>and</u> controllable parameter is stone diameter. The stone diameter is related to the cavity size. In literature is found that cavity size is related to biodiversity (Baptist, van der Meer, & de Vries, 2007). Different cavity sizes results in the contraction of habitats which are currently segregated due to the use of 'fixed' rock grading. So stone diameter has influence on favorable ecological conditions. On the other hand, stone diameter has influence on the stability of the bed protection, so the technical requirements.

The formulated steps are sketched in Figure 1-2:

- The green blocks are part of the ecological analysis;
- The brown blocks are part of the technical analysis; and
- The purple blocks combines the ecological analysis and the technical analysis and summarized the favorable ecological conditions and the technical requirements.

The conclusion of the literature study (Part I) is a list of controllable parameters for functional requirements, see lowest purple block in Figure 1-2.
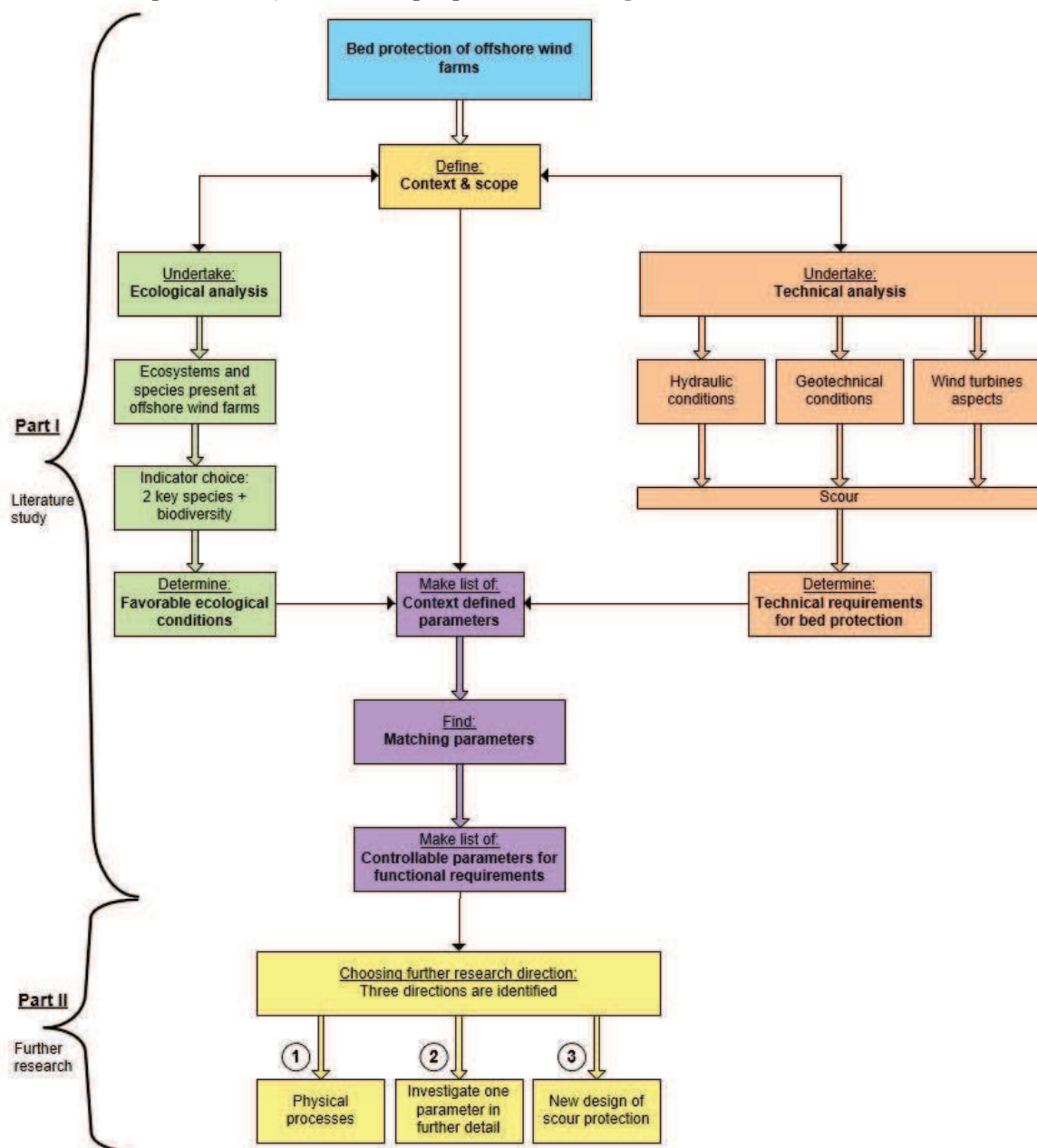
Figure 1-2: Scheme of the thesis structure with focus on part I.

Part II: Model and interpretation
The second part of this graduation work was not known in advance and depended on the results of the literature study. Three possible directions were conceived in advance:

1) Investigate the physical processes that determine the favorable ecological conditions. For example currents, turbulence through pores, or turbidity.
   This is the case if not a directly matching parameters will be found. If there is a parameter of influence, but this parameter has only effect on the favorable ecological conditions and not on the technical requirements. For example turbidity; turbidity has effect on the favorable ecological conditions, but does not have effect on the technical requirements. By researching the turbidity and its influences on the species new knowledge can be gained. Other examples for such parameters are currents or turbulence through pores. The flow through the pores does not directly determine the stability of the bed protection (in the bed protection design calculation), but it maybe determines the favorable ecological conditions for the species within the pores.

2) Research in further detail the found controllable parameter for functional requirements. For example material properties.
   This is the case if a (few) controllable parameters for functional requirements are found. The(se) parameter(s) has (have) influence on the favorable ecological conditions as well as the technical requirements. For example material properties; if another type of stone will be used for the bed protection this effects the ecological favorable conditions (more species can attach to soft stones) and also effects the technical requirements (soft stones wear).

3) Design a new bed protection that fulfills the technical requirements and create favorable ecological conditions?
   This is the case if many controllable parameters for functional requirements will be found. A revised bed protection design will be made and tested on stability

Due to the results of the literature study, presented in chapter 2, pore-size distribution is chosen as controllable parameter, see chapter 3. This means that above indicated direction 2 will be selected for further research and that one parameter will be investigated in detail, see Figure 1-3.
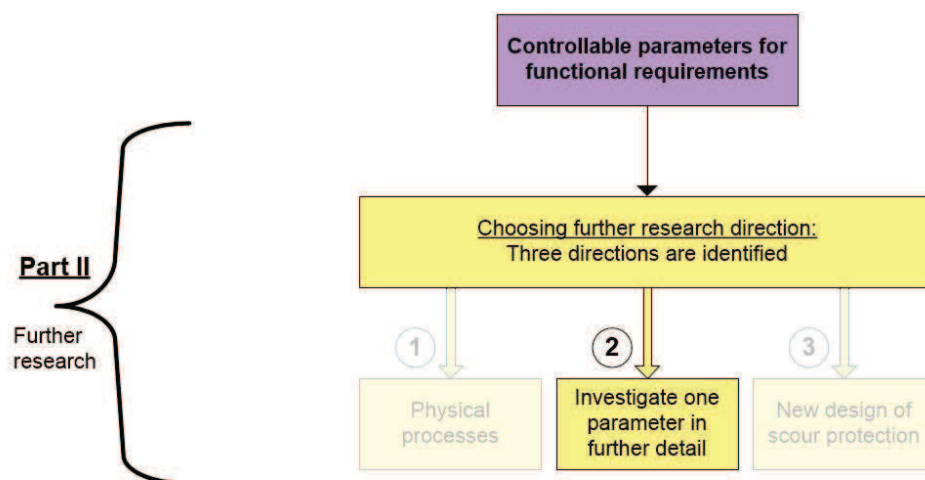

Figure 1-3: Three possible directions were conceived in advance and option 2 is chosen for further research.

In the second part of this thesis models will be proposed to expose the pores size distribution. The pore-size distribution will be determined with two different methods to validate the results. After validation an experimental program will be performed. The experimental program results in a formula for the pore-size distribution. This distribution will be compared with the favorable ecological conditions and the application of the model will be treated. The steps of part II of the research are sketched in Figure 1-4.
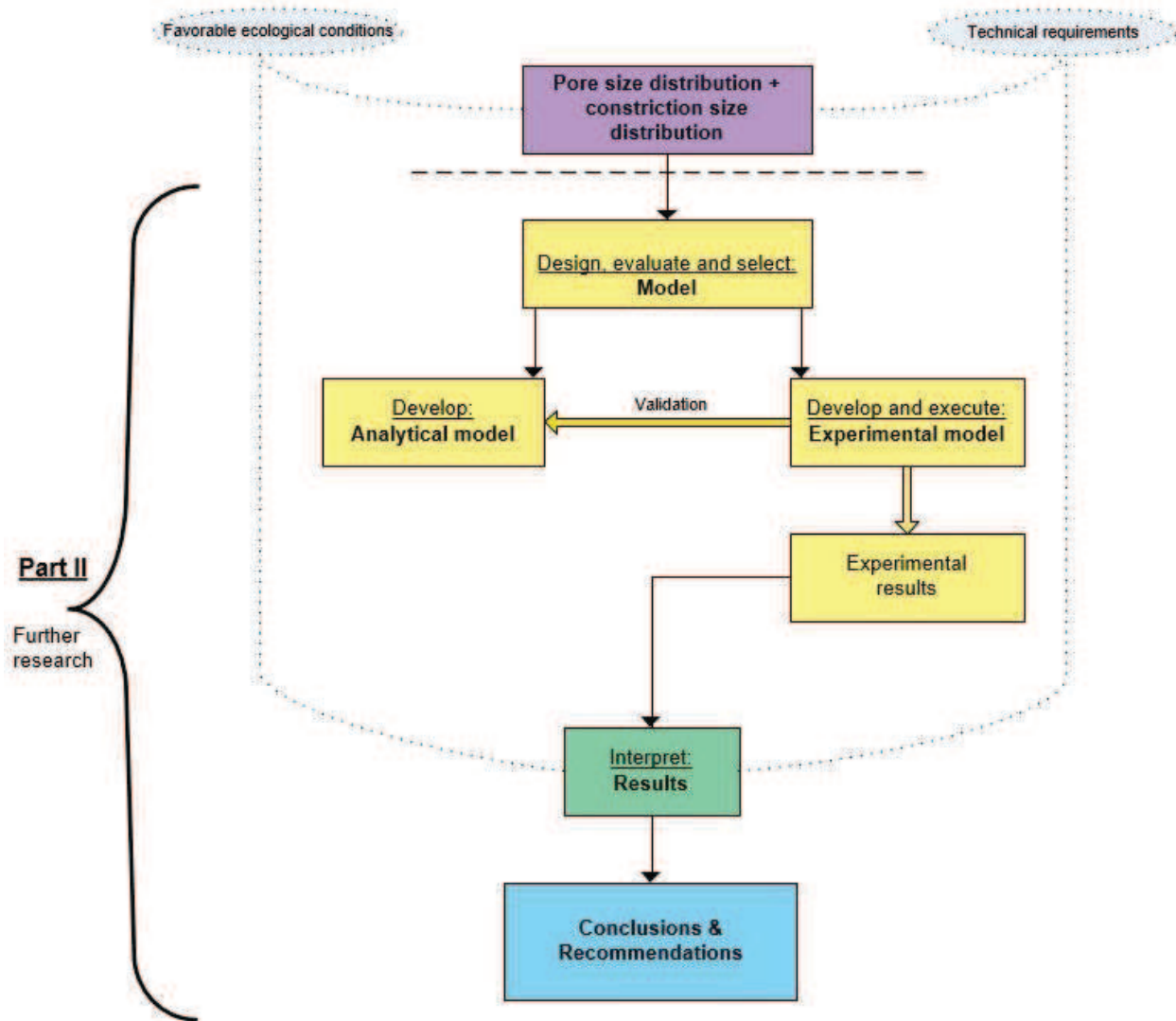

Figure 1-4: Scheme of the thesis structure of part II.

Part I and part II of the thesis are connected in the conclusions and recommendations to come up with a complete and coherent research, see Figure 1-6.

1.4   RESEARCH QUESTION

"Making calculations is not the goal, but the means"

The objective stated in 1.1 and the defined framework in Figure 1-2 lead to the following research question:

How can technical aspects of bed protection designs of offshore wind turbines be altered to provide favorable ecological conditions for marine life?

This thesis is split up in two parts as mentioned in 1.3 and drafted in Figure 1-2.
- The first part is the literature study and is trying to answer <u>which</u> aspects can be included or altered in bed protection design of offshore wind turbines to provide favorable ecological conditions for marine life.
- The subsequent part is further research and is trying to answer <u>how</u> the found aspect(s) can be included or altered in the bed protection design of offshore wind turbines to provide favorable ecological conditions for marine life.

In order to answer the research question conclusively the following sub questions are formulated:

<u>Part I: Literature review and parameter study</u>
In the first part of this research three sub questions are formulated to introduce the interdisciplinary topic and seek for the gaps/opportunities in literature.

1) Which species can be selected to provide favorable ecological conditions near offshore wind turbines and what are the parameters to describe these conditions?

2) What are the determining parameters for the technical requirements of a bed protection design of an offshore wind turbine?

3) What are the matching and controllable parameters between the *"favorable ecological conditions"* in question 1 and the *"technical requirements"* in question 2?

<u>Part II: Further research</u>
The subsequent part depends on the results of the literature study (answer on the above stated question 3). The parameter pore-size distribution is selected as chapter 2 will show. The following sub questions are formulated for the subsequent part of the thesis:

A) What are the relations between the stone-size distribution, the pore-size distribution, and the constriction-size distribution?

B) What cavity-sizes and opening-sizes are suitable to provide favorable ecological conditions for lobsters?

C) How can targeted cavities, which provide favorable ecological conditions for lobsters, be included in the technical design of a bed protection?

TUDelft Delft University of Technology

Boskalis

1.5   SCOPE

For a clear and defined thesis a research framework is constructed. This section will present the scope of the envisaged research. Because of the multidisciplinary topic of this graduation project the limitations and boundary conditions are categorized:

- Location and scale;
- Ecology;
- Hydraulic loads;
- Structure;
- Lifetime.

Per category limitations are stated and the focus related to these limitations will be substantiated. Figure 1-5 is a graphical representation of the area of interest.

1.5.1   Location and scale

- Worldwide offshore wind farms <----—> Dutch offshore wind farm

As mentioned in the introduction the Netherlands have already developed two offshore wind farms and at the moment three offshore wind farms are under construction. In the future the minister of Economic Affairs also announced more offshore wind farms in front of the Dutch coast. Therefore the **Dutch** part of the **North Sea** is selected as the study area of this thesis. The hydrodynamic conditions, the ecosystems and the species present in the North Sea form the context of this study.

- An offshore wind farm in its entirety <-----> One wind turbine

This research is not looking at prevailing waves/currents to establish patterns of sheltered areas to provide favorable ecological conditions at offshore wind farms. Also the cable to the shore is not within the boundaries of this thesis. The area of interest is **one offshore wind turbine** and its associated element of the bed protection. This boundary is chosen because of the interest of the author.

1.5.2   Ecology

The author conducted four interviews with ecologists to gain information about ecosystems and species and to define the ecological scope in this section, because of the technical background of the author.

- (Biodiversity) All species <-----> 1 key species (Biomass)

Ecological limitations have to be made for a defined thesis. The enhancement of the biodiversity is often the aim of anthropogenic interventions. Focusing on 1 key species is "making a farm for a certain species" and stimulating the biomass of one specie. This research will focus on **2 key species and biodiversity in general**. In the given amount of time this will result in a representative analysis of the favorable ecological conditions of the selected species. The two species chosen for this thesis are the **cod** (Gadus morhua) and the **European lobster** (Homarus gammarus), because of the following reasons (see also literature study in following chapter):

- Present at offshore wind farms;
- Economically attractive;
- Expert input;
- Stock decreasing;
- Literature available.

- Established species <-----> Pioneers (Ecological time scale)

Due to the installation of wind turbines the ecosystem will be disturbed. The number of species and the diversity will change. This study will concentrate on the established species and not the pioneers. Therefore the influences of bed protection will be evaluated for the **established species** which are present **after 3 years**. This lifetime is chosen because of the interest in long term effects and the life time expectancy of the species.

- Ecotope <----> Biotope (Ecological scale)

Ecotope is the smallest, ecologically distinct area in an ecological classification of landscapes. A biotope is an area with a uniform type of landscape in which certain organisms can thrive. Within a biotope multiple habitats can be distinguished. This study will focus on **ecotope** scale level. The choice for this ecological scale is related to the choice of looking at wind turbine scale.

- Supra littoral <----> sub littoral (ecological zone)

The ecological influences of a wind turbine will be investigated only on **sub littoral level**. Impact on birds and other kind of environmental 'damage' will not be part of this study. This limitation is related to the focus of the bed protection.

- Nature <----> No nature (Governance)

Governance aspects of ecology are **not taken into account**. The bed protection suits a technical purpose and a certain economic lifetime. Therefore the question arises if the bed protection is of a (temporary) nature of not? This lies outside the scope of this thesis. Also the governance aspects about fisheries management will not be treated here. The assumption is made that fisheries are prohibited at (future) offshore wind farms.

- Surrounding effects <-----> Bed protection (Ecological boundary)

The effect of scour holes at the end of the bed protection (edge scour) will not be treated with respect to the ecology. The boundary of the study area is at the end of the **bed protection**.

- Ecological testing <----> Only ecological hypothesis

This thesis aims to provide favorable ecological conditions. The real ecological effects have to be tested by other institutions for follow-up research, because this thesis focuses on the ecological effects of the established species (after 3 years). **Only a hypothesis** can be made about the expected ecological effects. Furthermore, ecology is not 100% predictable and Building with Nature is a process by "Learning by doing".

1.5.3   Hydraulic loads

- Waves <----> no waves
- Currents <----> no currents
- Storm conditions <----> no storm conditions
- Daily conditions<----> no daily conditions

This study will not ignore hydrodynamic conditions and aims to choose a representative set of **all situations**.

1.5.4   Structure

- All kind of foundations <----> monopiles (Type of wind turbine foundation)

In chapter 2.2 *Offshore Wind Turbines* of this document multiple foundation possible for wind turbines are treated. The selected foundation is related to the depth and the economic feasibility. Monopiles are the cheapest and most common type of foundation and are economical as well as technical feasible until a depth 30 meters. In deeper waters complex structures are applied such as tripods and jackets. The future Dutch offshore wind farms will probably be constructed in relatively shallow waters (not deeper than 30 meters). Therefore only **monopile founded structures** are researched in this thesis.

- All kind of measures to prevent scour <----> Only bed protection

The probability of failure of the wind turbine due to the scour around the monopile can be significantly reduced by the installation of a bed protection. This is commonly applied technique to prevent erosion. The bed protection reduces the load on the sand particles (bed material) and prevent the washout of these particles. Other load reduction measures to reduce the load are also possible. An examples can be a (cylindrical) vertical plate around the pile to reduce the down flow and thus reduce the load on the grain. However, the authorities of offshore wind farms want minimal interference with the monopile. Another option could be to omit the bed protection and let scour occur and anticipate on scour by applying more steel and drive the pile deeper. This study focuses only on the **bed protection** and not at other measures to prevent scour, because the existing literature shows already a positive effect on the ecosystem due to the bed protection.

- Different types of bed protections <-----> One type of bed protection

There are a number of different types of bed protection mentioned in section 2.5 of this document. The most common used bed protection is the installation of a layer of rock. This is due to the relatively easy installation method and it is the cheapest option comparing with other methods. The use of rock also restores the intrinsic character of the North Sea. Therefore only **bed protection consisting of rock** will be researched.

- Wind turbine failure <-----> Bed protection failure (technical effects)

Only the failure of the **bed protection** will be examined. Other aspect such as the behavior of the natural frequency of the wind turbine due to scour will not be discussed.

1.5.5   Lifetime

- Total life time <----> Operational phase (Structure cycle)

As mentioned in *1.5.2 Ecology* only the established species will be examined. Therefore this study will not focus on the construction and decommissioning phase with respect to the favorable ecological conditions. This research will focus only on the **operational phase** during the lifetime of 20 years (DNV, 2014).
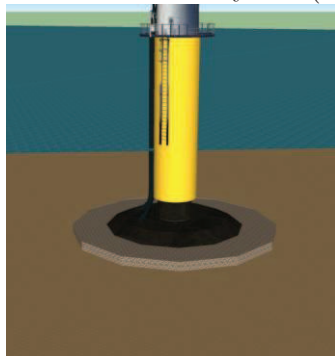

Figure 1-5: The scour protection of one offshore wind turbine is the area of interest.

1.6   REPORT STRUCTURE

This sections describes the elaborated subjects per chapter of this thesis. The report structure is on Figure 1-6.
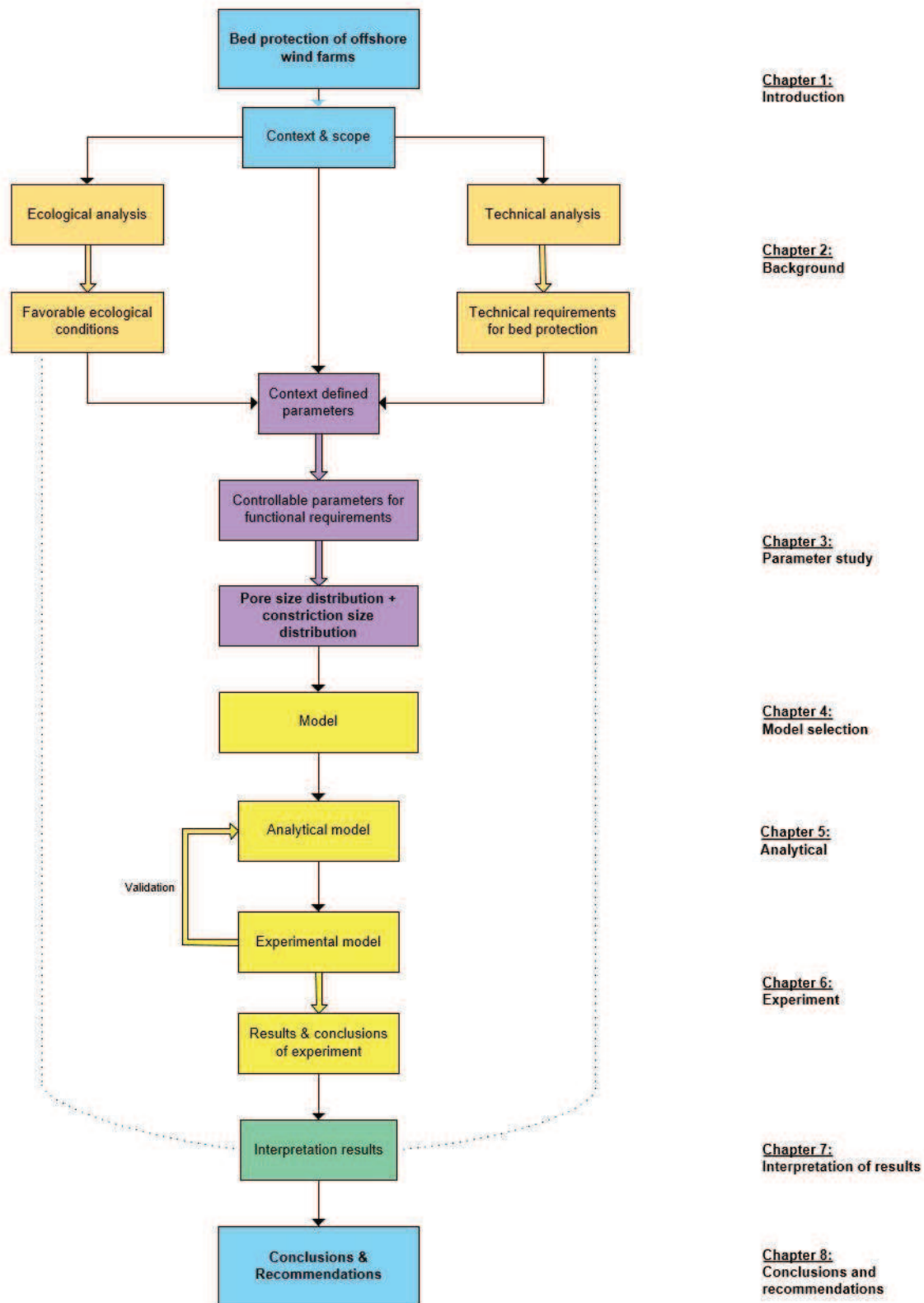

Figure 1-6: Report structure.

In **chapter 1** the **introduction** of this research is given.

In **chapter 2** the **literature study** is presented. A technical analysis and an ecological analysis is made. The offshore wind farms in Europe and in the Nederlands are discussed. Then this report zooming into a single wind turbine, the associated elements, and the installation method. Afterwards the technical requirements of the bed protection of a single offshore wind turbine and favorable ecological conditions will be discussed.

Chapter 3 contains a parameter study, derived from the literature study. A list of context-defined **parameters** is summarized. The non-matching and non-controllable parameters are filtered. The result is a list of controllable parameters for functional requirements. In the last section the parameter for further research is selected.

In **chapter 4**   models are presented to expose the pore-size distribution. These **models** are evaluated and two models are selected.

Chapter 5 elaborates the **analytical model**. For uniform spheres the pore-size distribution and the constriction-size distribution is derived. Only the constriction-size for multi-sized spheres are derived.

In **chapter 6** the **experimental model** is discussed. The set up of the experiment is elaborated and the possibilities and limitations are explained. The results of the model are presented and a general formula is derived. Also additional results are reported.

The elaborated models are both fundamental. In **chapter 7** is described how the fundamental **results** are **interpreted.**

The **conclusions and recommendations** are discussed in **chapter 8.**

2. BACKGROUND

This chapter provides background information about offshore wind farms, zooming in on a single wind turbine, presents parameters for favorable ecological conditions and summarizes the technical requirements for the bed protection. This literature chapter forms the basis to select controllable parameters for function requirements in chapter 3.

2.1 OFFSHORE WIND FARMS

In the last decades green energy has been a well-discussed topic in Dutch politics. The government has embraced the energy agreement of 14% sustainable energy production in 2020 (Rijksoverheid, 2014). In the same agreement the aim is to have 100% green energy in 2050. Nowadays only 4% is generated from sustainable sources. One of the measures to achieve this goal is an increase in the contribution of wind energy. The current production of wind energy is already a significant share of the total sustainable energy. The Netherlands is very flat and windy and therefore there is a lot of potential to create more wind farms. The generating of wind energy is envisaged to occur both on land and at sea.

In 2001 the governance launched a tender procedure for the first large offshore wind park in The Nederlands. In 2002 the consortium of Shell (Shell Wind Energy) and Nuon (Nuon Sustainable Energy) was assigned to exploit the offshore wind farm in the North sea in front of Egmond aan Zee (OWEZ). The first offshore wind farm consists of 36 wind turbines each with a capacity of 3MW and was constructed and operational in 2006 (Dekkers, 2007). A 3MW offshore wind turbine generate around 6.6 million kWh per year (Nederlandse Wind Energie Associatie, 2015) which is an efficiency of 25% with respect to the maximum capacity. The amount of generated offshore wind energy per turbine is enough to supply almost 2000 households. So, OWEZ can supply around 70.000 households per year.

Energy produced from fossil fuels and nuclear energy are called grey energy, because the extraction and transformation have negative effects on the environment or nuclear waste. The price (€/KWh) of green energy from offshore wind farms cannot compete against the price of most grey energies. This is the reason the government of the Nederlands provides subsidies for wind farms (Beurskens & van Kuik, 2004). The expectation is that future (technical) innovations will reduce the price of sustainable energy while the price of grey energy will rise and so the renewable energy will be relatively cheaper. These aspects make the investment in sustainable energy interesting.

At the moment there are two wind farms in the Netherlands:
- The *Noordzeewind* lies in front of the coast at Egmond aan Zee in section Q8 (OWEZ). The park contains 36 wind turbines with each with a capacity of 3MW.
- The *Prinses Amaliawindpark* lies just outside IJmuiden in section Q7. The park contains 60 wind turbines each with a capacity of 2MW.

At the moment three offshore wind farms are under construction (Rijksoverheid, 2014):

- *Luchterduinen* lies 23 km off the coast at Noordwijk aan Zee. The park will generate a maximum capacity of 150 MW.
- *Geminiparken:*
  - *Buitengaats* lies north of Ameland and will generate a capacity of 300 MW
  - *ZeeEnergie* lies north of Schiemonnikoog and will also generate a capacity of 300MW.

The overview of the Dutch wind farms are visible in Figure 2-1. The green areas are the two operational offshore wind farms (Noordzeewind & Prinses Amaliawindpark). The offshore wind farms under construction are sketched in yellow (Luchterduinen, west of Amsterdam) and in red (Buitengaats & ZeeEnergie). The potential areas for future wind mining are pink.

Figure 2-1: Map of the Dutch offshore wind farms. Green is operational, yellow and red is construction phase, and pink is future potential area (Global Offshore Wind Farms Database, 2014).

In the near future another 5 offshore wind farms will be built at three different locations in the Netherlands (Kamp & Schultz van Haegen, 26 september 2014). Each park will have a capacity of 700 MW (Rijksoverheid, Noordzeeloket, 2014), see Table 2-1.

Table 2-1: Future plans related to offshore wind farms of the Dutch minister of economic affairs.

Year	Plan	Location
2015	700 MW	Borssele
2016	700 MW	Borssele
2017	700 MW	Zuid Holland coast
2018	700 MW	Zuid Holland coast
2019	700 MW	Zuid Holland coast

The locations of the future offshore wind parks are the light blue areas in Figure 2-2. The operational and the under construction offshore wind farms are dark blue.
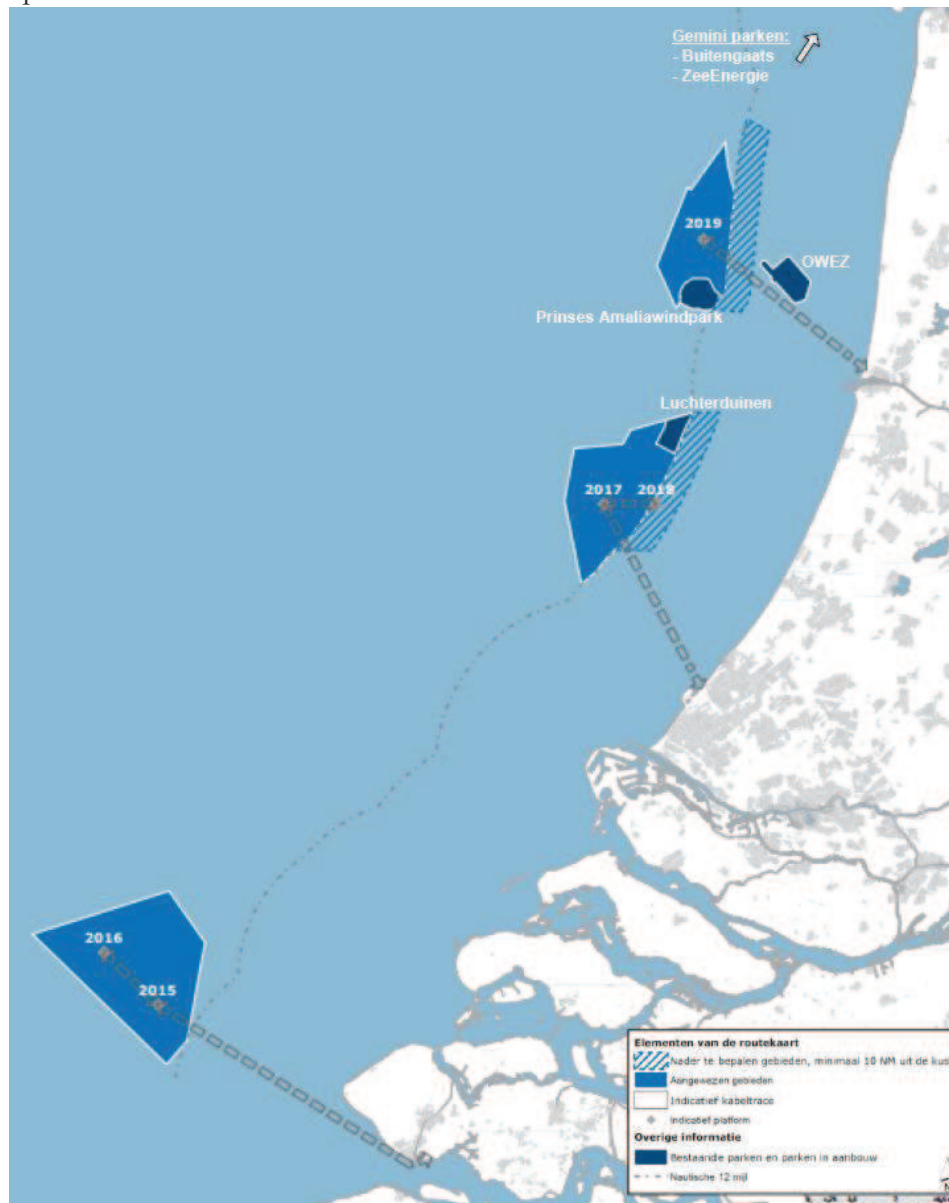
Figure 2-2: Future and operational offshore wind parks.

The Netherlands is not ahead of the wind energy market. Especially the UK, Denmark, and Germany are leaders in the market of offshore wind energy. In the North Sea and in the Baltic sea many offshore wind farms are constructed as visible in Figure 2-3.
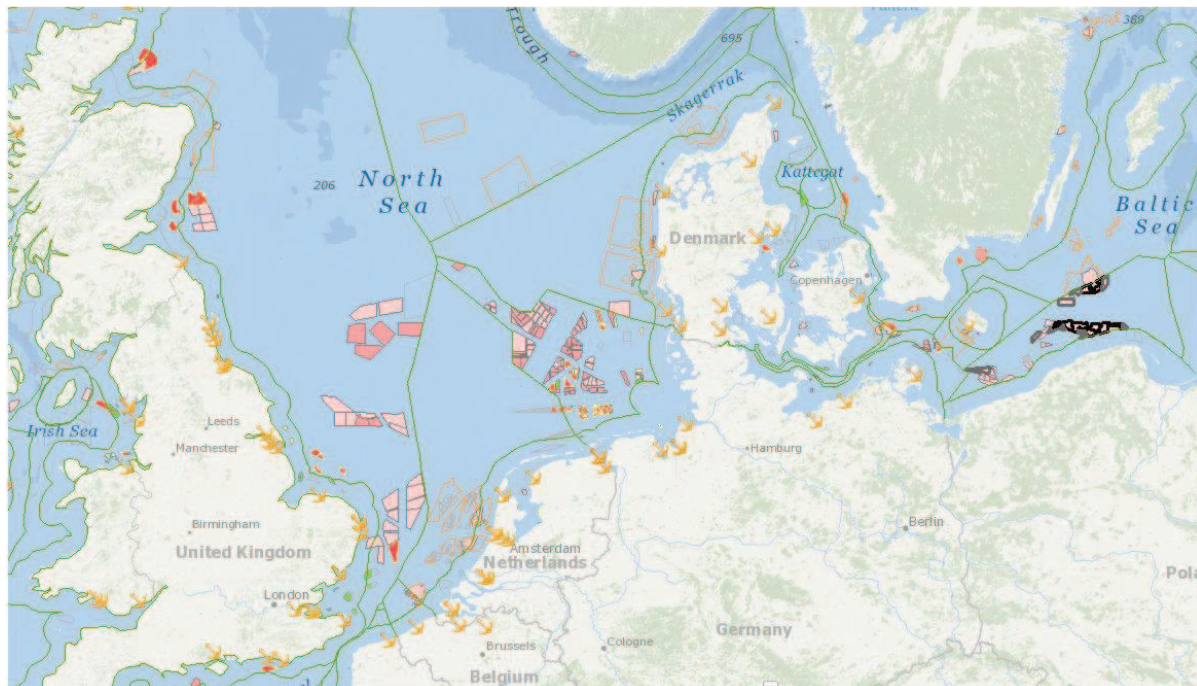

Figure 2-3: Map of the (future) offshore wind farms in North West Europe (Global Offshore Wind Farms Database, 2014).

The European Wind Energy Association stated that on 1 July 2014 the total number of installed offshore wind turbines is 2.304. These wind turbines have a combined capacity of 7.343 MW fully grid connected in European waters in 73 wind farms across 11 countries (EWEA, Key trends and statistics 1st half 2014, 2014). The generated electricity is comparable with the electricity consumption of 5 million households.

The European Wind Energy Association stated that in the first six months of 2014:
- 224 wind turbines were fully grid connected.;
- 233 foundations were installed in 13 farms;
- 282 turbines were erected in 8 farms.

The Dutch media has also adopted the discussion about offshore wind farms. The CPB (Netherlands Bureau for Economic Policy Analysis) calculated a cost of 5 billion euros for society. Nature & Environment comes to the conclusion that offshore wind farms are a "smart insurance". The plans of the Dutch government will lead to a cost of 1.2 billion euros or will lead to a gain of 12.3 billion euros. The calculation Nature & Environments takes climate damages due to the CO_2 emission into account (Natuur & Milieu, 2014). Overall, it can be concluded that the offshore wind energy market is dynamic.

2.2   OFFSHORE WIND TURBINES

This section provides the different foundation types and describe the dimensions and the construction method for the monopile foundation.

2.2.1   Foundation types

There is a variety of foundation types for offshore wind turbines. A lot of different foundation types of offshore wind turbines are listed below (DNV, 2014):

(a)   Monopile   (e)   Tripods
(b)   Gravity-based structure   (f)   Tri-pile
(c)   Floating   (g)   Twist jacket"
(d)   Jackets/Lattice structures

The last four listed foundation types (d, e, f, g) are called space frame foundations. A clear overview of all the foundation types is presented in Figure 2-5. Of the most applied foundation types (a, b, d, e) a technical drawing is shown in Figure 2-4 (Wind energy the facts, 2011) (Aber, 2012).
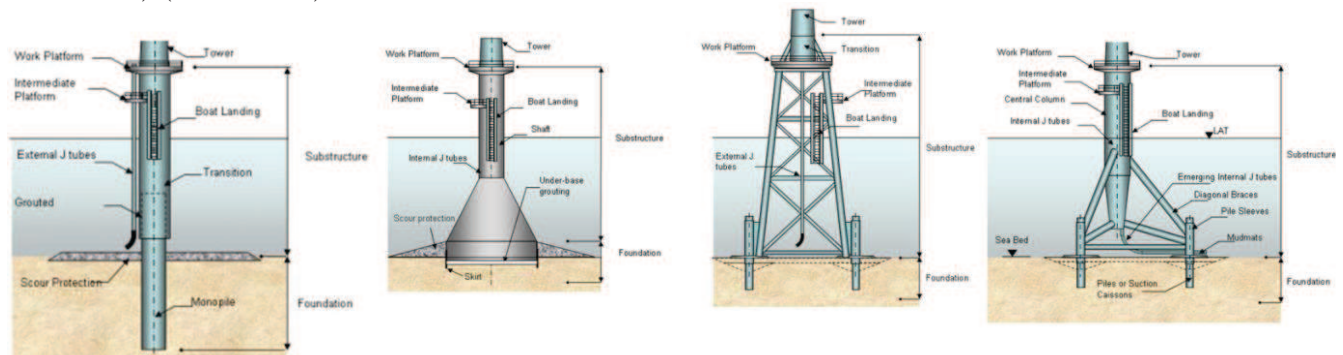

Figure 2-4: (a) monopile, (b) gravity-base structure, (d) space frame: jacket structure, and (e) space frame: tripod.

Based on the soil conditions, turbine specifications, and water depths the decision of foundation type is made. The monopile is a common and cost effective foundation. About 65% of the foundations of offshore wind turbines in Europe are monopiles(Redwave, 2014). It is suitable for depths up to 35 meter in less rocky soil conditions.

The gravity-based structures are applied in more rocky soil. Gravity-based foundations have a share of 25% of the offshore wind turbine foundations in Europe. The principle is easy to understand. A massive block is created to prevent sliding, tilting or uplifting. The excessive use of material is the main drawback of this design. Moreover, the construction time is long and the transport barges/vessels can only handle limited weight. An indication of the limiting depth of gravity-based structures is 25 meter because of the maximum bearing capacity of the transportation vessels/barges. In the future the limited depth may increase due to bigger equipment.

In deeper water space frame structures are financially and technically attractive. Due to its structure the jacket is stiff in comparison with the monopiles and the gravity-based structures. The jacket design and construction is expensive and therefore these foundation types are not economically feasible in waters shallower than 40 meters. The jacket can be anchored to the sea bed with suction buckets. These buckets are cylindrical piles with open bottom and a sealed hat. By means of vacuum the pile drives itself into the seafloor. The tripod is also a space frame structure and is designed for water depths between 30 and 40 meters.

(a) Monopile

(b) Gravity-based structure

(c) Floating

(d) Jacket

(e) Tripod

(f) Tri-pile

(g) "Twist Jacket'

Figure 2-5: Different types of wind turbine foundation.

To anticipate on future demand floating wind turbines are designed for deep waters. The technology for floating wind turbines is not yet fully developed and therefore floating wind turbines are not yet operational. The floating wind turbines are based on three different principles of floating structures, see Figure 2-6. A lot of research needs to be done, but for deep water the floating wind turbines have potential because of the wind conditions and the available space.

Mooring Line Stabilized
Tension leg platform with suction pile anchors

Ballast Stabilized
Spar buoy with catenary mooring, drag-embedded anchors

Buoyancy Stabilized
Barge with catenary mooring lines
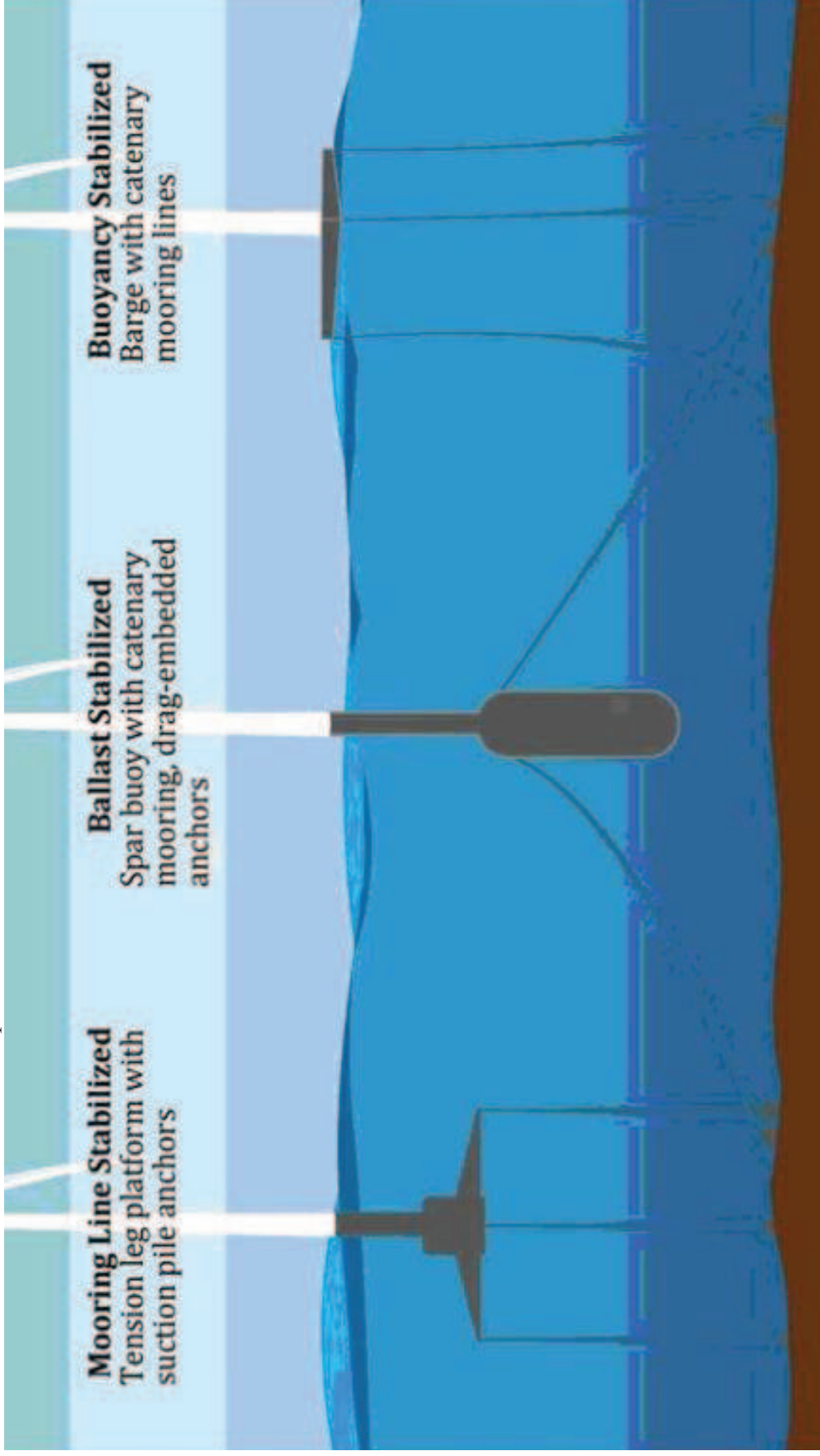
Figure 2-6: Floating offshore wind turbines (Alternative Energy in New York, 2014).

2.2.2   Dimensions

In the left sketch of Figure 2-7 the dimensions of a monopile founded offshore wind turbine are shown. This figure is included to give a indication of the size. The monopiles are giant steel pipes with a diameter of 2.5 – 7m and have a length of 35-70 meters (Lawson, 2013). Monopile foundations are economically feasible up to a maximum depth of 35 meters below mean sea level. A 70 meter long monopile with a width of 5 meters has a weight of about 550 ton (Belwind, 2014). The transition piece is between 25 meters and 40 meters, see Figure 2-7. A good indication of the transition piece height above sea level is 20 meters, but the actual height depends on the set up and the wave height (Schaumann & Keindorf Ingenieurges, 2014). The shaft height of the wind turbines are often around 100 meters, depending on the blade length.

An indication of the dimensions of the bed protection is presented in the right section of Figure 2-7 (Raaijmakers, Joon, Segeren, & Meijers, 2014). The volume of the bed protection has a magnitude of 1000m^3 and the stone size (d_{50}) of the armour layer will be around 50cm. This depends of course on the location and conditions, but the numbers are only mentioned to get an indication of the magnitude.
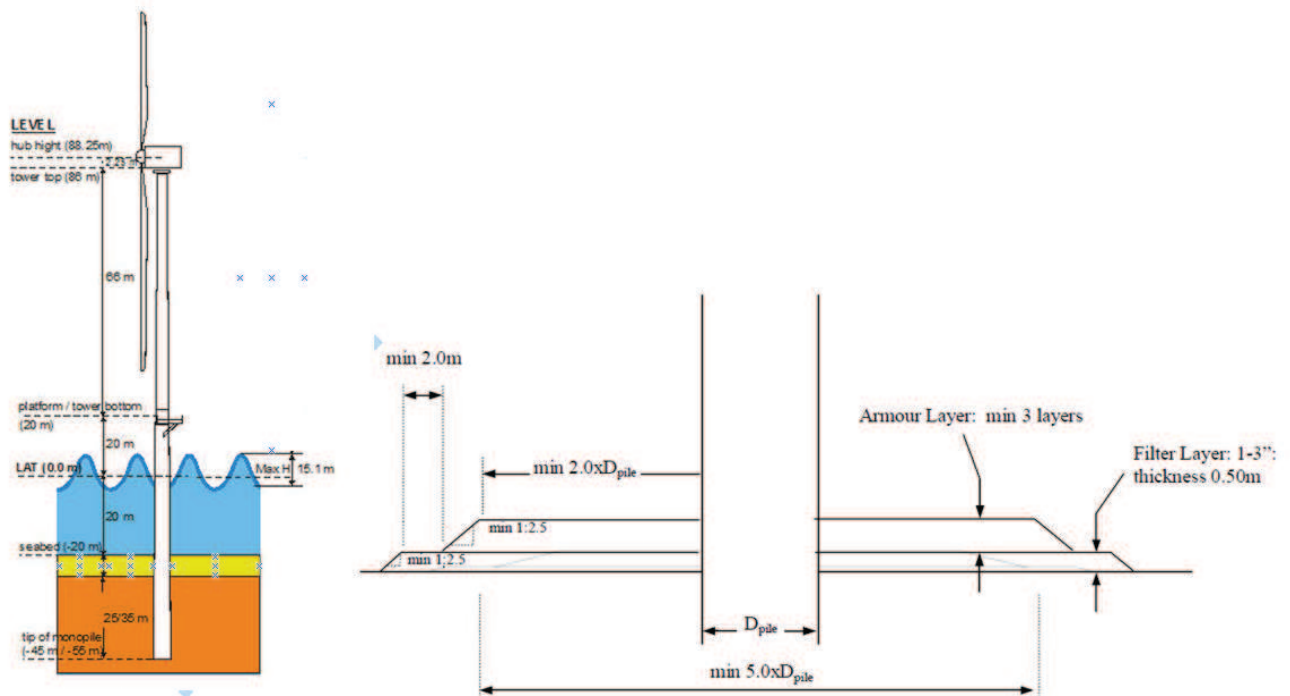

Figure 2-7: Indication of the dimensions of an offshore wind turbine (left) and indication of the dimensions of an associated scour protection (right).

2.2.3   Installation of monopile foundation

This sub section will explain the procedure of the installation of a monopile founded offshore wind turbine with bed protection, because this is the most applied foundation. The installation of other foundation types will not be treated here. The monopile foundation elaborated here consists of a bed protection around the monopile.

There are four phases in the lifetime of a offshore wind farm:
- Design phase
- Construction phase
- Operational / maintenance phase
- Removal phase

The first step of construction of a wind turbine is placing a filter layer on the bed. The filter layer consist of small stones. The stone size and the grading are calculated (see 2.5.4) and often dumped by a side stone dumper. After the inspection of the filter layer the monopile is lifted by jack-up vessel or pontoon crane. The position will be fixed by a special mold. Once the pile is in the right place and perfectly vertical, the pile will be hammered or drilled into the ground. If the monopile has reached the desired depth, a transition part is placed over the monopile (at a fixed height above sea level) and a special grout is injected in between. The height of the transition piece above the water level is location specific and depends on the wave set up and the wave height. After the installation of the transition piece an armour layer is dumped on the filter layer around the monopile. The stone size and grading is calculated (see 2.5.4) and placed by fallpipe vessel or side stone dumper. The side stone dumper is less accurate and more material is needed. The complete sequence is sketched in Figure 2-8.
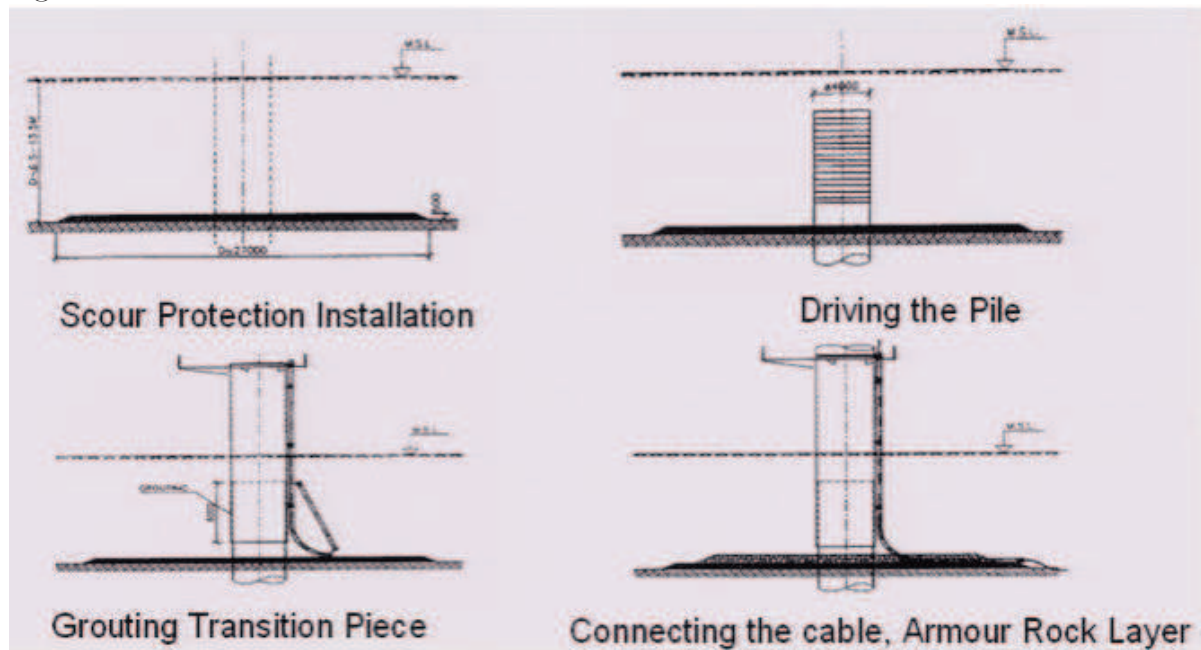

Figure 2-8: Monopile installation sequence (Sustainable Energy Technology, 2006).

At this stage the proceedings end for traditional contractors like Boskalis, Van Oord, and Ballast Nedam. The placement of the tower on top of the transition piece requires also a lot of installation work. This will be done by other parties and are outside the scope of this thesis.

To get a better impression of the installation of the monopile the installation sequence is presented in Figure 2-9 with four impression. The monopile is a simple structure that consists of one cylindrical tube of steel. The steel tube is in its entirety made in the factory on shore. Afterwards it is transported by pontoon vessels to its location, see upper left picture in Figure 2-9. Sometimes both ends of the tube are closed and the pile is floating and dragged by tug.

At the location already filter layer is installed before the monopiles arrive. The arrived monopiles will be lifted by jack-up vessel or pontoon crane. By a special mold the monopiles will be placed at the exact location and be hold vertical while driven or hammered, see upper right in Figure 2-9. If the monopile is installed a transition piece will be placed over the monopile, see bottom left in Figure 2-9. The transition piece and the monopile are connect together by grout injection. After installation of the transition piece a armour layer will be placed with a fallpipe vessel, see bottom right in Figure 2-9.
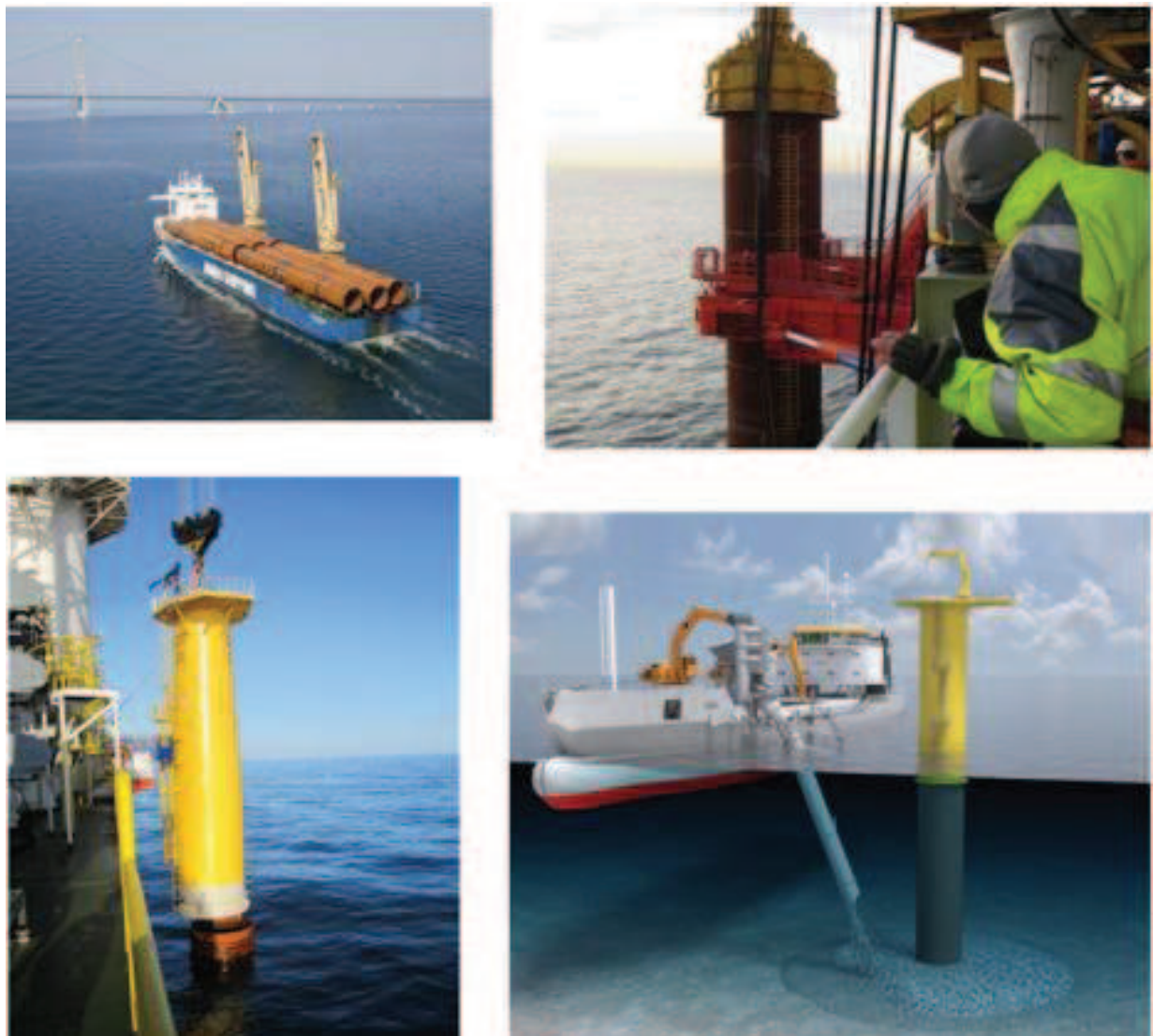
Figure 2-9: Execution of monopile installation in practice.

2.3   ECOLOGICAL ANALYSIS

How to combine favorable ecological conditions and technical requirements at offshore wind farms? Technical requirements consist of calculations and model tests and are (for the author at least) more straightforward than the broad spectrum of ecosystems and species. What are the favorable ecological conditions for species and how do these conditions interact? What kind of species will be focused on and why? And another question that arises: why is stimulation of the favorable ecological conditions needed in the first place? What is the social acceptability?

In this section the ecological analysis is presented. First of all the social acceptability and the current environmental impact assessment procedure is very briefly stated. The next sub section discusses the ecological zones and classification systems. Then the monitored ecosystems and species at operational offshore wind farms are described. In sections 2.3.6 and 2.3.7 is substantiated which species are selected including their favorable ecological conditions. This ecological analysis concludes with a list of parameters which are of influence to provide favorable ecological conditions for the selected species. In chapter 3 this list of parameters is compared with the parameters for technical requirements.

Note: Building with Nature is "learning by doing".

2.3.1   Social acceptability

The current trend is to foresee and anticipate on the environmental impact of new civil works. The Dutch water sector embraces this thought by Building with Nature instead of Building in Nature. Building with Nature is a program that aims to utilize natural processes and provide opportunities for nature while realizing hydraulic infrastructure (Ecoshape, 2014). The program is administrated, represented and carried out by the consortium called EcoShape. The consortium of private parties such as engineering consultants and dredging contractors as well as public agencies academic research institutes and government agencies. The American counterpart is called Engineering with Nature.

Most of the time eco-solutions are designed to create and stimulate biodiversity. A larger diversity of plant species means a great variety of crops which increases the species diversity. This ensures natural sustainability for all life forms and a healthy ecosystem that can better withstand and recover from disasters (Shah, 2014). This research is aiming to search for and provide favorable ecological conditions for certain species at offshore wind turbines by investigating influences of the bed protection. Therefore this research topic almost implies bioengineering. This thesis' approach can also be seen as an eco-hydraulic approach.

To win tenders and gain assignments contractors of offshore wind farms need to have unique selling points. So if a contractor has a better understanding of the impact on the environment during installation and lifetime of the civil structure the contractor can score on this point with respect to their competitors. The image of the client and corporate responsibility of the contractor is of great importance, so often a 'green solution' is preferred when economically feasible.

From this point of view it is clear that a contractor is interested in a study that takes place at the dividing line between favorable ecological conditions and technical feasibility. The questions rise if it is really necessary to provide favorable ecological conditions or that it is just a market strategy to boast image?

Four interviews are conducted with ecologists gain more knowledge in the field of ecology and to answer the question about the social acceptability. The following persons are interviewed:
1. Victor Beumer, eco-engineer, Deltares and
   Tim Raaijmaker, scour protection engineer, Deltares.
2. Joop Coolen, marine ecologists, Imares and
   Babeth van der Weide, ecological researcher, Imares.
3. Annemiek Hermans, marine ecologist, Boskalis and
   Astrid Kramer, marine ecologist, Boskalis.
4. Luca van Duren, senior researcher and specialist of the relation between aquatic organisms and fluid dynamics, Deltares.

Joop Coolen is a marine ecologist at Imares specializing in biodiversity of reefs in the North Sea. He looks at offshore installations such as oil and gas production platforms and wind farms and studies natural reef biology and shipwrecks in the North Sea. His research is related to the ecology part of this graduation work. He said about the social acceptability and the approach of this thesis: "The installation of offshore wind farms is not natural and human interferences are in principal not good. However, in the past a significant part of the North Sea floor consisted of hard substrate, but due to trawling activities by humans this is removed. Nowadays the North Sea floor consists of sand and by dumping stones for the bed protection of offshore wind farms hard substrate will be added which was present in the past. Furthermore, offshore wind turbines will be build, so then it is better to build it properly and in consultation with the environment". The other ecologists agreed on the last comment: "If it has to be build, build it properly". By providing favorable ecological conditions on top of the technical requirements a proper interdisciplinary project can be accomplished.

Substantiated the motivation of this thesis is clients image, the corporate responsibility of the contractor, the historical hard substrate conditions of the North Sea, and the conception of the ecologists.

2.3.2   Legislation

The European legislation requires an assessment about the impact on the environment for civil engineering projects such as offshore wind farms. This is done in an Environmental Impact Assessment (EIA). The necessary steps to be taken in an EIA is presented in Figure 2-10 (MER, 2014).
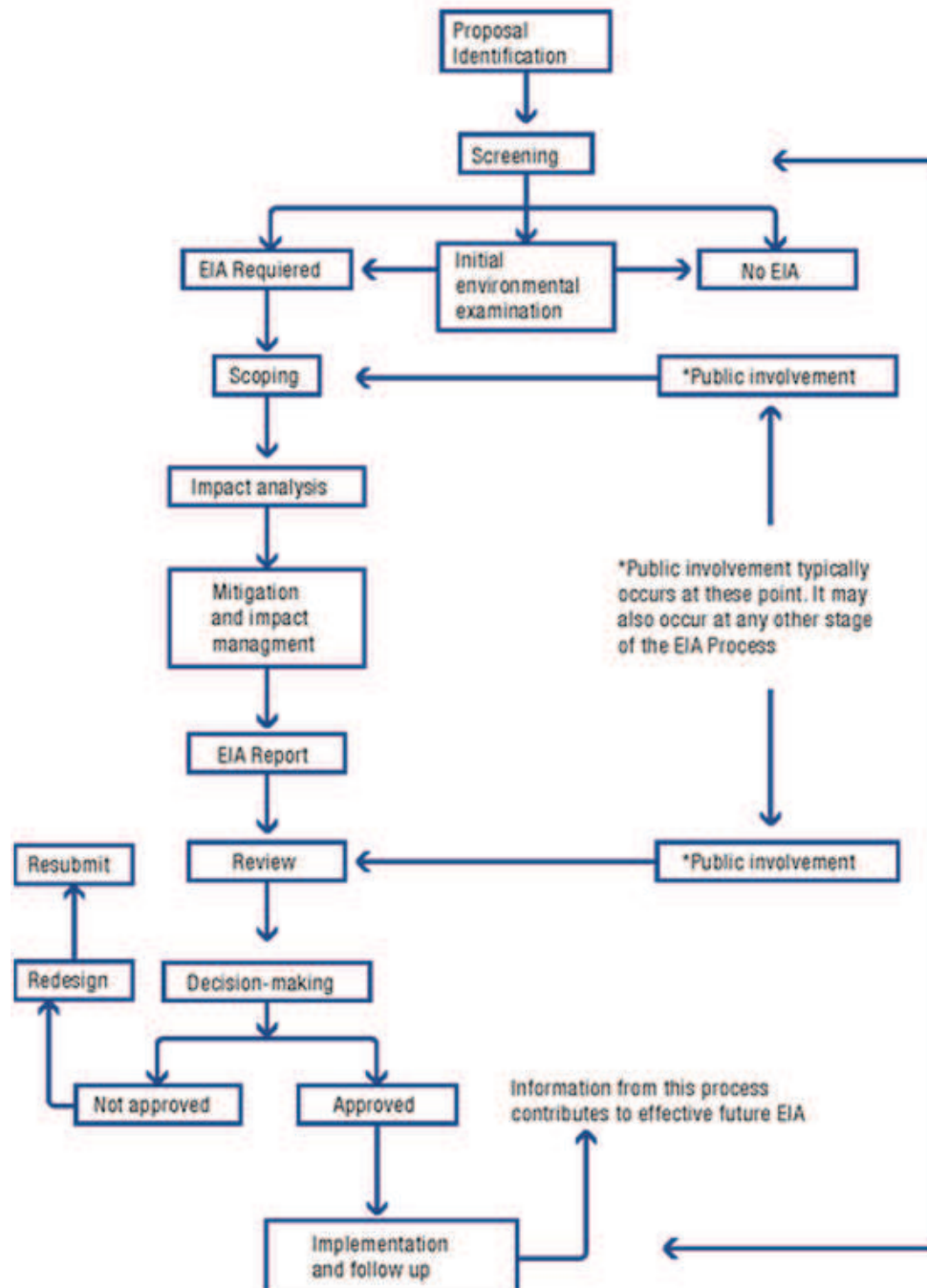

Figure 2-10: Structure of EIA processes.

The Dutch EIA commission stated that there is insufficient structural vision for offshore wind energy. Further investigation on the impact on birds and underwater life is essential (Windenenergie-nieuws, 2014). This news article strengthen the social acceptability of this thesis, because this thesis seeks for favorable ecological conditions for certain species (underwater life).

2.3.3   Area of interest & ecological zones

The focusing area is the North Sea in front of the Dutch coast. As mentioned in section 2.1, the Netherlands have already developed two offshore wind farms and at the moment three offshore wind farms are under construction. The minister of Economic Affairs also announced more offshore wind farms in front of the Dutch coast. Therefore the study area of the North Sea is selected.

Due to the building of offshore wind farms the ecosystem changes. The wind turbines and especially the blades causes collisions with birds (Birdlife, 2009). This topic is outside the scope of this thesis. This research focuses on the ecosystem related to the water body.

There are three major environmental zones to distinguishable (Bolier, 2006):
- Littoral zone
- Pelagic zone
- Benthic zone
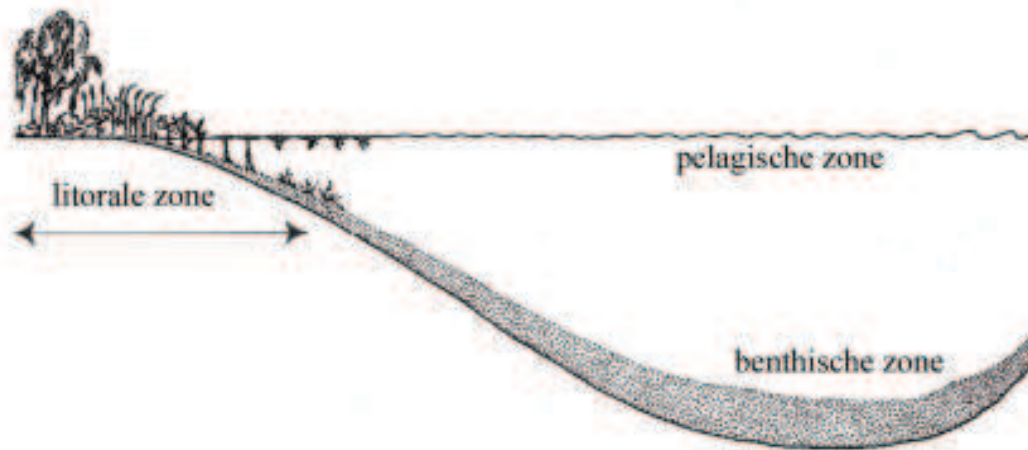
Figure 2-11: Defined zones in water system.

Within the littoral zone also three areas can be defined (Baptist, van der Meer, & de Vries, 2007).
- Supra littoral (above tidal zone)
- Eu littoral (in tidal zone)
- Sub littoral (below tidal zone)

The littoral zones listed above are depth related and are in the intertidal area. During low tide some parts will fall dry and during high tide some areas are submerged or are wetted by splash water. The offshore wind parks are further offshore and (the area around) the bed protection is completely submerged, so the littoral zone is not further investigated. If the study area of this research also included the ecosystem and species present at the monopile/transition piece, than the littoral zone would be of importance. The area of interest of this thesis is the pelagic zone and the benthic zone.

Both zones (pelagic and benthic) are characterized by abiotic components such as light intensity, turbidity, temperature, temperature, soil minerals etc. Abiotic components include also the hydrodynamic conditions (wave exposure and currents). The biotic components always influence the presence of certain species.

The biotic and abiotic components indicate if certain species can be found in a zone. Below both zones are more elaborated on and an example is given for the species found in these zones.

- Pelagic zone;
  The species in this zone are neither close to the bottom nor near the shore. The species are in the water column between mean sea level and a distance from the bottom. Fish that lives in this zone are called pelagic fish. Within the pelagic fish two types can be distinguished:

  - There are predator pelagic fish like sharks who eat smaller fish in the pelagic zone; and

  - Forage pelagic fish like herring and sardine which are eaten by bigger pelagic fish.

- Benthic zone (demersal zone);
  The species in this zone living in the water column near the bottom. In this zone also two types are differentiated.

  - Benthopelagic;
    Benthopelagic fish lives just above the bottom in the water column. Most demersal fish are benthopelagic fish like cod.

  - Benthic zone
    In the benthic zone live organisms on, in or near the seabed. The community is called benthos. An example are the colonization of hard substrates like mussels. Lobsters can also be found in this zone.

So, different kinds of species can be distinguished in the pelagic and benthic zone. All species have their own favorable ecological conditions and thrive in a specific section of the ecosystem.

The definition of an ecosystem:
An ecosystem is a community of biotic components in conjunction with the abiotic components interacting as a system.

The abiotic components are the nonliving chemical and physical parts of the environment that affect living organisms and the functioning of the ecosystem. The biotic components are the living things that shapes the ecosystem. The comprehensive term is called ecology.

2.3.4 Ecosystems and species present at offshore wind farms

Frequently stories about offshore wind farms appear in the media. A lot of these stories are economically related (as already discussed 2.1), but also articles are written about the impact on the environment. The stories are often based on a new published article from scientists. In 2012 Trouw published the article: "Mussels, oysters, and skate thrive on wind farms" (Wesseling, 2012). In this article is stated: "Nature and people seems to have a love-hate relationship with offshore wind farms. The people are struggling with the degradation of the landscape, but see also the positive environmental effects of it. In nature there are 'winners' and 'losers'. The wind turbines provide a new habitat for many species such as cod and cormorants, but it also have negative effects for certain birds."

Two fundamental reports and their conclusions are listed below to indentify the conducted researches on the environmental impacts of offshore wind farms.

- Short-term ecological effects of an offshore wind farm in the Dutch coastal zone; a compilation (Lindeboom, Kouwenhoven, Bergman, & Bouma, 2011):
  In this paper the short-term (two years) results are compiled on a large number of faunal groups obtained so far. Impacts were expected from the new hard substratum, the moving rotor blades, possible underwater noise and the exclusion of fisheries. The results indicate no short-term effects on the benthos in the sandy area between the generators, while the new hard substratum of the monopiles and the scouring protection led to the establishment of new species and new fauna communities.
  Overall, the OWEZ wind farm acts as a new type of habitat with a higher biodiversity of benthic organisms, a possibly increased use of the area by the benthos, fish, marine mammals and some bird species and a decreased use by several other bird species.

- Positive environmental impacts of offshore wind farms (DTU-Aqua, 2012):
  On-going monitoring programmes in Horns Rev 1 offshore wind farm show that the stock of some fish species increased. Starting before wind farm construction in 2002, scientists from the Aquatic Department of the Technical University of Denmark mapped the fish life in the area. The biologists compared those results with the situation in the area seven years later. The survey showed that the offshore project had no negative effects on the fish life and that boulder structures functioned as artificial reefs, providing good breeding conditions with a wide selection of food and shelter from currents. The boulder structures attracted fish species that usually prefer rocky soils, and as such the wind turbines provided habitats for a range of new species

Following these researches, the hard substrate have a positive effect on the environment. The exact explanation and physics behind it are not (yet) fully understand. The positive effects are more 'a coincidence' than that it is designed on purpose to enhance for example biodiversity. This thesis, inspired on the Building with Nature program, aims therefore to see the bed protection of offshore wind turbines from the technical point of view as well as the ecological point of view. An integral design which foresee favorable ecological conditions and fulfill the technical requirements is the ultimate goal. Dual functions of bed protection have a much better chance of maximizing the return for investment (Linley, Wilding, Black, Hawkins, & Mangi, 2007).

Note: It is not known if abundance of species is taken from other areas of the sea or that the count species are due to new juveniles.

2.3.5   Classification of favorable ecological conditions

The favorable ecological conditions can be quantified in ecotopes classes or in separate parameters.

To understand species population dynamics, the underlying processes have to be understood. Such processes are rates of birth (i.e. recruitment), immigration, emigration and death. These factors form a complex web of demographic rates. Larval and juvenile stages can contain both a pelagic and a benthic phase, thus making it difficult to study the natural development of individual cod and populations (Andersson, 2011).

A method to quantify favorable ecological conditions for species per parameters is with the Habitat suitability index (in dutch: Habitat Geschiktheids Index (HGI)). This method describes per parameter (such as depth, current, etc) how suitable the condition is for the selected species (van Breukelen, 1992). If the score is 0, than it means non suitable and if the score is 1.0 than the selected species can thrive perfectly in this condition. Deltares published these kind of graphs on their wiki (Deltares Mytilus edulis, 2014). An example will be given for the mussel:

stroomsnelheid (m/s)	HGI
<0.2	0
0.5	0.5
0.8	1
1	0.75
1.2	0.4
1.5	0.2
>1.8	0

orbitaalsnelheid (m/s)	HGI
0	0.4
0.2	1
0.3	0.5
0.5	0.2
>0.6	0

Referentie: #1
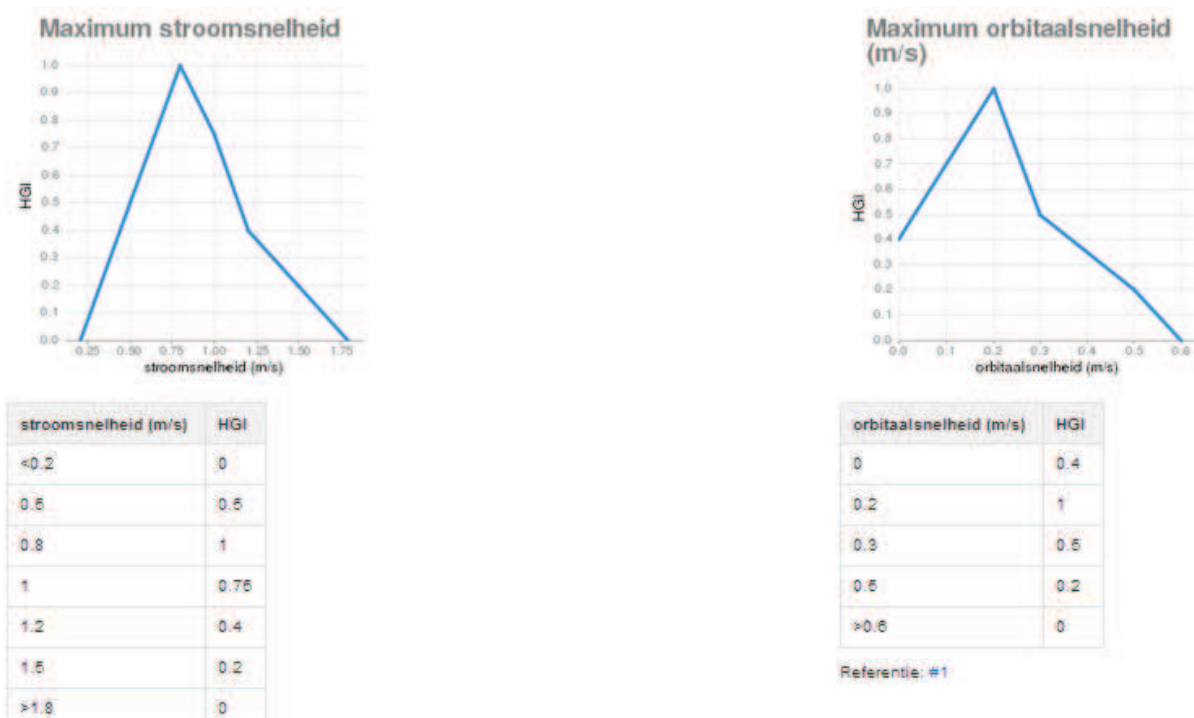
Figure 2-12: Habitat suitability indexes of the mussel for certain parameters.

For a few parameters the HGI of the mussel is established. It can be read from Figure 2-12, upper left figure and below left table, that the current has to be between 0.25 m/s and 1.75 m/s for the mussel to survive. If the current is less than 0.25 m/s the mussel will migrate or die (probably due to the lack of food supply). If the current is higher than 1.75 m/s the mussels will be washed away. The best current speed for the mussel to thrive is 0.8 m/s, see Figure 2-12.

However, remarks can be made about the quantification of this method. These HGI are probably derived from experiments in the flume and these indexes cannot be one-to-one adopted in real situations. All kind of parameters interact and are related to each other. The favorable ecological conditions for species has to be seen as an interacting system and to derive this from flume experiments is arbitrary says Tim Raaijmakers (Raaijmakers T. ,

Ecology-based bed protection of offshore wind turbines interview, 2014). Moreover, the interpretation of ecological data is often difficult due to unknown influences, making it partly depending on expert judgment as Joop Coolen states (Coolen & van der Weide, 2014).

Other Habitat suitability models for the estimation of the impact of human interventions on species are investigated (Bult, Stikvoort, & Willemse, 1999). Other studies concluded that ecological systems should be based on ecotopes, rather than habitat parameters (Leewis, Dankers, & de Jong, 1998).

However, this thesis will continue with the focus on parameters and not ecosystems as a whole. This is comparable with a HGI index. The research structure/framework is as follows:
- The 'ecological' parameters for favorable ecological conditions will be compared with the 'technical' parameters for technical requirements
- All the context-defined parameters will be listed
- Controllable parameters for functional requirements will be researched in detail.

2.3.6   Indicator choice of species

Ecology is the branch of biology that deals with the relations of organisms to one another and their physical surroundings (Oxford dictionary, 2014). So, ecology entails a wide range of (interacting) aspects and therefore the ecological analysis of this thesis is limited to two attractive species and the enhancement of biodiversity. The biodiversity is selected because it is an important topic at the international agenda for the Natura2000 areas, which is a European network of protected areas (Royal-HaskoningDHV, 2014).

The two species this research will focus on are cod (*Gadus morhua*) and European Lobster (*Homarus gammarus*). These species are selected because of the following arguments:

- Present at offshore wind farms
  Juvenile cod (Winter, Aarts, & van Keeken, 2010) and juvenile lobsters (Krone & Schmalenbach, 2011) are found during ecological impact monitoring at offshore wind farms.

- Economically attractive
  Cod and lobster are commercially important in the Netherlands/North Sea.

- Expert input
  Expert information is gained in four interviews with ecologists. These ecologists are experienced and able to indicate a realistic and feasible scope of this research. There opinion is included in the selection and decision procedure.

- Stock decreasing
  The stock of both species are significantly decreased in the recent decades due to overfishing.

- Literature available
  The availability of literature is essential to succeed and to come to a realistic thesis.

The favorable ecological conditions of these species are discussed in the following paragraphs.

2.3.7   Favorable ecological conditions

The favorable ecological conditions of the cod and the lobsters will be elaborated in this section.

1. <u>European lobster (Homarus gammarus)</u>

European lobsters are crevices dwellers, burrow dwellers or live in cavities. The European lobster has big claws and is a solitary species, see Figure 2-13. Adult specimen can grow up to a meter long. However, due to overfishing the possibility of seeing such a big lobster is almost zero.

The European lobster must shed in order to grow (Ecomare; common lobsters, 2014). After discharging their old shell the lobster is vulnerable and a easy prey. Therefore during this phase the lobster has to find shelter in a hole. Crawling out of their old shell, the lobsters can absorb more water and increase their size by at least 15%. Then their new carapace begins to harden. Depending on the calcium content in the water a strong carapace is created in several hours to several weeks.

Adults and juvenile lobsters are not necessarily found in the same place since habitat requirements vary. Juvenile lobsters under 35 mm carapace length (CL) are considered to be burrow dwellers, while the lobsters above 35 mm CL are considered to be crevice dwellers. Growth rate of juvenile lobsters can vary considerably (Jensen, Wickings, & Bannister, 2000). The legal landing size of lobsters is 85mm CL which is reached after 4-6 years.
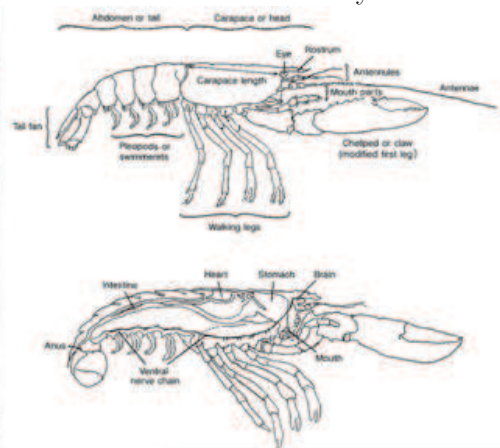
Figure 2-13: European lobster.

In most areas lobsters do not mature before an age of 5-8 years, depending on water temperature (Prodöhl, Jørstad, Triantafyllidis, Katsares, & Triantaphyllidis, 2006). They mate every in 2 to 3 years and only when the females are in a freshly molted state. After mature, the females carry the eggs (around 150.000 in total) around for a year in her tail. After hatching, the young larvae are zooplankton and 'swim' 2 to 7 weeks around in the water before molting into small lobsters. In total the planktonic larvae molt four times and in stage five they settle on the bottom of the sea. The small lobsters are then 10-13 mm long (Havforskningsinstituttet, 2007). However, most of the small lobsters are forage for pelagic species.

The hole, the 'home' of the lobster, has a front and back entrance so that they can escape from all precarious situations. During day time they are hiding in these holes and during night time the lobsters are going out to find food. Lobsters play an important role within the North Sea's ecosystem. As omnivores, they top the food chain, thriving on algae, mussels, snails and worms and ensuring that other species don't become pests. However, research has

to be done whether the lobsters will eat each other in the restricted confines of the wind turbine foundations. The German scientist Frank, who is researching the replenish of the lobster habitat of Helgoland: "Lobsters recognize one another by smell. Once they have tested their strength against one another, they accept the results." (Scientist plan to settle lobsters in wind farms, 2013). In the same article stated that scientists calculated that each square meter can provide a home up to five lobsters.

European lobsters can be found in the North Sea and prefer a complex habitat such as old ship wrecks and thus also offshore wind farms. Besides providing additional habitat, the wind turbines and ship wrecks can represent as stepping stones which enhance the connectivity of the North Sea lobster population (Krone & Schroder, 2010).

Adult lobsters occupy shelters in a wide variety of habitats. They prefer the crevices in natural rock, boulders and scree formations, but lobsters readily occupy suitable holes in man-made structures. When food reserves within and close to the burrow of providing complete sustenance, the lobster starts to forage further afield seeking shelter whenever necessary to avoid strong currents and predators (Jensen, Wickings, & Bannister, 2000).

2. Cod (Gadus morhua)

Fish move to exploit resources, mainly food and shelter. Basically, fishes select foraging areas to maximize food intake and minimizing threats by available shelter. The new hard substrate of Offshore Wind farm Egmond aan Zee (OWEZ) provides shelter and food for fish species like North Sea cod (Lindeboom, Kouwenhoven, Bergman, & Bouma, 2011).

The behavior of cod in offshore wind farms is well documented in the report Residence time and behaviour of sole and cod in the OWEZ (Winter, Aarts, & van Keeken, 2010). Due to the observed seasonal and diurnal patterns of cod in the wind farm the suggestion is made that the monopile habitat attracts at least part of the cod population. The telemetry experiments could not relate noise and vibrations produced by wind turbines with the presence of cod. It is likely that the wind farm is used for foraging and refuse, but because most, if not all, of the tracked cod were immature, the significance for spawning is not determined. The report also concluded that if fishing remains effectively banned from the OWF, it can act as a refuge against fishing cod.

In the telemetry experiments no adult was present. The cod varied from 24-47 cm, so most of them were juvenile cod. Three reasons to explain this:
- Adult cod behave differently than juvenile and tend to avoid the wind farm or show less attraction
- Due to the young age of the wind farm colonization of the newly created monopile habitats was mostly performed by dispersing juvenile cod
- There are no adult cod presented in the coastal zone where OWEZ lies because of the temperature.

Due to overfishing the cod population in the North Sea is decreased significantly, see Figure 2-14 (Compendium, 2014). Therefore the minimum legal landing size of cod is 35 cm in the North Sea.
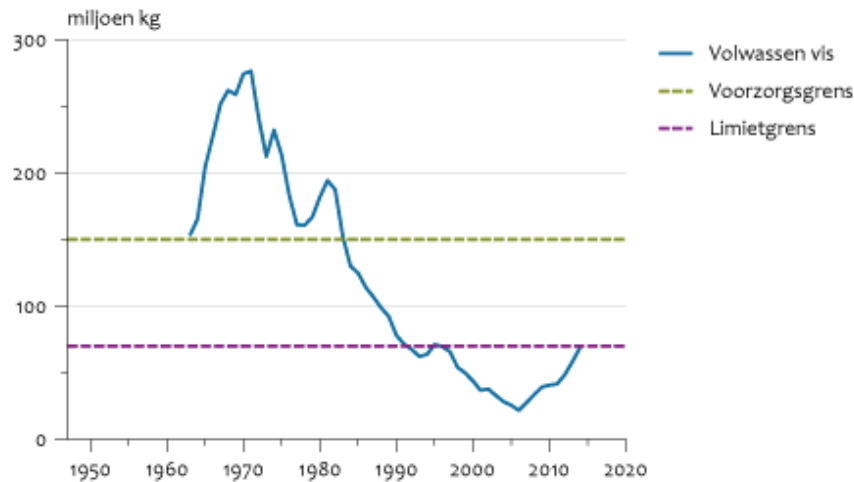

Figure 2-14: Cod stock in North Sea.

The method that cod use to find directions during migration is not fully understood. It is possible that adults recognize sea currents by temperature and salinity. For spawning the water temperature and the current directions is of importance and in the North Sea this if the cod is at least 3 years. The fecundity (the amount of eggs) depends on the length of the female. Moreover, also the quality of the eggs increase. The females can produce up till 500.000 eggs per kilogram bodyweight.

Figure 2-15: Cod.

The larvae phase takes around three months. The larvae drift in the water column (plankton). After three months the juvenile cod becomes benthic and have a length of about 4-7 cm. Juvenile cod can thrive in higher temperatures than adult cod. They profit from foraging in shallow waters. Adult cod are predators and can eat fish up to 70% of its own length. Adult cod also consume juvenile cod. The only major predator of the cod in the North Sea are the fishermen (Breve, 2013).

2.3.8   Conclusion of ecological analysis

All the ecological related parameters for the favorable ecological conditions are summarized in this subsection with the focus on *cod, European lobster*, and *biodiversity* in general. This summarized list is presented below. These parameters will be compared with the technical parameters in chapter 3.

Because of the amount of parameters, the parameters are organized per theme. The themes are:

- Physical conditions;
- Bed protection;
- Material properties;
- Water quality;
- External effects.

<u>Physical conditions</u>
There are four ecological parameters distinguished and categorized in the theme 'physical conditions':

- Waves
  High and/or long period waves cause a strong orbital velocity at the bed in shallow and transitional waters. This orbital velocity at the bed determines the settlement of organisms/species and determines if organisms/species remain settled. In intertidal areas (inapplicable here), the waves can prevent dehydration of organisms/species (Bolier, 2006). In literature there is not a quantitative defined relation found between cod - waves and lobsters – waves, such as Habitat suitability indices. However, after a severe storm in OWEZ the presence of cod was reduced (Winter, Aarts, & van Keeken, 2010).

- Currents
  Currents determine the settlement of organisms/species and determine if organisms/species remain settled (Bolier, 2006). Currents also determine the food supply for example for bivalves. In literature there is not a quantitative defined relation found between cod - currents and lobsters – currents. However, cod prefers shelter habitats so probably there is a relationship, but just not yet defined.

- Kinetic energy (turbulence)
  Highly turbulence flow reduces the probability of settlement of species and make it hard to remain settled for species. In literature there is not a quantitative defined relation found between cod – turbulence and lobsters – turbulence.

- Depth
  Species have depth limited zones where they thrive. This can be related to the amount of light penetration, predators, temperature etc. The cod prefers a depth between 10-200 meters and the lobsters prefers a depth between 0-150 meters.

Bed protection
There are ten ecological parameters distinguished and categorized in the theme 'bed protection':

- Type of bed protection
  Hard substrate might have the function as refuges and stepping-stones for non-native species. Species could find a new suitable habitat on the bed protection (Andersson, 2011). It is noticed that cod and lobsters are attracted to hard substrate (Winter, Aarts, & van Keeken, 2010) (Krone & Schmalenbach, 2011).

- Stone size of the armour layer and its grading
  The applied stone size and the associated grading of bed protections is related to (the amount of) rocking, cavities sizes, cracks and crevices. This parameter is therefore indirect related to favorable ecological conditions for the cod/lobster, see cavity size.

- Filter layer and its grading
  In literature no influencing information about cod and lobsters is found related to the filter layer. The filter layer is 'unreachable' for cod and lobsters. These species find only shelter in the armour layer.

- Cavity size
  Cavity size of importance for cod, lobsters, and for the biodiversity (Baptist, van der Meer, & de Vries, 2007). A variety of cavity sizes stimulate the biodiversity. A wide spectrum of cavity sizes will result in a more complete habitat by telescoping of habitats which are now separated by the use of fixed grading of stones. This attracts in its turn new species because of the availability of food. In principal more small cavities are needed, because there are more small organism (Kamerik, 2014). Experiments with manufactured holes in artificial reefs show higher abundance of fish and crabs compared with the surroundings (Langhamer & Wilhelmsson, 2009).
  Cod find shelter in cavities and food around hard substrate bottoms. For lobsters the cavities function as their 'house'. The right dimensions of cavities (depends on the age of the lobsters) can stimulate the lobster stock. In a pilot it can be tested if more 'houses' lead to more lobsters.

- Horizontal dimension of the bed protection (surface of the bed protection)
  Species such as cod and lobsters could find a new suitable habitat on the bed protection. More surface of the bed protection provides more favorable ecological conditions.

- Vertical dimension of the bed protection (height, or in ecological terms, ecological landscaping)
  An in height varying landscape creates gradients and diversity of conditions which can stimulate the enhancement of the biodiversity. It can provide more favorable ecological conditions for hard substrate species and shelter places for fishes such as cod.

- Orientation
  The orientation of the bed protection can create more lee sides or more areas which are (not) sheltered where species can settle.

- Water retention capacity
  This parameter determines the hydration of the substrate and organisms during ebb tide; substrate that stays submerged is more attractive for certain species. Because of the offshore location the bed protection is always in the water column. This parameters is inapplicable here.

- Porosity / Packing
  The packing/porosity of the bed protection layer is probably correlated with the installation method (fallpipe vessel/side stone dumper). However,
  in literature no relation is found between the porosity and favorable ecological conditions. In literature is also not found if the smaller stones are on top of the bed protection layer because of the fall velocity.

- Inclination of the surface
  In literature is not found if the slope of the have effect on favorable ecological conditions for species. In general gradients are preferable for the ecosystems and species.

- Edge scour
  The scour holes just after the bed protection stops creates extra gradients. So maybe if the scour hole is fully developed it can enhance the biodiversity, but in literature no proof is found.

Material properties of rock
There are seven ecological parameters distinguished and categorized in the theme 'material properties of rock':

- Color
  Temperature changes occur more at dark stones, which is not preferable for organisms (Baptist, van der Meer, & de Vries, 2007). However, this is assumed non significant because of the depth of offshore wind turbines.

- Roughness/texture/rugosity
  The roughness of the material determines the (extra) possibility of settlement, especially at places with high (orbital) currents. The type of stone has influence on the roughness and thus on the biodiversity (Baptist, van der Meer, & de Vries, 2007).

- Shape of the rock
  The shape of the rock determines the complexity and the cavity sizes which is of importance for favorable ecological conditiosn of the species. Cracks in rock increase the complexity and can result in the enhancement of biodiversity.

- Density
  The density is of influence for the technical requirements (see later on), but not for favorable ecological conditions. However, density is related to hardness which is of influence for the ecology, see below.

- Hardness
  Some species drive into the stone which is easier in limestone than hard basalt or granite. So the use of soft stones have potential to enhance the biodiversity (Baptist, van der Meer, & de Vries, 2007).

- Chemical composition
  Due to leaching toxic substances can be released in the water column. Due to erosion the material (rock) can wear and become more smooth (Baptist, van der Meer, & de Vries, 2007).

- pH Value
  The settlement of new organisms depends on the PH value of the material. For artificial reefs a PH value of 8.3 is recommended (Kamerik, 2014).

Water quality
There are six ecological parameters distinguished and categorized in the theme 'water quality':

- PH value
  The PH value in front of the Dutch Coast (12kilometer offshore) is assumed constant and not controllable.

- Turbidity
  Turbidity determines the amount of light penetration. This determines the limit of the zone were seaweed and algae can thrive (Baptist, van der Meer, & de Vries, 2007). Recruit abundances in OWEZ were correlated with mud content, but most likely to be attributed to the absence of fisheries and not to the presence of the OWF (Lindeboom, Kouwenhoven, Bergman, & Bouma, 2011).

- Light penetration
  Quantity and quality of light penetration is decisive for the growth of micro- and macro algae and aquatic plants on the construction.

- Oxygen &Nutrients
  Water circulation patterns are associated with nutrients and prevent stagnant water and anoxic areas (Kamerik, 2014). Profiting from upwelling, and thus increasing nutrients, is preferable for ecosystems and species.

- Salinity
  The range of the salinity is decisive for the presence of species, not only the mean but also the extremes. The salinity in front of the Dutch coast is determined by the Atlantic Sea and the discharge of rivers. Further offshore the salinity is higher than close to the coast. Salinity is assumed context-defined and not controllable.

- Temperature
  The temperature is of importance for species and especially for cod. During summer the North Sea temperature is around 20 ° and during wintertime the temperature drops to 5°. The temperature in front of the Dutch Coast (12kilometer offshore) is assumed context-defined and not controllable.

External effects
There are five ecological parameters distinguished and categorized in the theme 'external effects':

- Sound / vibrations
Marine species rely on hearing for feeding, mating and defense. Swim bladders amply a great range of sounds and therefore cod is particularly sensitive for sounds. Shipping, commercial fishing, ferries and other vessels expose marine species to a noisy environment. This make it difficult to estimate the influence by offshore wind turbines. It is anticipated that human influences have the potential to (Island-Institute, 2012):
    - mask species' communication and navigation vocalizations;
    - damage hearing of animals that venture too close; and
    - cause stress-related responses.

It is not proven that sounds and vibrations have effects on species during operational phase of the wind turbine (Zucco, Wende, Merck, Kochling, & Koppel, 2006).

- Electromagnetic fields (EMF)
The lobster use the earth's magnetic field to aid in orientation and direction. EMF emissions have the potential to disorientate marine species (Island-Institute, 2012).
Non of the performed studies have found substantial behavioral or biological impact of the undersea cables on migratory fish (Zucco, Wende, Merck, Kochling, & Koppel, 2006).

- Available food
Without food availability the species will mitigate. The right habitat is not only the abiotic components, but also the biotic components. The area must contain a rich biodiversity, so enough food is available for cod and lobsters. These species are at the top of the food chain, so they are the predators and they need smaller species to forage.

- Catchment/Nursery
Fishing is prohibited in the offshore wind farm and safety zone of OWEZ. Therefore offshore wind farms can function as nursery areas for fish communities and benthos (Lindeboom, Kouwenhoven, Bergman, & Bouma, 2011). The increase of the fish assemblages and benthos are attributed to new habitat in offshore wind farms and the impact of not trawling (EWEA, Positive environmental impacts of offshore wind farms, 2013).

- Collision
The increased vessel traffic in and around offshore wind farms during construction and maintenance activities may increase the probability of collisions with marine species (Island-Institute, 2012).

Note: All the parameters are abiotic components and there are no biotic components discussed. The biological regenerative cycle is not included in the parameters. The component that partly represents the biotic components is the parameter 'food'.

2.4   TECHNICAL ANALYSIS

In this section the technical analysis of offshore wind turbines is elaborated and only treated from technical point of view. Currents and waves cause a(n) (orbital) flow (load) just above the bed and therefore first of all the hydraulic loads are discussed. In the followed subsection the extra induced load by the monopile will be elaborated (wave/currents-structure interaction). In subsection 482.4.3 the hydraulic strength of the bed around an offshore wind turbine at the North sea is discussed. The geotechnical conditions of the North Sea bed and the force on a single grains is presented. In the last subsection 2.4.4 the hydraulic load and strength come together in the scour process around monopiles. In section 2.5 prevention methods of scour(holes), in the form of bed protections, are treated including the design requirements.

2.4.1   Hydraulic conditions

The hydraulic loads on the bed are caused by currents and waves. The extra induced hydraulic load due to the created vortices by the monopile are discussed in the next subsection.

<u>Currents</u>

Currents are generated by tide. The tidal flow is semi-diurnal along the North Sea coast, see Figure 2-16 (Louwersheimer, 2007). During flood the tidal flow is in northern directions and during ebb the flow is in southern direction. The average tidal flow reach a maximum of 0.7 m/s during spring tide.
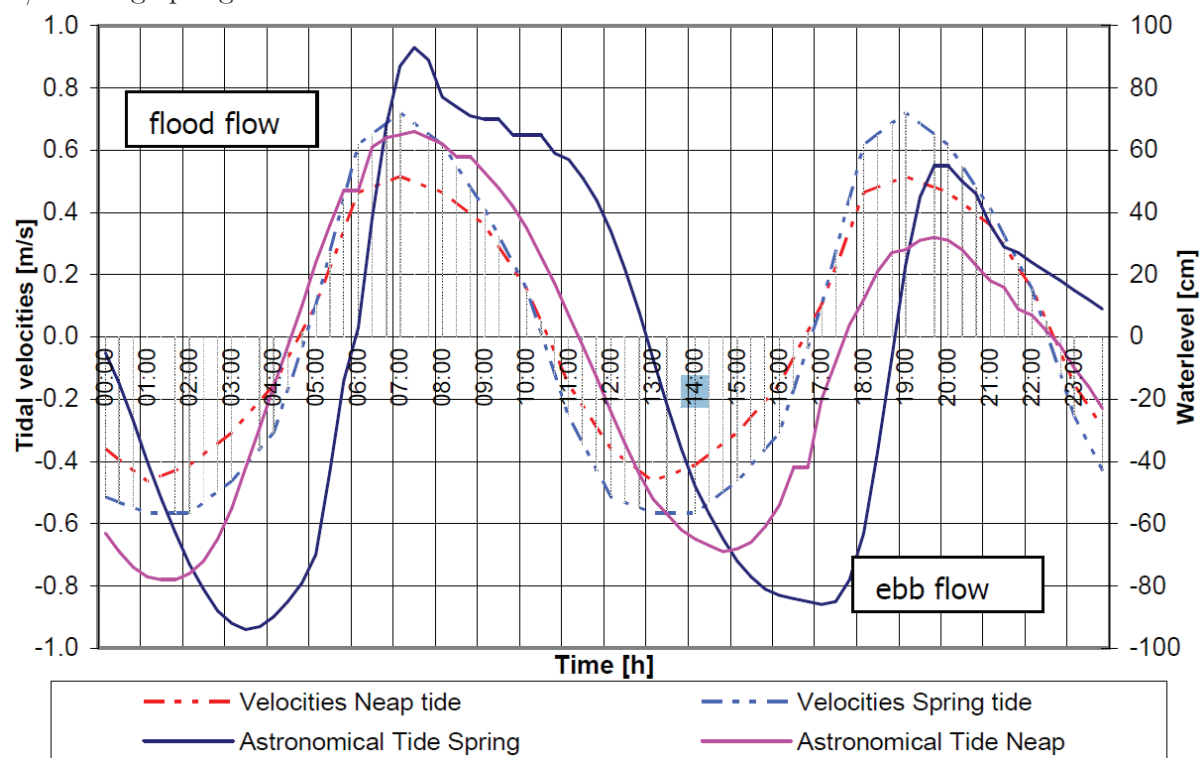
Figure 2-16: Indication of water levels and flow in front of the Dutch coast due to tide.

Waves

In deep water waves can propagate undisturbed, but this change if waves start noticing the bottom, see Figure 2-17 (Holthuijsen, 2007). Undisturbed wave propagation depends on the relative water depth, which is determined by the wave length (wave period) an the water depth. There are three relative water depths classified in the linear wave theory:

- Deep water
- Intermediate depth
- Shallow water
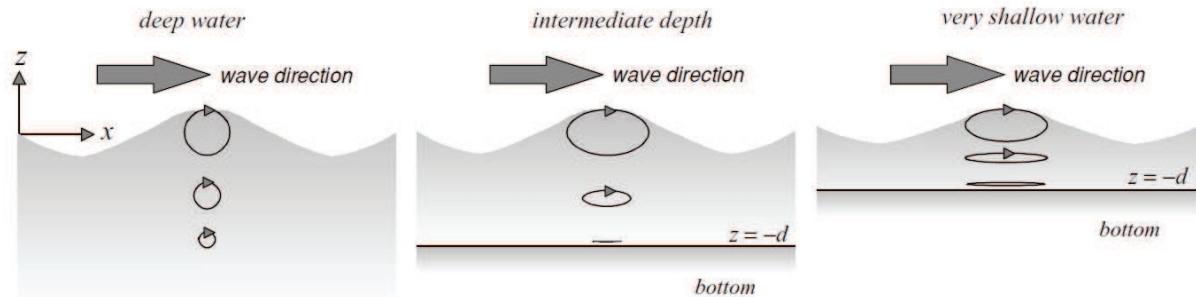
Figure 2-17: The orbital motion depends on the relative water depth.

The relative water depth criteria are defined in Table 2-2 (Schiereck, 2001).

Table 2-2: Relative depth criteria.

	Shallow water	Intermediate water depth	Deep water
Relative depth criteria	0.05 < h/L	0.05 < h/L < 0.5	h/L > 0.5

In which:

h   water depth   [m]
L   wave length   [m]

The wave length is formulated in equation (2.1).

$$L = \frac{gT^2}{2\pi} tanh(kh)$$ (2.1)

In which:

L   wave length   [m]
g   acceleration of gravity   [m/s^2]
T   wave period   [s]
k   wave number (=2 π/L)   [m^{-1}]
h   water depth   [m]

Example 1 (first part):
The significant wave height is 0.5 meters with a period of 7 seconds. The offshore wind turbine will be installed at a depth of 25 meters.

In this case the wave length (L) will be 74.3 meters.
The relative depth criteria (h/L) will be 0.34, so in this case the water depth is intermediate.

The wave shape is related to the water motion in the wave. The validity of various wave theories are presented in Figure 2-18 (Schiereck, 2001). In case of the example above the linear wave theory is valid.
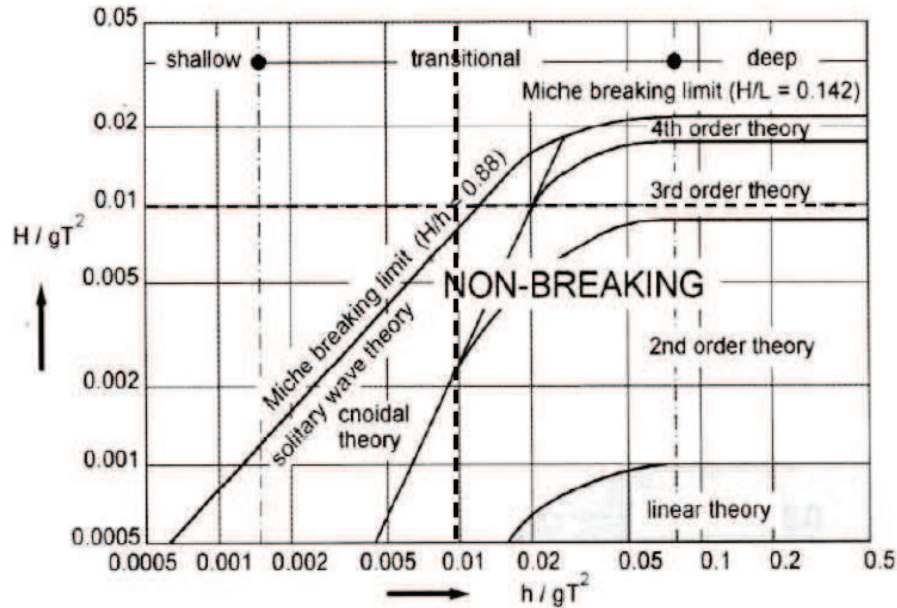
Figure 2-18: Validity of wave theories (Le Méhauté, 1976)

The orbital motion is circular in deep water and elliptical in shallow and intermediate waters, see Figure 2-17. To determine the flow velocities at the bed, the particle velocities are calculated at the bottom. The particle velocities are formulated in equation (2.2) and (2.3) .

$$u = \omega a \, \frac{\cosh k(h+z)}{\sinh kh} \sin(\omega t - kx) \tag{2.2}$$

$$w = \omega a \, \frac{\sinh k(h+z)}{\sinh kh} \cos(\omega t - kx) \tag{2.3}$$

In which:

ω	wave frequency (=2 π/T)	[s^{-1}]
k	wave number (=2 π/L)	[m^{-1}]
a	wave amplitude (=H/2)	[m]
z	interesting depth	[m] , see Figure 2-17

The near bed velocity is only horizontal, so it can be calculated with equation (2.2) by filling in z=-d. The maximum near bed velocity for the linear wave theory (1st order) can also be calculated with equation (2.4).

$$u_{w,max} = \frac{\pi H}{T \sinh kh} \tag{2.4}$$

Example 1 (second part):
The example will be continued. The linear wave theory is valid for this example. Therefore maximum near bed velocity can be calculated with equation (2.2) or (2.4). The maximum near bed velocity is 0.05 m/s.

Breaking waves can increase the scour potential. Waves break when the steepness is exceeded. Miche stated equation (2.5) in 1944.

$$\left[\frac{H}{L}\right]_{max} = \frac{1}{7} \tanh(kh) \tag{2.5}$$

2.4.2   Wave/currents - monopile interaction

Current – monopile interaction

The monopile is an obstruction for the 'free propagating' flow generated by the tide. The shape, surface roughness, and diameter of the monopile determine the magnitude of obstruction. The flow will accelerate and decelerate along the monopile. Separation of the flow occur when the flow cannot follow the monopile surface, see Figure 2-19.
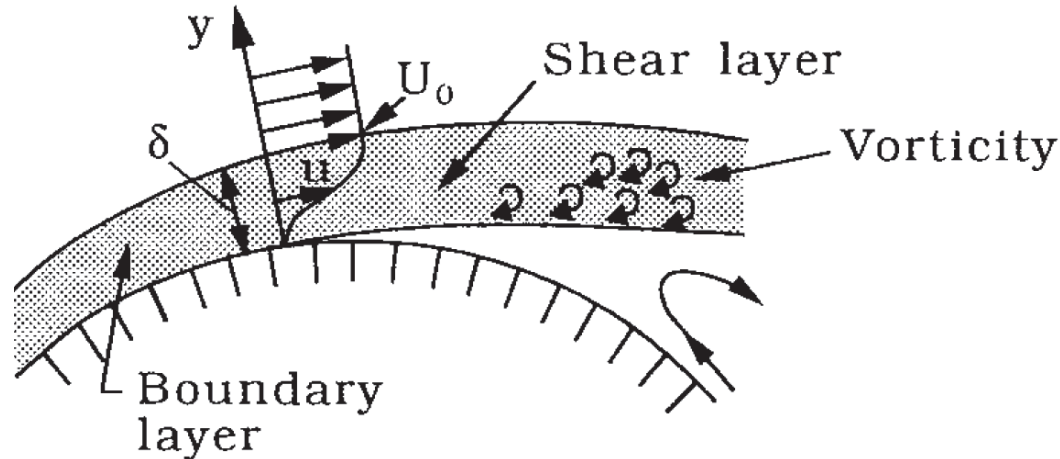
Figure 2-19: Flow separation and the formation of lee-wake vortices.

The flow separation depends on the Reynolds number.

$$Re = \frac{uD}{v} \qquad (2.6)$$
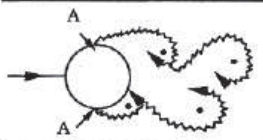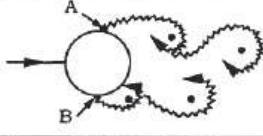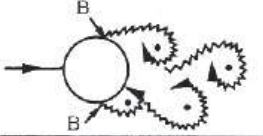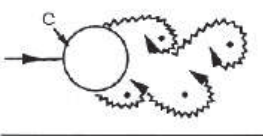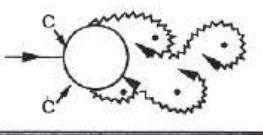
In which:

Re   Reynolds number   [-]
D   Monopile diameter   [m]
v   kinematic viscosity $(=10^{-6})$ [m^2/s]

There are nine different flow regimes classified, see Table 2-3 (Sumer & Fredsøe, 2002). So, for a pile diameter of 5 meters and a flow of 0.7 m/s the Reynolds number will be
Re = 3.5 * 10^6. This is class h) in Table 2-3. The boundary layer is completely turbulent on one side of the cylinder. The other side is partly laminar and party turbulent. If the Reynolds number will be larger than 4*10^6 both sides are completely turbulent.

Table 2-3: Flow regimes around a smooth, circular cylinder in a steady current.

a)	No separation. Creeping flow	Re < 5
b)	A fixed pair of symmetric vortices	5 < Re < 40
c)	Laminar vortex street	40 < Re < 200
d)	Transition to turbulence in the wake	200 < Re < 300

		Description	Reynolds range
e)		Wake completely turbulent. A:Laminar boundary layer separation	$300 < Re < 3 \times 10^5$ Subcritical
f)		A:Laminar boundary layer separation B:Turbulent boundary layer separation;but boundary layer laminar	$3 \times 10^5 < Re < 3.5 \times 10^5$ Critical (Lower transition)
g)		B: Turbulent boundary layer separation;the boundary layer partly laminar partly turbulent	$3.5 \times 10^5 < Re < 1.5 \times 10^6$ Supercritical
h)		C: Boundary layer completely turbulent at one side	$1.5 \times 10^6 < Re < 4 \times 10^6$ Upper transition
i)		C: Boundary layer completely turbulent at two sides	$4 \times 10^6 < Re$ Transcritical

Wave –monopile interaction

The monopile is also an obstacle for the 'free developing' orbital movement generated by waves. The influence of the pile is expressed in the Keulegan-Carpenter number (KC-number) and the diffraction parameter (D/L).

The pile can be seen as 'vertical wall' if the wave length is much smaller than the pile diameter. In this case the pile is classified as a large pile. If the wave length is much larger than the pile diameter, the wave 'hardly notice' the presence of the pile. In this case the pile is classified as a slender pile. The classification of the pile is based on the KC numbers, see Table 2-4.

In equation (2.7) the KC number is expressed (valid for linear wave theory):

$$KC = \frac{u_{max}T}{D} = \frac{\pi H}{D \sinh kh} \qquad (2.7)$$

In which:

KC	Keulegan-Carpenter	[-]
u_{max}	maximum orbital velocity near the bottom	[m/s], see equation (2.4)
T	wave period	[s]
D	monopile diameter	[m]

The pile classification related to the KC number is given in Table 2-4.

Table 2-4: Pile classification.

KC range	pile definition
KC < O(1)	large
O(1)< KC < 6	intermediate
KC >O(6)	slender

Flow changes due to the increase of the KC number is classified Table 2-5. The classification is made for $Re = 10^3$ in which Re is defined as (Sumer & Fredsøe, 2002):

$$Re = \frac{DU_{max}}{v}$$
(2.8)

Table 2-5: Flow regimes around a smooth, circular cylinder in oscillatory flow.

a)	No separation. Creeping (laminar) flow.	KC < 1.1
b)	Separation with Honji vortices. See Figs. 3.3 and 3.4	1.1 < KC < 1.6
c)	A pair of symmetric vortices	1.6 < KC < 2.1
d)	A pair of symmetric vortices. Turbulence over the cylinder surface (A).	2.1 < KC < 4
e)	A pair of asymmetric vortices	4 < KC < 7
f)	Vortex shedding	7 < KC Shedding regimes

Sumer and Fredsøe (2002) showed that the threshold of reflection of waves lies at D/L=0.2. However, Hoffmans and Verheij believed that diffraction is significant for D/L>0.1. A overview of pile classification can found in Figure 2-20.
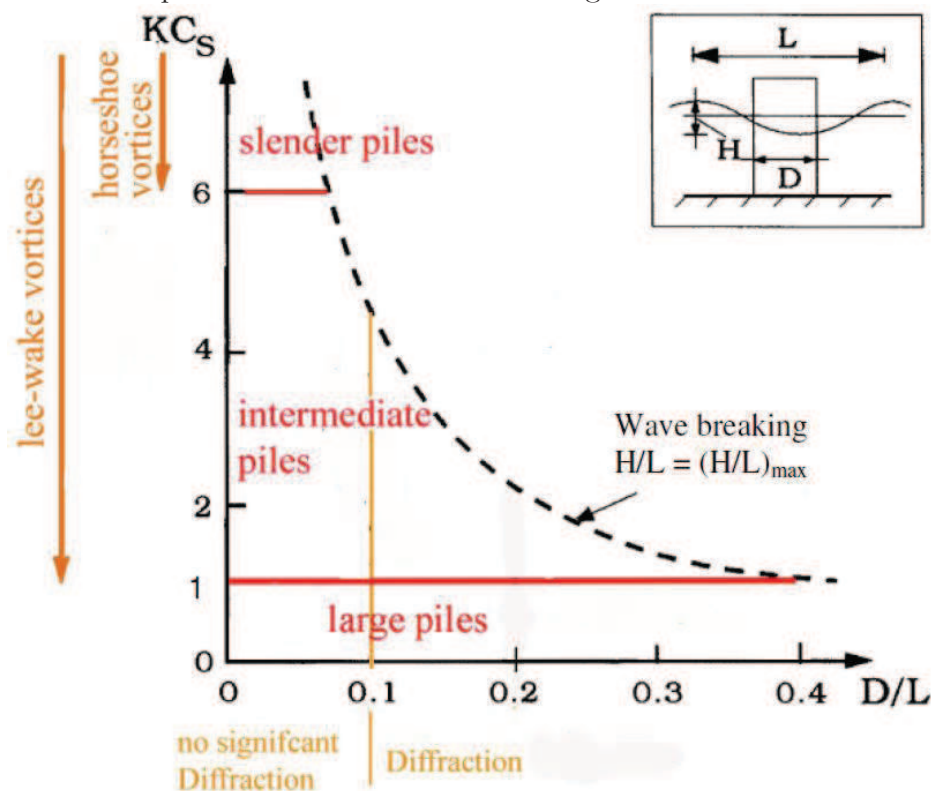
Figure 2-20: Overview of the pile classifications and the associated requirements of KC and D/L.

Current and waves – monopile interaction (vortices)

- Lee-side vortices
  After flow separation from the pile, lee-side vortices are formed. The lee-side vortices are generated by flow and the wake is present over the whole depth. Due to turbulence higher local velocities and disturbances may occur. The boundaries are set to KC>O(1) or Re>5. Vortex shedding occurs when Re>40, see Figure 2-21.
  Vortex A will grow in size and strength so that it will draw vortex B across the wake (left sketch of Figure 2-21). This will lead to the shedding of vortex A, see right sketch of Figure 2-21.
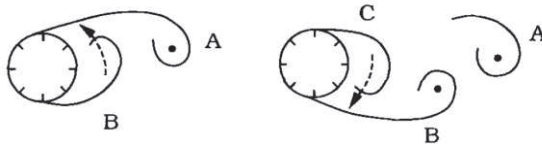
Figure 2-21: Vortex shedding.

- Horseshoe vortices
  Due to the deceleration of the flow pressure differences occur which result in down flow. Due to an unequal velocity distribution in the bed layer rotations can occur in the incoming boundary layer. These vortices are called horseshoe vortices because the vortices roll up in front and along the pile in an area shaped like a horseshoe. Under waves horseshoe vortices occur when KC> O(6).
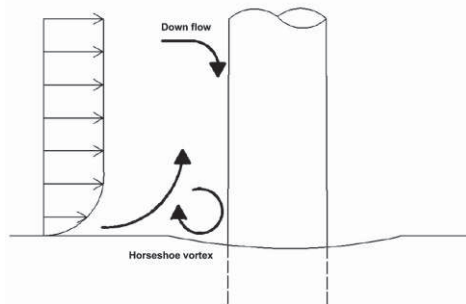
Figure 2-22: Formation of horseshoe vortices.

- Wave induced flow
  The lee side vortices and the horseshoe vortices are only generated by waves for large piles. By the disturbance of the monopile the waves are reflected and diffracted around the pile. In the disturbed situation near the monopile the oscillatory motion has a cycle-to-cycle variation. This cycle-to-cycle variation results in a phase shift every next wave. This results in a wave induced flow called steady streaming.

A overview of vortices related to the pile classification is sketched in Figure 2-23.
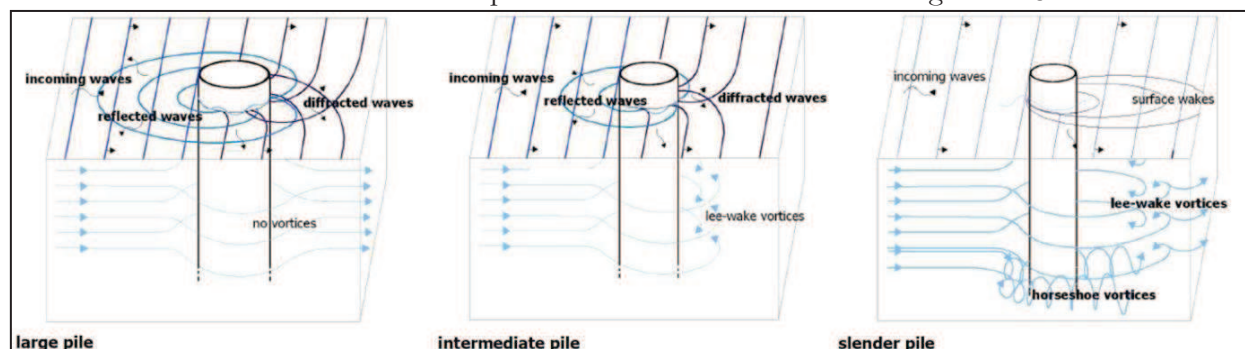
Figure 2-23: Sketch of flow regimes and vortices.

2.4.3   Force on the grain

Before diving into the scour development due to hydraulic loads, the initiation of movement will be described first. The forces on a grain particle (or stone) are sketched in Figure 2-24 (Schiereck, 2001).
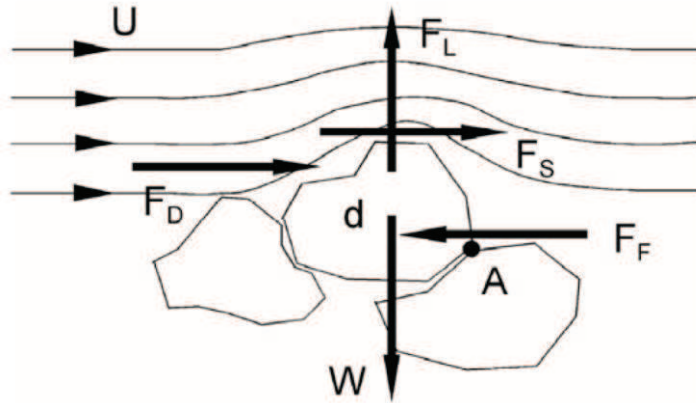
Figure 2-24: Forces on a grain in flow.

The forces that hold the grain in place are the resistance forces. The resistance forces are the friction force (F_F) and the weight of the stone (W). The forces that lead to movement of the grain are called load forces. The load forces are:

$$\left. \begin{aligned} Drag\ force\ F_D &= \frac{1}{2} C_D\,\rho_w\,u^2\,A_D \\ Shear\ force\ F_S &= \frac{1}{2} C_F\,\rho_w\,u^2\,A_S \\ Lift\ force\ F_L &= \frac{1}{2} C_L\,\rho_w\,u^2\,A_L \end{aligned} \right\} F \sim \rho_w\,u^2\,d^2 \tag{2.9}$$

In which:

F	Force	[N]
C_i	coefficients	[-]
ρ_w	density of water	[kg/m³]
u	velocity	[m/s]
A_i	exposed surface	[m²]
d	representative size	[m]

Balance of forces leads to equation (2.10):

$$\left. \begin{aligned} \sum H &= 0 \quad F_D + F_S = F_F \\ \sum V &= 0 \quad F_L = W \\ \sum M &= 0 \quad F_D O(d) + F_S O(d) = WO(d) \end{aligned} \right\} \quad \rho_w\,u^2\,d^2 \sim (\rho_s - \rho_w)gd^3 \tag{2.10}$$

This lead to the following relation between load and strength:

$$u_c^2 \sim \left(\frac{\rho_s - \rho_w}{\rho_w}\right) gd = \Delta gd \;\rightarrow\; u_c^2 = K\Delta gd \tag{2.11}$$

In which:

u_c	critical velocity	[m/s]
ρ_s	density of stones	[kg/m³]
g	acceleration of gravity	[m/s²]
K	constant	[-]

All formulas on grain/rock stability come down to this proportionality. Izbash did experiments to dam a river and he found the K factor of about 2.9 for the equation (2.11). This formula works quite well for big stones in not too deep water. Probably he used the velocity near the bed. The disadvantage of this formula is that the velocity near the stone is not good measurable for small grains.

Shields applied another method for the stability relation. He used the momentum balance to measure the shear stress over the bottom. This formula is not based on the flow velocity which is good because the flow velocity near the bed is hard to measure. The formula of shields is stated in equation (2.12).

$$\Psi_c = \frac{\tau_c}{(\rho_s - \rho_w)gd} = \frac{u_*^2}{\Delta gd} = f(Re_*) = f\left(\frac{u_* d}{v}\right) \qquad (2.12)$$

This shields relation is presented in two curves in Figure 2-25 (Schiereck, 2001). The left figure (a) is the classical Shields form. The critical Shields values (Ψ_c) are plotted against the Reynolds numbers (Re$_*$). For high Reynolds numbers the critical Shields value becomes constant at 0.055. The right figure (b) of Figure 2-25 describes the same stability relation, but the Reynolds number is replaced for the dimensionless particle parameter (d$_*$) by Van Rijn (1984).
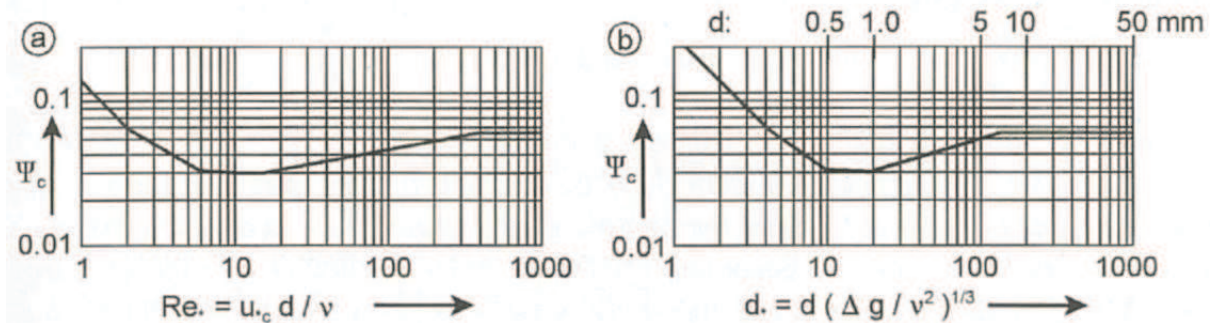
Figure 2-25: Critical shear stress according to Shields - van Rijn.

In fact, no such thing as critical velocity exists (Schiereck, 2001). The stability of every individual grain is different due to irregularities of natural stones, the position, the protrusion and thus the exposure of stones. Therefore Figure 2-25a can be better interpreted as Figure 2-26.

1) no movement at all
2) occasional movement at some locations
3) frequent movement at some locations
4) frequent movement at several locations
5) frequent movement at many locations
6) frequent movement at all locations
7) continuous movement at all locations
8) general transport of grains
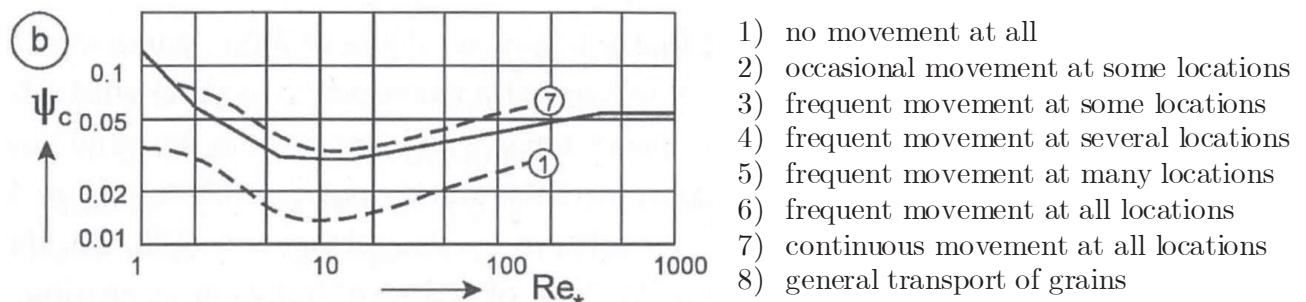
Figure 2-26: Incipient motion of stones.

The movement of the stones in the bed are classified in different curves. The shields criterion fits stage 6 rather well.

The North Sea bottom is consists mainly of sand (63 – 2000 µm). At some places gravel, silt or clay can be present. In general the grain size decreases at the surface from south to north (Noordzeeloket, 2015).

2.4.4   Scour (holes)

Scour principle
In the last subsection the incipient motion is treated, but scour is caused by the imbalance of sediment transport. The general expression for the conservation of mass for sediments reads (Schiereck, 2001):

$$\frac{\partial z_b}{\partial t} + \frac{\partial S}{\partial x} = 0 \qquad (2.13)$$

In which:
z_b: position of the bed level   [m]
S: Sediment transport per unit width   [m^2/s]

There are three possibilities for local scour which will be explained according to the sketch of Figure 2-27:
  (a) Dynamic equilibrium $S_2 = S_1 > 0$;
  (b) Clear-water scour $S_2 > S_1 = 0$;
  (c) Live-bed scour $S_2 > S_1 > 0$.
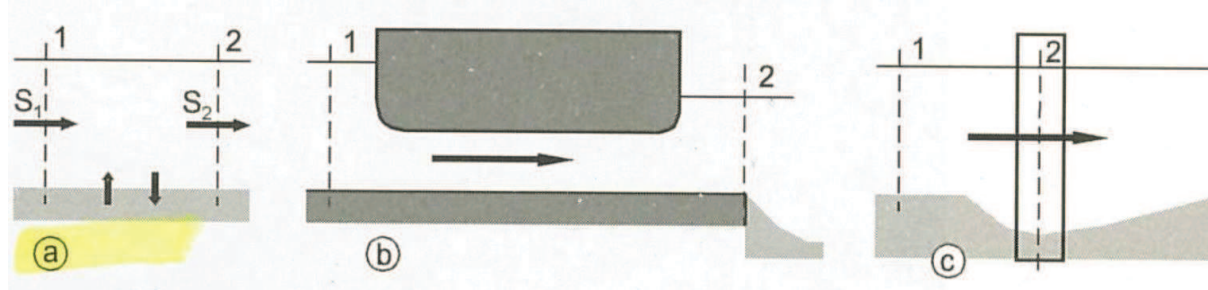
Figure 2-27: Local scour.

Scour hole at slender piles
Due to the complexity of the 3D situation of flow around objects a first design formula is proposed by Breusers et al. (1977) for slender piers (Schiereck, 2001):

$$\frac{h_s}{D} = 2\,K\,tanh(\frac{h_0}{D}) \qquad (2.14)$$

In which:
h_s scour depth   [m]
h_0 depth   [m]
D   pile diameter   [m]
K   factor for shape, angle of attack, and velocity   [-]

Slender piers are classified by Breusers et al (1997) if the water depth/diameter ratio is 2-3. Sumer and Fredsøe call piles slender if KC > O(6) and D/L <0.1 (Sumer & Fredsøe, 2002).

$$\frac{S}{D} = 1.3\left[1 - exp\left(-m(KC - 6)\right)\right] \qquad (2.15)$$

In which:
m   =0.03 for regular waves
m   =0.06 for nonlinear waves
S   = equilibrium scour depth   [m]
D   = pile diameter   [m]
KC   = Keulegan-Carpenter numebr   [-]

Due to breaking waves the scour can be considerable higher, up to three times the pile diameter (Bijker & de Bruyn, 1988). The scour extent for slender piles are cylindrical and for a steady flow it can lead to a scour area of 5 times the pile diameter behind the monopile (Whitehouse 1998).

<u>Scour holes at Intermediate piles</u>
No predictions directed to scour at intermediate piles are found in literature.

<u>Scour hole at large piles</u>
In Table 2-6 a summary is given for the maximum scour depth for large piles. No general accepted prediction exists (Haddorp, 2005). For each method also the associated definitions are given for large piles.

Table 2-6: Summary of scour predictions of the diffraction regime.

	Maximal scour depth	Definition of large piles
May and Wiloughby (1980)	$3\,^{h}/_{d}$	D/L > 0.2, h/D < 2
Rance (1980)	$0.06 \cdot D$	D/L > 0.1
Katsui and Toue (1993)	$0.04 \cdot D$	KC < 0.5
Verheij and Hoffmans (1997)	"nil"	KC < 6, D/L < 0.1
Sumer and Fredsoe (2002)	$0.03 \cdot D$	KC < 1.2, D/L < 0.27

Sumer and Fredsøe measured the bed topography during experiments. For D=100 cm, T=3.5 s, L=6.8 m, D/L=0.15, and KC=0.61 the bed topography is present in Figure 2-28.
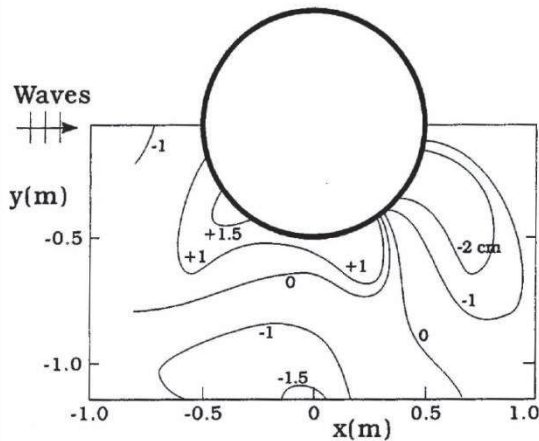
Figure 2-28: Contour plot of bed topography of equilibrium state.

The extension of the scour hole is likely to depend on the wave length. Range (1980) stated that the extension of the scour hole is up to 0.75 meters of the pile diameter (Haddorp, 2005).

2.5 TECHNICAL REQUIREMENTS OF BED PROTECTION

In this section the motivation to apply bed protection will be given. The different types of bed protections will be elaborated including the failure mechanisms. For the rock bed protection the design requirements (the stone size, the filter properties, and dimensions) will be discussed.

2.5.1 Scour related to monopile failure

Figure 2-29 gives an overview of the dimensions and the active forces on a wind turbine. Three basic requirements needs to be verified to prevent failure of the monopole (DNV, 2014) (Haddorp, 2005):

- Static analysis
  The maximal moment of the monopile needs to be transferred into the ground over the foundation length

- Dynamic analysis
  Resonance must be avoided, so the natural frequency of the structure must not correspond with the natural frequency of the loading waves

- Fatigue analysis
  The monopile needs to resist all the loads during life time.

All the three analysis are related to the scour depth. The first two analysis are straightforward and also the scour – fatigue relation is established (van der Tempel, Zaaijer, & Subroto, 2004).
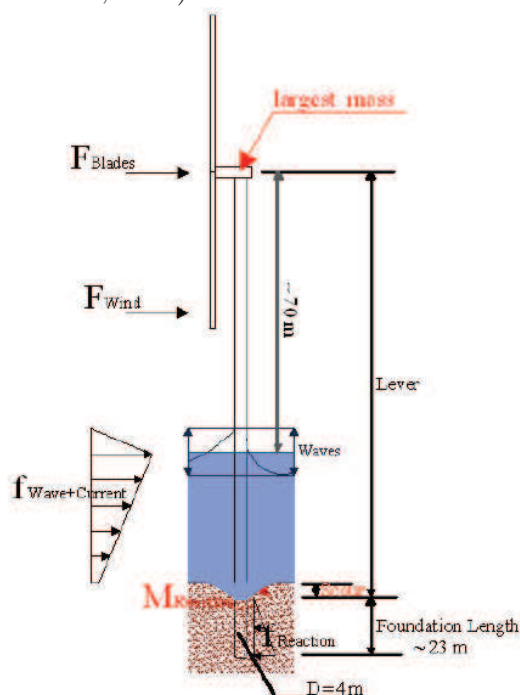
Figure 2-29: Sketch of a monopile founded wind turbine including the forces.

Bed protection to prevent scour can be omit by driving the pile deeper into the ground, but mostly bed protection is applied (Raaijmakers, Joon, Segeren, & Meijers, 2014). This is mainly based on economic feasibility. By omitting of scour protection the piles must be extended and extra steel must be applied. Otherwise scour protection has to be applied to guarantee a constant pile fixation level.

2.5.2 Bed protections

Several types of bed protections around offshore wind turbines are possible to prevent scour, see Figure 2-30:
- Concrete or asphalt mattresses
- Vegetation like sea grass
- Geohooks
- Mats, for example of old car tyres to entrap sediment (Maritime Journal, 2014)
- Rock
    - Loose rock: static protection
    - Loose rock: dynamic protection
    - Single layer Rock (Raaijmakers T. , Handbook offshore scour protection methods, 2015)
    - High density rock
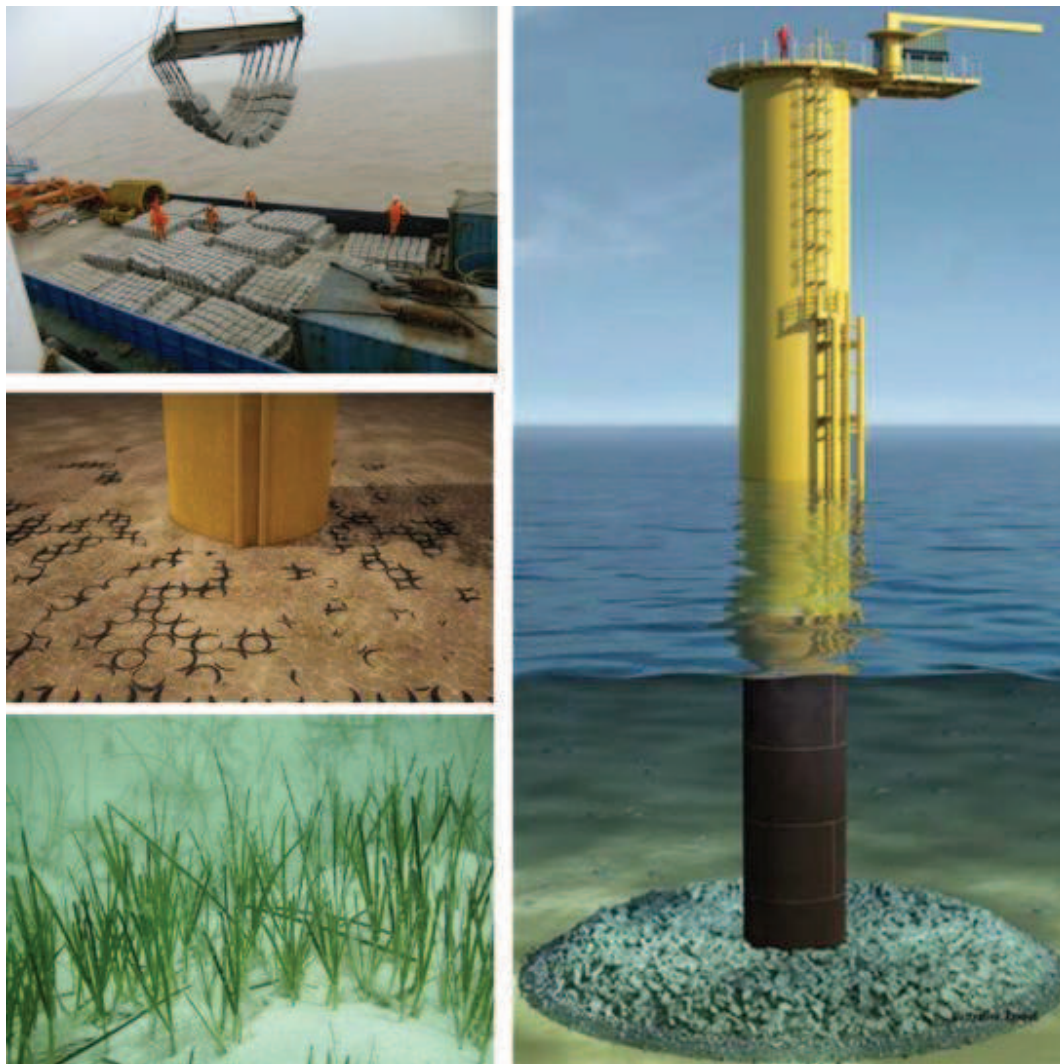
Figure 2-30: Different types of bed protection.

The dimensions and roughness of the bed protection are of influence of the stability. Very rough protections will introduce more turbulence, but lower bottom velocity. Smooth bed protections however are associated with higher bottom velocities. It turns out that in general the smooth bed protection lead to higher alpha values (the amplification factor for the velocity which indicates the amount of turbulent fluctuations and disturbances in flow).

Concrete mattresses require costly offshore installation (van der Tempel, Zaaijer, & Subroto, 2004). Probably vegetation will die around offshore wind farms because of the depth and the strong (orbital) velocity says Tim Raaijmaker (Raaijmakers T. , Ecology-based bed protection of offshore wind turbines interview, 2014). The mats of old tyres is still in the pilot phase. Therefore most of the time crushed rock is dumped around the piles.

The idea behind the placement of rock is to reduce the hydrodynamic loads (waves & currents) on the soil particles. The bed protection consists of at least two layers, see Figure 2-31 (KED-Ingenieure-GmbH, 2011):
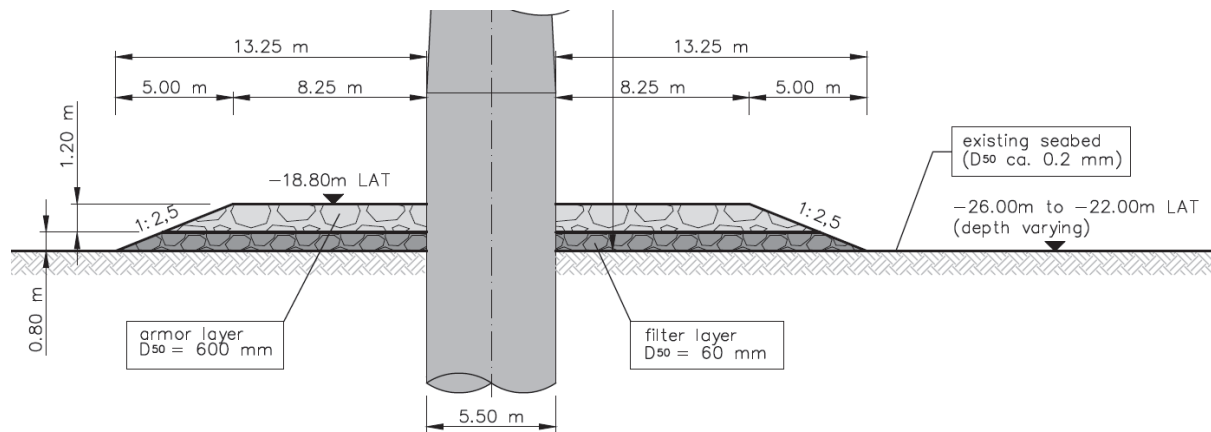
Figure 2-31: Filter and Armour layer of bed protection.

- Filter layer
  The main function of the filter layer is to prevent of the covered subsoil (seabed).

- Armour layer
  The top layer (armour layer) has to resist the hydrodynamic forces and to protect the removal of the filter layer.

First of all the needed stone size (D_{50}) will be calculated for the armour layer. The needed D_{50} depends on the acceptable probability of failure for the bed protection. The probability of failure can be calculated with equation (2.16).

$$P = 1 - e^{-f*T} \tag{2.16}$$

In which:
P   Probability of failure   [-]
f   Frequency   [1/year]
T   Lifetime   [year]

An offshore wind farm is typically planned for a 20-year design lifetime (DNV, 2014) and is designed based on a 1/100 years storm conditions. This means that clients accept a probability of failure of 18% for the armour layer.

If the stone size for the armour layer is determined and the grain size of the sand particles of the sea bed is known, the filter layer (the layer in between) can be determined.

At the end the bed protection will be tested with a physical model study to optimize the design. The design calculations of these layers is present in the following subsections.

2.5.3   Failure modes of bed protection

The main function of a bottom protection is not to minimize scour, but to keep the scour hole far away from the structure that needs protection, see Figure 2-32. So from technical point of view a scour hole does not directly lead to failure of the structure.
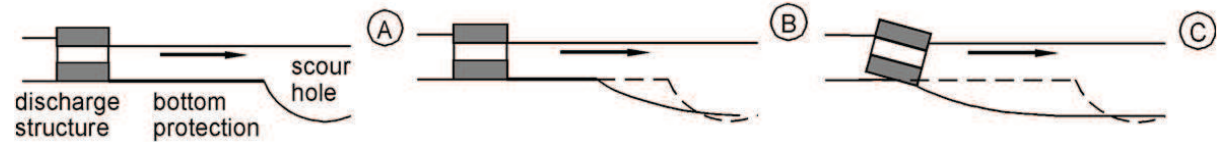
Figure 2-32: Only scour close to the structure leads to failure.

There are four relevant failure mechanisms for the bed protection around a monopile foundation (de Vos, 2011):

a) Erosion of the top layer caused by the flow, possibly leading to scour near the structure;

b) Loss of subsoil through the scour protection, which may lead to sinking of the top layer in the bed. This can be an iterative process, eventually leading to scour holes near the construction;

c) Due to the edge scour, which originates from the abrupt change in roughness between the riprap and the bed, stones may disappear at the edge of the scour protection, leading to an undersized scour protection (horizontal dimensions);

d) When the scour hole is to steep, flow slide may damage the scour protection from the edge.

The four failure mechanisms can be seen in Figure 2-33 (de Vos, 2011).
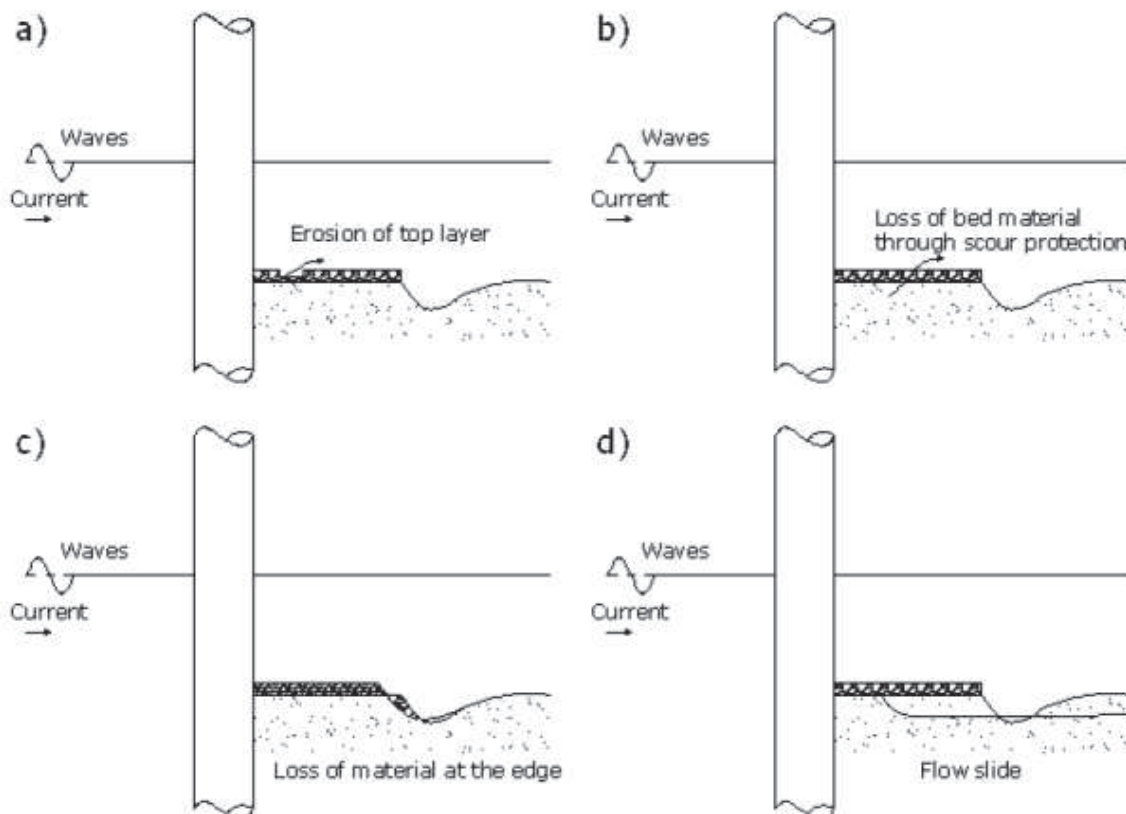
Figure 2-33: Failure mechanisms for bed protection around an offshore monopile foundation.

2.5.4   Design calculation of armour layer

The required stone size of the armour layer is mainly determined by failure mechanism a), the erosion of the top layer caused by flow, see Figure 2-33.

The formula of Van de Meer or the formula of Hudson is used to calculate the required stone diameter of the armour layer for breakwater design. However, in this case the armour layer of a bed protection needs to be determined and not a revetment on a slope. Therefore the formula of van de Meer and Hudson is not applicable here. Extra difficulty for determining the bed protection is the extra turbulence caused by the monopile, see section 2.4.

The principle to calculate the required stone diameter for the armour layer is based on the Shields criteria. When the bed shear stress exceeds the critical bed shear stress, the stones of the armour layer will move.

In this thesis two methods to determine the D_{50} of the armour layer are elaborated:
- the traditional/classical approach
- de Vos method

The traditional approach
The bed shear stress for a steady, uniform flow is defined as:

$$\tau_c = \frac{1}{2}\rho_w f_c \, U_c{}^2 \tag{2.17}$$

In which:

τ_c	bed shear stress due to flow	[N/m^2]
ρ_w	density of water	[kg/m^3]
f_c	friction coefficient of the bed	[-]
U_c	flow velocity	[m/s]

The dimensionless friction factor f_c depends on the Chezy coefficient:

$$f_c = \frac{2g}{C^2} \tag{2.18}$$

The bed shear stress due to waves is defined as:

$$\tau_w = \frac{1}{2}\rho_w f_w \, U_m{}^2 \tag{2.19}$$

In which:

τ_w	bed shear stress due to waves	[N/m^2]
ρ_w	density of water	[kg/m^3]
f_w	wave friction coefficient of the bed	[-]
U_m	maximal orbital velocity	[m/s]

The maximal orbital velocity just above the bed can be derived with linear wave theorem:

$$U_m = \frac{\pi * H}{T_w} \frac{1}{\sinh\left(\frac{2\pi d}{L}\right)} \tag{2.20}$$

In which:

U_m	max orbital velocity near bed	[m/s]
H	Significant wave height	[m]
T_w	wave period	[s]
d	water depth	[m]
L	wave length	[m]

Several expressions for the wave friction coefficient f_w exists:
- Dixon et al (2008)
- Soulsby (1997)
- Fredsøe and Deigaard (1992)
- Nielsen (1992)
- Kamphuis

The different formulas of the wave friction coefficient (f_w) result in a spreading of the outcome of the expressions. Due to this scatter the result in terms of wave induced bed shear stress depends also on the chosen formula, see Figure 2-34 (de Vos, 2011).
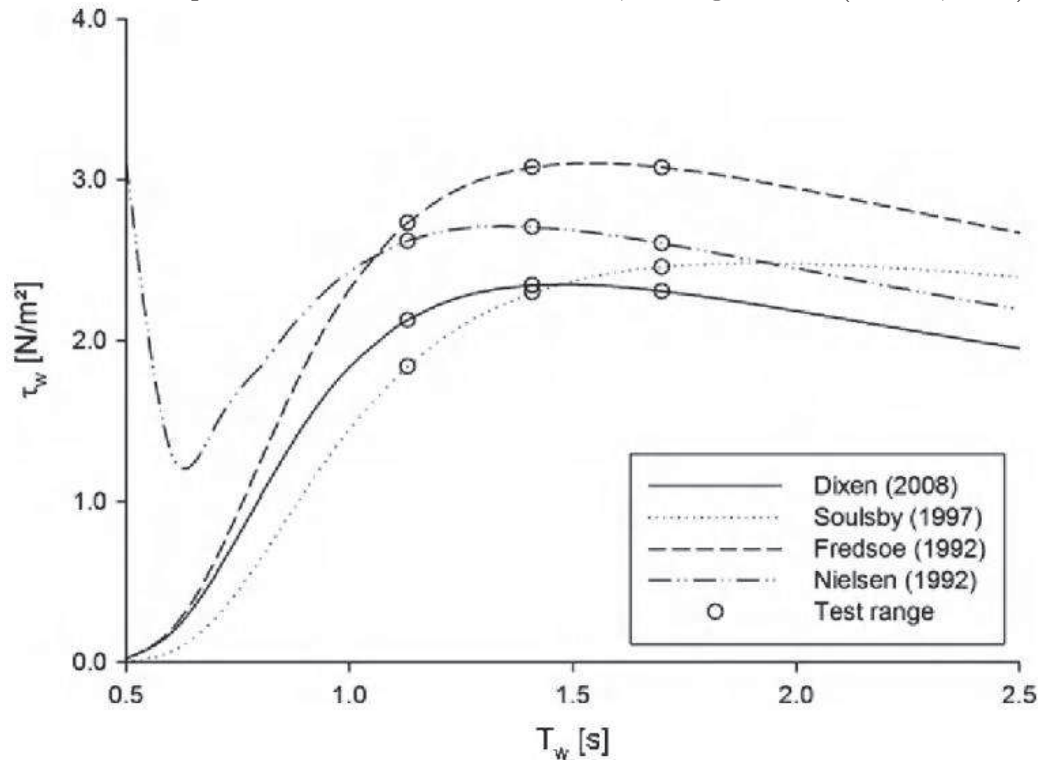
Figure 2-34: Wave related bed shear stress τ$_w$ as a function of the wave period Tw.

Currents and waves occur not separately in marine environments. The interaction between currents and waves give a combined influences which is not the same as a linear sum of their separate influences. Several models have been proposed to calculate the bed shear stress of their combined influence leading to considerable difference in the prediction of the combined wave-current bed shear stress. The actual bed shear stress due to currents and waves (undisturbed situation) is defined as follows (Van den Bos, 2006):

$$\tau_{bed,w+c} = \sqrt{\tau_c{}^2 + \tau_w{}^2 + 2\,\tau_c\,\tau_w \cos\beta} \tag{2.21}$$

In which:

τ_c	bed shear stress due to flow	[N/m^2]
τ_w	bed shear stress due to waves	[N/m^2]
β	angle between the current and the waves	[°]

Due to the monopile the flow pattern changes (disturbed situation) and increase the local sediment transport capacity, as mentioned in 2.4. The increase of bed shear stress is expressed in terms of an amplification factor (α) which is defined as:

$$\alpha = \frac{\tau_b}{\tau_{b,\infty}}$$

(2.22)

In which:

τ_b actual bed shear stress $[\text{N/m}^2]$
$\tau_{b,\infty}$ actual bed shear stress $[\text{N/m}^2]$

The amplification factor close to monopiles due to currents is defined as follows:

$$K_c = \min\left\{11; 3.5\left(\frac{x}{D}\right)^{-0.5}\right\}$$

(2.23)

The amplification factor close to monopiles due to waves is defined as follows:

$$K_w = \left[1 + \left(\frac{0.5\,D_{pile}}{0.5\,D_{pile} + x}\right)^2\right]^2$$

(2.24)

Marine / biological fouling is monitored at OWEZ. The transition piece is for 90% covered by marine growth and the monopile showed almost 100% coverage (Bruijs, 2010). Biological fouling can increase the pile diameter. It can be noticed that the pile diameter is of importance for the amplification factors. This should be included in the calculations.

The actual bed shear stress due to waves and currents in the disturbed situation (Louwersheimer, 2007):

$$\tau_{bed,w+c} = \sqrt{(K_c\tau_c)^2 + (K_w\tau_w)^2 + 2\,K_c\tau_c\,K_w\tau_w\cos\beta}$$

(2.25)

The minimum required stone size diameter (D_{50})of the armour layer for a dynamically stable situation:

$$D_{50A}(x) = \frac{\tau_{bed,w+c,dist}(x)}{\Psi_{cr} * \rho_w * \Delta * g}$$

(2.26)

In which:

D_{50} required stone size $[\text{m}]$
$\tau_{bed,w+c}$ bed shear stress in disturbed situation $[\text{N/m}^2]$
Ψ_{cr} critical Shields parameter $[-]$
ρ_w density of water $[\text{kg/m}^3]$
Δ relative density $[-]$
g acceleration of gravity $[\text{m/s}^2]$

Soulsby (1997) suggest a value of α=2.2 for the amplification factor of the bed shear stress due to waves. Most of the time a value of α=4 is used for the amplification factor of the bed shear stress due to currents.

<u>De Vos method</u>
The method of de Vos et al. (2011) is another way to calculate the required stone size of the armour layer. This method is based on 40 model tests and the combined wave en current induced bed shear stress is fitted (regression analysis). Therefore this method can only be applied in a small range of KC values.

The bed shear stress due to currents is calculated in the same manner, see equation (2.17).

The bed shear stress due to waves contain other wave friction coefficient of the bed (f_w). The best result for the regression analysis was obtained by the following formulas for the wave friction coefficient:

$$f_w = 0.32 \left(\frac{A}{k_s}\right)^{-0.8} \quad for \quad 0.2 < \frac{A}{k_s} < 10 \tag{2.27}$$

$$f_w = 0.4 \left(\frac{A}{k_s}\right)^{-0.75} \quad for \quad 10 < \frac{A}{k_s} < 50 \tag{2.28}$$

In which:
f_w wave friction coefficient of the bed   [-]
A   amplitude of orbital movement at the bed   [m]
ks   bed roughness   [m]

It is important to note that $2.5D_{50}$ is used for the bottom roughness (k_s). The amplitude is defined in equation (2.29).

$$A_{bed,max} = \frac{U_{w,bed,max}}{\omega} \tag{2.29}$$

In which:
U_m max orbital velocity near bed   [m/s]
ω wave frequency (=2 π/T)   [s^{-1}]

De Vos obtained a good result by using $H_{1/10}$ and T_p to calculate the orbital velocity at the bed in equation (2.20).

The combined current and wave bed shear stress is empirical established as:
$$\tau_{cr,pred} = 83 + 3.569\tau_c + 0.765\tau_w \tag{2.30}$$

The required stone size ($D_{67,5}$ instead of D_{50}) can be calculated with the total bed shear stress, see formula 2.16.

$$D_{67.5} = \frac{\tau_{cr}}{\Psi_{cr} * g * (\rho_s -* \rho_w)} \tag{2.31}$$

In which:
D_{50} required stone size   [m]
τ_{cr} total bed shear stress   [N/m^2]
Ψ_{cr} critical Shields parameter   [-]
g   acceleration of gravity   [m/s^2]
ρ_w density of water   [kg/m^3]
ρ_s density of rock   [kg/m^3]

The critical shields parameter (Ψ_{cr}) is assumed 0.035. In de Vos et al (2011) is stated:
The value of $D_{67.5}$ is used instead of D_{50} to calculate τ_{cr} as the results showed that **stones in a scour protection with a smaller grading tend to move faster than those in a scour protection with a wide grading.**

The corresponding D_{50} is a function of the grading range (D_{85}/D_{15}), see equation (2.32).

$$\log\left(\frac{D_{67.5}}{D_{50}}\right) = 0.25 \log\left(\frac{D_{85}}{D_{85}}\right) \qquad (2.32)$$

De Vos studied also a dynamic bed protection approach. The static design method is conservative and smaller stone sizes can be used by maintenance reparations after storms. In this dynamic approach a damage parameter is added in the stability formula. De Vos et al (2011) assumed failure of the bed protection when the filter is exposed by a minimum area of four armour units ($4D_{50}{}^2$). Tim Raaijmakers said during the interview that this value is arbitrary.

2.5.5   Design calculation of filter layer

There are two types of filter layers possible in bed protections (for monopiles):

- Geometrically closed filters
  These filter layers are designed in successively coarser layers proceeding outward from the underlying finer soil. The first layer should hold the subsoil (base layer) and each following layer has to be able to hold the underlying one. Most of the time more layers need to be installed. The geometrically layers have to fulfill the following requirements (Schiereck, 2001):

  $Stability: \dfrac{d_{15F}}{d_{85B}} < 5 \qquad\qquad Int.stability: \dfrac{d_{60F}}{d_{10F}} < 10 \qquad\qquad Permeability: \dfrac{d_{15F}}{d_{15B}} > 5$

- Geometrically open filters
  In geometrically open filter particles of the subsoil can penetrate through the filter layer. However, a stable geometrically open filter is designed in such a way that the hydraulic loads on the subsoil are reduced. The filter layer(s) prevent(s) the particles from moving entirely through the rock bed by this load reduction (van de Sande, 2013).
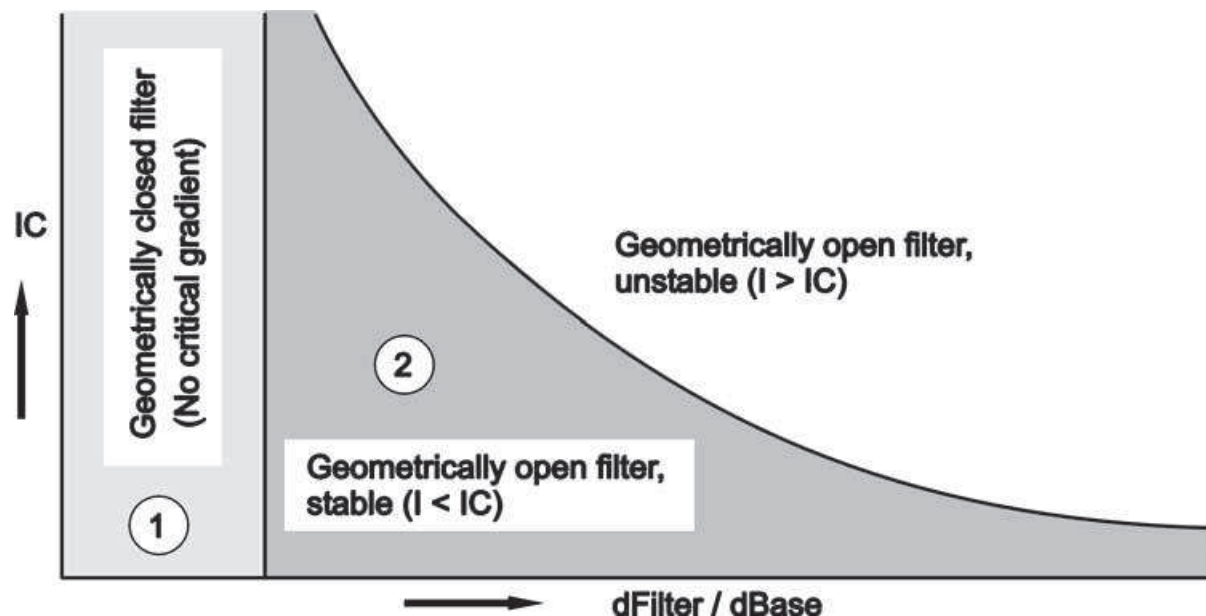
Figure 2-35: Design criteria for granular filters (Schiereck, 2001).

2.5.6   Design aspects of horizontal and vertical dimensions

Horizontal

In literature different extent of the horizontal bed protection dimensions can be found. This is probably due to the different hydrodynamic conditions and the structure interaction (pile classification) and the subsoil conditions. A compiled review is found in (Loosveldt & Vannieuwenhuyse, 2012), see Figure 2-36.
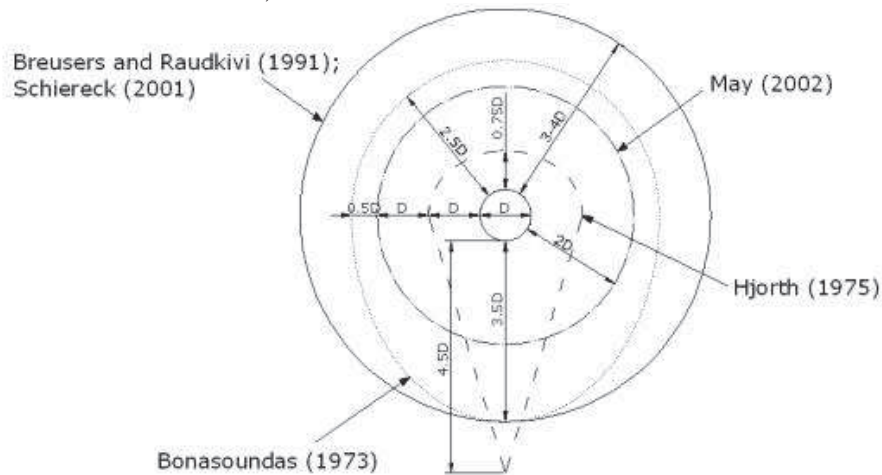
Figure 2-36: Recommendation for the extent of a bed protection.

Carstens, Sumer and Fredsøe suggest a bed protection as far as the scour hole would reach:

$$L_s = F_s S_e \cot \varphi \qquad (2.33)$$

In which:

L_s	radial distance to edge of the scour hole	[m]
F_s	safety factor	[-]
S_e	scour depth	[m]
φ	angle of repose	[°]

This formula is made visible in Figure 2-37.
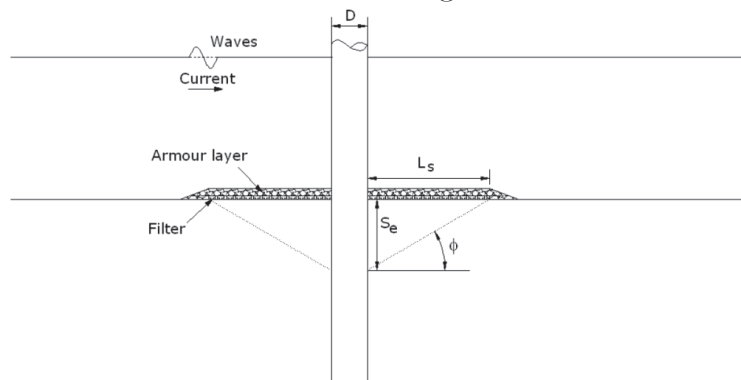
Figure 2-37: Horizontal extent of bed protection.

Sumer and Fredsøe (2002) recommend a radius of the scour protection of 2 times the pile diameter for slender piles. Whitehouse (1998) recommends a radius of 5, while Halfschepel (2001) and Zaaijer (2004) recommends a scour protection of 7 times the pile diameter because of the high uncertainties (Haddorp, 2005).

Vertical

The layer thickness of the layers must be at least two times D_{50} for stability with a minimum of 0.3 meters (for installations procedures).

2.5.7   Conclusion of technical analysis

All the technical related parameters for the technical requirements of a bed protection of a offshore wind turbine are summarized in this subsection. This summarized list is presented below. These parameters will be compared with the technical parameters in chapter 3.

- Waves
  Waves create an orbital flow just above the bed level. The magnitude of the orbital motion at the bed is related to relative water depth and influenced by the period and height of the wave. Larger waves (in significant wave height and/or period) increase the orbital motion. Higher orbital flows at the bed will increase the bed shear stress. Higher bed shear stress results in deeper scour holes or (in case of bed protection) larger armour units need to be applied.

- Currents
  Currents are related to the bed shear stress. Higher bed shear stress results in deeper scour holes or (in case of bed protection) larger armour units need to be applied.

- Kinetic energy (turbulence)
  A rough bed protection results in higher turbulences near the bed. Higher turbulences can affect the stability of the bed protection.

- Depth
  The depth is important for the wave classification. However, the depth is only context-defined and not controllable.

- Stone size of the armour layer and its grading
  The stone size determine the weight of the stones and is <u>the</u> factor for stability. De Vos (de Vos, 2011) stated that bed protection with smaller grading lead to less stable bed protections.

- Filter layer and its grading
  The filter layer has to coverage the subsoil and prevent erosion of the subsoil.

- Pore size
  The pore size is related to the installation method (stone packing), stone size, and its grading. These three aspects are also of great importance for the stability of the bed protection. However, the bed protections are not designed based to create certain pore sizes.

- Vertical dimension of the bed protection
  The vertical dimensions determine the load reduction on the covered subsoil.

- Orientation
  The dominant flow and wave direction can lead to an elliptical bed protection design instead of a round bed protection.

- Porosity / Packing
  The porosity/packing is related to the installation method (stone placing), stone size, and its grading and is therefore related to the stability of the bed protection.

- Inclination of the surface
  The slope of the bed protection influences the failure mechanism and determines therefore also the stability of the bed protection.

- Edge scour
  Scour is not directly related to failure of the bed protection. The purpose of bed protections is not prevent scour holes, but to keep the scour hole away from the structure.

- Horizontal dimension of the bed protection (surface of the bed protection)
  The horizontal dimension is to keep the scour hole far away of the structure.

- Shape of the rock
  The shape of rock determines the stability of the bed protection. Stones with protrusions interlock which strengthen the bed.

- Density
  The stability of stones is related to the weight. Smaller stones can be applied if the density is higher. Moreover, smaller stones result in less bed roughness. From technical point of view high stone densities are preferable.

- Hardness
  Hard stones wear less than soft stones which is preferable during the lifetime of the bed protection.

- Chemical composition
  This material property determines the hardness of the stone.

- Salinity
  The salinity of the seawater is of influence relative density and thus the stability of stones. However, the salinity is only context-defined and not controllable.

- Pile diameter
  The pile diameter is present in the calculations to determine the load forces.

3. PARAMETER STUDY

The favorable ecological conditions and the technical requirements of bed protections of offshore wind turbines are treated in chapter 2. In this chapter is searched for parameters that are of influence for the technical requirements and to provide favorable ecological conditions.

The total list of context-defined parameters are presented in section 3.1. In section 3.2 the controllable and matching parameter are listed. In section 3.3 'cavity size' is selected and substantiated as controllable parameter for functional requirements. The selected parameter 'cavity size' will be investigated in chapter 4.

3.1 CONTEXT-DEFINED PARAMETERS

In chapter 2 the list of *context-defined parameters* to provide favorable ecological conditions and the list of context-defined parameters for technical requirements is presented and substantiated. Context-defined means that no distinction is made whether the parameter is controllable or not.

A example of a context-defined parameter is salinity. A lot of species, such as cod, are sensitive to salinity. However, salinity is assumed non-controllable for bed protections in the North Sea. Therefore salinity is a context-defined parameter and not a *controllable parameter*. Controllable parameter means that the parameter is controllable by adaptations in design or installation method.

Moreover, salinity determines the relative density which is an important parameter to determine the stability of the bed protection. So, salinity is a matching parameter, but non-controllable. The term *matching* means that the parameter is relevant for both the technical part as well as the ecological part of the bed protection.

Intermezzo: extreme events vs. daily conditions
The bed protection of offshore wind farms are designed based on the extreme events. The bed protection may not fail for storm conditions of a certain level. The favorable ecological conditions have to be designed for 'daily use' and are based on daily conditions.

All the context-defined parameters are listed in Table 3-1. In this table no distinction is made between matching or non matching. The table is organized per subject to present a clear overview. The subjects are:

- Physical conditions;
- Bed protection;
- Material properties;
- Water quality;
- External effects.

Table 3-1: List of context-defined parameters.

Physical conditions	Bed protection
• Waves • Currents • Kinetic energy • Depth	• Type of bed protection • Stone size of the armour layer and filter layer • Horizontal dimension of the bed protection (surface of the bed protection) • Vertical dimension of the bed protection (height, or in ecological terms, ecological landscaping) • Orientation • Rocking
Material properties of rock	**Water quality**
• Color • Roughness • Porosity • Cavity size • Shape of the rock • Density • Water retention capacity • Hardness • Chemical composition • PH Value	• PH value • Turbidity • Light penetration • Oxygen • Salinity • Temperature • Nutrients
External effects	
• Sound • Electromagnetic fields • Food • Catchment/Nursery • Collision • Pile diameter	

In the next section the table above will be reduced to the matching and controllable parameters for functional requirements.

3.2   CONTROLLABLE   PARAMETERS   FOR   FUNCTIONAL REQUIREMENTS

In Table 3-1 there are six concrete controllable parameters for functional requirements found. These are listed below.

1. Waves
   The waves in the North Sea the waves are non-controllable of course, but maybe the waves around wind turbines are controllable or the wave force on the bed protection is controllable.

Target:	Create favorable (orbital) flow patterns
How:	A structure around the wind turbine (for instance a floating breakwater) can create favorable flow patterns and other/lighter bed protections can be applied. Moreover, the extra structure can also function to provide favorable ecological conditions. Another examples are a horizontal plate around the foundation or new configuration of rocks at the bottom.

2. Currents
   Same concept as described above at 'Waves'.

3. Dimensions of the bed protection (add more hard substrate)

Target:	Create more hard substrate
How:	By adapting the length, width, or height (ecological landscaping) more hard substrate can be added.

4. Pore-size distribution

Target:	Create suitable hard substrate cavities
How:	By exposing the relationship between rock size distribution and pore-size distribution targeted shelter places ('houses') can be developed.

5. Turbidity

Target:	Reduce turbidity
How:	Map the water quality and search for adjustments in the bed protection design to create a better water quality.

6. Properties of rock

Target:	Create better settlement positions
How:	Apply different material properties (softness, roughness) in the bed protection

3.3   SELECTED PARAMETER

In this subsection the parameter for further research is selected. The dimensions of the bed protection, the water quality, and the material properties of rock are more related to ecological investigations. The options for waves and currents are not further elaborated, because this require large adaptations in the bed protection designs. Therefore, the selected parameter for further research is the **pore-size distribution**.

The pore-size distribution, which are cavities for species, determines the favorable ecological conditions for the lobster and juvenile cod. A variety of pore sizes also stimulate the biodiversity (Baptist, van der Meer, & de Vries, 2007). Therefore the distribution of cavities is a very attractive parameter in terms of ecology to investigate in detail.

There are many uncertainties and unexposed relations for the pore-size distribution. The pore-size distribution depends on the stone size (D_{50}), stone grading (D_{85}/D_{15}), porosity, and the shape of the stones. These variables directly affect the technical requirements for stability.

However, the relation between the pore-size distribution, the stone-size distribution, porosity, and the shape of the stones is not yet defined. Bed protections have been applied for years, but how large is the space between the rock?

Other reasons to select the pore-size distribution for further research is because of:
- This parameter is affiliated to the work field of Boskalis
- More insight in pore-size distribution is interesting for other fields as well:
    o Filter behavior
    o Wave damping
    o Permeability

Moreover, the controllable parameter "*stone size and grading*" is also attractive because of the $D_{67.5}$ used by the de Vos method. De Vos stated:
The value $D_{67.5}$ is used instead of D_{50} to calculate the τ_{cr} as the results showed that some stones in a scour protection with a smaller grading tend to move faster than those in a scour protection with a wide grading. The reason why scour protections with a wide grading appear to be more stable is probably due to the fact that in widely graded material, smaller stones find a better shelter thanks to the larger stones.

The parameter pore-size distribution is selected to investigate in further detail. Part II of this thesis, chapter 4, chapter 5, chapter 6, and chapter 7 is searching to expose the relation between the pore-size distribution, the stone-size distribution, porosity, and the shape of the stones. After this technical study the link is made again with the preferred cavities for lobsters. This is summarized in Figure 1-4.

4. MODEL SELECTION

The space between rocks of the bed protections of offshore wind farms is of importance for favorable ecological conditions for cod and lobster as described in chapter 3. These species find shelter in the cavities. A great variety of cavity sizes provide also favorable ecological conditions for the enhancement of biodiversity.

Bed protections of offshore wind farms are designed to withstand storm conditions with a certain probability of occurrence. On these conditions, the stone-size distribution of the armour layer is determined. The hypothesis is made that the stone-size distribution is directly related with the pore-size distribution. This means the number of cavities and the cavity sizes. However, the (technical) design requirements for the bed protection are not based on the pore-size distribution. In fact, the relation between the stone-size distribution and the pore-size distribution is not exposed.

In this chapter models are proposed to investigate the relation between the stone-size distribution and the pore-size distribution. After a short introduction of the terms and the terminology the model considerations are discussed. In section 4.2 is substantiated why the analytical and the experimental model are selected. In chapter 5 the analytical model will be elaborated and in chapter 6 the experimental model is discussed.

Note: Artificial (concrete) structure can also be applied to provide specified cavities. Multiple artificial structures can possibly act as a bed protection. This is not further investigated in this research.

4.1 INTRODUCTION

How to make the translation from the stone-size distribution to the pore-size distribution? To answer this question first some general terms and terminology are discussed.

4.1.1 Porosity

Porosity is the measure of 'empty' spaces in a material or packing. The porosity is defined as the sum of the empty spaces [m3] (which are filled with water in case of bed protection of an offshore wind turbine) divided by total volume, see equation 4.1.

$$\phi = \frac{V_{total} - V_{Stone}}{V_{total}} \tag{4.1}$$

The pore number is another way of presenting the porosity. The pore number is defined as the sum of the empty spaces divided by the volume of the material, see equation 4.2.

$$e = \frac{V_{total} - V_{Stone}}{V_{stone}} = \frac{\phi}{1 - \phi} \tag{4.2}$$

4.1.2   Stone-size distribution

The applied stones of a bed protection are classified in mass M (kg), sieve size D (m), and nominal diameter D_n(m).

- Sieve size D
  The median sieve size D_{50} [m] is the sieve size when 50% of the mass is passed. The number after the 'D' is related to the percentage of the total mass passed. So, the D_{85} is the sieve size when 85% of the total mass of stones is passed.

- Nominal diameter D_n
  The median nominal diameter D_{n50} is related to the dimensions of the equivalent cube of a stone with mass $W_{50,}$ see equation 4.3.

$$W_{50} = \rho * D_{n50}{}^3 \tag{4.3}$$

The relation between Dn50 and D50 is experimentally determined by Laan (1981), see equation 4.4 (Rockmanual, 2007).

$$D_n = 0{,}84 * D \tag{4.4}$$

- Stone grading
  Stones are not uniform due to the mining in the quarry. A batch of stones will display a range of sieve sizes. The grading width is often given by equation 4.3 (Schiereck, 2001).

$$grading\ width: \frac{D_{85}}{D_{15}} \tag{4.5}$$

It is called a narrow gradation is if D_{85}/D_{15} is smaller than 1.5.
It is called a wide gradation is if D_{85}/D_{15} is between 1.5 and 2.5.
It is called a very wide gradation is if D_{85}/D_{15} is between 2.5 and 5.0.

- Stone-size distribution
  The different stone sizes of a batch, the stone-size distribution, is often graphical presented, see Figure 4-1. The x-as contains the sieve diameter and the y-as contains the passing percentage by weight lighter. The stone-size distribution is most of the time presented in a:
    o   Mass probability density function
    o   Mass cumulative density function

  Another way of presenting is also possible by looking at the number of stones and the corresponding sizes of a batch. This is the stone-number distribution. The number distribution can be obtained with equation 4.6.

$$\Delta p_i = \frac{(\Delta m_i/d_i)^3}{\sum (\Delta m_i/d_i)^3} \tag{4.6}$$

The stone-number distribution can be presented in a:
- o   Number probability density function
- o   Number cumulative density function

The stone-number distribution is not often applied in civil engineering, but the number of stones are interesting for the pore-size distribution. The x-as of the number distribution contains the sieve diameter and the y-as contains the passing percentage by number smaller. In Figure 4-1 the four different types of presenting a stone-size distribution are sketched. The input data of the graph is presented in Table 4-1. The yellow cells has to be filled in by hand.

Table 4-1: Input data for Figure 4-1.

Designed grain distribution														
Sieve sizes [mm]	7,1	10	12,5	14	16	20	22,4	25	31,5	40	50	63	71	90
Stone classes		[7,1-10]	[10-12,5]	[12,5-14]	[14-16]	[16-20]	[20-22,4]	[22,4-25]	[25-31,5]	[31,5-40]	[40-50]	[50-63]	[63-71]	[71-90]
mean stone class (di)	7,1	8,55	11,25	13,25	15	18	21,2	23,7	28,25	35,75	45	56,5	67	80,5
Mass distribution														
Mass probability density (Δm)		0%	0%	0%	2%	5%	13%	30%	34%	12%	4%	0%	0%	0%
Mass cumulative probability density		0%	0%	0%	2%	7%	20%	50%	84%	96%	100%	100%	100%	100%
Number distribution														
number of stones (Δm/diˆ3)	0	0,00E+00	0,00E+00	0,00E+00	5,93E-06	8,57E-06	1,36E-05	2,25E-05	1,51E-05	2,63E-06	4,39E-07	0,00E+00	0,00E+00	0,00E+00
p (number of stones)	0%	0%	0%	0%	9%	12%	20%	33%	22%	4%	1%	0%	0%	0%
P (number of stones)	0%	0%	0%	0%	9%	21%	41%	74%	96%	99%	100%	100%	100%	100%

Σ(Δm/diˆ3)
6,88E-05
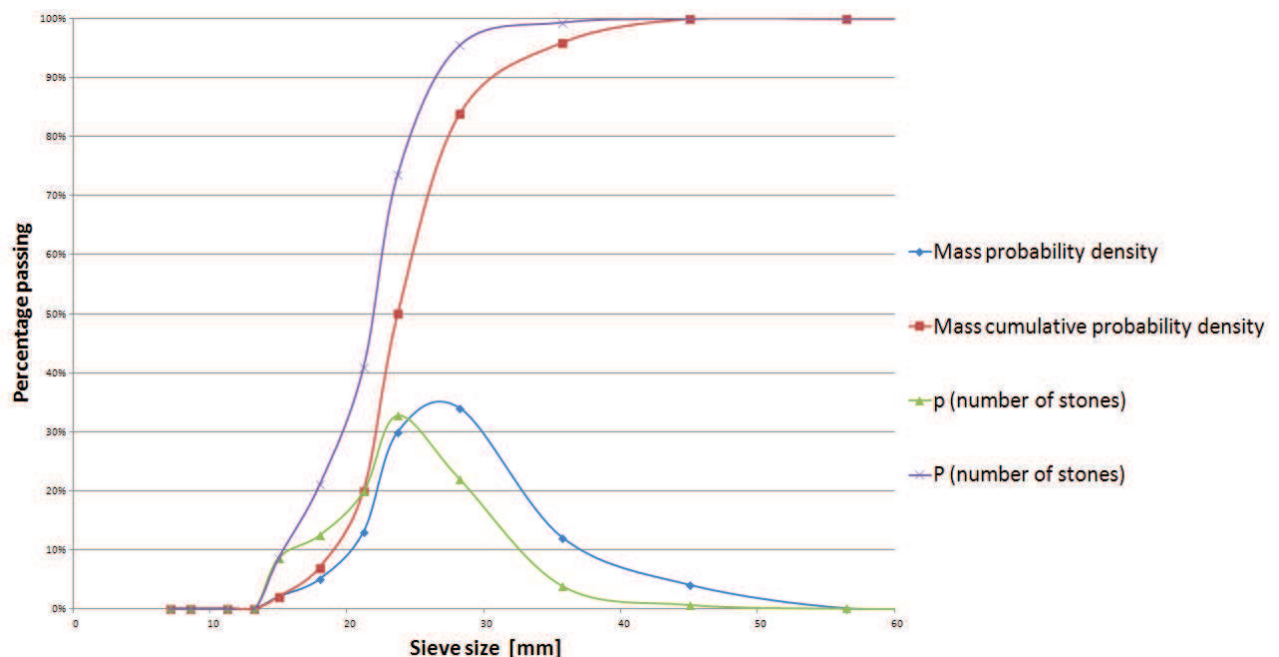
Figure 4-1: Mass probability density function (blue), Mass cumulative probability density function (red), Number probability density function (green), Number cumulative probability density function (purple).

The output in numbers of Figure 4-1 is presented in Table 4-2.

Table 4-2: Output in numbers of Figure 4-1.

D50 (mass)	25,00	D50 (number)	23,12
D85 (mass)	32,21	D85 (number)	28,37
D15 (mass)	21,48	D15 (number)	18,04
D85/D15 (mass)	1,50	D85/D15 (number)	1,57

4.1.3   Stone shape

There are two methods to classify the stone shape:

- Blockiness
  The blockiness is defined as the volume of the stone divided by the volume of the enclosing XYZ orthogonal box with a minimum volume, see equation 4.7 and Figure 4-2 (Rockmanual, 2007). The blockiness of a cube is 100%.

$$BLc = \left(\frac{M}{\rho} * \frac{1}{X * Y * Z}\right) * 100 \tag{4.7}$$
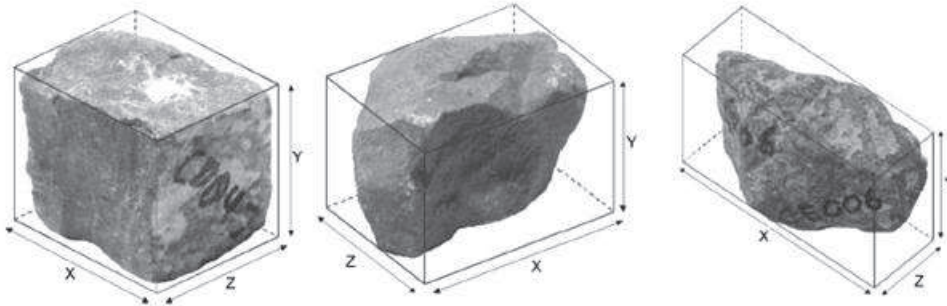
Figure 4-2: Blockiness examples; left BLc=80%, middle BLc=60%, right BLc=40%.

- LT
  The length-to-thickness ratio (LT) is defined as the maximum length divided by the minimum distance. The LT of a cube is 1.73.

4.1.4   Terminology

In literature different terms are found to explain the same phenomena.

Pore size:
There are different terms for the pore size:
- Pore body
- Void size
- Cavity size
- Pore diameter
- Pore scale

In this thesis the term cavity size is used if it is about the space for species. Otherwise the term pore size is used. Multiple pores and with different sizes is called pore-size distribution.

Constriction-size:
The cavity openings are important for the species to go in en out the cavity. These openings are the narrowest cross sections along any possible pathway. Also for the cavity openings are different terms used:
- Pore opening
- Pore throat (Al-Kharusi & Blunt, 2006)
- Pore channel
- Constriction-size

In this thesis the term cavity openings is used if it is about the openings for species. Otherwise the term constriction-size is used. Multiple constrictions and with different sizes is called constriction-size distribution.

4.2 MODEL OPTIONS

How to extract the pores from a batch of stones and come up with the translation from stone-size distribution to pore-size distribution? This question is graphical presented in Figure 4-3.
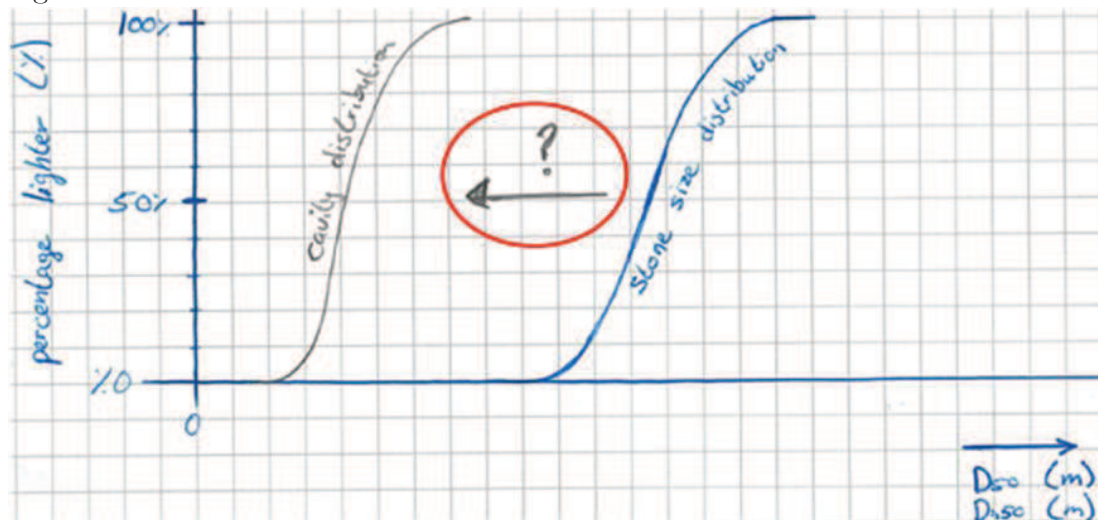
Figure 4-3: How to derive the pore-size distribution from a stone-size distribution?

Different kind of models are considered to expose the relation between the stone-size distribution and the pore-size distribution. The models are separated into an analytical model, numerical model, or experimental model. The models are obtained from literature in the field of granular filters (Etzer, Aufleger, & Muckenthaler, 2012) and the oil and gas industry (Silin & Patzek, 2003) (Enbaia, 2014) and conceived by the author.

Analytically:
   A) Geometrically analysis with spheres

Numerically:
   B) Analysis with Blender; a software package used in the movie industry for film animations. Blender has also a python interface.

Experimentally:
   C) Imaging analysis with Avizo Fire; the image can be created with
         o   a MRI scanner (3D image) (Kleinhans, 2008)
         o   a CT scanner (3D image)
         o   a photo camera (2D image)

   D) Physical experiment by measuring the porosity per layer; fill a container with stones, add water in the container, measure the water level in the container, and reduce the container size stepwise.

   E) Physical experiment by saw slices of a packing (Vincens, Witt, & Homberg, 2014)
         o   Fill a container with stones, add elastic material/glue, remove the stones, and make slices of the glue structure
         o   Make a mold of stones, make elastic/plastic stones, make a packing of the stones, glue the stones together, make slices of the structure.

F) Physical experiment by dropping glass balls; fill a container with stones, drop mono-sized (uniform) glass balls in the container. Some glass balls will fit in the pores and occupy these pores. Leave the glass balls that fit in the pores in the pores. Remove the glass balls that stay on top of the stones. Repeat the experiment with smaller glass balls. So drop smaller uniform glass balls in the container. Leave the glass balls that occupy pores in the pores and remove the glass balls that stay on top of the stones. Repeat this again for X times. Count the number of glass balls and their associated sizes in the end. This will result in a number distribution of pores. This experiment takes the pore size and pore openings into account. It is very practical, because it also computes only the top layer of a bed protection, which is the interesting area with respect to species.

G) Mercury capillary tests (Nimmo, 2004); inject mercury, measure the mercury that enters the sample and measure the associated increasing pressure.

The considered models are different from nature: some models are fundamental science while others are more applied sciences and 'fit for duty'. The 'fit for duty' models focuses at the top layer of the bed protection (the area of interest for the species) and also includes openings and not only cavity sizes.

4.3   SELECTED MODEL

In Figure 4-4 the challenge for the model is visible. There are three parameters which determine the pore-size distribution:

  A. Grain packing/porosity
  B. Grain shape factor
  C. Grain size factor

Secondly, the scaling effects and the number of pores are to be investigated.
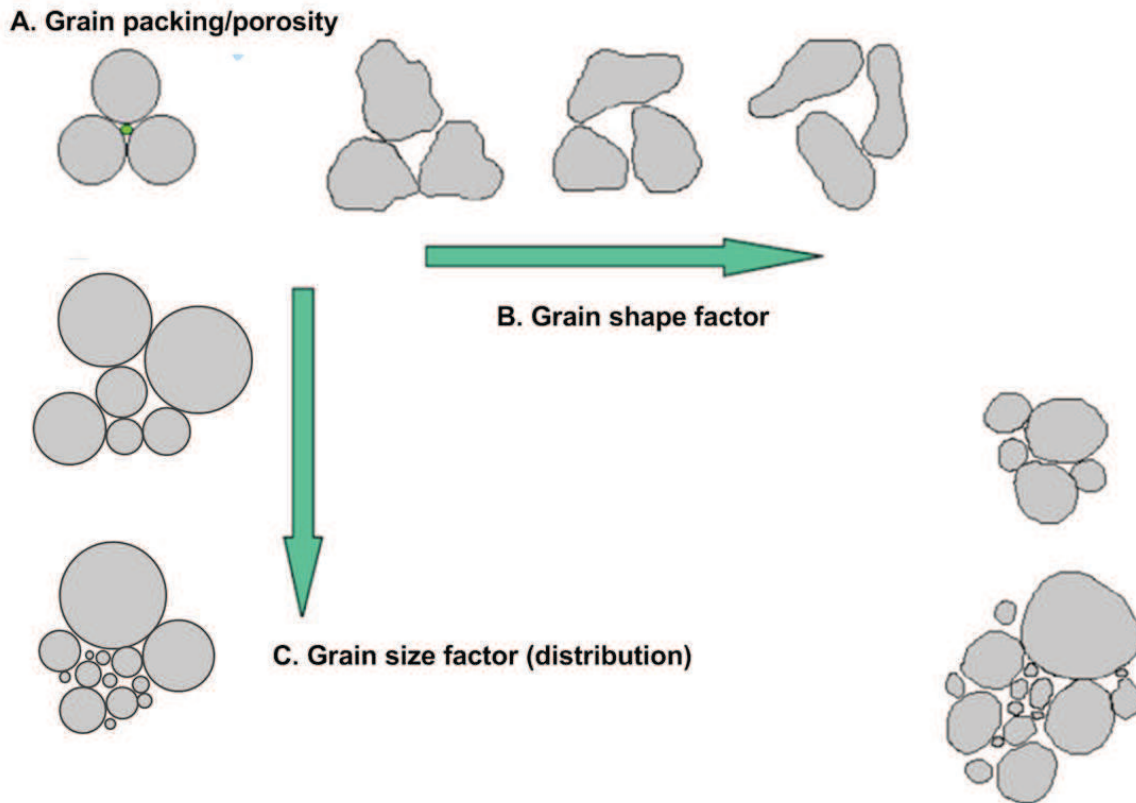
Figure 4-4: Grain packing (porosity), grain shape, and grain distribution.

The analytical model with spheres and the experimental imaging model are selected to crack the problem. The experimental imaging model is chosen, because it is innovative in this field and it is a fundamental approach. This model is able to include all three parameters (A, B, and C). The imaging model computes the 3D pore structure and also the constriction-size of the pores. The analytical model is elaborated to give indications and to validate the experimental imaging model. The analytical model only include parameter A en C. Both models deal with scaling effects.

Both models are fundamental and therefore in a later stage (chapter 7) the pore-size distribution size will be used in the context of species.

5. ANALYTICAL APPROACH

The analytical approach is selected to get an indication and to validate the experimental model. The analytical approach is based on geometry and statistics. All grains are seen as spheres in the analytical model.

The different packing types for spheres will be explained first. For the most dense and most loose packing the constriction-size (distribution) will be determined. The constrictions sizes are important because these are the openings for the species to get into the cavities. In the last section the pore-size distribution will be elaborated.

5.1   PACKING

The packing of spheres is related to the porosity, the constriction-size, and pore size. A overview of the different packing arrangements are presented in Figure 5-1 (Albers, 2005).
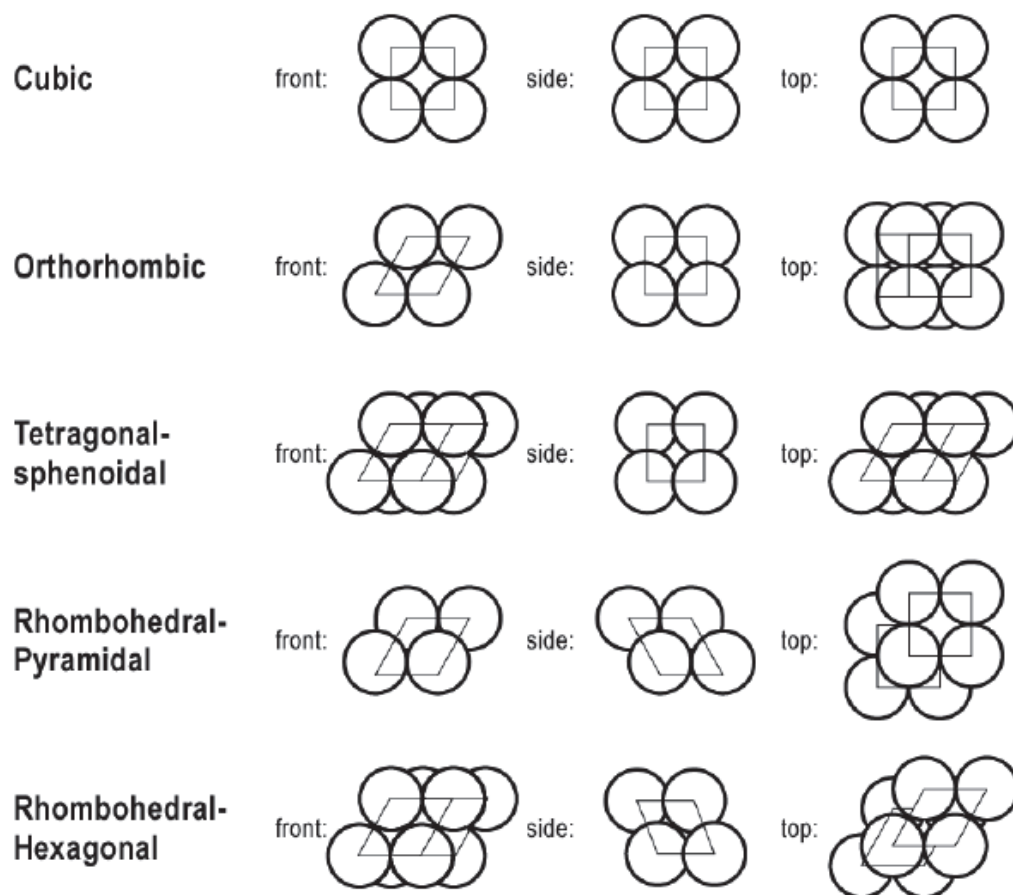
Figure 5-1: Packing arrangements.

The cubic packing is 'most loose' packing possible. The 'most dense' packing is the rhombohedral-hexagonal packing. This is also called Kepler conjecture or face-centered cubic. The proof that this is the 'most dense' packing is delivered in 1998 by Thomas Hales. Hales' proof is a proof by exhaustion and referees are "99% certain" of the correctness of the proof (Hales, 2005). In Figure 5-2 a 3D impression is given of the two packings.
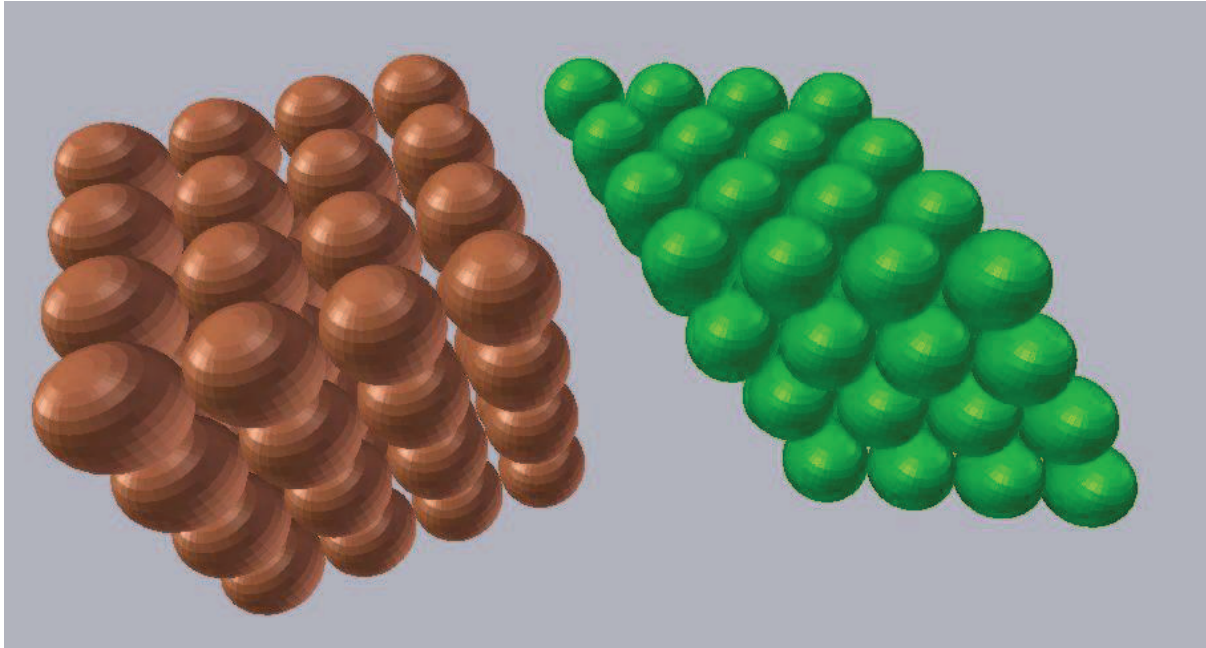
Figure 5-2: Sketch (3D) of cubic packing (left) and rhombohedral-hexagonal packing (right).

The porosity of the cubic packing and rhombohedral-hexagonal packing are derived.

- Cubic packing porosity
  The porosity of cubic packing is relatively easy to derive compared to the rhombohedral-hexagonal packing. It is the volume of a cube (see Figure 5-3) minus the volume of the spheres inside the cube divided by the volume of the cube, see equation 5.1. The porosity is 47,6%.
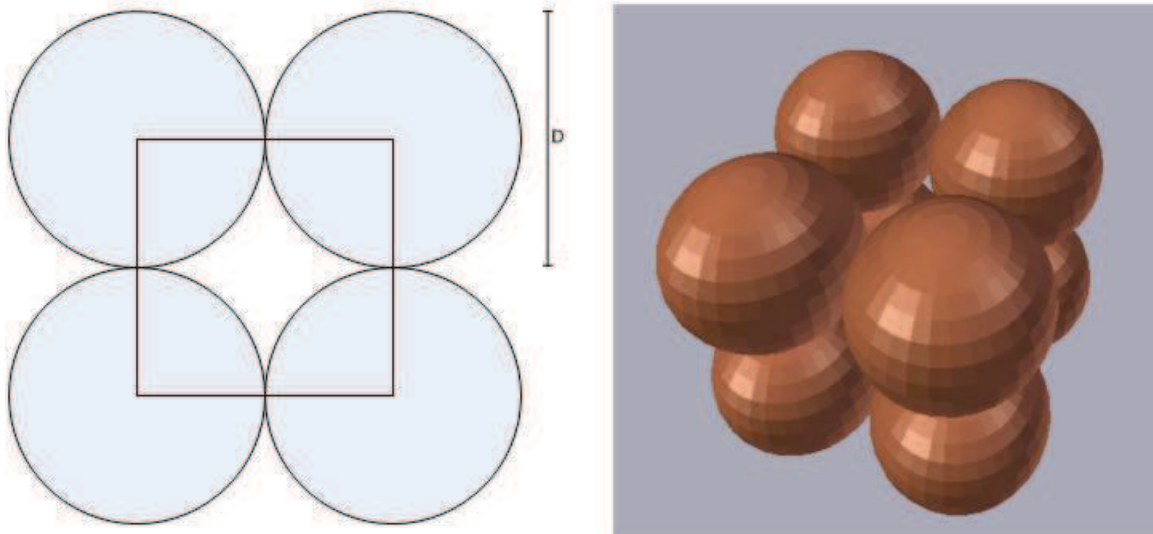
Figure 5-3: 2D sketch (left) and 3D impression of cubic packing.

$$Porosity = \frac{V_{cube} - V_{spheres}}{V_{cube}} = \frac{D^3 - \frac{4}{24}\pi D^3 * \frac{1}{8} * 8}{D^3} = 1 - \frac{\pi}{6} \approx 0.4764 \qquad (5.1)$$

- Rhombohedral-hexagonal packing porosity
  The Rhombohedral-hexagonal packing is sketched in Figure 5-4. The porosity is derived by defining a box (not a cube, but a parallelepided). The porosity is the volume of the box minus the volume of the spheres in the box dived by the volume of the box, see equation 5.2. The porosity is 25.95%.
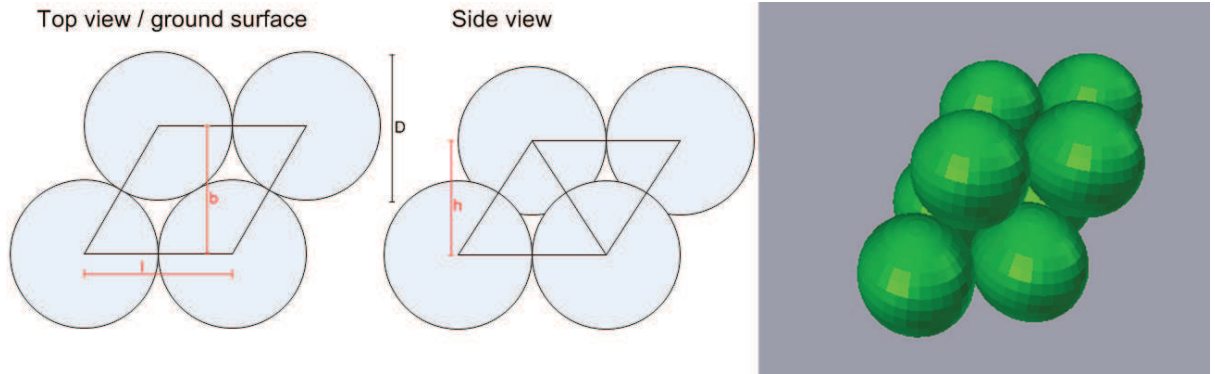
Figure 5-4: 2D sketches and 3D impression of rhombohedral-hexagonal.

$$Porosity = \frac{V_{cube} - V_{spheres}}{V_{cube}} = \frac{l*b*h - \frac{4}{24}\pi D^3}{l*b*h} = 1 - \frac{1}{6}\sqrt{2}\pi \approx 0.2595 \tag{5.2}$$

o   The length of the box (l) is D.

o   The width of the box (b) is de $\frac{1}{2}\sqrt{3}$ (=sin 60°)

o   The height of the box (h) is more difficult to determine because the sphere is dropped down as visible in the side view of Figure 5-4. After deriving the height is established at $\sqrt{\frac{2}{3}}D$, see Figure 5-5.

o   The volume of the spheres in the box is exactly the volume of one sphere.
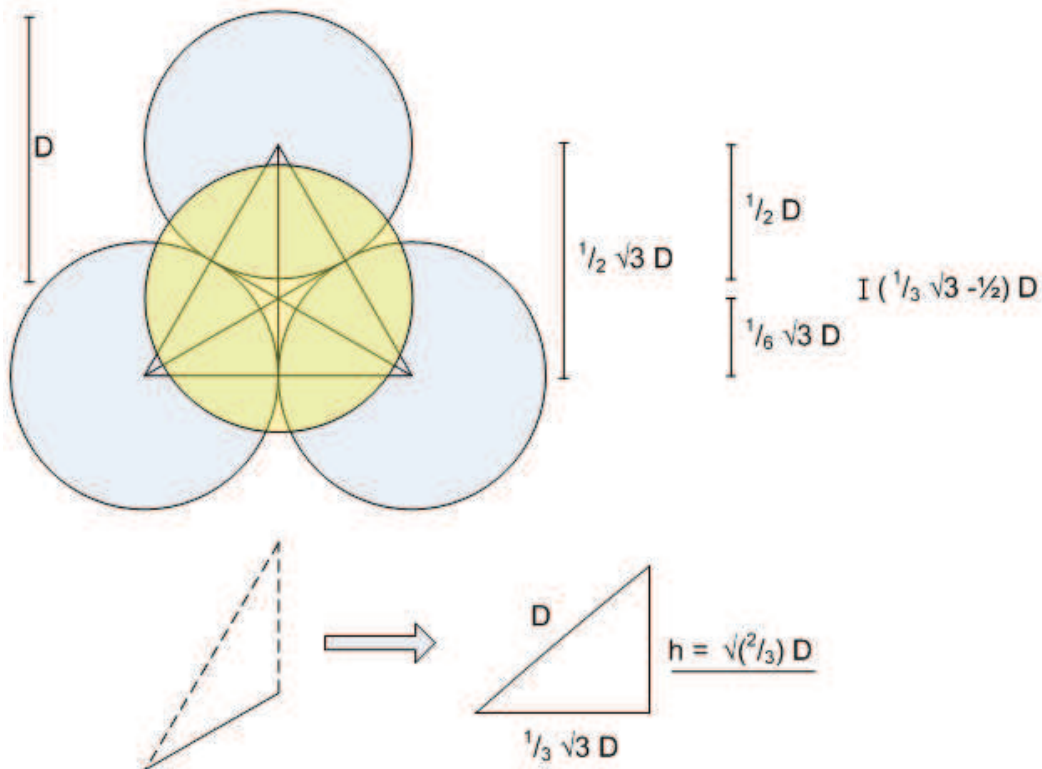
Figure 5-5: The height of the rhombohedral-hexagonal packing box.

5.2   CONSTRICTION-SIZE DISTRIBUTION

The constriction-size is the narrowest opening and is 2D accessed. First of all the constriction-size is determined for *mono-sized spheres* for:
- Cubic packing / 'most loose' packing
- Rhombohedral-hexagonal packing / 'most dense' packing

Secondly the constriction-sizes are determined for *multi-sized spheres*. This results in a constriction-size distribution. The constriction-size distribution is also determined for:
- Cubic packing / 'most loose' packing
- Rhombohedral-hexagonal packing / 'most dense' packing

5.2.1   Mono-sized spheres:

- Cubic packing construction size
  The constriction-size for cubic packing for uniforms spheres is 0.414D, see Figure 5-6 and equation 5.3.
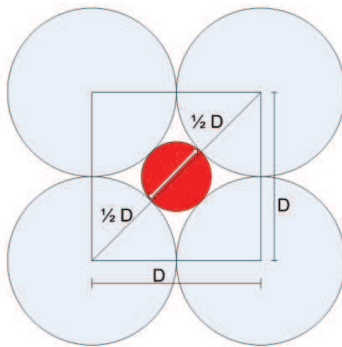
Figure 5-6: Constriction-size cubic packing.

$$Constriction\ size = \sqrt{D^2 + D^2} - D = (\sqrt{2} - 1)D = 0,414\ D \qquad (5.3)$$

- Rhombohedral-hexagonal packing constriction-size
  The constriction-size for rhombohedral-hexagonal packing for uniforms spheres is 0.155 D, see Figure 5-7 and equation 5.4.
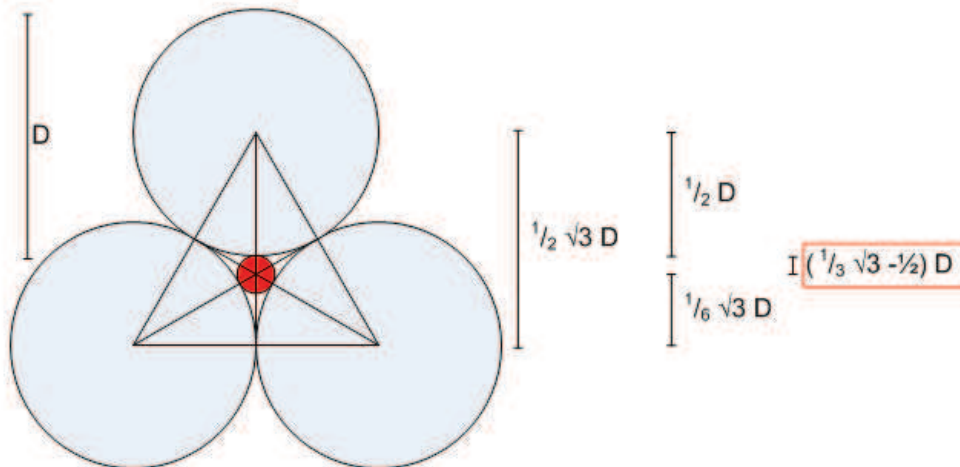
Figure 5-7: Constriction-size rhombodedral packing.

$$Constriction\ size = 2 * (\frac{1}{3}\sqrt{3} - \frac{1}{2}) = 0.155\ D \qquad (5.4)$$

- Overview

The construction size for uniform spheres is determined for the 'most loose' and 'most dense' packing, see Table 5-1. In Geohydraulik (Busch, Luckner, & Tiemer, 1993) a linear relation is suggested between the construction size and the porosity for $0.2595 < \phi < 0.476$. This relation is presented in Figure 5-8 and stated in equation 5.5.

Table 5-1: Overview of packing types, porosity, and constriction-size for mono-sized spheres.

Packing	Porosity	Constriction-size
Cubic	47.64%	0.414 D
Rhombohedral-Hexagonal	25.95%	0.155 D
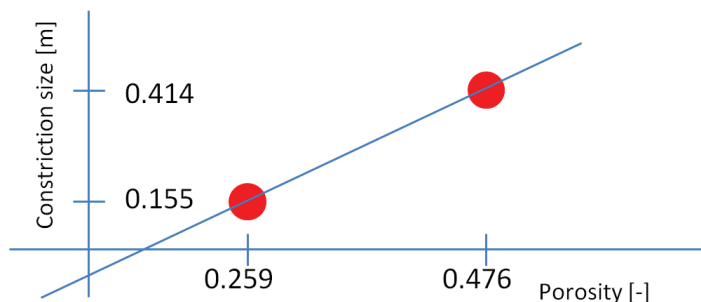
Figure 5-8: Relation between constriction-size and porosity.

$$Constriction\ size = -0{,}154 + 1{,}19\ \phi \qquad\qquad (5.5)$$

The relation in equation 5.5 is only valid for uniform spheres. In the next paragraph the relation is derived for multi-sized spheres.

5.2.2   Multi-sized spheres

In the paragraph above the constriction-size is determined for uniform spheres. In this paragraph the constriction-size is determined if the spheres are not uniform, but have different sizes (multi-sized). Different sphere sizes lead to different constriction-sizes. Therefore a constriction-size distribution is derived. First the constriction-size distribution will be derived for the 'most loose' packing (comparable with the cubic packing) and secondly the constriction-size distribution will be derived for the 'most dense' packing (comparable with the rhombohedral-hexagonal packing).
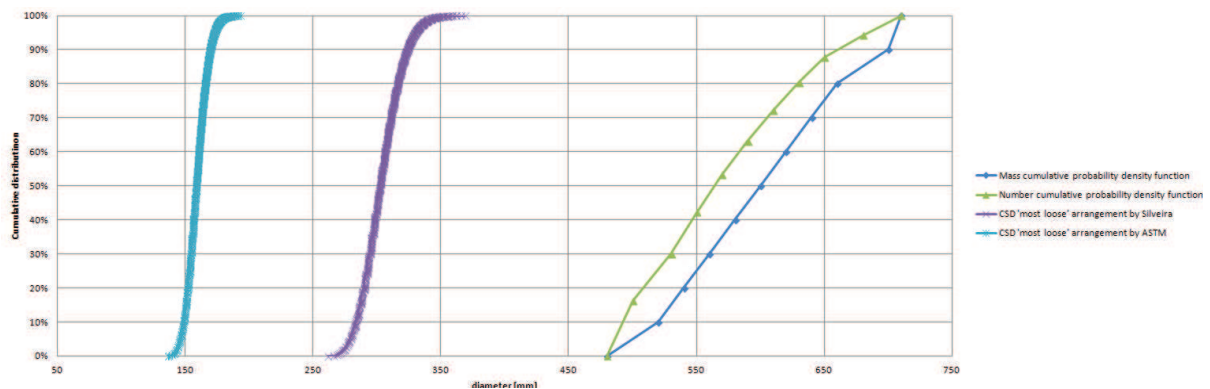
- Constriction-size distribution for the 'most loose' packing

  The constriction-size distribution for the 'most loose' packing depends on the constriction-size per combination, the combinations possible, the probability of occurrence of a sphere and the definition of the constriction-size.

  o Constriction-size

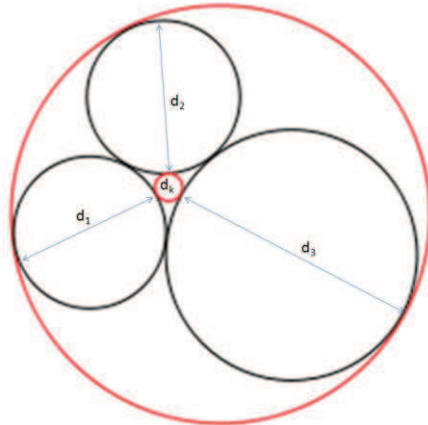 The constriction-size for the 'most loose' packing is defined by four spheres. There are two configurations limits, see Figure 5-9:
  - α_{min}
  - α_{max}
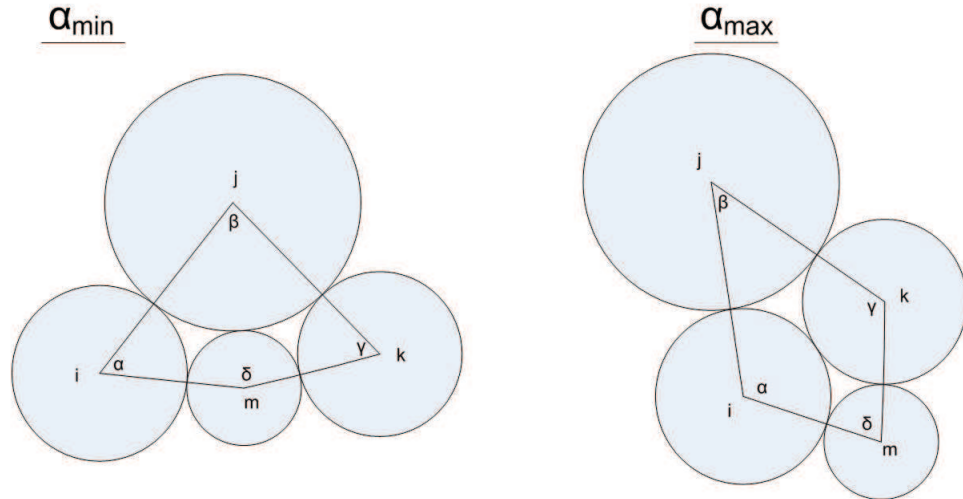
Figure 5-9: Configuration of α_{min} and α_{max}.

The angles $(\alpha,\beta,\gamma,\delta)$ for α_{min} and α_{max} can be calculated with equation 5.6 and 5.7 (Moraci, Mandaglio, & Ielo, A new theoretical method to evaluate the internal stabilty of granular soils, 2012).

$$\tan\left(\frac{\alpha_{min}}{2}\right) = \left[\frac{D_j D_m}{D_i(D_i + D_j + D_m)}\right]^{0.5} \qquad (5.6)$$

$$\alpha_{max} = \alpha' + \alpha'' \qquad (5.7)$$

$$\tan\left(\frac{\alpha'}{2}\right) = \left[\frac{D_j D_k}{D_i(D_i + D_j + D_m)}\right]^{0.5}$$

$$\tan\left(\frac{\alpha''}{2}\right) = \left[\frac{D_k D_m}{D_i(D_i + D_k + D_m)}\right]^{0.5}$$

The opening within the four spheres (S_v) is determined by the surface of two triangles minus the area of the four spheres, see equation 5.8 (Reboul, Vincens, & Cambou, 2009) and Figure 5-10.

$$S_v(\alpha) = A_{triangle\,1} + A_{triangle\,2} - A_{spheres} \qquad (5.8)$$

$$S_v(\alpha) = \frac{1}{8}\big[(D_i + D_j)(D_i + D_m)\sin(\alpha) + (D_j + D_k)(D_k + D_m)\sin(\gamma) - (\alpha D_i{}^2 + \beta D_j{}^2 + \gamma D_k{}^2 + \delta D_m{}^2)\big]$$
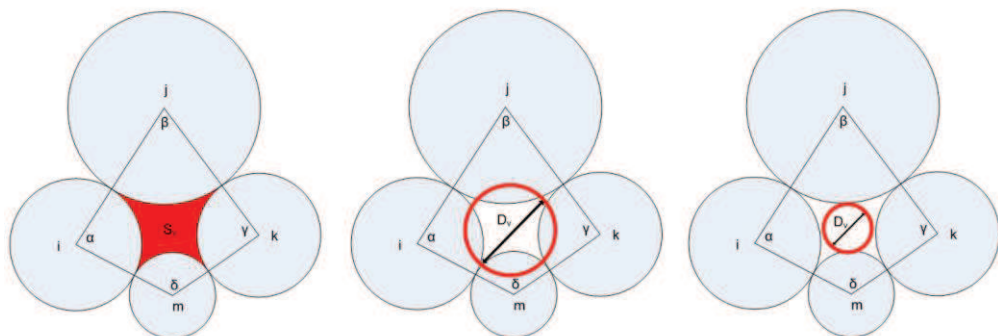
Figure 5-10: Constriction-size for the 'most loose' packing for multi-sized spheres.

The opening (S_v) is maximum for a certain alpha value. The constriction-size is determined with the maximum S_v. There are two possibilities to calculate the constriction-size. The constriction-size by Silveira (1975) is stated in equation 5.9 and the constriction-size by ASTM (2002) is stated in equation 5.10 (Moraci, Mandaglio, & Ielo, Reply to the discussion by Dallo and Wang on 'A new theoretical method to evaluate the internal stability of granular soils'., 2012). ASTM (2002) stated that the equation of Silveira (1975) overestimates the constriction-size. In Figure 5-11 (TO, Scheuermann, & Williams, 2012) it is clearly visible that the representing constriction-size overestimates the 'real' constriction-size.
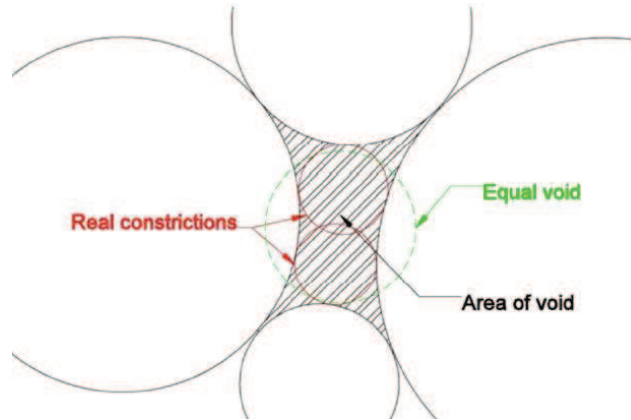
Figure 5-11: Difference in represented constriction-size.

$$D_v = \left(\frac{4S_v}{\pi}\right)^{0.5} \tag{5.9}$$

$$D_v = 4\left(\frac{S_v}{P_v}\right) \tag{5.10}$$

In which:
P$_v$:   perimeter   [m]

o   Combinations
The number of sphere sizes determines the number of different combinations. The combinations possible are stated in equation 5.11.

$$Combinations\ possible = \frac{(n + k - 1)!}{k!\,(n - 1)!} \tag{5.11}$$

In which:
n: number of spheres sizes
k: number of spheres that create the opening

The constriction-size for the 'most loose' packing is defined by four spheres, so k=4. So for example, in case of 10 different sphere sizes the number of combinations possible is $\frac{(10+4-1)!}{4!(10-1)!} = 715$.

o Configurations
A combination can have several configurations.

In case of four spheres:
$1,1,1,1 \rightarrow \binom{4}{0} = 1$ configuration
$1,1,1,2 \rightarrow \binom{4}{1} = 4$ configurations
$1,1,2,2 \rightarrow \binom{4}{2} = 6$ configurations
$1,1,2,3 \rightarrow \binom{4}{1}\binom{3}{1} = 12$ configurations
$1,2,3,4 \rightarrow \binom{4}{1}\binom{3}{1}\binom{2}{1} = 24$ configurations

o Probabilities of occurrence of a sphere
The probability of occurrence of a sphere is calculated with equation 5.12. This formula is based on the translation from a mass distribution to a number distribution.

$$\Delta p = \frac{\dfrac{\Delta m_i}{d_i^{3}}}{\sum \dfrac{\Delta m_i}{d_i^{3}}} \tag{5.12}$$

o Overview constriction-size distribution 'most loose' packing

Table 5-2 is the overview of Figure 5-12. In this figure the mass and number probability density functions are sketched and the constriction-size distributions for the 'most loose' packing.

Table 5-2: Constriction-size, combinations possible, configurations and probability of occurrence of a sphere lead to the constriction-size distribution for the 'most loose' packing.

number	combination				diameter grain/rock				Occurrence sphere				Configurations	Probability	Cum. distr.	CSD Silveira	CSD ASTM	Surface area (Sv)	Perimeter	alpha
	i	j	k	m											0					
															0,000%	260,22	136,01			
1	1	1	1	1	500	500	500	500	0,16	0,16	0,16	0,16	1	7,06E-04	0,071%	261,36	136,62	53650,46	1570,796	90,0
2	1	1	1	2	500	500	500	530	0,16	0,16	0,16	0,14	4	2,37E-03	0,308%	265,21	138,66	55241,76	1593,637	90,8
3	1	1	1	3	500	500	500	550	0,16	0,16	0,16	0,12	4	2,12E-03	0,520%	267,70	140,00	56283,21	1608,105	91,4
11	1	1	2	2	500	500	530	530	0,16	0,16	0,14	0,14	6	2,99E-03	0,819%	269,04	140,64	56850,88	1616,911	91,9
4	1	1	1	4	500	500	500	570	0,16	0,16	0,16	0,11	4	1,91E-03	1,009%	270,13	141,33	57310,02	1622,008	91,9
12	1	1	2	3	500	500	530	550	0,16	0,16	0,14	0,12	12	5,34E-03	1,544%	271,58	142,01	57927,79	1631,659	92,5
5	1	1	1	5	500	500	500	590	0,16	0,16	0,16	0,10	4	1,72E-03	1,716%	272,51	142,65	58322,88	1635,38	92,3
56	1	2	2	2	500	530	530	530	0,16	0,14	0,14	0,14	4	1,67E-03	1,883%	272,96	142,66	58517,52	1640,759	92,8
20	1	1	3	3	500	500	550	550	0,16	0,16	0,12	0,12	6	2,39E-03	2,122%	274,00	143,24	58963,87	1646,586	93,1
13	1	1	2	4	500	500	530	570	0,16	0,16	0,14	0,11	12	4,80E-03	2,602%	274,06	143,37	58989,68	1645,836	93,0
6	1	1	1	6	500	500	500	610	0,16	0,16	0,16	0,09	4	1,56E-03	2,758%	274,83	143,96	59322,45	1648,251	92,8
290	2	3	6	9	530	550	610	680	0,14	0,12	0,09	0,06	24	2,34E-03	65,071%	308,06	161,27	74532,90	1848,651	96,7
174	1	5	6	9	500	590	610	680	0,16	0,10	0,09	0,06	24	2,26E-03	65,297%	308,10	160,95	74552,60	1852,871	101,3
130	1	3	7	10	500	550	630	705	0,16	0,12	0,08	0,06	24	2,27E-03	65,524%	308,10	161,17	74556,75	1850,386	100,5
519	4	4	6	6	570	570	610	610	0,11	0,11	0,09	0,09	6	5,85E-04	65,583%	308,16	161,09	74583,98	1851,974	92,2
710	8	10	10	10	650	705	705	705	0,07	0,06	0,06	0,06	4	5,84E-05	99,985%	360,91	188,60	102301,49	2169,679	94,1
713	9	9	10	10	680	680	705	705	0,06	0,06	0,06	0,06	6	8,52E-05	99,994%	361,90	189,18	102867,19	2175,032	91,2
714	9	10	10	10	680	705	705	705	0,06	0,06	0,06	0,06	4	5,10E-05	99,999%	365,17	190,87	104730,96	2194,796	91,8
715	10	10	10	10	705	705	705	705	0,06	0,06	0,06	0,06	1	1,14E-05	100,000%	368,52	192,63	106662,48	2214,823	90,0

Figure 5-12: Constriction-size distribution for the 'most loose' packing.

- Constriction-size distribution the 'most dense' packing
  The constriction-size distribution for the 'most dense' packing depends also on the constriction-size per combination, the combinations possible, the probability of occurrence of a sphere and the definition of the constriction-size.

  o Constriction-size
    The constriction-size for the 'most dense' packing is defined by three spheres, see Figure 5-13.

Figure 5-13: Constriction-size for the 'most dense' packing for multi-sized spheres.

The red enclosed circle of Figure 5-13 is the constriction-size for the 'most dense' packing. The diameter of this circle can be found with the Descartes' theorem, see equation 5.13.

$$d_{k,m} = \left[\frac{1}{d_1} + \frac{1}{d_2} + \frac{1}{d_3} + 2 * \left(\frac{1}{d_1 d_2} + \frac{1}{d_1 d_3} + \frac{1}{d_2 d_3} \right)^{\frac{1}{2}} \right]^{-1} \qquad (5.13)$$

  o Combinations
    The combinations possible are calculated with equation 5.11. The constriction-size for the 'most dense' packing is defined by three spheres, so k=3. So for example, in case of 10 different sphere sizes the number of combinations possible is $\frac{(10+3-1)!}{3!(10-1)!} = 220$.

  o Configuration
    A combination can have several configurations. In case of three spheres:
    1,1,1 --> $\binom{3}{0}$= 1 configuration
    1,1,2 --> $\binom{3}{1}$= 3 configurations
    1,2,3 --> $\binom{3}{1}\binom{2}{1}$= 6 configurations

  o Probabilities of occurrence of a sphere
    The probability of occurrence is calculated with equation 5.12.

  o Overview constriction-size distribution 'most dense' packing
    Table 5-3 are the underlying values of Figure 5-14. In this figure the mass and number probability density functions are sketched and the constriction-size distributions for the 'most dense' packing.

Table 5-3: Constriction-size, combinations possible, configurations and probability of occurrence of a sphere lead to the constriction-size distribution for the 'most dense' packing.

number	combination			diameter grain/rock			CSD	Occurrence			Configurations	Probability	Cum. distr.
							76,76					0,00E+00	0,000%
1	1	1	1	500	500	500	77,35	0,16	0,16	0,16	1	4,33E-03	0,433%
2	1	1	2	500	500	530	78,85	0,16	0,16	0,14	3	1,09E-02	1,524%
3	1	1	3	500	500	550	79,79	0,16	0,16	0,12	3	9,76E-03	2,501%
11	1	2	2	500	530	530	80,39	0,16	0,14	0,14	3	9,16E-03	3,417%
4	1	1	4	500	500	570	80,69	0,16	0,16	0,11	3	8,77E-03	4,294%
12	1	2	3	500	530	550	81,37	0,16	0,14	0,12	6	1,64E-02	5,933%
5	1	1	5	500	500	590	81,56	0,16	0,16	0,10	3	7,91E-03	6,724%
56	2	2	2	530	530	530	81,99	0,14	0,14	0,14	1	2,56E-03	6,980%
13	1	2	4	500	530	570	82,30	0,16	0,14	0,11	6	1,47E-02	8,453%
20	1	3	3	500	550	550	82,36	0,16	0,12	0,12	3	7,34E-03	9,187%
6	1	1	6	500	500	610	82,39	0,16	0,16	0,09	3	7,16E-03	9,902%
57	2	2	3	530	530	550	83,00	0,14	0,14	0,12	3	6,88E-03	10,591%
7	1	1	7	500	500	630	83,19	0,16	0,16	0,08	3	6,50E-03	11,240%
14	1	2	5	500	530	590	83,20	0,16	0,14	0,10	6	1,33E-02	12,568%
21	1	3	4	500	550	570	83,32	0,16	0,12	0,11	6	1,32E-02	13,886%
216	8	10	10	650	705	705	106,09	0,07	0,06	0,06	3	7,53E-04	99,841%
218	9	9	10	680	680	705	106,46	0,06	0,06	0,06	3	7,33E-04	99,915%
219	9	10	10	680	705	705	107,75	0,06	0,06	0,06	3	6,57E-04	99,980%
220	10	10	10	705	705	705	109,06	0,06	0,06	0,06	1	1,97E-04	100,000%
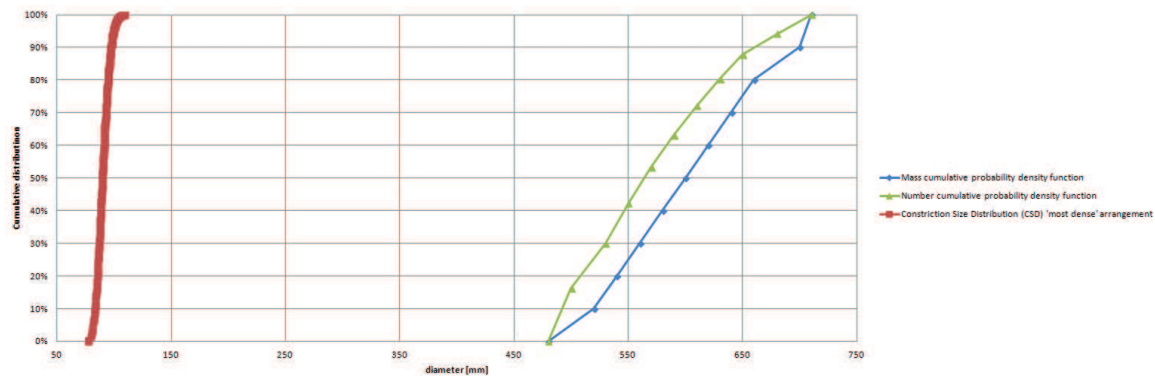
Figure 5-14: Constriction-size distribution for the 'most dense' packing.

- Overview of constriction-size distribution for multi-size spheres
  The constriction-size distribution can be derived with the formulas 5.6 t/m 5.13. The only input is a mass distribution of spheres, see Table 5-4. The output is the constriction-size distributions in Figure 5-15.

Table 5-4: Input parameters for construction size distribution.

Mass cumulative probability density	0%	10%	20%	30%	40%	50%	60%	70%	80%	90%	100%
Sieve size of sphere	480	520	540	560	580	600	620	640	660	700	710
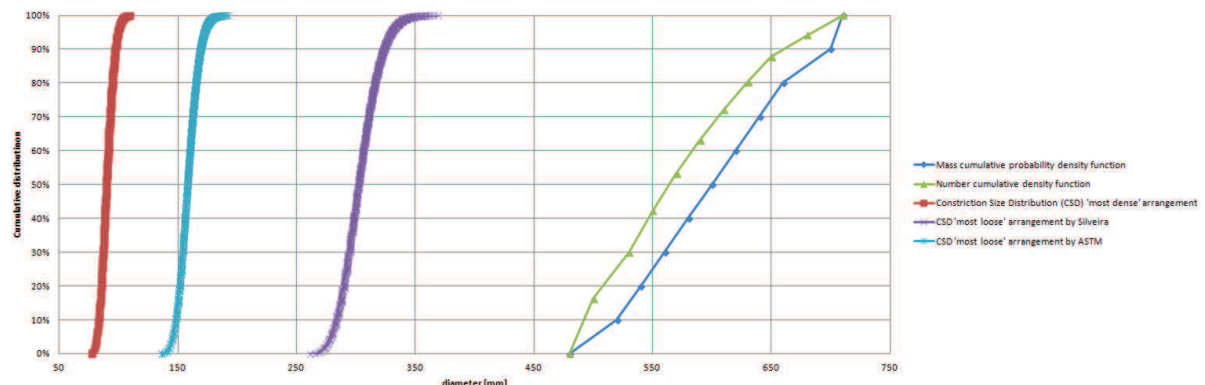
Figure 5-15: Constriction-size distributions for the 'most loose' and the 'most dense' packing.

To come to a general formula for the constriction-size distribution, the constriction-size distribution will be schematized with a curve fit (normal distribution), see Figure 5-16. The input is a stone-size distribution with a D50 of 25mm and a D85/D15 of 1.5.
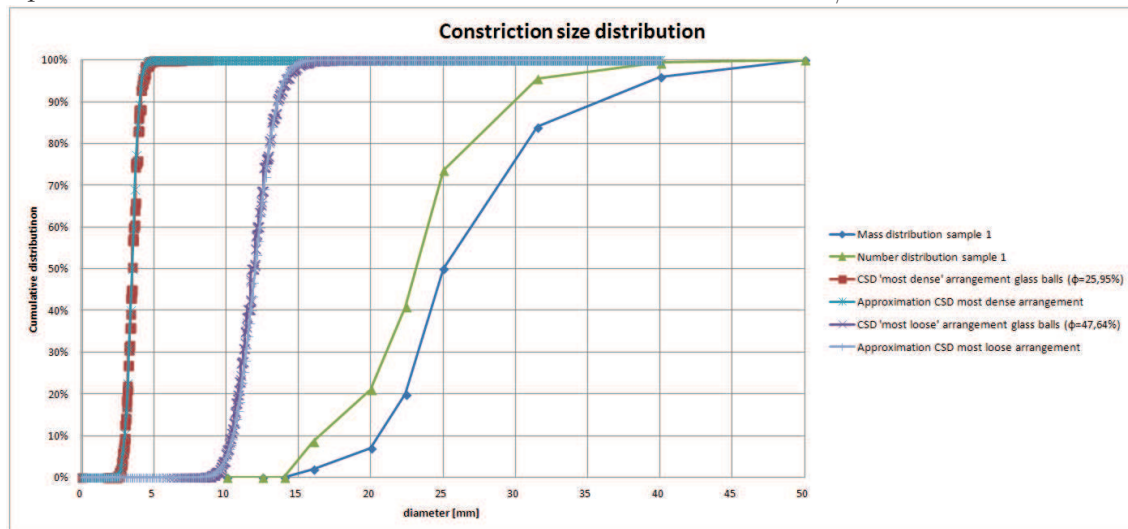
Figure 5-16: Curve fit of most dense and most loose arrangement of the CSD for D50=25mm and D85/D15=1.5.

The constriction-size distribution of the most dense arrangement is approximated with the normal distribution: N(3.5,0.4).
The constriction-size distribution of the most loose arrangement is approximated with the normal distribution: N(12,1.2).

The same trick is repeated for a stone-size distribution with a D50 of 25mm and a D85/D15 of 4. This is done to include the grading influences, see Figure 5-17.
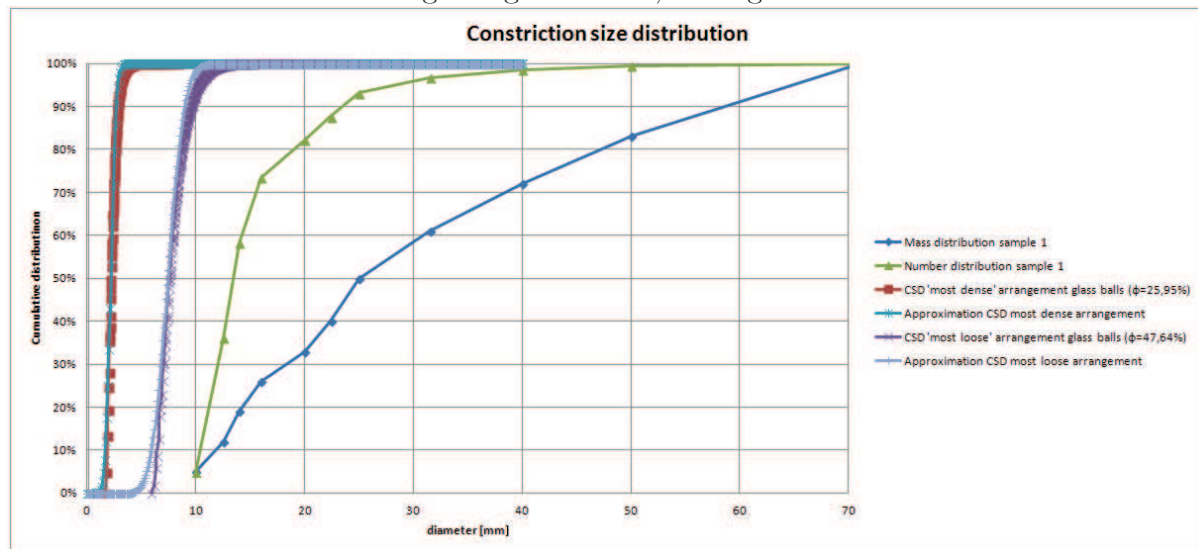
Figure 5-17: Curve fit of most dense and most loose arrangement of the CSD for D50=25mm and D85/D15=4.

The constriction-size distribution of the most dense arrangement is approximated with the normal distribution: N(2.2,0.4)
The constriction-size distribution of the most loose arrangement is approximated with the normal distribution: N(7.5,1.2)

To do an analysis based on these curve fit, the porosity has to be included. The porosity is for the most dense packing is assumed 25.9% and the porosity for the most loose packing is assumed 47.6%. The values are summarized in Table 5-5.

Table 5-5: Summarizing table of curve fits.

D85/D15=1.5	dense	loose
D50	25	25
mu	3.5	12
mu/D50	0.14	0.48
porosity	0.26	0.48
sigma	0.4	1.2
sigma/D50	0.016	0.048

D85/D15=4	dense	loose
D50	25	25
mu	2.15	7.5
mu/D50	0.086	0.3
porosity	0.26	0.48
sigma	0.4	1.2
sigma/D50	0.016	0.048

	dense	loose	Mean
mu/mu	0.614	0.625	0.62
D85/D15	1.5	4	
factor mu	1	0.62	

Based on this table two plots are made, see Figure 5-18 which results in equation 5.14.
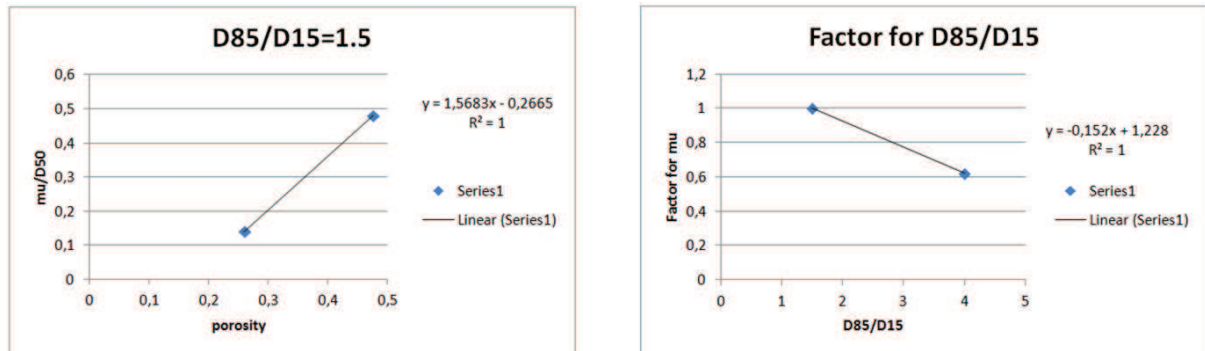
Figure 5-18: Plots to describe the mu of the constriction-size distribution.

$$\mu = (1.57 * \phi - 0.267) * D50 * \left(-0.152 * \frac{D85}{D15} + 1.23\right) \qquad [m] \qquad (5.14)$$

The assumption is made that the factor for sigma only depends on the D50 and the porosity, not on the grading. This relation is plotted in Figure 5-19 and stated in equation 5.15.
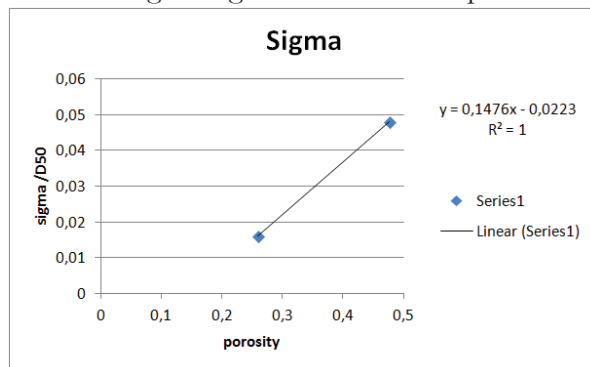
Figure 5-19: Plot to describe the sigma of the constriction-size distribution.

$$\sigma = (0.148 * \phi - 0.0223) * D50 \qquad [m] \qquad (5.15)$$

A quick indication of the constriction-size distribution for spheres can be obtained by filling in equation 5.14 and equation 5.15.

5.3   PORE-SIZE DISTRIBUTION

The pore size is the largest sphere that fits into the spheres of the packing.
- First of all the pore size is determined for mono-sized spheres for
  - 'Most loose' packing
  - 'Most dense' packing
- Secondly is explained why the pore-size distribution not can be derived.

5.3.1   Mono-sized spheres

- Cubic packing porosity
  The porosity is 47.6% as derived in section 5.2.

- Cubic packing pore size
  The pore size for cubic packing for uniforms spheres is 0.732D, see Figure 5-20 and equation 5.16.
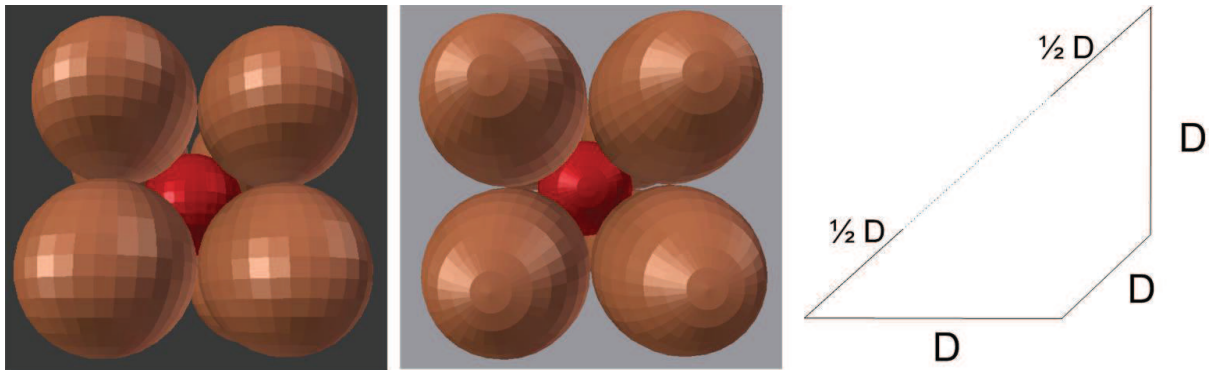
Figure 5-20: Pore size cubic packing.

$$d_{k,m} = Diagonal - 2 * \frac{1}{2}D = \sqrt{D^2 + D^2 + D^2} - 2 * \frac{1}{2}D = (\sqrt{3} - 1)D \qquad (5.16)$$

- Rhombohedral-hexagonal packing porosity
  The porosity is 25.9% as derived in section 5.2.

- Rhombohedral-hexagonal packing pore size
  The pore size for the rhombohedral-hexagonal packing is more difficult to derive. Two equation are derived based on Figure 5-21, see equation 5.17 and equation 5.18. The pore size for uniforms spheres is 0.22D. 'r' is the radius of the pore size and 'y' is the y-coordinate of the midpoint of the pore size.

$$r = \sqrt{\left(\frac{1}{3}\sqrt{3}D\right)^2 + y^2 D^2} - \frac{1}{2}D = \left(\sqrt{\frac{1}{3} + y^2} - \frac{1}{2}\right)D \qquad (5.17)$$

$$r = \sqrt{\frac{2}{3}}D - \frac{1}{2}D - yD \qquad (5.18)$$

After rewriting equation 5.17 and 5.18 the largest 'r' possible is established at r=0.1124. The associate 'y' is than y=0.2041.

The midpoint of the pore is at $\frac{1}{2}D + y = 0.7041$.

To validate the formula $\frac{1}{2}D + y + r$. must be $\sqrt{\frac{2}{3}}$, which is correct in this case.
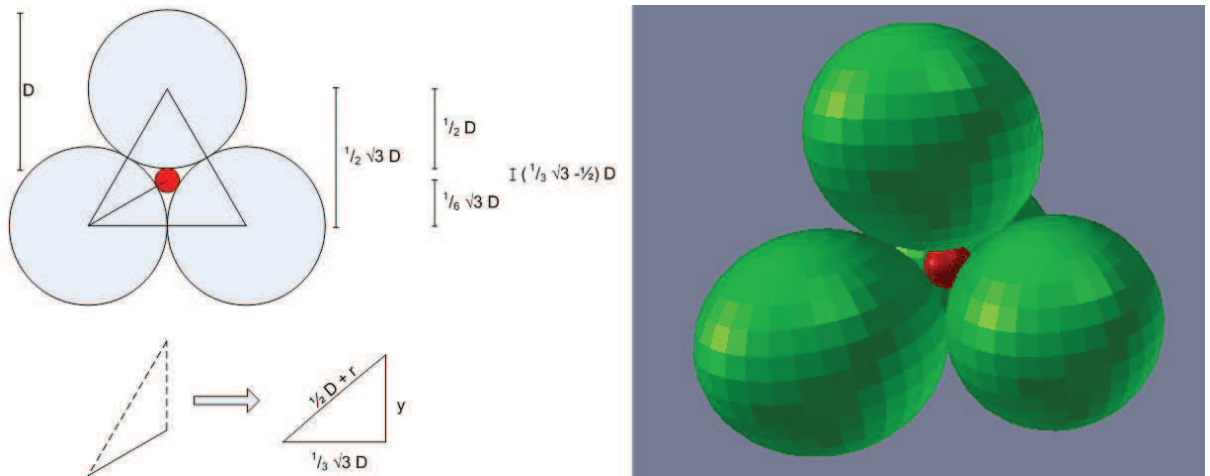
Figure 5-21: Pore size rhombohedral-hecagonal packing.

- Overview
  The pore size for uniform spheres is determined for the 'most loose' and 'most dense'
  packing, see Table 5-6. A linear relation is suggested between the pore size and the
  porosity for $0.259 < \phi < 0.476$. This relation is presented in Figure 5-22 and stated in
  equation 5.19.

Table 5-6: Overview of packing types, porosity, and pore size for mono-sized spheres.

Packing	Porosity [-]	Pore-size [m]
Cubic	47.64%	0.73 D
Rhombohedral-Hexagonal	25.95%	0.22 D
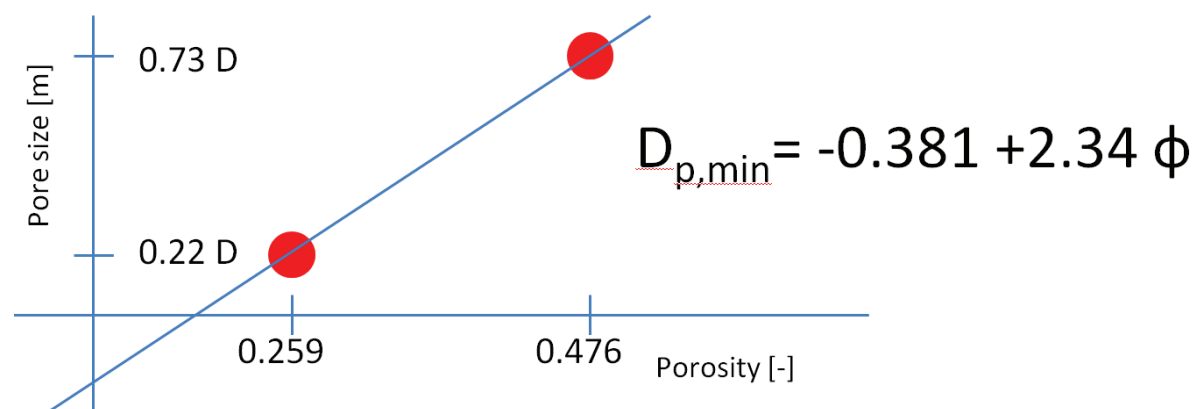
Figure 5-22: Relation between pore size and porosity.

$$Pore\ size = -0.381 + 2.34\ \phi \qquad [m] \qquad (5.19)$$

The relation in equation 5.19 is only valid for uniform spheres. In the next paragraph
is discussed why the author was not able to derive the pore-size distribution for
multi-sized spheres.

5.3.2   Multiple sized spheres

The arrangement of spheres for the cubic packing is visible in Figure 5-23 for the multi-sized spheres. It can be noticed that the left figure contains a floating sphere which is not realistic. In the right figure the floating sphere dropped down and this is the final arrangement of spheres. Therefore it is not possible to derive the pore-size distribution for multi-sized spheres. This also holds for the rhombohedral-hexagonal packing. To obtain the pore-size distribution a numerical or physical experiment has to be carried out, because geometrical calculations are not valid anymore due to the unknown packing.
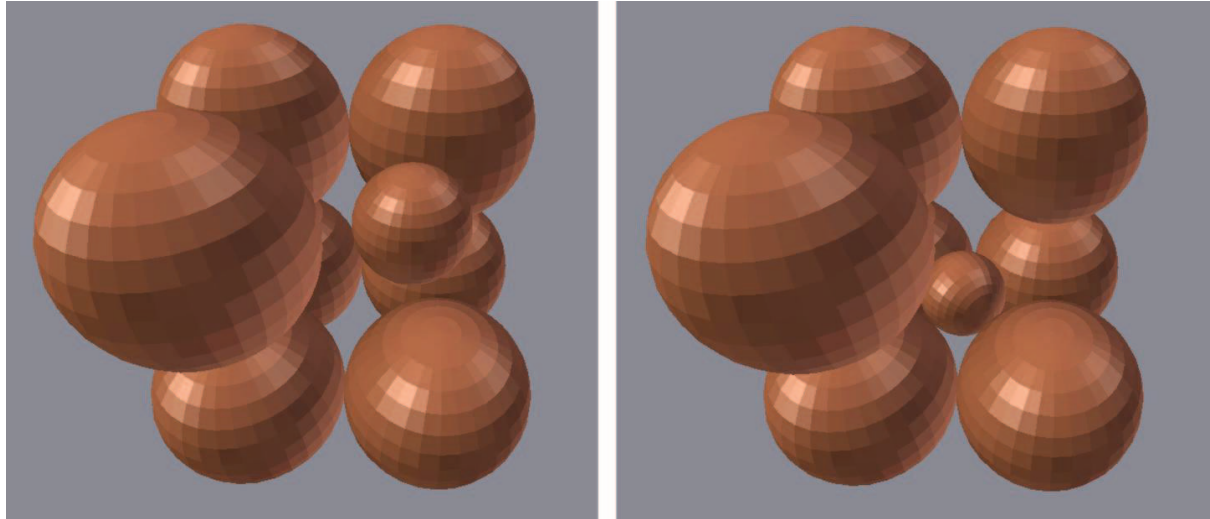
Figure 5-23: Result for packing due to multi-sized spheres.

6. EXPERIMENTAL APPROACH

In this chapter the experimental approach will be elaborated. A test scan is performed to identify the possibilities and limitations of the experiment. Based on this scan the experimental steps are described in section 6.1. The experimental model is validated in section 6.2. Based on the experienced possibilities and limitation of the model an experimental program is designed and executed. The results of this program are presented in section 6.4. In section 6.5 a general formula is found to describe the pore-size distribution. The constriction-size distribution found during the experiment is presented in 6.6. In the last section the additional findings are presented.

6.1 EXPERIMENTAL STEPS

The experiment is conducted with a medical CT scanner in the Geosciences lab of the Faculty of Civil Engineering and Geosciences. First a bucket of stones is filled. After scanning the bucket of stones with the CT scanner the image is analyzed with Avizo Fire. The data produced by Avizo Fire is processed in numbers and figures. This obtained data is analyzed to find relations. In the next subsections the following experimental steps are treated step by step based on the test scan:

- Input
- CT scanner
- Avizo Fire
- Output

Intermezzo: anecdote

The experiment is carried out by geosciences and the background of the author is civil engineering. The scale of accuracy of both worlds is of another magnitude. When the civil engineer is talking about 'pretty accurate', he is talking about a mm, cm, or sometimes a meter. However, 'pretty accurate' for a geoscientist is in the order of a µm. So when the author discussed the accuracy of the experiment with the geoscientist for executing the experiment it was an eye opener for both.

Secondly, the geoscientist most of the time analyze a natural samples. Therefore the geoscientist was very interested how to fill the bucket with stones and how to keep the stones in the 'right' position. However, the civil engineer creates artificial objects such as bed protection of stones. So placing the stones in the bucket (artificial) is simulating the reality. This was the second eye opener for the geoscientist.

6.1.1   Input

The input of the CT scan is a bucket of stones. The bucket is filled with stones of a certain stone-size distribution. This stone-size distribution is obtained by sieving and weighting stones (see section 6.3). This means, before scanning it is exactly know what is inside the bucket. There are a few practical issues for the input:

- The bucket has to be round and rotated 90 degrees (see Figure 6-1), because of undesired matrix effects.

- The bucket has to be aligned horizontal, vertical, and centered for an accurate scan and post-processing reasons.

- The maximum diameter of the bucket is limited, otherwise the X-radiation cannot penetrate entirely through the bucket. The resolution of the core of the bucket will be too poor.

- The CT scanner costs 7 euro per scan second and generates slices, see Figure 6-2. A smaller bucket (the height in upright position) is quicker to scan because less slices are needed. This reduces the costs. Moreover, if the volume of the bucket is decreased, the stone sizes in the bucket has to be reduced as well. Otherwise the number of stones (and pores) are too low from statistical point of view. In this case also less stones are needed to fill a smaller bucket which also reduces the costs. However, too small stones are not easy to sieve and less easy to handle. Making a sieve curve of small stones is hard and not accurate (scaling problems). Furthermore, the resolution of the CT scanner must be large enough, because otherwise the image analysis is not accurate and will contain large errors. Resolution means the number of voxels per stone. Therefore the stones may not be too small, because this results in too little voxels per stone (this will be treated in the next section). All those considerations have led to a sample bucket with a radius of 10 cm and a height of 15 centimeters and stones sizes of around a D_{50} of 25mm.

- Before closure of the bucket, the bucket is filled with paper. This paper is placed to prevent rolling of the stones if the bucket is rotated 90 degrees. The density of the paper is significantly different than the density of stones/air, so the paper is removed in the analysis by applying a threshold.

Figure 6-1: Input of test CT scan.

6.1.2   CT scan

CT scan stands for Computed Tomography (Lindner, 2015). This means making cross sections using the computer. In Figure 6-2 the working of the CT scanner is sketched.
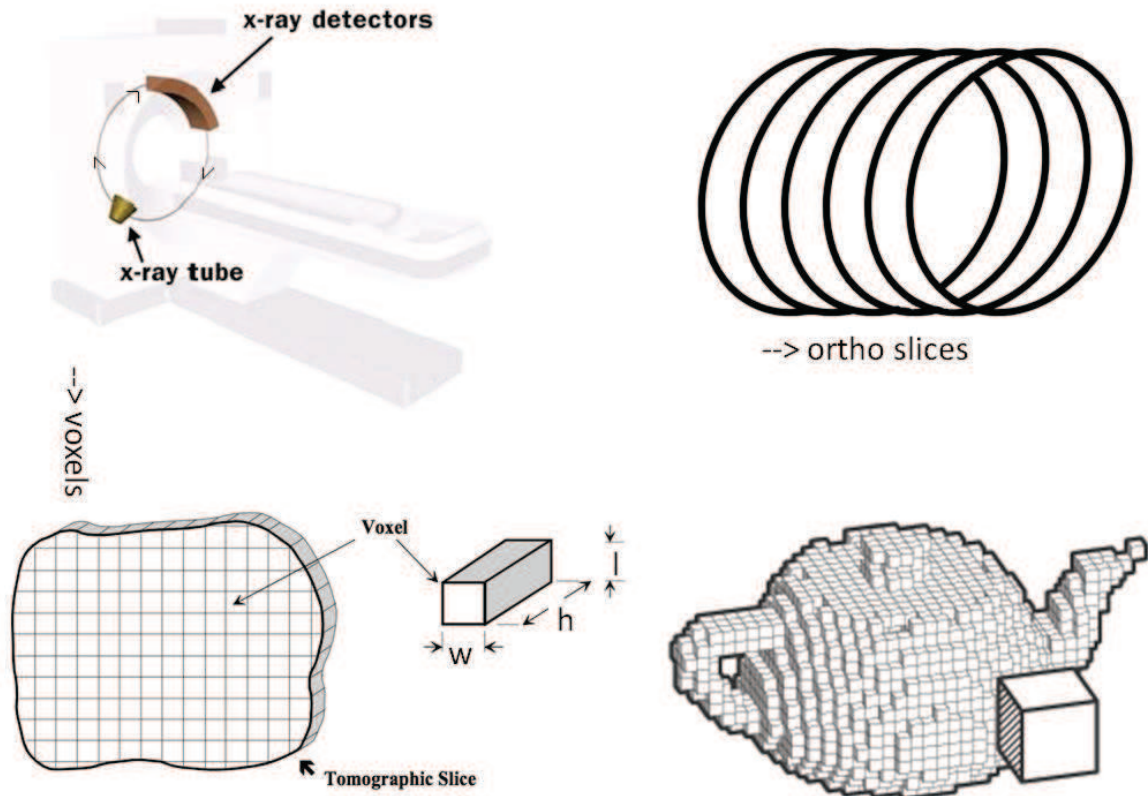
Figure 6-2: Working of a CT scanner.

The scan is made with X-radiation. The x-ray source (x-ray tube in Figure 6-2) and the x-ray detector rotate around the sample (which is normally a human body). The x-ray tube transmits X-radiation which penetrates through the sample/body and received by the detector.

The X-radiation is weakened due to the sample. The magnitude of weakening (received by the detector) is determined by the densities within the sample. The difference in densities is converted in shades of gray which forms the image. The sample consists of slices and is computed in voxels. The voxel size is 0.48 x 0.48 x 1mm. This means that the slices are generated every 1mm.

Intermezzo: anecdote

The used CT scanner is a medical CT scanner and the settings are not changed. This means that every sample has to be classified in a man or woman. Moreover, the amount of X-radiation (mSv) is limited per scan. The exposure time of persons are limited and therefore this is also the case for scanning stones. So, if the amount of X-radiation is higher per second, the maximum scanning time is reduced to stay within the limits of the maximum mSv.

6.1.3   Imaging analysis

The generated data with the CT scanner is analyzed with Avizo Fire 8.01. An algorithm connects all the slices and creates a 3D picture. A volume is edited/selected which will be analyzed. On this volume a threshold of gray patterns is applied. In this way only pores (or only stones) can be selected. The pores are separated with a mathematical operations and all the separated pores are labeled. These followed steps to analyze the image are sketched in Figure 6-3.
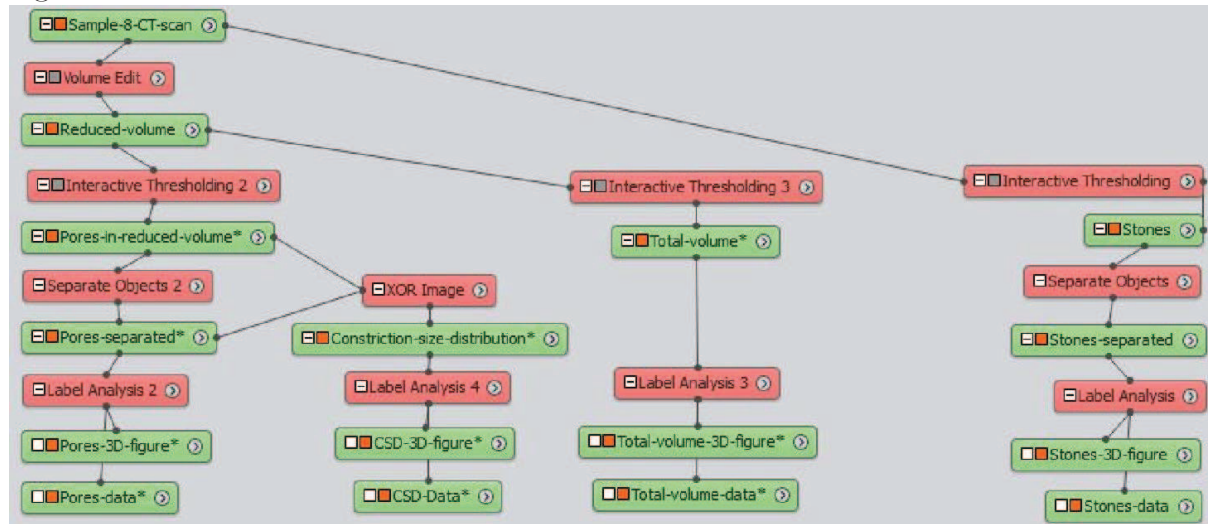
Figure 6-3: Steps of imaging analysis .

All the steps in Figure 6-3 are treated in detail below.

1. Loading CT scan data

The result of a CT scan is a set of slices in a xy-plane. The first step is loading these slices and connect the slices to a 3D object. This 3D object is generated by an algorithm which computes the xz-plane and the yz-plane, see Figure 6-4. This is a mathematical operation of voxels.
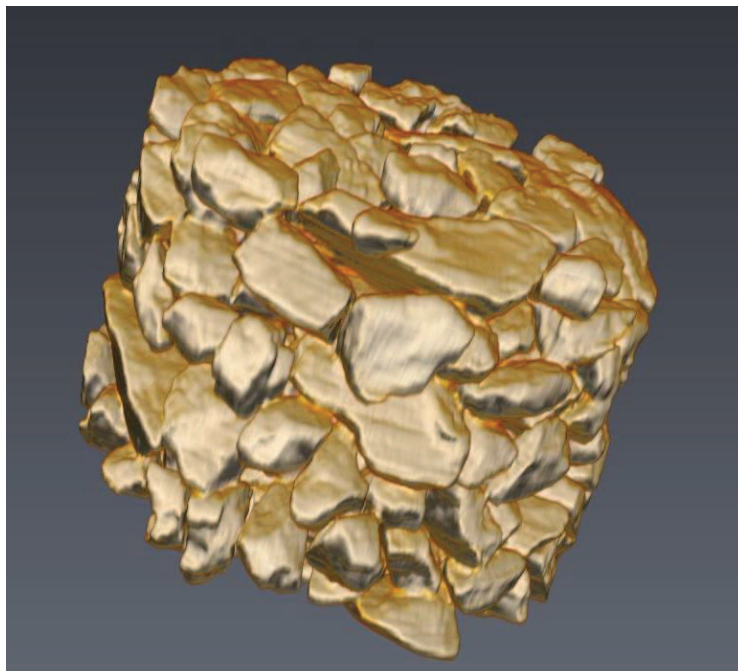
Figure 6-4: Render of the volume of the CT scan.

2. Select volume

The volume of the bucket can be edited, see Figure 6-5. By editing the volume of the bucket the error at the boundaries is solved. The volume should not be too small, otherwise some stones of the sieve curve are neglected.
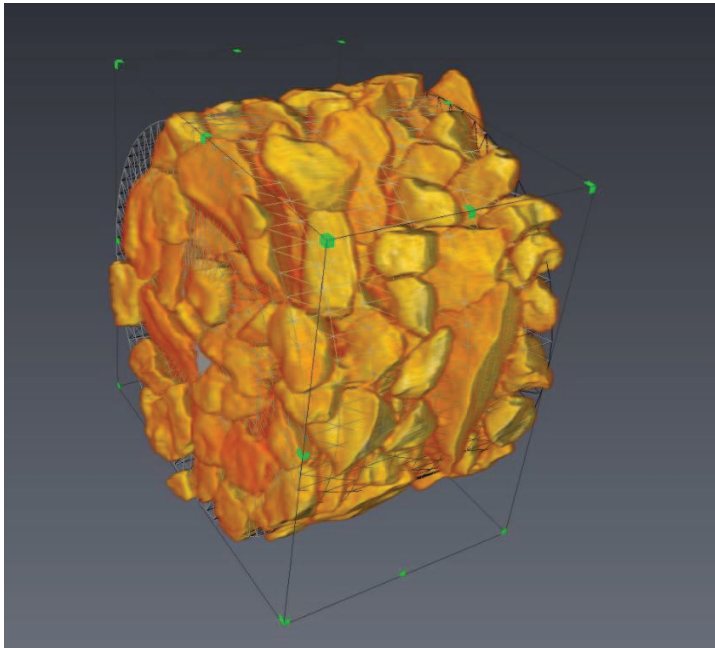
Figure 6-5: Edit volume of image.

3. Threshold

A threshold is applied on the gray patterns, see the red box in Figure 6-7. The area between 617 and 3071 contains the gray patterns of the stones. The values between -1775 and 617 contains the gray patterns of the pores. By applying the threshold between -1775 and 617 the pores becomes blue and the stones become gray, see Figure 6-6.
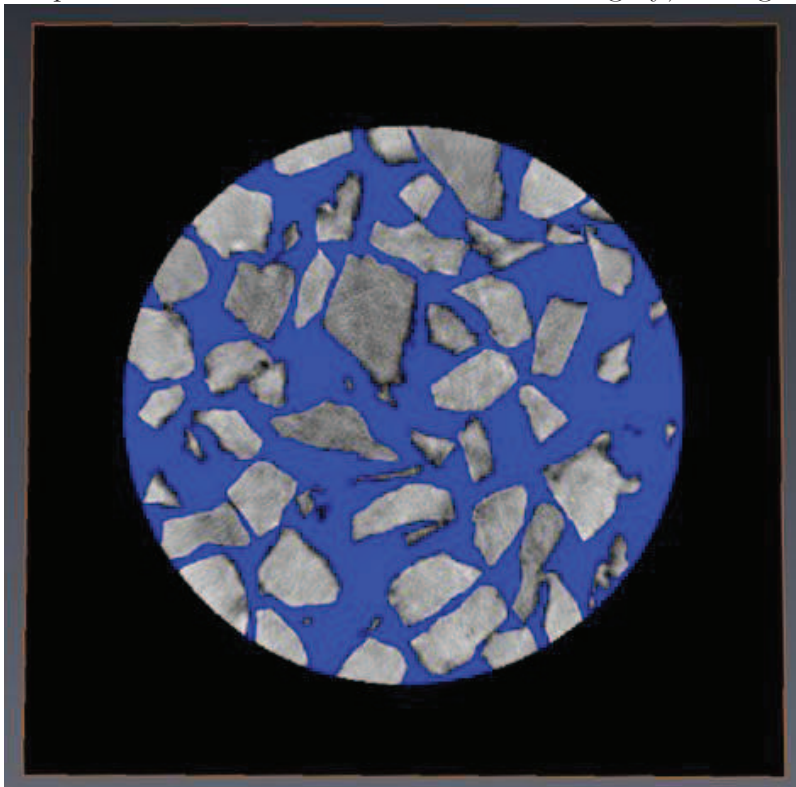
Figure 6-6: Threshold stones of image.
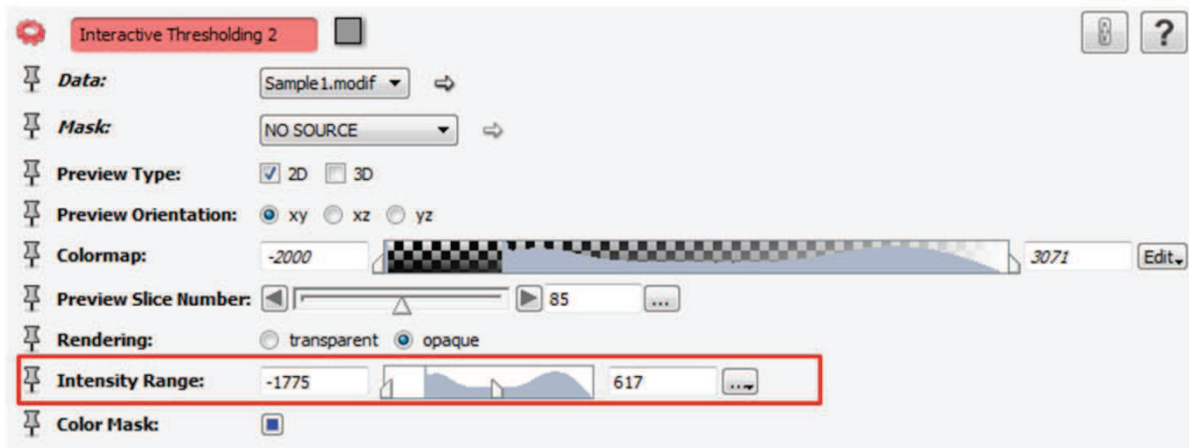
Figure 6-7: Threshold settings.

4. Separate objects

The next step is to separate the pores which is done with the command *bin separate*. The pore area (actually it is a volume, but it is 2D presented) is blue and separated by the black lines, see Figure 6-8. In fact, the black lines are also a volume.
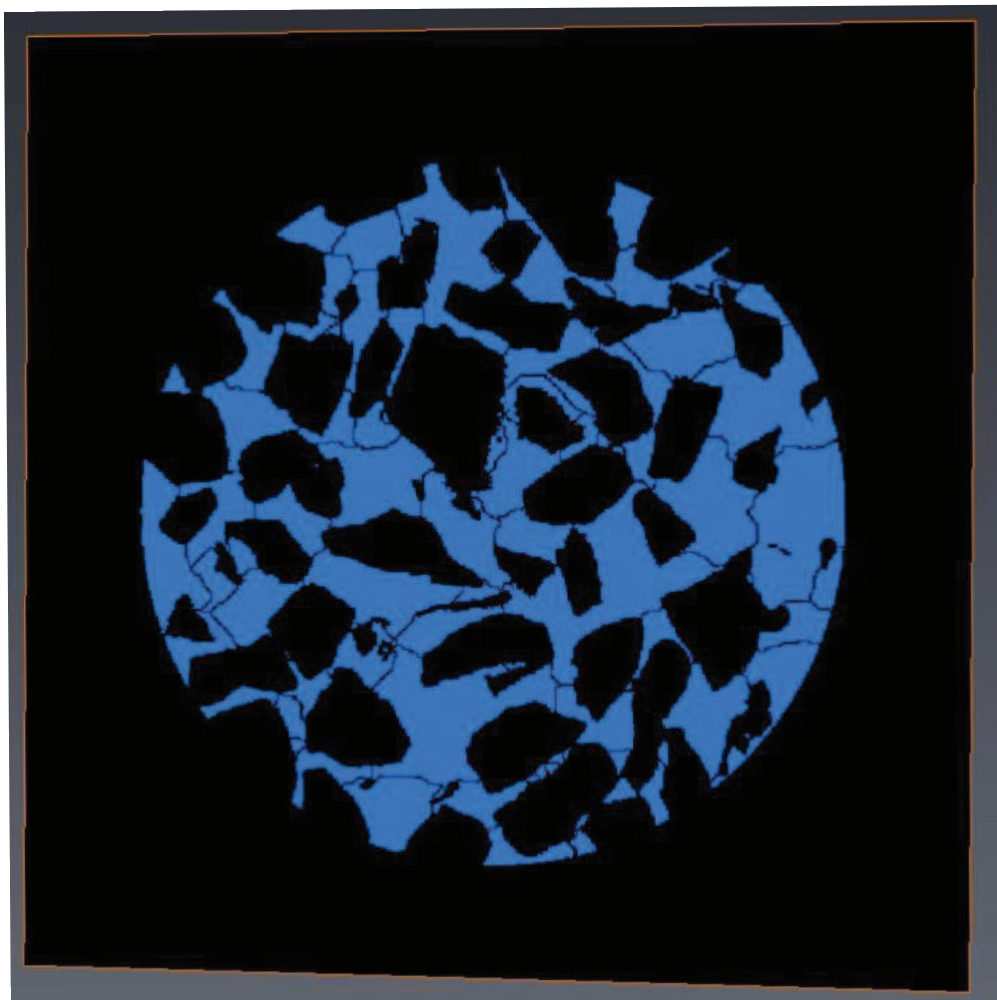
Figure 6-8: Separate pores of image.

How does bin separation work? This is illustrated in Figure 6-9. The outer layer of voxels will be eroded. If the voxels are cut loose, Avizo will 'remember' this. The last step is the

dilatation and the pores grow back to their original size and shape. Only one row of voxels is stored as separation volume.
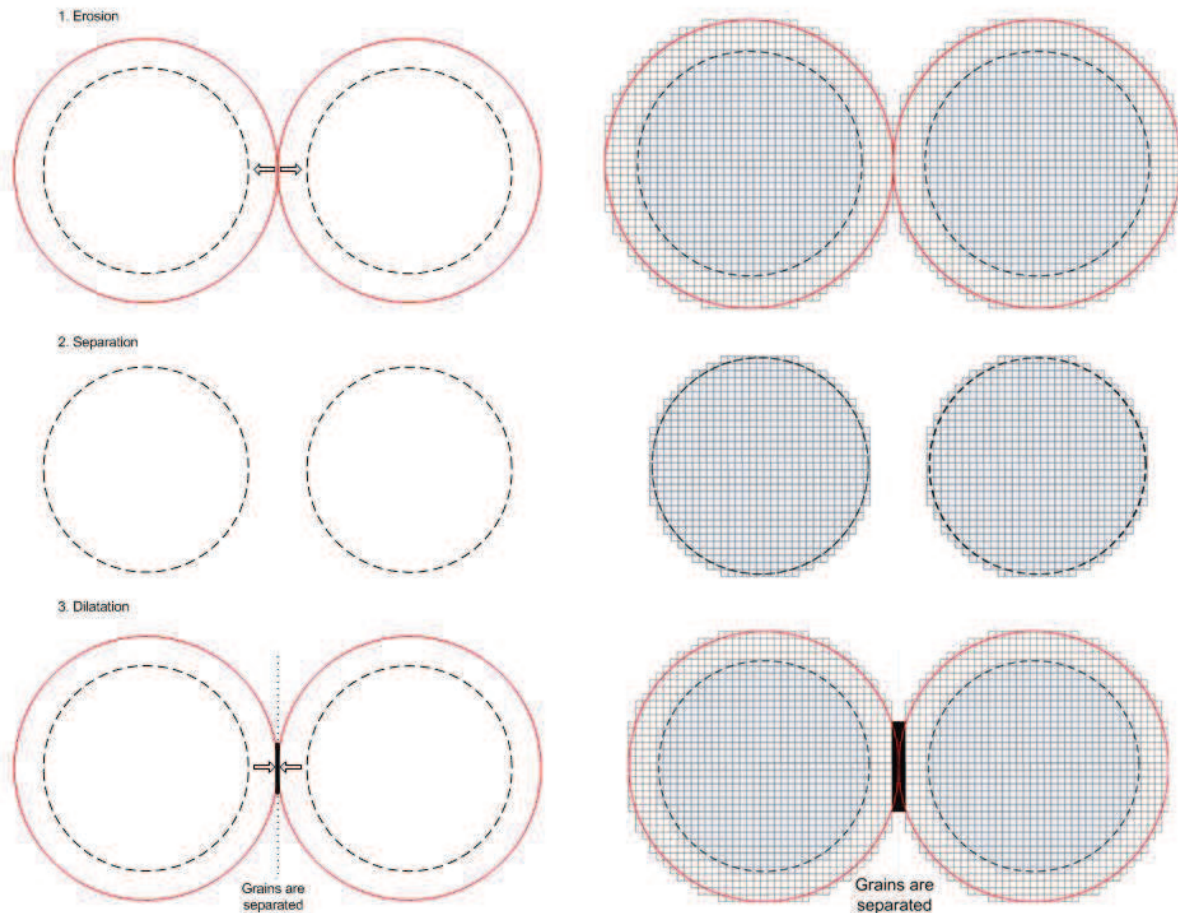
Figure 6-9: Steps of separating pores.

Resolution has a large influence on the separation of pores. In Figure 6-9 the resolution is high and the separation of the image (which still is a mathematical operation of voxels) is possible and accurate. In Figure 6-10 an example if given of a poor resolution. Avizo 'sees' not the two red circles, but the voxels in the lower right corner of Figure 6-10. Mathematical operations are hard to perform. To increase the resolution, the voxels needs to be smaller or the pores need to be bigger.
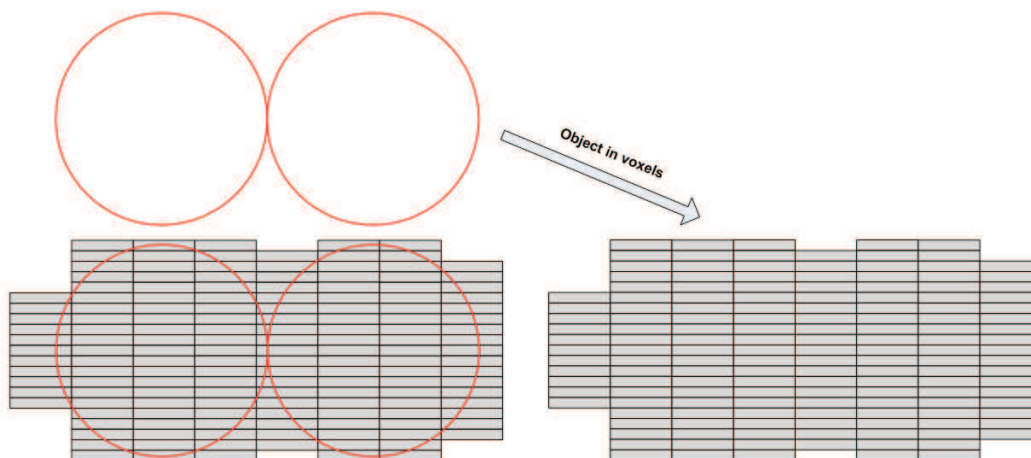
Figure 6-10: Example of poor resolution.

<u>5. Label pores</u>

After the pores are separated the pores are labeled. Labeled means that the different pores are recognized and numbered. All the pores get a color, see Figure 6-11. The properties of all the pores are measured separately.
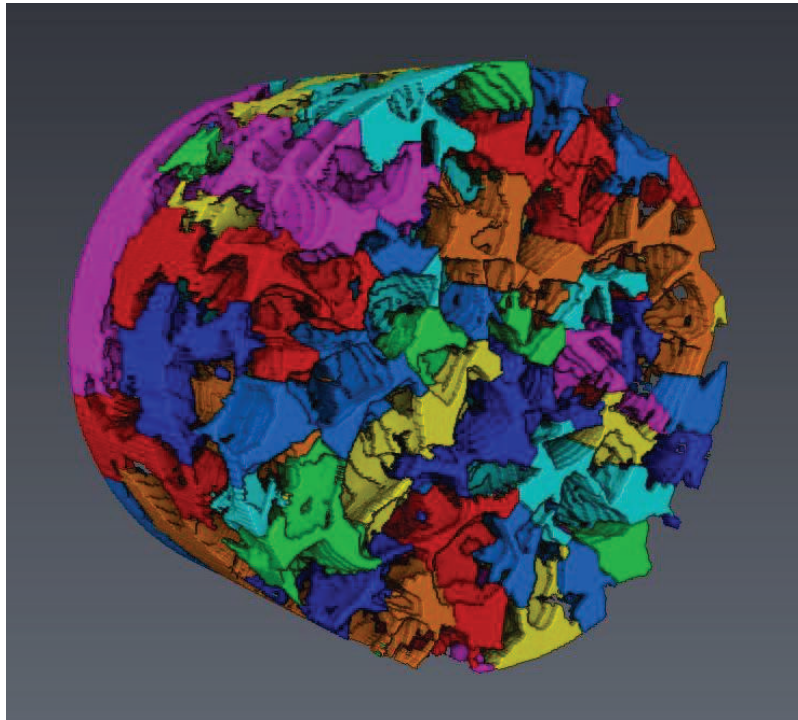
Figure 6-11: Label pores of image.

<u>6. Exclusive or operation --> constriction-size</u>

The XOR operation measures the difference between the result of step 3 *threshold* and the result of step 4 *separation*. The difference between step 3 and step 4 is the separation lines/volumes. This are the constriction-sizes or openings, see Figure 6-12.
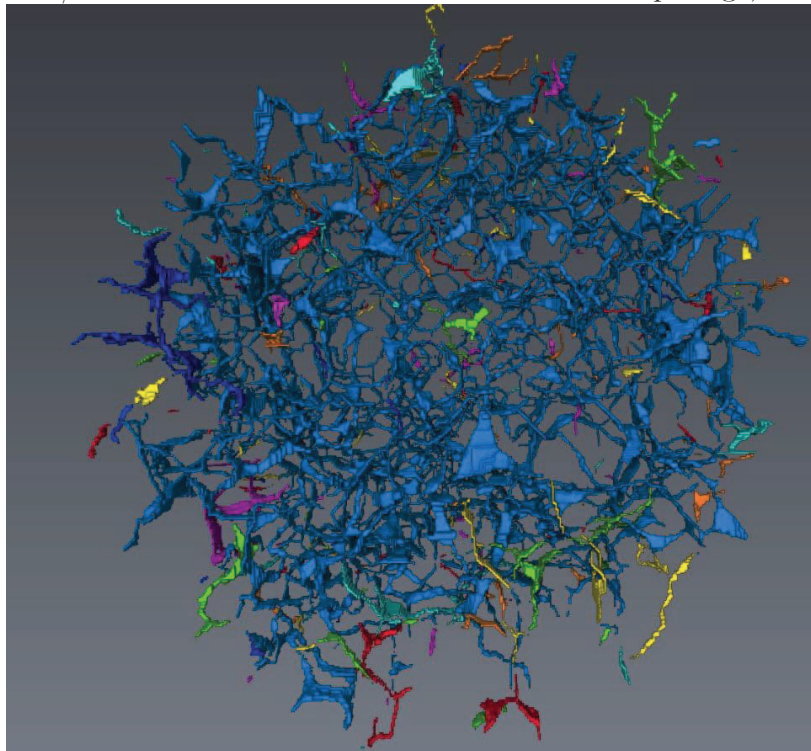
Figure 6-12: Constriction-sizes of the stones.

6.1.4 Output

The output of the image analysis is the number of pores and per pore the following properties are measured:

- Coordinates
- Volume
- Area3D
  Total outside surface.
- Shape
  The shape is defined as equation 6.1. This means that the shape of a sphere is 1 and a shape of a cube is almost 2.

$$Shape = \frac{Area3D^3}{36*\pi*Volume^2} \qquad (6.1)$$

- Length of pore
  This is the maximum feret diameter.

These properties are also obtained for the constriction-sizes (opening). The constriction-size is thus a volume (!), see Figure 6-13. The magnitude of the volume depends on the direction of the voxel relative to the constriction direction, because the voxel is not a cube but a beam! The minimal voxel size of the used medical CT scanner is l = w = 2*h.
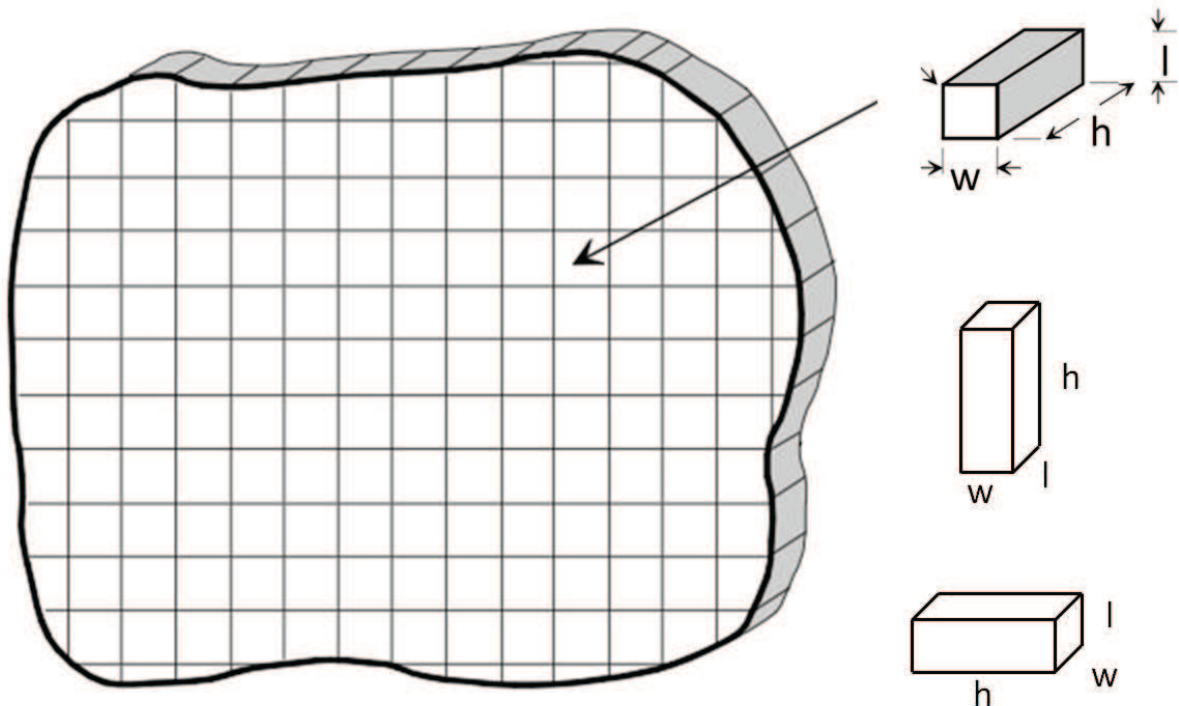
Figure 6-13: Sketch of construction size distribution.

For example: assume that the constriction volume of Figure 6-13 is 100 mm³ and that l = w = 2*h. If the voxel direction is 90 degrees rotated relative to the constriction, the volume of the constriction is reduced to 50mm³. Thus volume is not a representative indication of the constriction-size.

Another output parameter is the area3D. This is a more representative parameter for the constriction-size, but also the voxel direction relative to the constriction influence the magnitude, but not as strong as the volume output.

6.2   VALIDATION OF MODEL

The experimental model is validated with the analytical model. In chapter 5 is determined what the porosity and the pore size are for the cubic packing of uniform spheres. These geometrical determined values are compared with the experimental results for a sample of cubic packed uniform spheres. This sample is made with glass balls, see Figure 6-14.

Figure 6-14: Sample of cubic packed uniform spheres.

The first images of the CT scan are presented in Figure 6-15. By comparing Figure 6-14 and Figure 6-15 the scan seems to be successful. However, it is not about the image, it is about the produced data.
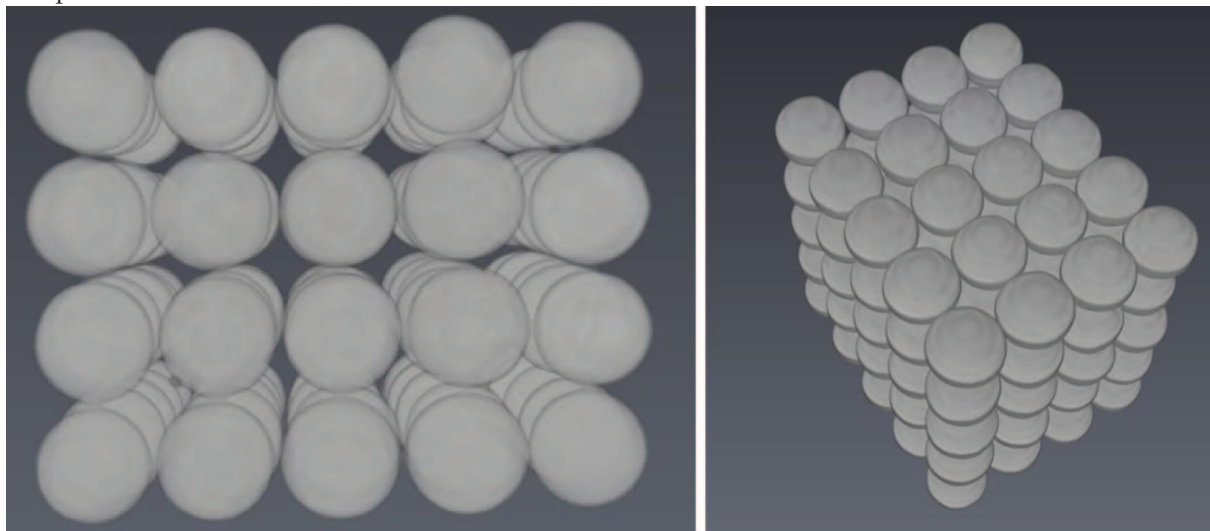
Figure 6-15: Image of the results of the test scan.

6.2.1   Input

The input of the scan is:
- 100 glass balls
- 25 mm (on the label of the manufacturers)
- Cubic packing of spheres

6.2.2   Scan and imaging analysis

First a scan is made with slices of 3 mm, see left image of Figure 6-16. It is visible that the resolution of the right scan (1mm) is higher.
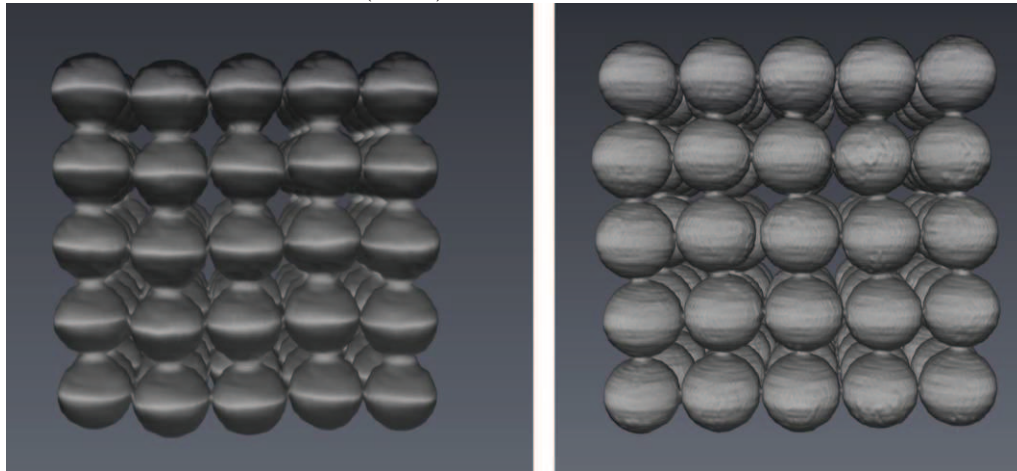
Figure 6-16: Image of validation scan with 3mm (left) and with 1mm (right).

The scan is analyzed by applying a threshold, separating the spheres and labeled the spheres. The result of the low resolution (3mm) is visible in Figure 6-17. The spheres are separated in the xy-plane, but in the due to the low resolution in z-direction the pores are not separated in yz-plane and xz-plane. Only 20 of the 100 spheres are recognized by the software. The spheres in xy-plane are all 'recognized', but in z-direction the spheres on top of each other are 'seen' as one sphere.
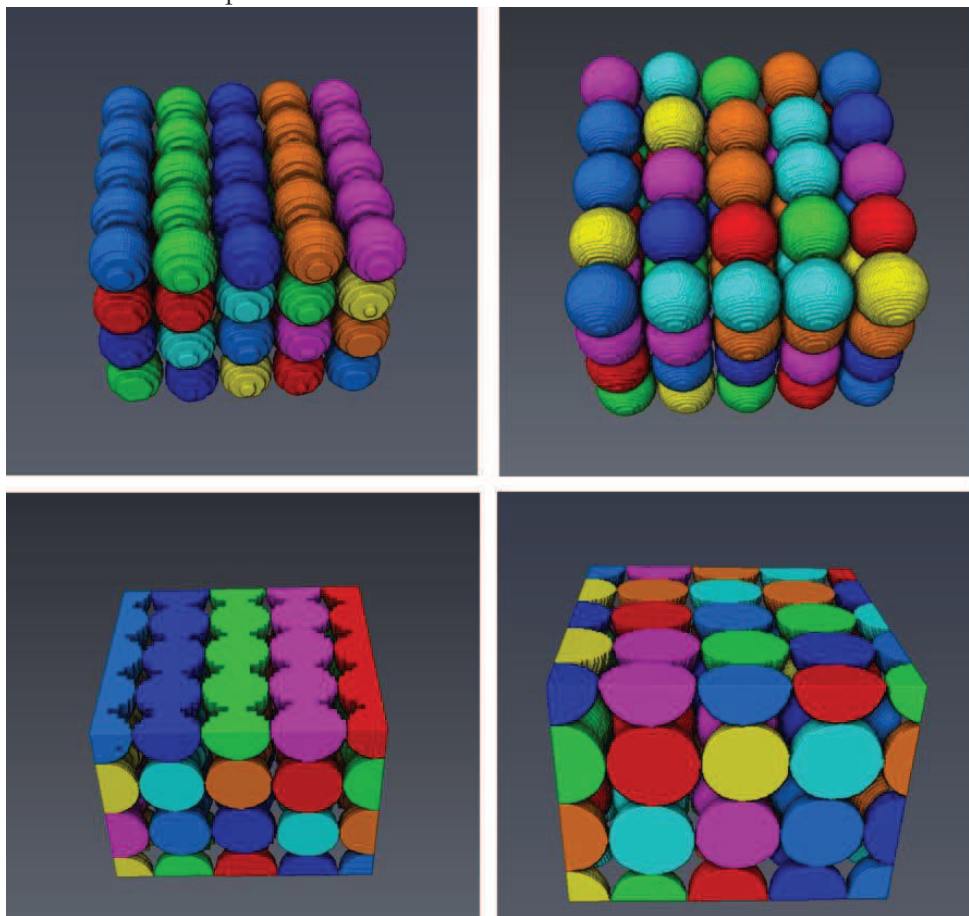
Figure 6-17: Image of validation scan after separation of spheres with slices of 3mm (left) and 1mm (right).

6.2.3   Output

The outcome of the CT scan and analysis is presented in Table 6-1 and in Figure 6-18. This is for the CT scan with slices of 1mm.

Table 6-1: Outcome of 1mm validation scan.

		Analytical	Experimental
Number of spheres	[-]	100	100
Sphere diameter	[mm]	25	25.0 ± 0.42
Number of pores	[-]	48	48
Volume of one pore	[mm^3]	7444	7270 ± 240
Porosity	[-]	0.476	0.470
Number of constriction-sizes	[-]	104	102
Construction size	[mm^2]	134	139.0 ± 5.8

The analytical model calculates the exact values of the cubic packing of 100 spheres. This is based on the ideal situation. The 'real' scanned sample of cubic packed spheres is packed by the author and therefore close to the ideal situation, but not exactly. This results in a small error. Furthermore, the spheres are manufactured and have not exactly the same size and shape.

The experimental model contains a range of values which is presented as a normal distribution. This is also the reason that an exact error cannot be identified for the sizes, volumes, and porosity. For the number of spheres, the number of pores, and the number of construction sizes an exact error is computed. Overall the conclusions can be drawn that the results are very accurate.
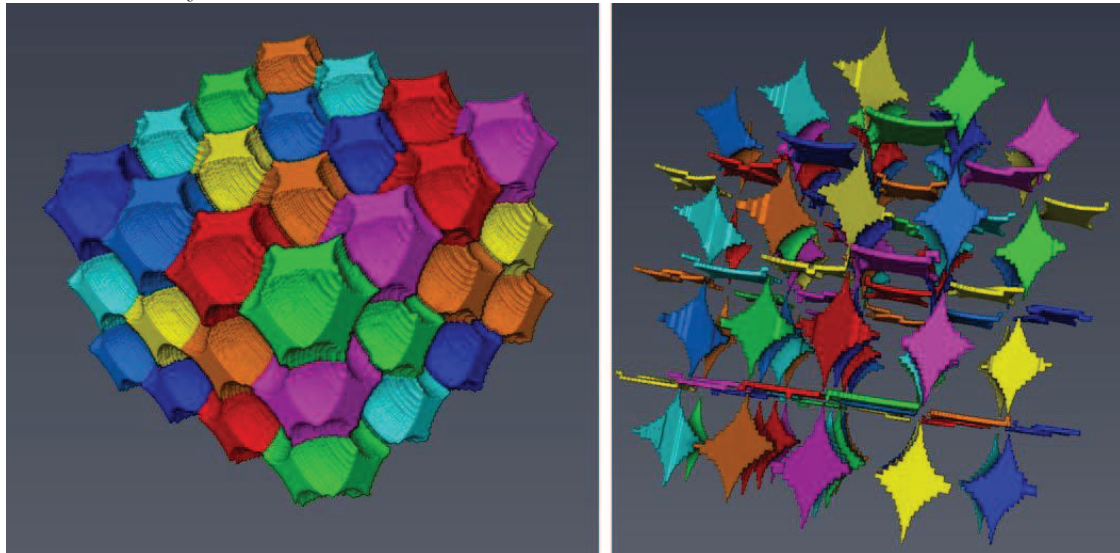
Figure 6-18: Pores (left) and constriction-sizes (right) of validation scan.

6.2.4   Conclusions of validation

The resolution is of importance for the accuracy of the output of the scan. The spheres are most unfavorable packed for the software to identify the different spheres. Despites this all the spheres are observed during the imaging analysis. The conclusion can be drawn that slices of 1mm are accurate for spheres of 25 mm and that slices of 3mm are not accurate for spheres of 25mm.

6.3   EXPERIMENTAL PROGRAM

In the test scan the possibilities and limits are identified and the validation scan gives confidence about the outcome of the results. Therefore an experimental program is designed and executed. The program is discussed in the next subsection. In subsection 6.3.2 the method to make the samples is explained, followed by the settings of Avizo Fire. In section 6.4 the results of the experimental program is elaborated.

6.3.1   Experimental set up

The goal is to derive the pore-size distribution and the constriction-size distribution for the following parameters:
- D_{50}
- D_{85}/D_{15}
- Porosity
- Shape

To find this relation 10 test scan are designed. An overview is given in Table 6-2.
- The first three scans are made of one bucket with the same stones (sample 1, 8, and 9). Between the scans the bucket is emptied, the stones are mixed, and the bucket is filled again. For the first scan the bucket is not compacted. For the second scan the bucket is shaken a bit to compact the stones (lower porosity). In the third scan the stones are even more compacted. The shape of the stones, the grading, and the D_{50} of the stones is the same. Only the porosity is variable.
- In the next three scans (sample 5, 6, and 7) the D_{50} is the variable parameter. The three buckets are filled with a other D_{50} while keeping the grading constant. The shape is assumed constant. The difference in porosity can be correct because this relation is known.
- In scan 2, scan 3, and scan 4 the D_{50} is kept constant and the grading (D_{85}/D_{15}) is the variable parameter. The shape is assumed constant and difference in porosity can be corrected.
- The last scan is made of a bucket with another material. The bucket is filled with gravel instead of the quarry material in the first 9 scans.

Table 6-2: Overview of experimental samples.

Sample	D50	D85/D15	Material	Packing/porosity	Purpose			
					Porosity	Stone size	Stone grading	Stone shape
1	25	1.5	Quarry run	Loose	■			
2	25	2	Quarry run	Compaction			■	
3	25	1	Quarry run	Compaction			■	
4	25	4	Quarry run	Compaction		■		■
5	15	1.5	Quarry run	Compaction			■	
5	35	1.5	Quarry run	Compaction		■		
6	45	1.5	Quarry run	Compaction		■		
8	25	1.5	Quarry run	Semi loose	■			
9	25	1.5	Quarry run	Compaction	■		■	
10	15	1.5	Gravel	Compaction				■
					3	4	4	2

The stone-size distributions of the table above have been established by finding an optimum between:
- Sieve sizes available
- Stones available
- Costs of stones

- Number of stones in bucket for statistical analysis
- Costs of CT scanner
- Resolution of CT scanner

6.3.2   Making samples

The designed stone-size distributions are mainly determined by the available sieve sizes. The following steps are executed to make the 10 samples that can be scanned.

1. Buy stones

The stones are bought in three available classes:

- 8 - 16mm
- 16 – 32 mm
- 40 – 80 mm

More stones [kg] are bought to guarantee there are sufficient stones in every bin after sieving.

2. Sieve stones

The were 14 sieve sizes available at Boskalis Dolman. Most sieves fit in the automatic sieving machine, but also a few hand sieves are used. The stones are sieves and sort in bins, see Figure 6-19.

Figure 6-19: Compilation of sieve process.

3. Fill buckets

The stone-size distribution is determined based on the sieve sizes. The stone-size distribution is designed by filling in the yellow cells of Table 6-3. If the stone-size distribution is designed, the bucket has to be filled with the values which are automatically calculated in the dark green cells. Per stone class the bucket is filled, see Figure 6-20. The total weight of the added stones per class has to be filled in the blue cells. The table is based on the formulas in chapter 4.

Table 6-3: Overview of stone-size distribution and weights needed per class.

Sample 1																
Designed grain distribution																
Sieve sizes [mm]	7,1	10	12,5	14	16	20	22,4	25	31,5	40	50	63	71	90		
Stone classes		[7,1-10]	[10-12,5]	[12,5-14]	[14-16]	[16-20]	[20-22,4]	[22,4-25]	[25-31,5]	[31,5-40]	[40-50]	[50-63]	[63-71]	[71-90]		
mean stone class	7,1	8,55	11,25	13,25	15	18	21,2	23,7	28,25	35,75	45	56,5	67	80,5	90	
Mass distribution																
Mass probability density		0%	0%	0%	2%	5%	13%	30%	34%	12%	4%	0%	0%	0%		
Mass cumulative probability density		0%	0%	0%	2%	7%	20%	50%	84%	96%	100%	100%	100%	100%		
Number distribution																
number of stones		0,00E+00	0,00E+00	0,00E+00	5,93E-06	8,57E-06	1,36E-05	2,25E-05	1,51E-05	2,63E-06	4,39E-07	0,00E+00	0,00E+00	0,00E+00		6,88E-05
p (number of stones)	0%	0%	0%	0%	9%	12%	20%	33%	22%	4%	1%	0%	0%	0%	0%	
P (number of stones)	0%	0%	0%	0%	9%	21%	41%	74%	96%	99%	100%	100%	100%	100%	1,00	

D50	25,0
D85	32,2
D15	21,5
D85/D15	1,50

What is (needed) in the bucket															
Stone classes		[7,1-10]	[10-12,5]	[12,5-14]	[14-16]	[16-20]	[20-22,4]	[22,4-25]	[25-31,5]	[31,5-40]	[40-50]	[50-63]	[63-71]	[71-90]
Amount needed in bucket [kg]		0,000	0,000	0,000	0,150	0,375	0,974	2,248	2,548	0,899	0,300	0,000	0,000	0,000	7,493
Cumulative amount needed in bucket [kg]		0,000	0,000	0,000	0,150	0,524	1,499	3,746	6,294	7,193	7,493	7,493	7,493	7,493	
Amount possible in bucket		OK	OK	OK	OK	OK	OK	OK	OK	OK	OK	OK	OK	OK	
Really added in bucket [kg]		-	-	-	150,00	526,00	1.500,00	3.749,00	6.292,00	7.203,00	7.484,00	-	-	-	7484,00
Mass probability density		0%	0%	0%	2%	5%	13%	30%	34%	12%	4%	0%	0%	0%	
Mass cumulative probability density		0%	0%	0%	2%	7%	20%	50%	84%	96%	100%	100%	100%	100%	
number of stones		0,00E+00	0,00E+00	0,00E+00	5,94E-06	8,61E-06	1,37E-05	2,26E-05	1,51E-05	2,66E-06	4,12E-07	0,00E+00	0,00E+00	0,00E+00	6,89E-05
p (number of stones)	0%	0%	0%	0%	9%	12%	20%	33%	22%	4%	1%	0%	0%	0%	0%
P (number of stones)	0%	0%	0%	0%	9%	21%	41%	74%	96%	99%	100%	100%	100%	100%	1,00

D50	25,0
D85	32,1
D15	21,5
D85/D15	1,50
Stone density	2650 [kg/m^3]
Weight W50	0,02 [kg]
Volume	4,71 [L]
Estimated porosity in bucket	40% [-]
Estimated stone volume	2,83 [L]
Weight of bucket	7,49 [kg]
Estimated stones in bucket	328 [-]
Estimated stones in bucket	309 [-]
Count stones	309 [-]

Grain distribution (chart: Mass cumulative probability density; Mass probability density)
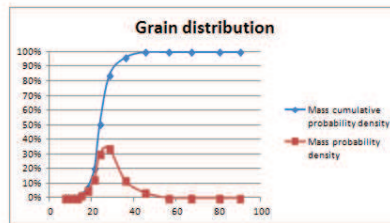
Figure 6-20: Filling the bucket with a specified stone-size distribution.

4. Wash stones

In principle the buckets are ready to scan. However, to increase the accuracy the stones are washed to remove the dust.

5. Dry stones

Wet stones can give errors during scanning. After washing the stones, the stones are dried with a towel and above a heater.

6. Fill buckets again

The buckets are filled again and transported to the CT scanner at the TU Delft.

Figure 6-21: Washing, drying, and transporting.

6.3.3   CT scan

The settings of the CT scanner are:
- Voxel size is 0.48 x 0.48 x 3 mm

The settings of Avizo Fire are:
- Threshold values
    - Pores: gray value between -1775 and 617
    - Stones: gray value between 617 and 3071
- Bin separate
    - Method: Chamfer – Conservative
    - Interpretation: 3D
    - Neightborhood: 26
    - Marker Extent: 1
    - Output type: split
    - Algorithm mode: repeatable

6.4   PORE-SIZE DISTRIBUTION RESULTS

In this section the results of the experiment will be presented, while in the next section the results will be discussed and relations are elaborated. The results are also depicted in appendix A.

The result of the experiment is the pore-size distribution. The pore-size distribution can (just as a stone-size distribution) be presented as a:
- Mass distribution
- Number distribution

There are five parameters which determine the pore-size distribution:
A. Stone shape factor
B. Stone packing/porosity
C. Median stone sieve size D50(scaling effects)
D. Grading (D85/D15)
E. Number of pores

The pores volumes are presented as Dpore [m] which are calculated with equation 6.2.

$$D_{pore} = \left[Volume_{pore} \right]^{\frac{1}{3}} \qquad [m] \tag{6.2}$$

6.4.1   Stone shape factor

No usable results are found to determine the stone shape factor. The resolution of the scans is too low to get representative results for the stone shape factor. Sample 5 and sample 10 are therefore ignored. The chosen stone-size distribution is are too small. However, an interesting fact is found about the stone shape factor which is presented in section 6.7.

6.4.2   Porosity

To define the porosity relation three scans are made of one bucket with the same stones. These scans are sample 1, sample 8, and sample 9. Between the scans the bucket is emptied, the stones are mixed, and the bucket is filled again. The input of the three scans is the same mass and number distribution, see the input in Table 6-4. The output is given in Figure 6-22, Figure 6-23, and Table 6-5.

Table 6-4: Input for the porosity analysis.

Mass distribution; cumulative probability density function													
Sieve sizes [mm]	7,1	10	12,5	14	16	20	22,4	25	31,5	40	50	63	71	90
Sample 1, 8, 9 Mass cumulative probability density	0%	0%	0%	0%	2%	7%	20%	50%	84%	96%	100%	100%	100%	100%

Number distribution; cumulative probability density function													
Sieve sizes [mm]	7,1	10	12,5	14	16	20	22,4	25	31,5	40	50	63	71	90
Stone class [mm]		[7,1-10]	[10-12,5]	[12,5-14]	[14-16]	[16-20]	[20-22,4]	[22,4-25]	[25-31,5]	[31,5-40]	[40-50]	[50-63]	[63-71]	[71-90]
Sample 1 number distribution	0%	0%	0%	0%	9%	21%	41%	74%	96%	99%	100%	100%	100%	100%

Table 6-5: Output of porosity analysis.

PORES: Mass distribution							
	D15, pore	D50, pore	D85, pore	D85, pore / D15, pore	Porosity	Number of pores	Cylinder volume
Sample 1	13,81	17,96	23,36	1,69	38,06%	199	2291030
Sample 8	14,22	19,29	24,92	1,75	36,82%	188	2449550
Sample 9	14,25	20,21	25,40	1,78	38,31%	184	2551460

PORES: Number distribution							
	D15, pore	D50, pore	D85, pore	D85, pore / D15, pore	Porosity	Number of pores	Cylinder volume
Sample 1	11,17	14,75	19,68	1,76	38,06%	199	2291030
Sample 8	10,68	15,21	20,44	1,91	36,82%	188	2449550
Sample 9	11,40	15,37	21,14	1,85	38,31%	184	2551460
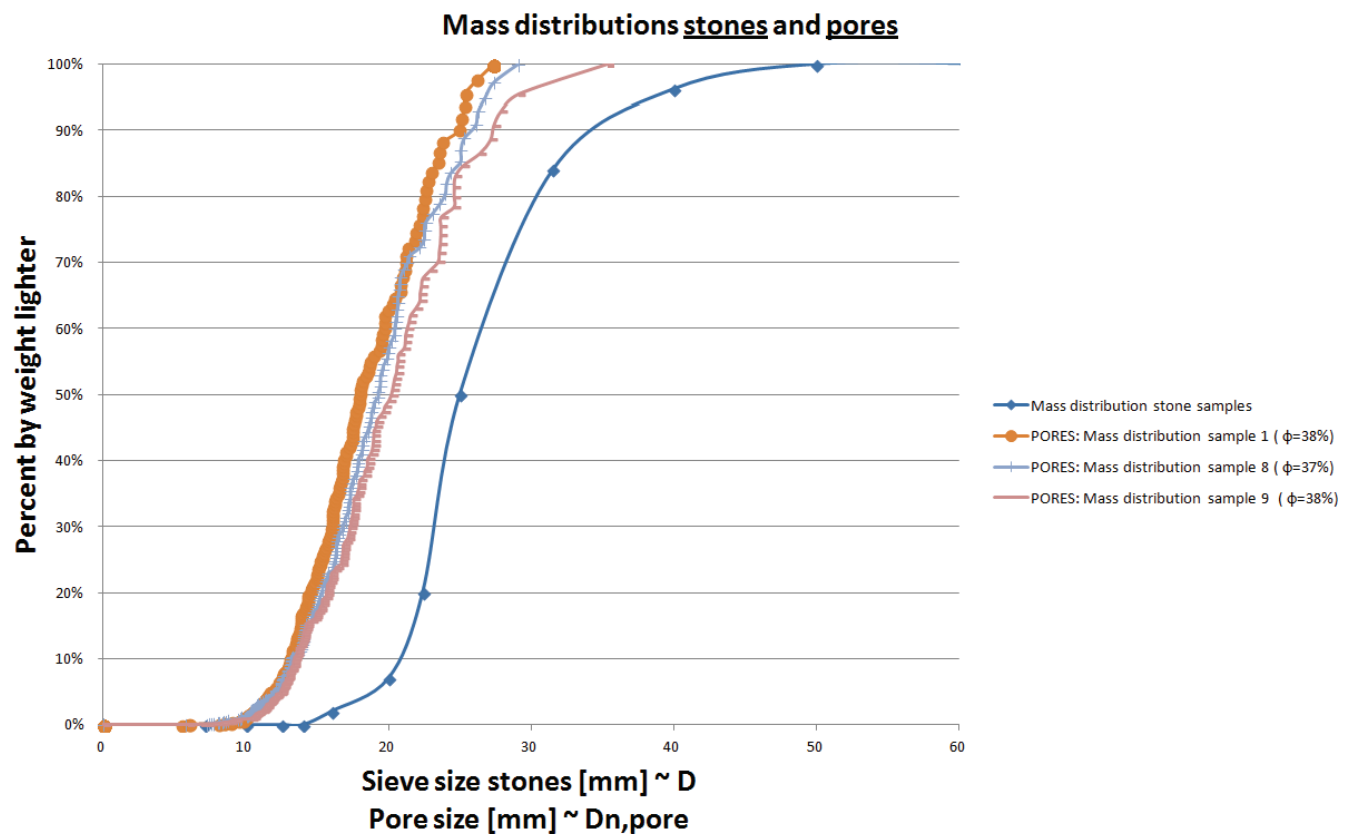
Figure 6-22: Mass distribution of stones and pores.
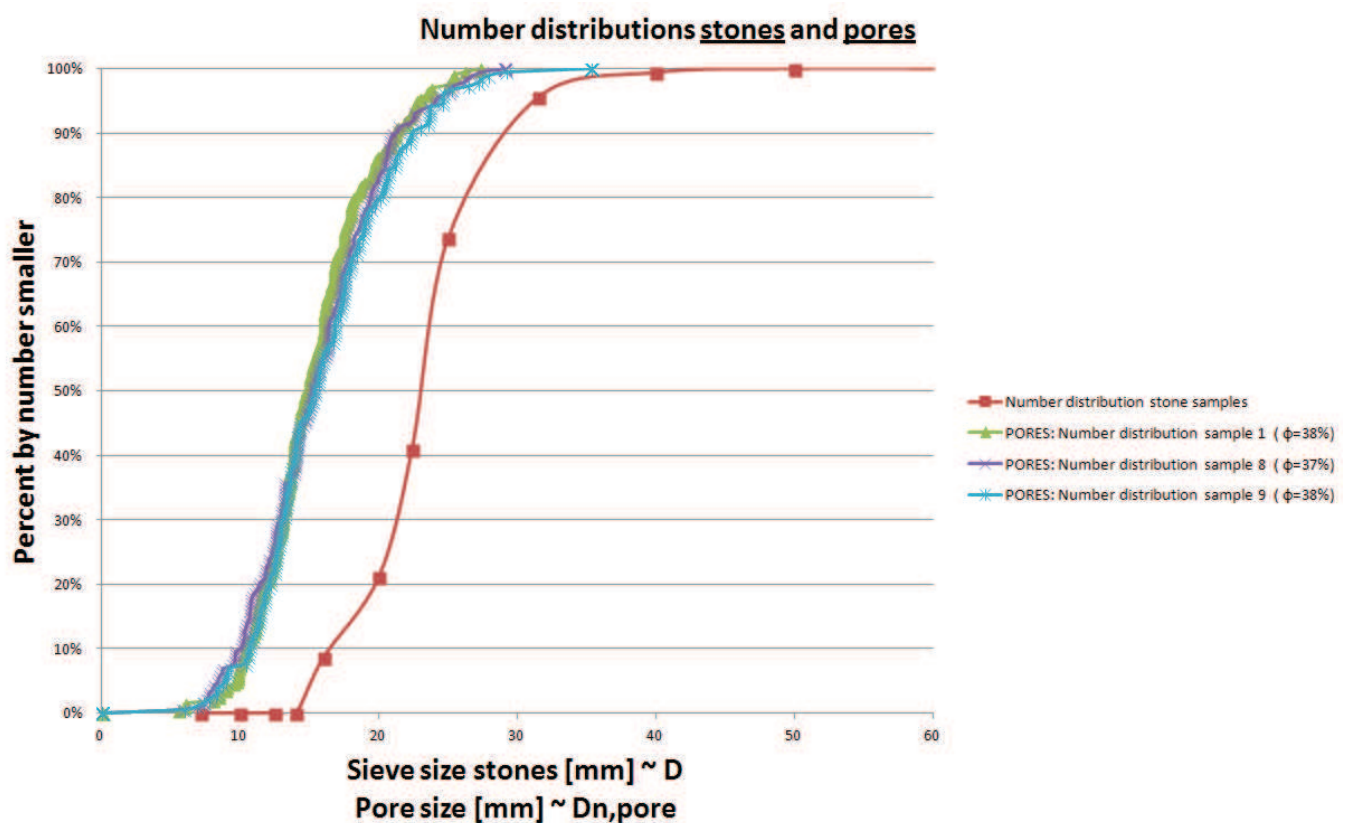
Figure 6-23: Number distribution of stones and pores.

6.4.3   Scaling effect (D50)

In the next three scans the D_{50} is the variable parameter. These scans are sample 1, sample 6, and sample 7. Three buckets are filled with another D_{50} while keeping the grading constant (D85/D15 = 1.5). The shape is assumed constant, because it is all quarry material. The difference in porosity is small.

Table 6-6: Input for the D50 analysis.

Mass distribution; cumulative probability density function														
Sieve sizes [mm]	7,1	10	12,5	14	16	20	22,4	25	31,5	40	50	63	71	90
Sample 1 Mass cumulative probability density	0,00%	0,00%	0,00%	0,00%	2,00%	7,03%	20,04%	50,09%	84,07%	96,25%	100,00%	100,00%	100,00%	100,00%
Sample 6 Mass cumulative probability density	0,00%	0,00%	0,00%	0,00%	0,00%	0,00%	0,13%	6,01%	27,04%	83,11%	94,69%	100,00%	100,00%	100,00%
Sample 7 Mass cumulative probability density	0,00%	0,00%	0,00%	0,00%	0,00%	0,00%	0,00%	1,00%	3,97%	23,01%	76,79%	100,00%	100,00%	100,00%

Number distribution; cumulative probability density function														
Sieve sizes [mm]	7,1	10	12,5	14	16	20	22,4	25	31,5	40	50	63	71	90
Stone class [mm]		[7,1-10]	[10-12,5]	[12,5-14]	[14-16]	[16-20]	[20-22,4]	[22,4-25]	[25-31,5]	[31,5-40]	[40-50]	[50-63]	[63-71]	[71-90]
Sample 1 number distribution	0%	0%	0%	0%	9%	21%	41%	74%	96%	99%	100%	100%	100%	100%
Sample 6 number distribution	0%	0%	0%	0%	0%	0%	1%	16%	50%	94%	99%	100%	100%	100%
Sample 7 number distribution	0%	0%	0%	0%	0%	0%	0%	6%	15%	46%	90%	100%	100%	100%

Table 6-7: Output of D50 analysis.

PORES: Mass distribution							
	D15, pore	D50, pore	D85, pore	D85, pore / D15, pore	Porosity	Number of pores	Cylinder volume
Sample 1	13,8	18,0	23,4	1,69	38,0%	196	2291030
Sample 6	16,8	22,1	27,4	1,63	36,0%	104	2308120
Sample 7	20,5	27,6	43,7	2,13	35,0%	52	2308340

PORES: Number distribution							
	D15, pore	D50, pore	D85, pore	D85, pore / D15, pore	Porosity	Number of pores	Cylinder volume
Sample 1	11,3	14,9	19,7	1,75	38,0%	196	2291030
Sample 6	13,3	18,5	24,0	1,80	36,0%	104	2308120
Sample 7	14,7	21,5	29,1	1,98	35,0%	52	2308340

The mass and number distribution of stones and the pore-size distribution is presented per sample in Figure 6-24, Figure 6-25, and Figure 6-26.

The mass distributions of sample 1, sample 6 and sample 7 are presented in Figure 6-27. The number distributions per samples are presented in Figure 6-28. The pore-size distributions of sample 1, sample 6, and sample 7 are presented in Figure 6-29. It can be obtained that the D50 pore (number distribution) increases if the D50 stone (mass distribution) increases.
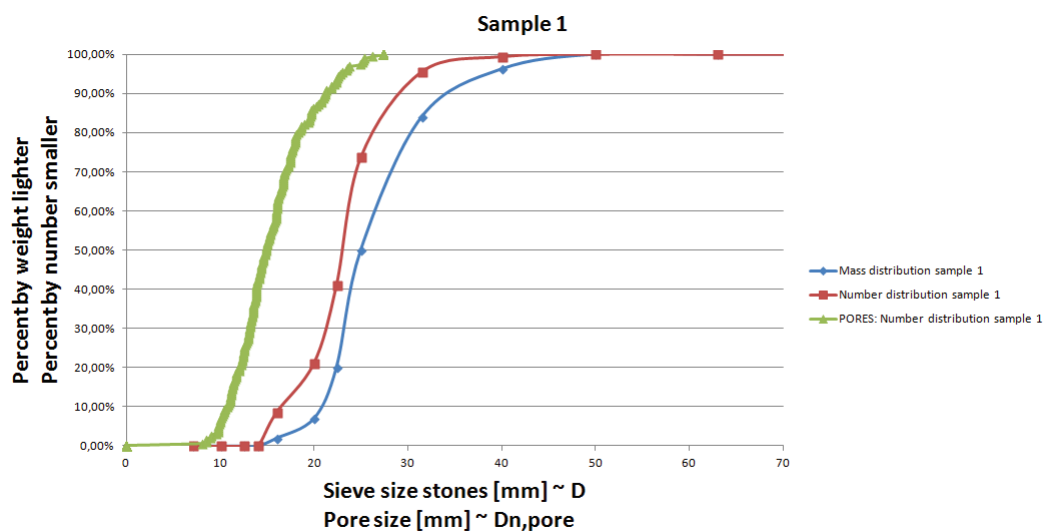
Figure 6-24: Stone and pore-size distribution of sample 1.
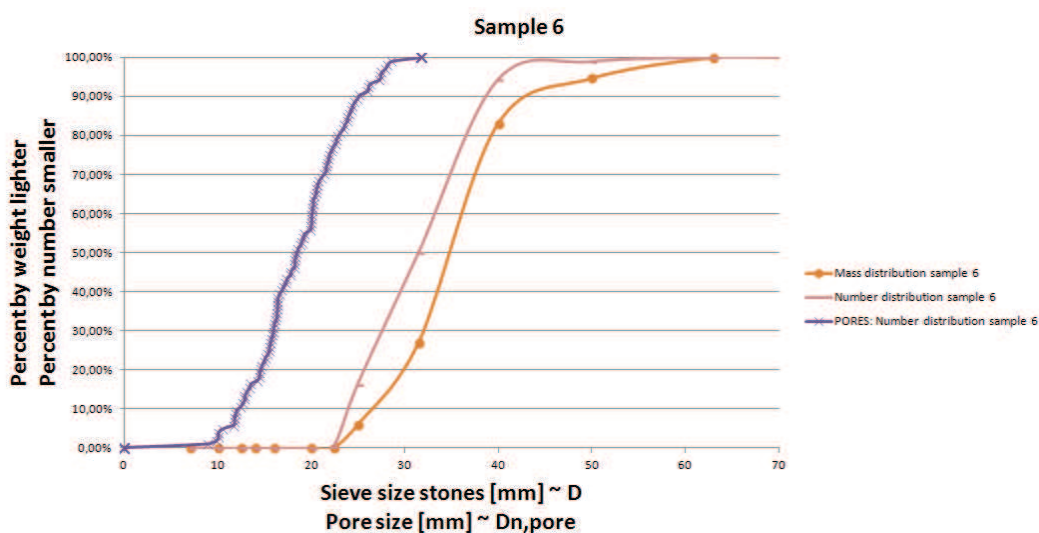
Figure 6-25: Stone and pore-size distribution of sample 6.
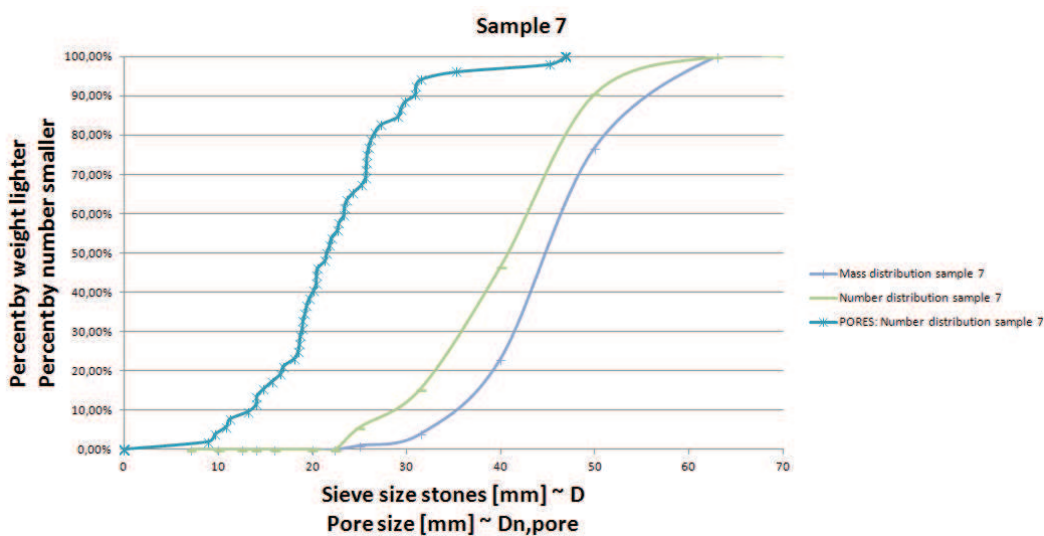
Figure 6-26: Stone and pore-size distribution of sample 7.
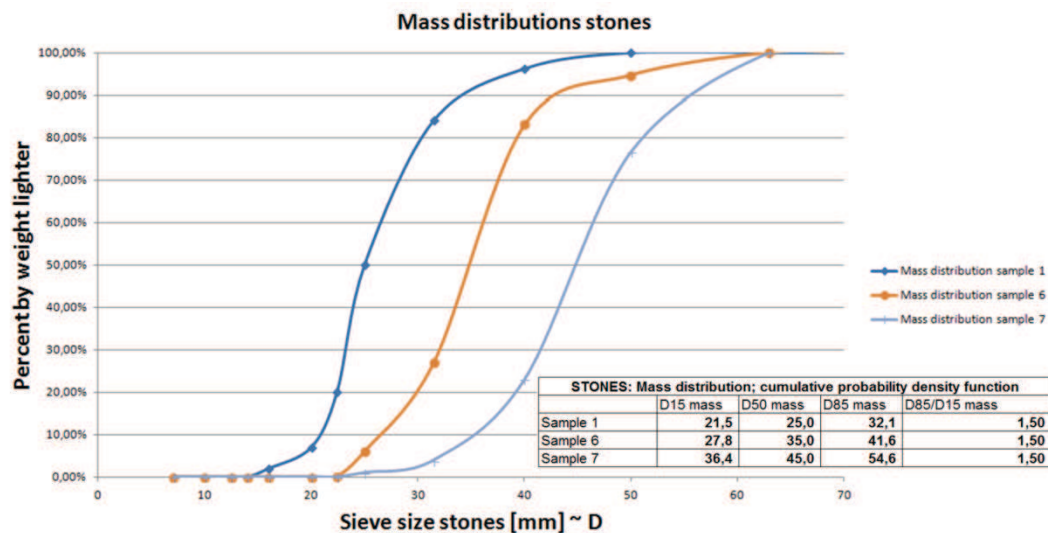
Figure 6-27: Mass distributions of stones of sample 1, 6, and 7.
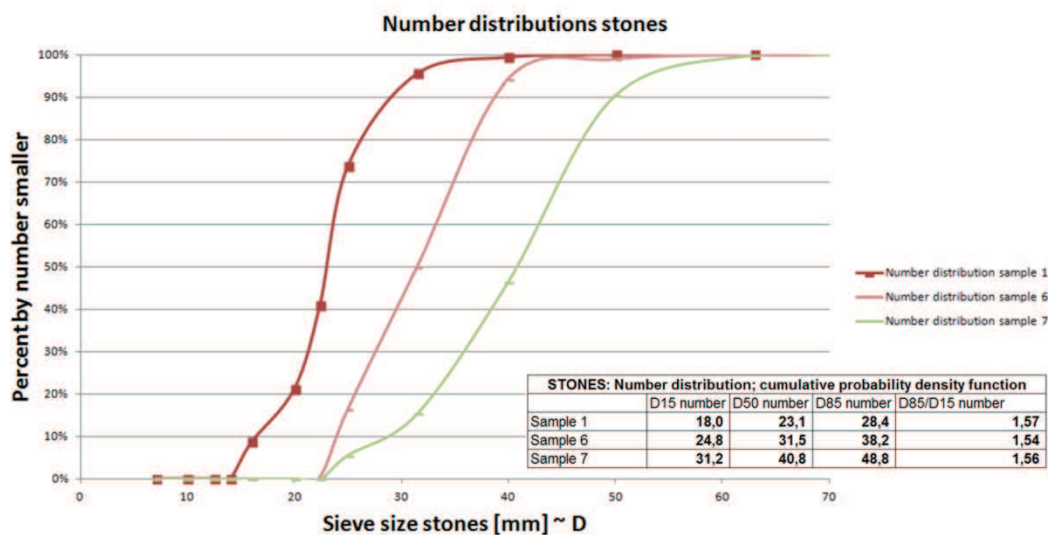
Figure 6-28: Number distributions of stones of sample 1, 6, and 7.
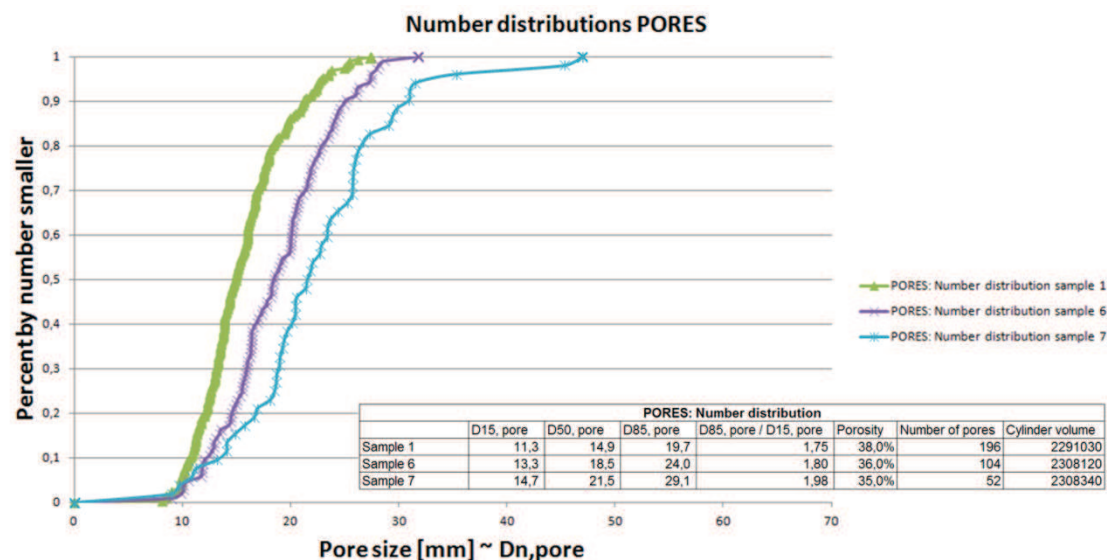
Figure 6-29: Number distributions of pores of sample 1, 6, and 7.

6.4.4   Grading (D85/D15)

In the next three scans the D_{50} is kept constant and the grading (D_{85}/D_{15}) is the variable parameter. These scans are sample 1, sample 2, and sample 4. The shape is assumed constant, because it is all quarry material. The difference in porosity is small.

Table 6-8: Input for the grading analysis.

Sieve sizes [mm]	7,1	10	12,5	14	16	20	22,4	25	31,5	40	50	63	71	90
Mass distribution; cumulative probability density function														
Sample 1 Mass cumulative probability density	0,00%	0,00%	0,00%	0,00%	2,00%	7,03%	20,04%	50,09%	84,07%	96,25%	100,00%	100,00%	100,00%	100,00%
Sample 2 Mass cumulative probability density	0,00%	0,00%	2,00%	5,02%	8,31%	18,02%	29,00%	49,96%	72,01%	90,89%	100,00%	100,00%	100,00%	100,00%
Sample 4 Mass cumulative probability density	0,00%	5,01%	12,03%	19,03%	26,03%	33,04%	40,07%	50,09%	61,14%	72,13%	82,90%	92,21%	100,00%	100,00%

Sieve sizes [mm]	7,1	10	12,5	14	16	20	22,4	25	31,5	40	50	63	71	90
Number distribution; cumulative probability density function														
Stone class [mm]		[7,1-10]	[10-12,5]	[12,5-14]	[14-16]	[16-20]	[20-22,4]	[22,4-25]	[25-31,5]	[31,5-40]	[40-50]	[50-63]	[63-71]	[71-90]
Sample 1 number distribution	0%	0%	0%	0%	9%	21%	41%	74%	96%	99%	100%	100%	100%	100%
Sample 2 number distribution	0%	0%	15%	28%	38%	56%	68%	84%	95%	99%	100%	100%	100%	100%
Sample 4 number distribution	0%	37%	60%	74%	83%	89%	92%	96%	98%	99%	100%	100%	100%	100%

Table 6-9: Output of grading analysis.

PORES: Number distribution							
	D15, pore	D50, pore	D85, pore	D85, pore / D15, pore	Porosity	Number of pores	Total volume
Sample 1	11,2	14,7	19,7	1,76	38,1%	199	2291030
Sample 2	9,8	13,8	19,3	1,98	35,4%	208	2288040
Sample 4	9,0	12,3	17,5	1,94	35,6%	230	2215500

The mass and number distribution of stones and the pore-size distribution is presented per sample in Figure 6-30, Figure 6-31, and Figure 6-32.

The mass distributions of sample 1, sample 2 and sample 4 are presented in Figure 6-33. The number distributions per samples are presented in Figure 6-34. The pore-size distributions of sample 1, sample 2, and sample 4 are presented in Figure 6-35. It can be obtained that the D50 pore (number distribution) decreases if the stone grading (D85/D15 stone mass distribution) increases.
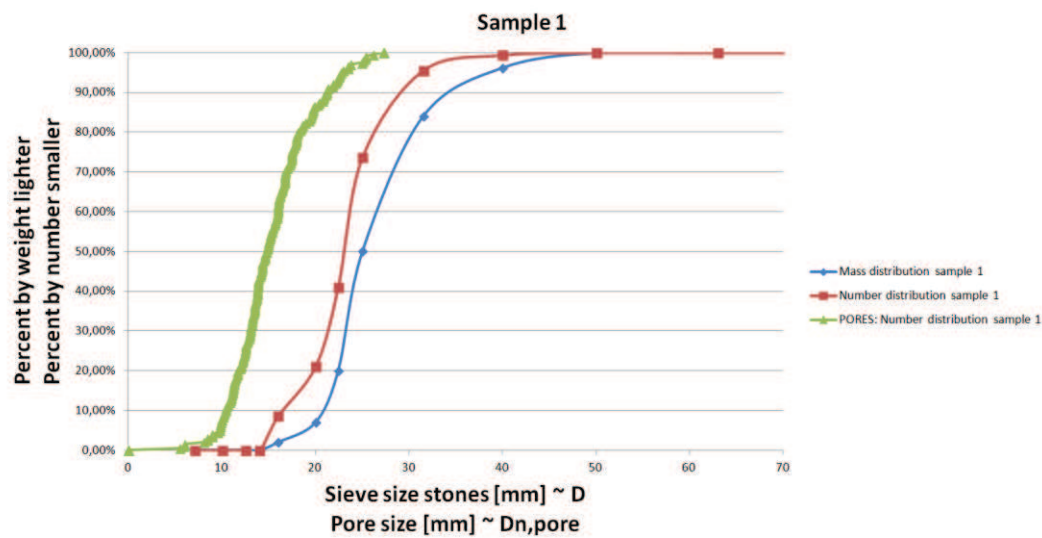
Figure 6-30: Stone and pore-size distribution of sample 1.
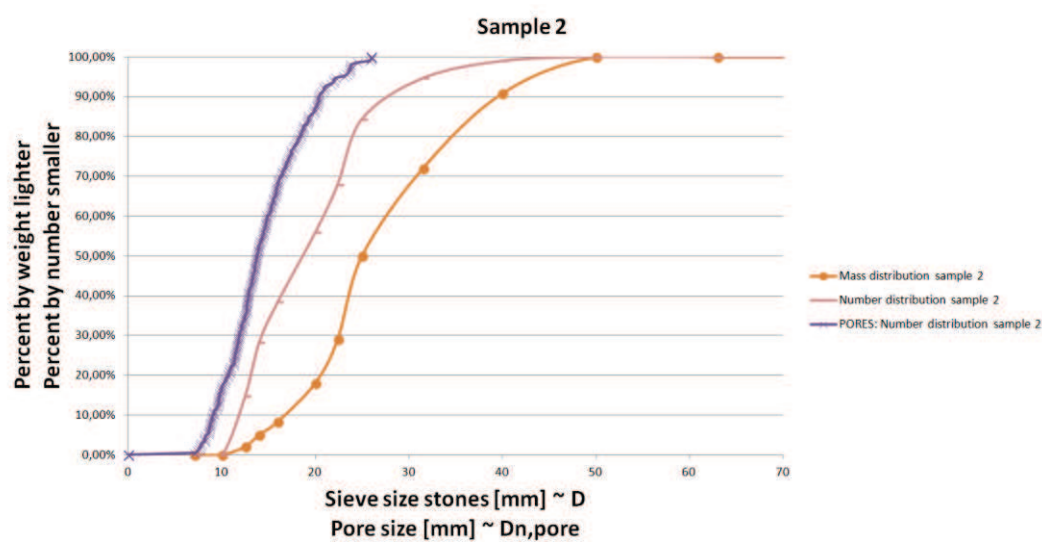
Figure 6-31: Stone and pore-size distribution of sample 2.
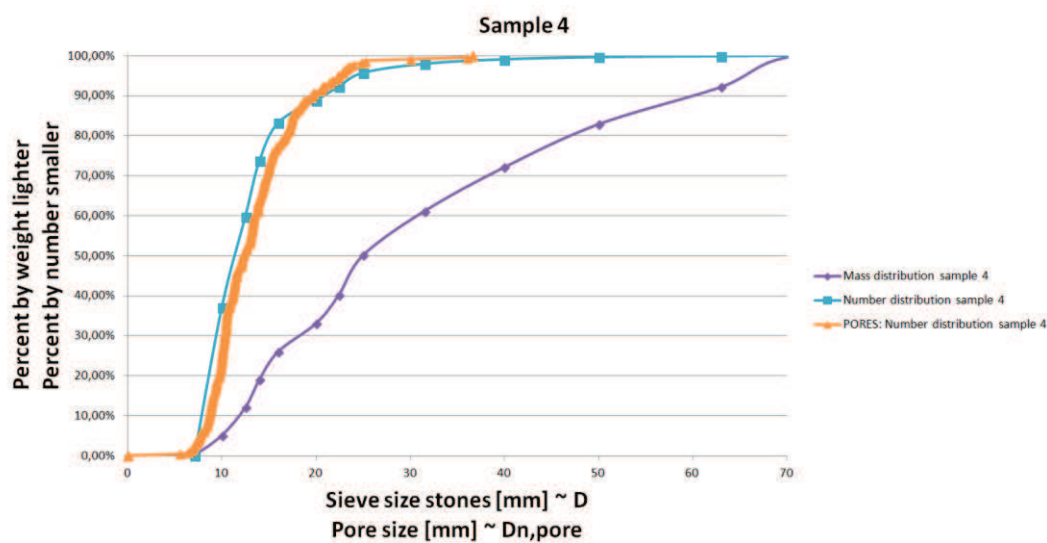
Figure 6-32: Stone and pore-size distribution of sample 4.
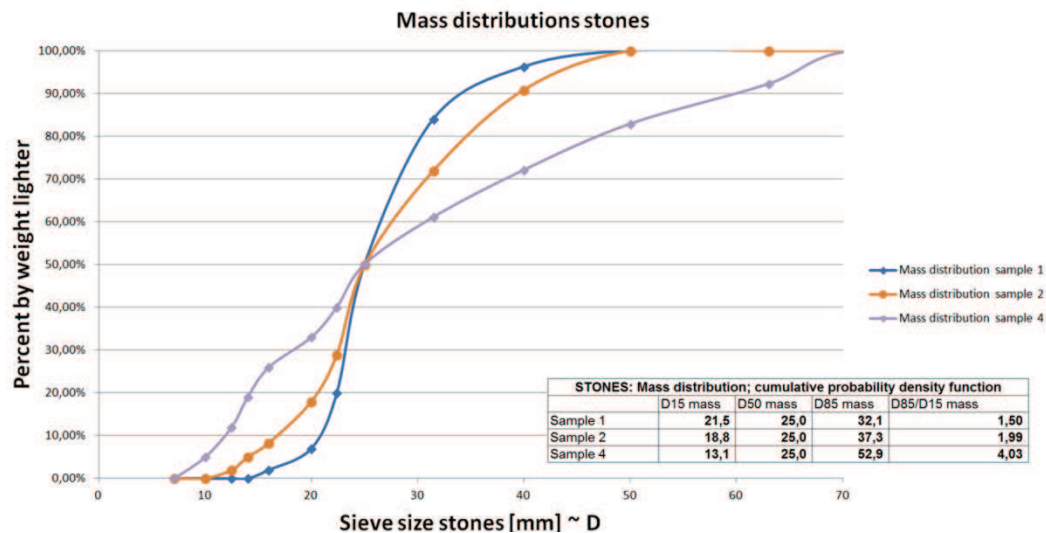
Figure 6-33: Mass distribution of stones of sample 1, 2, and 4.
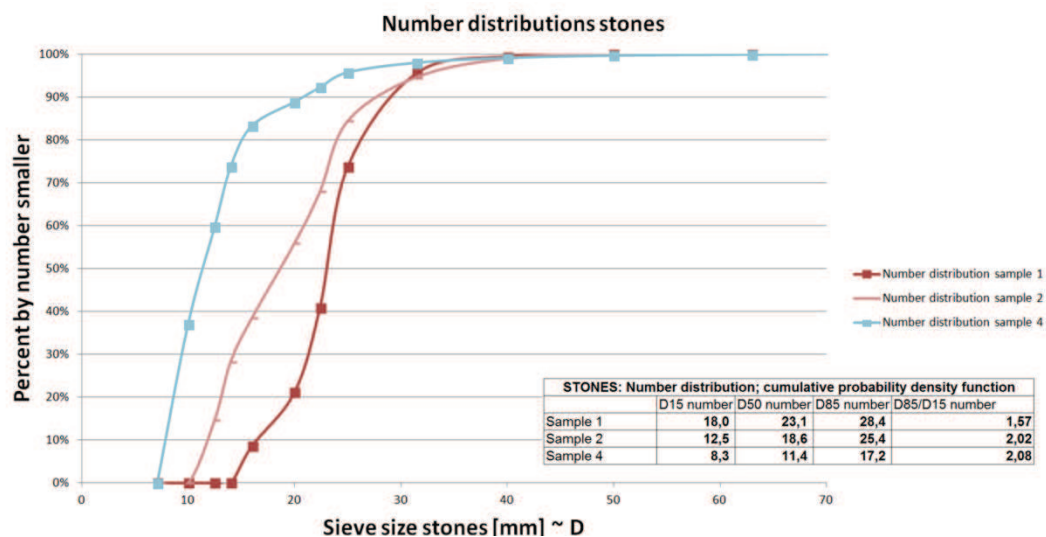
Figure 6-34: Number distributions of stones of sample 1, 2, and 4.
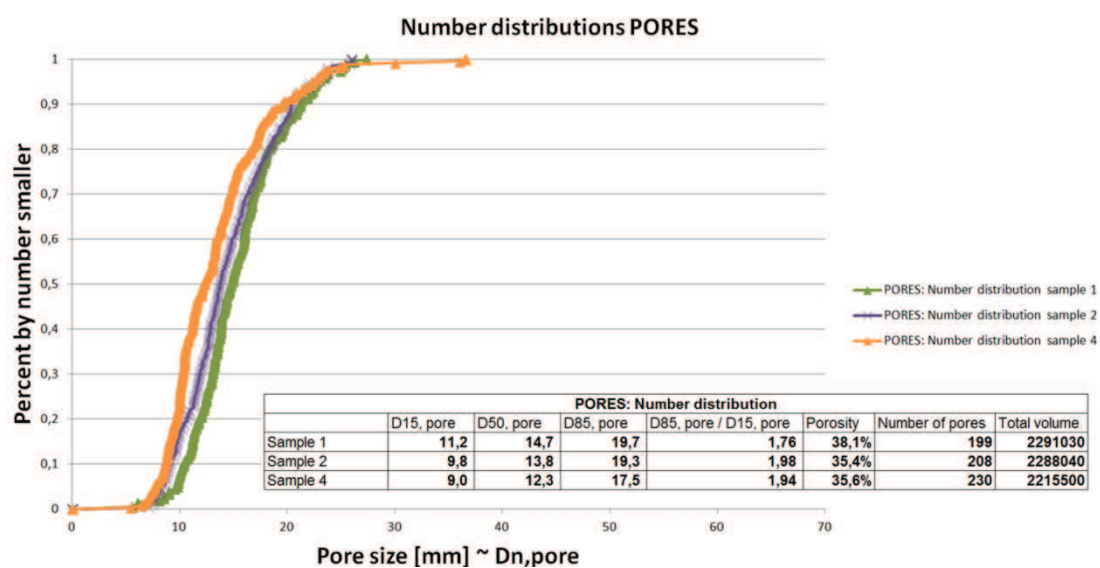
Figure 6-35: Number distribution of pores of sample 1, 2, and 4.

6.4.5 Number of pores

As explained in the experimental steps, a cylindrical volume is selected of the bucket of stones. The number of pores within this cylinder is count of all the samples. Also the number of stones in this cylinder is count. The input for the analysis of the number of pores is presented in Table 6-10 and the stone distributions presented in Table 6-11. In section 6.5 the relation of the number of pores is discussed.

Table 6-10: Output of number of pores analysis.

	PORES: General data				
	Number of pores in cylinder	Cylinder volume	Porosity	Amount of stones in cylinder	Amount of stones
Sample 1	199	2291030	0,38	238	310
Sample 2	208	2288040	0,35	286	410
Sample 3	205	2460550	0,38	299	361
Sample 4	230	2215500	0,36	494	784
Sample 6	107	2308120	0,36	118	147
Sample 7	53	2308340	0,35	56	69
Sample 8	188	2449550	0,37	254	318
Sample 9	184	2551460	0,38	267	314

6.4.6 Overview of results

An overview of all the results are summarized in Table 6-11. All the conducted analysis in the next sections are based on this data.

Table 6-11: Overview of the results.

STONE distributions				
STONES: Mass distribution; cumulative probability density function				
	D15 mass	D50 mass	D85 mass	D85/D15 mass
Sample 1	21,5	25,0	32,1	1,50
Sample 2	18,8	25,0	37,3	1,99
Sample 3	22,8	23,7	24,6	1,08
Sample 4	13,1	25,0	52,9	4,03
Sample 6	27,8	35,0	41,6	1,50
Sample 7	36,4	45,0	54,6	1,50
Sample 8	21,5	25,0	32,1	1,50
Sample 9	21,5	25,0	32,1	1,50

STONES: Number distribution; cumulative probability density function				
	D15 number	D50 number	D85 number	D85/D15 number
Sample 1	18,0	23,1	28,4	1,57
Sample 2	12,5	18,6	25,4	2,02
Sample 3	22,8	23,7	24,6	1,08
Sample 4	8,3	11,4	17,2	2,08
Sample 6	24,8	31,5	38,2	1,54
Sample 7	31,2	40,8	48,8	1,56
Sample 8	18,0	23,1	28,4	1,57
Sample 9	18,0	23,1	28,4	1,57

PORE distributions				
PORES: Mass distribution				
	D15, pore	D50, pore	D85, pore	D85, pore / D15, pore
Sample 1	13,8	18,0	23,4	1,69
Sample 2	13,2	18,4	23,5	1,78
Sample 3	14,2	18,6	22,3	1,57
Sample 4	12,3	18,1	26,1	2,12
Sample 6	16,8	22,1	27,4	1,63
Sample 7	20,5	27,6	43,7	2,13
Sample 8	14,2	19,3	24,9	1,75
Sample 9	14,2	20,2	25,4	1,78

PORES: Number distribution				
	D15, pore	D50, pore	D85, pore	D85, pore / D15, pore
Sample 1	11,2	14,7	19,7	1,76
Sample 2	9,8	13,8	19,3	1,98
Sample 3	11,0	15,5	19,7	1,78
Sample 4	9,0	12,3	17,5	1,94
Sample 6	12,9	18,3	23,9	1,85
Sample 7	14,1	21,4	29,1	2,06
Sample 8	10,7	15,2	20,4	1,91
Sample 9	11,4	15,4	21,1	1,85

PORE general data				
	Number of pores in cylinder	Cylinder volume	Porosity	Amount of stones in cylinder	Amount of stones
Sample 1	199	2291030	0,38	238	310
Sample 2	208	2288040	0,35	286	410
Sample 3	205	2460550	0,38	299	361
Sample 4	230	2215500	0,36	494	784
Sample 6	107	2308120	0,36	118	147
Sample 7	53	2308340	0,35	56	69
Sample 8	188	2449550	0,37	254	318
Sample 9	184	2551460	0,38	267	314

6.5   GENERAL FORMULA FOR PORE-SIZE DISTRIBUTION

The results of the experiment are presented in the previous section. The analysis to find the relation between stone-size distribution and the pore-size distribution is discussed in this section. The analysis also include the number of pores. In the last subsection the derived formula is validated.

Two approaches are elaborated to find the formula for the pore-size distribution. The first approach is presented in appendix B. This approach is based on finding the D50 of the pore size number distribution. The second approach is presented in section 6.5.1. This approach is based on approximation function that describes approximates the pore-size distribution.

6.5.1   Approximation function of pore-size distribution

The pore-size distributions, as found in Figure 6-23, Figure 6-29, and Figure 6-35, have a S-curved shape. Therefore the pore-size distributions are approximated with an adapted Rosin Rammler distribution. The equation of the Rosin Rammler distribution is stated in equation 6.3.

$$f\left(x, P_{80}, m, F\right) = 1 - \ e^{\ln(0.2) * \left(\frac{x-F}{P_{80}}\right)^m} \qquad for\ x > F \qquad (6.3)$$

The Rosin Rammler distribution depends on three parameters:
- P80   : this parameter determines the slope of the distribution
- m   : this parameter determines the shape of the distribution
- F   : this parameter determines start point the distribution

In Figure 6-36 all the pore-size distributions of the experiment are plotted and all the pore-size distributions are approximated (curve fitting) with a Rosin Rammler distribution. The used factors of the Rosin Rammler distributions are presented in Table 6-12. The values are manually found with trial and error.

Table 6-12: Used factors for the approximation with Rosin Rammler per sample.

Rosin Rammler approximations				
		slope	shape	Start point
	LN	P80	m	Factor
Sample 1	0.2	12	2	7
Sample 2	0.2	12	2	6
Sample 3	0.2	12	2	7
Sample 4	0.2	10	1.5	6.5
Sample 6	0.2	12	2	10.5
Sample 7	0.2	12	2	14
Sample 8	0.2	12	2	7
Sample 9	0.2	12	2	7
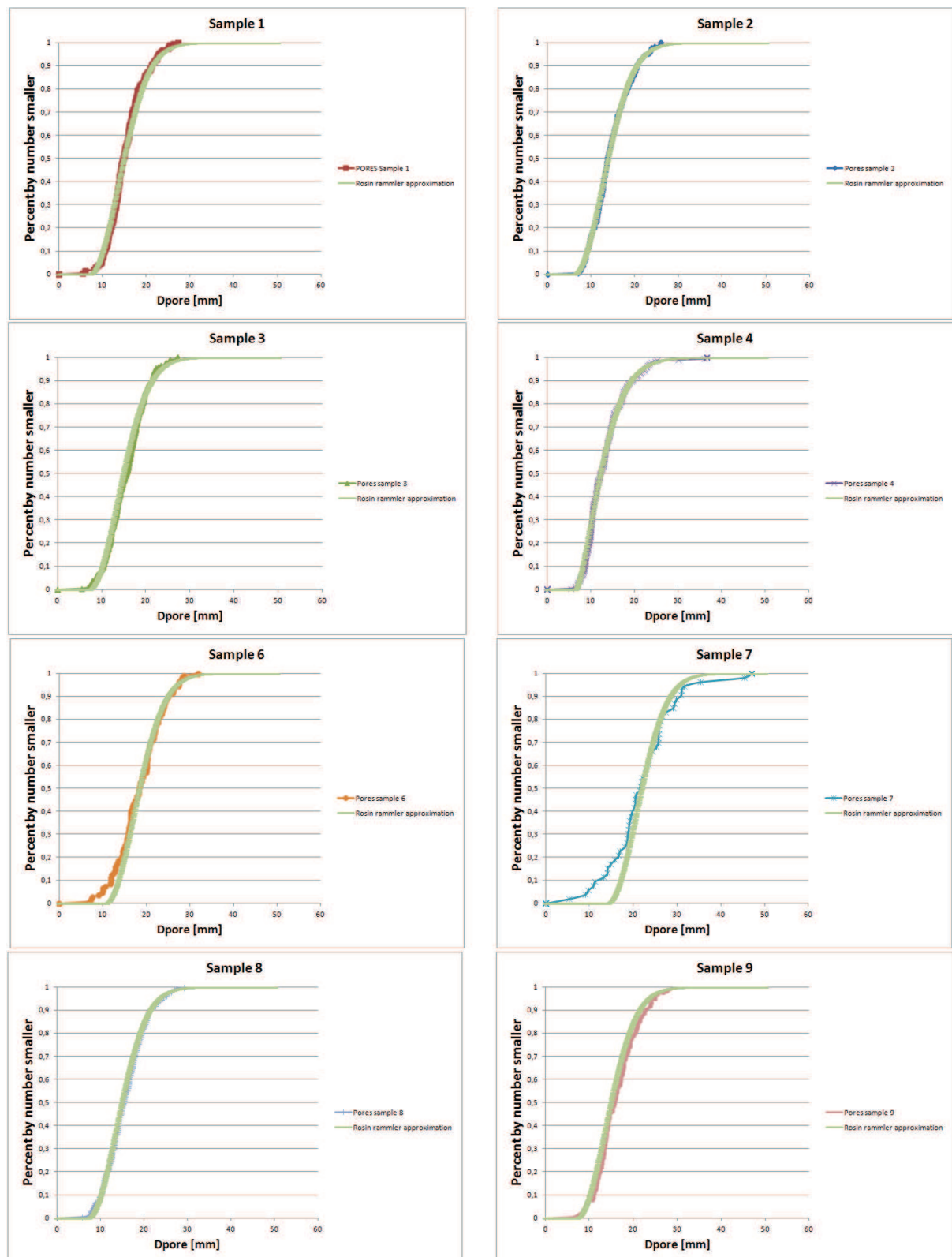
Figure 6-36: Pore-size distribution and approximation with Rosin Rammler distribution of all the samples.

The aim is to search if the found parameters of the curve fitting formula have a correlation with the stone-size distribution. The stone-size distribution parameters are:

- D50 stone
- D85/D15
- Porosity
- Stone shape

Due to a lack of data the stone shape is not taken into account*. However, all the scans are performed on quarry material. It is assumed that the stone shape factor is negligible for further analysis.

*It is is tried to find a relation for the shape factor by comparison with the glass ball validation scan, but because of the high porosity and grading difference (uniform pores and high porosity) no representative results are found. However, an interesting fact is found about the stone shape factor which is presented in section 6.7.

Slope factor P80

The factor for the slope of the Rosin Rammler distribution (P80) is assumed correlated to the porosity and the stone grading, see equation 6.4.

$$P_{80} = \left\{ \left[\frac{D85}{D15} stone\right]^a, [\phi]^b \right\} \qquad (6.4)$$
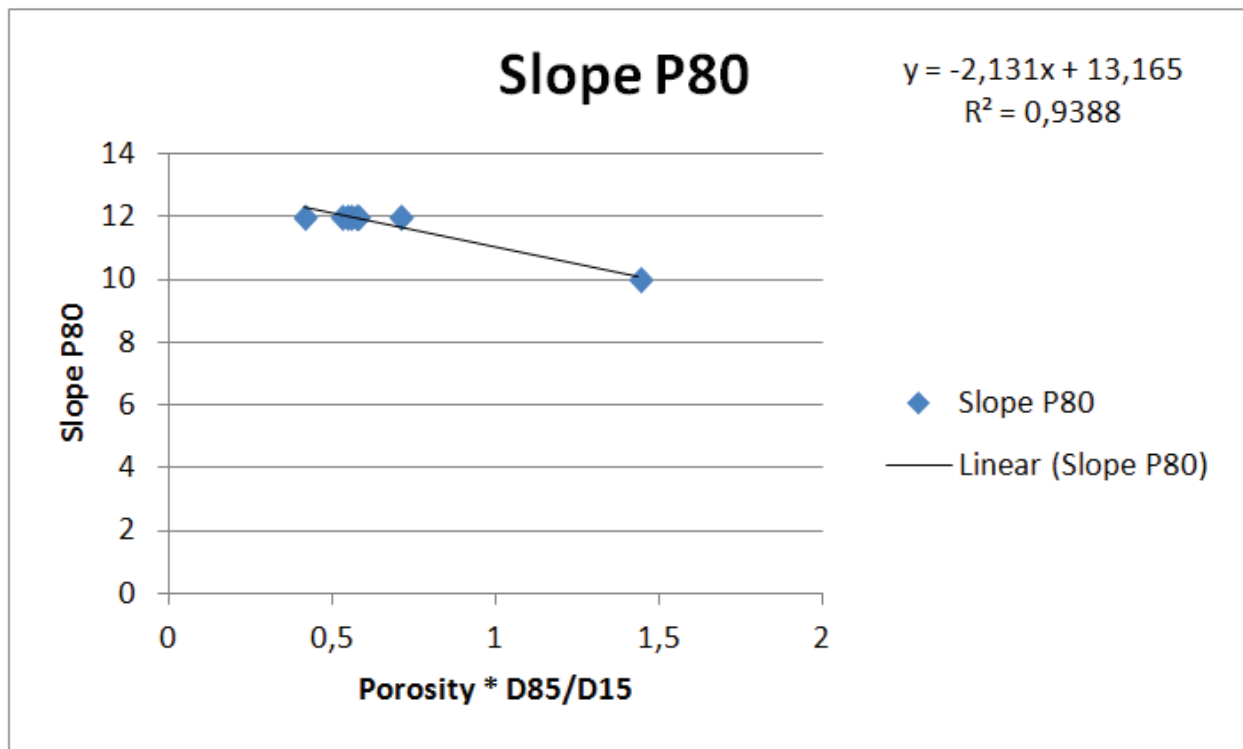
Figure 6-37: Correlation between P80 and the porosity times the stone grading.

Figure 6-37 is obtained for a=1 and b=1 of equation 6.4. Furthermore, the slope P80 is scaled linear with the D50 and therefore the formula in equation 6.5 is found for the factor P80.

$$P_{80} = \left(-2.13 * \phi * \frac{D85}{D15} + 13.2\right) * \frac{D50}{25} \qquad (6.5)$$

Shape factor m
The factor for the shape of the Rosin Rammler distribution (m) is also assumed correlated to the porosity and the stone grading, see equation 6.6.

$$m = \left\{ \left[\frac{D85}{D15} stone \right]^a , [\phi]^b \right\}$$

(6.6)
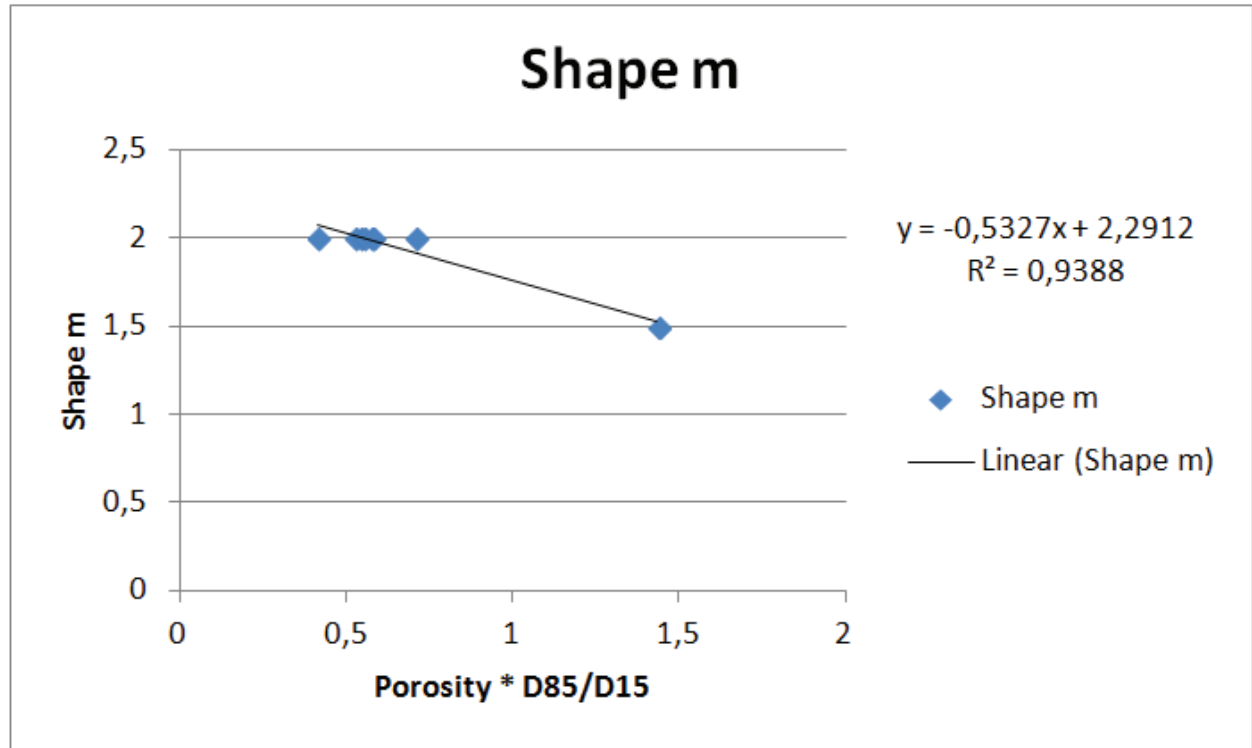
Figure 6-38: Correlation between m and the porosity times the stone grading.

Figure 6-38 is obtained for a=1 and b=1 of equation 6.6. The formula for the shape of the Rosin Rammler distribution (m) is stated in equation 6.7.

$$m = \left(-0.533 * \phi * \frac{D85}{D15} + 2.29 \right)$$

(6.7)

<u>Start point F</u>
The factor for start point of the Rosin Rammler distribution (F) is assumed correlated to the
porosity and the stone size, see equation 6.8.

$$F = \{ \ [D50]^a \ , [\phi]^b \ \} \tag{6.8}$$
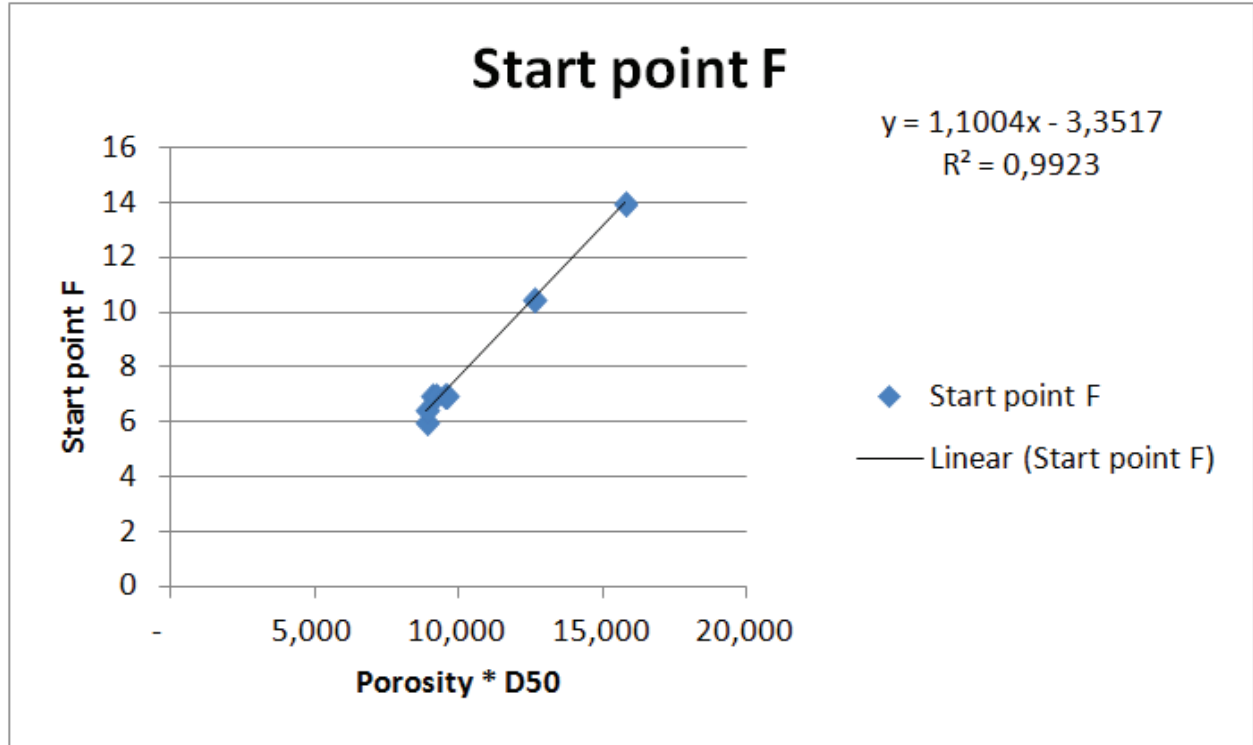
Figure 6-39: Correlation between F and porosity times median stone size.

Figure 6-39 is obtained for a=1 and b=1. Afterwards start point (F) is scaled linear with the
D50 and therefore the formula in equation 6.9 is found for the factor F.

$$F = (27.5 * \phi - 3.35) * \frac{D50}{25} \tag{6.9}$$

The function of the pore-size distribution found is presented in equation 6.10.

$$f\left(x, P_{80}, m, F\right) = 1 - e^{\ln(0.2)*\left(\frac{x-F}{P_{80}}\right)^m} \qquad [m] \qquad for \ x > F \tag{6.10}$$

With
$$P_{80} = \left(-2.13 * \phi * \frac{D85}{D15} + \ 13.2\right) * \frac{D50}{25}$$
$$m = \left(-0.533 * \phi * \frac{D85}{D15} + \ 2.29\right)$$
$$F = (27.5 * \phi - 3.35) * \frac{D50}{25}$$

In subsection 6.5.3 the formula is checked.

6.5.2   Number of pores

There are three equations possible to describe the number of pores, see equation 6.11, equation 6.12, and equation 6.13.

$$Number\ of\ pores = \left\{ \left[\frac{D85}{D15} stone \right]^a , [\phi]^b , \left[\frac{V}{D50^3} \right]^c \right\} \tag{6.11}$$

$$Number\ of\ pores = \left\{ [\phi]^a , \left[\frac{V}{D50pore^3} \right]^b \right\} \tag{6.12}$$

$$Number\ of\ pores = \{\ number\ of\ stones\ \} \tag{6.13}$$

In equation 6.11 the number of pores are related to the stone-size distribution (D50 and D85/D15), the porosity, and the total volume. Equation 6.12 is based on the total pore volume divided by the mean pore volume. In this case the mean pore volume has to be calculated first. In equation 6.13 the number of pores are related to the number of stones. The number of stones have to be calculated first to use this formula.

Therefore equation 6.11 is preferable because the number of pores are directly related to the input parameters. Figure 6-40 is obtained for equation 6.11 with a=0.25, b=1, and c=1. Because linear scaling is assumed (if the volume is increased by factor 2, the number of pores should also be increased by factor 2) the trend line goes through the origin of the coordinate system. The two outliers on the left can be explained by a low ratio of volume divided by D50. The formula for the number of pores is stated in equation 6.14.

$$Number\ of\ pores = 1.81 * \left(\frac{D85}{D15} stone \right)^{0.25} * \frac{V * (1 - \phi)}{D50^3} \tag{6.14}$$
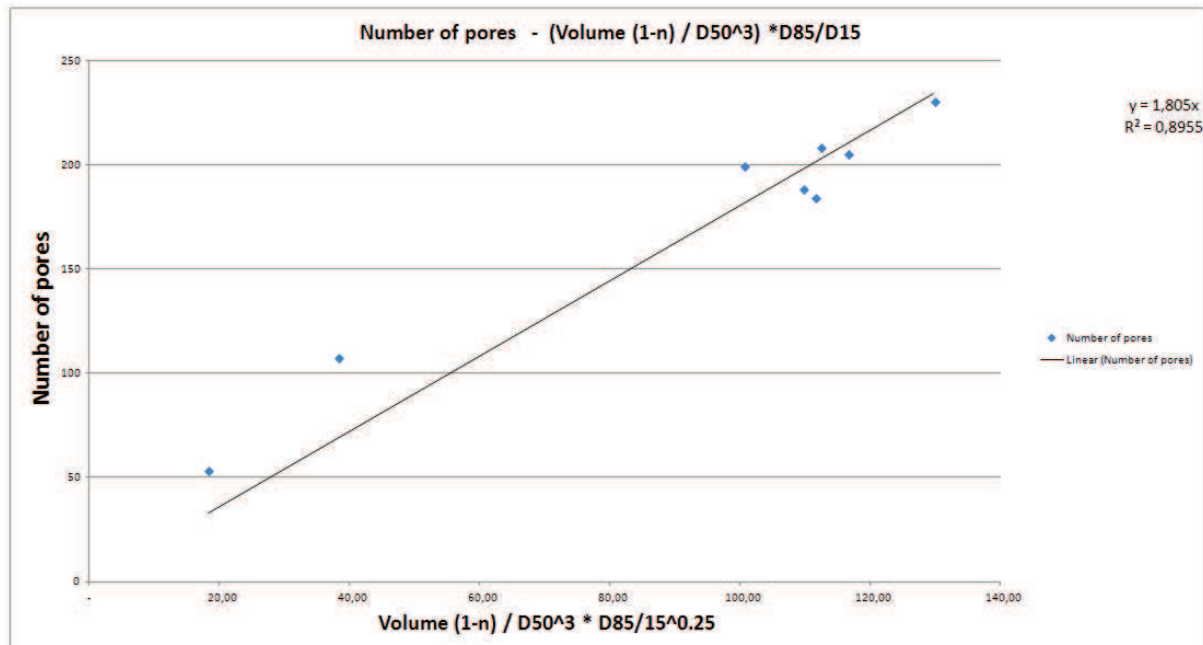
Figure 6-40: Correlation between number of pores and the stone-size distribution, porosity, and volume.

To find the correlation of equation 6.12 the D50pore has to be calculated first. This is an extra step which brings inaccuracy. Furthermore, in Figure 6-41 is visible that the correlation is low. This method is not suitable to predict the number of pores.
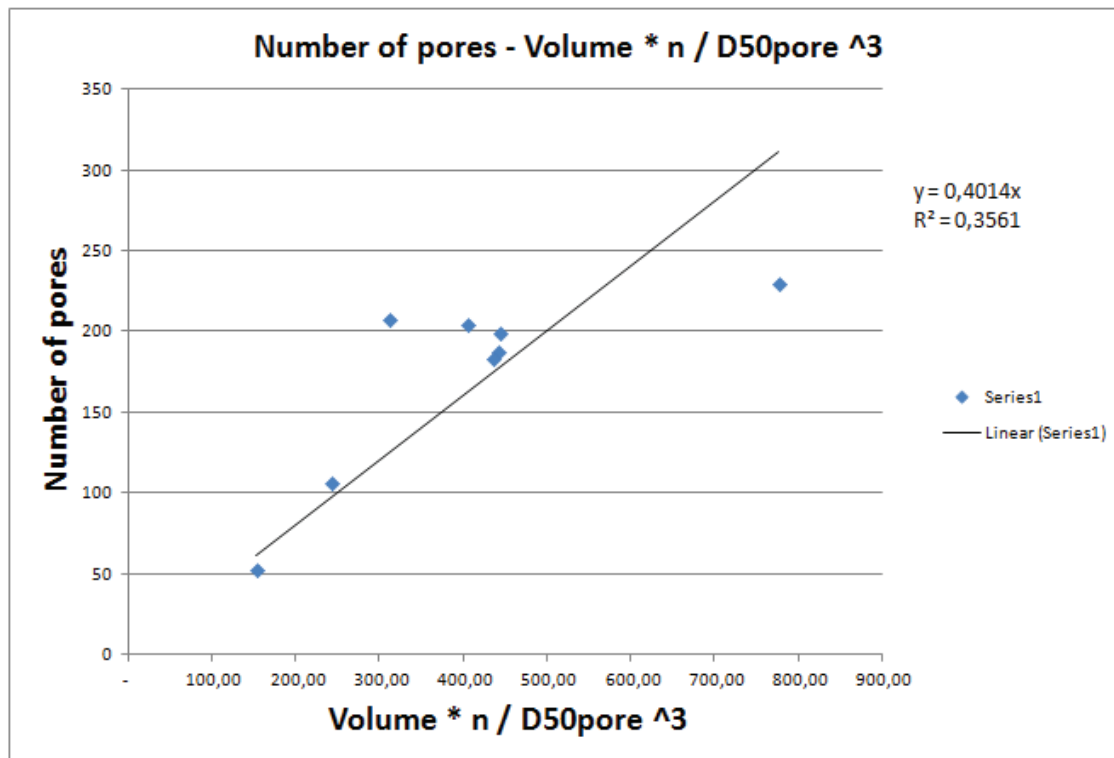
Figure 6-41: Correlation between number of pores and mean pore size, porosity, and volume.

The number of pores can also be obtained by plotting the number of pores against the number of stones, see Figure 6-42. It is visible that there definitely is a trend, but that there is one outlier.
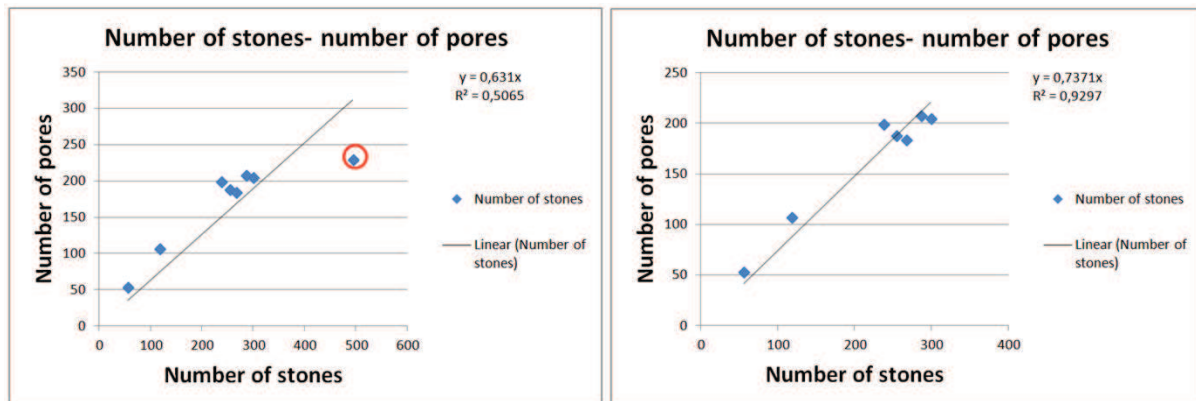
Figure 6-42: Correlation between number of pores and number of stones.

Including this outlier equation 6.15 is obtained and if the outlier is ignored equation 6.16 describes the number of pores.

$$Number\ of\ pores = 0.631 * number\ of\ stones \qquad (6.15)$$

$$Number\ of\ pores = 0.737 * number\ of\ stones \qquad (6.16)$$

Still a disadvantage of this method, with respect to equation 6.14, is that the number of stones has to be estimated.

6.5.3   Accuracy of the derived formula

In this subsection the accuracy of the derived formula for the pore-size distribution (equation 6.10) and the formulas that describe the relation of the number of pores (equation 6.14 and equation 6.16) are discussed. The formula for the pore-size distribution (equation 6.10) is applied to all the stone distributions of the samples and plotted against the pore-size distributions found with the CT scanner and Avizo Fire, see Figure 6-43.
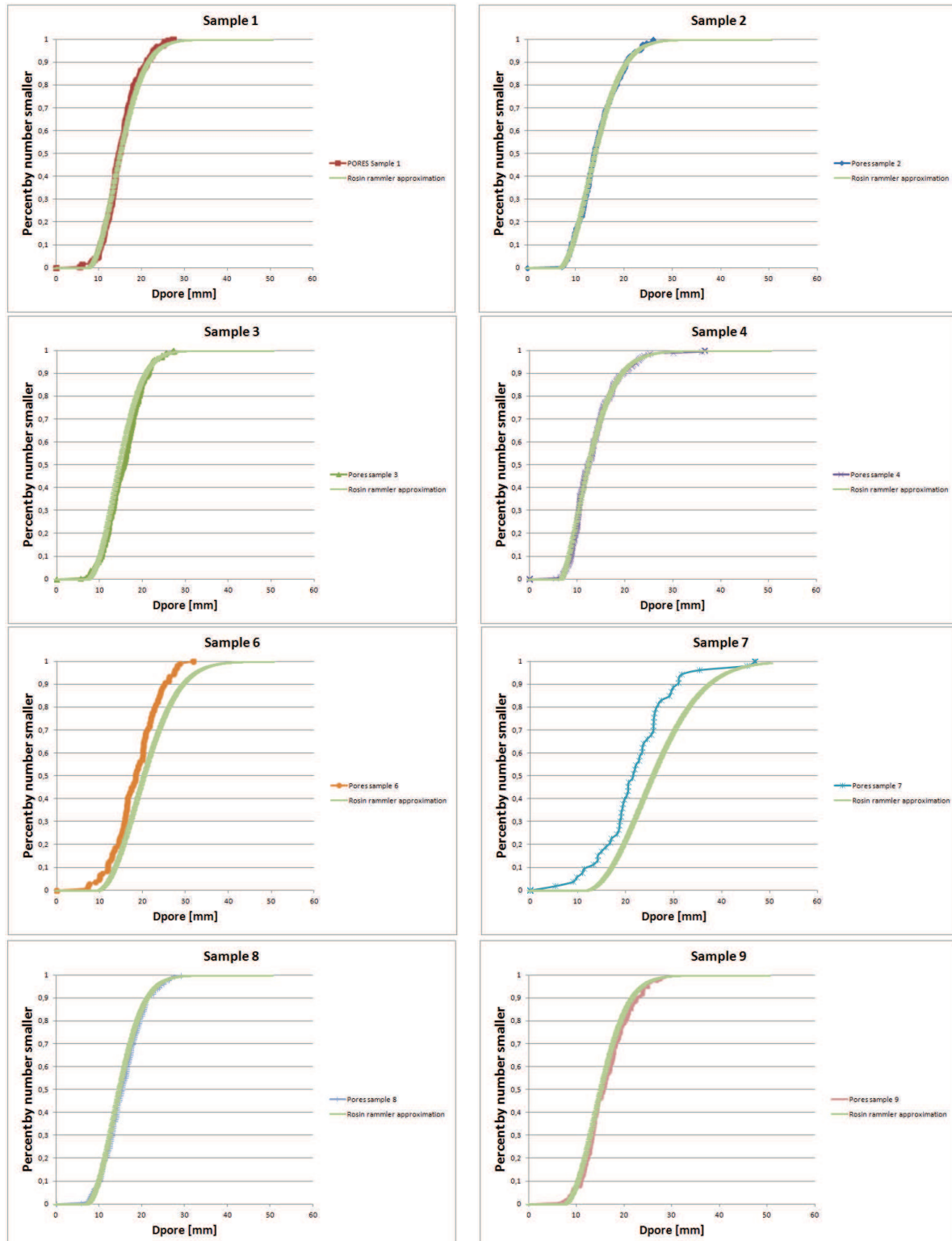
Figure 6-43: General formula of pore-size distribution (Rosin Rammler) and pore-size distributions found with the CT scanner and Avizo Fire.

Sample 6 and sample 7 contain a small error, see Figure 6-43. It is possible, the error is caused by the approximation distribution or by the experiment. The buckets of sample 6 and sample 7 are filled with bigger stones, so less stones are inside the bucket. This means that there are also less pores inside the bucket. The pore-size distribution of the experiment is a number distribution and therefore sensitive if the number of pores are low. Therefore the error of sample 6 and sample 7 are assumed mostly related to the experiment.

To check the formula even more, a D50 of 10 times the D50 of sample 1 is used in the formula. The stone grading and the porosity is kept the same as sample 1. The result is visible in Figure 6-44. The outcome of the pore sizes of the sample 1 (determined with the CT scanner and Avizo Fire) is also multiplied with a factor 10. The formula for the pore-size distribution give accurate results and are assumed representative for indication purposes.
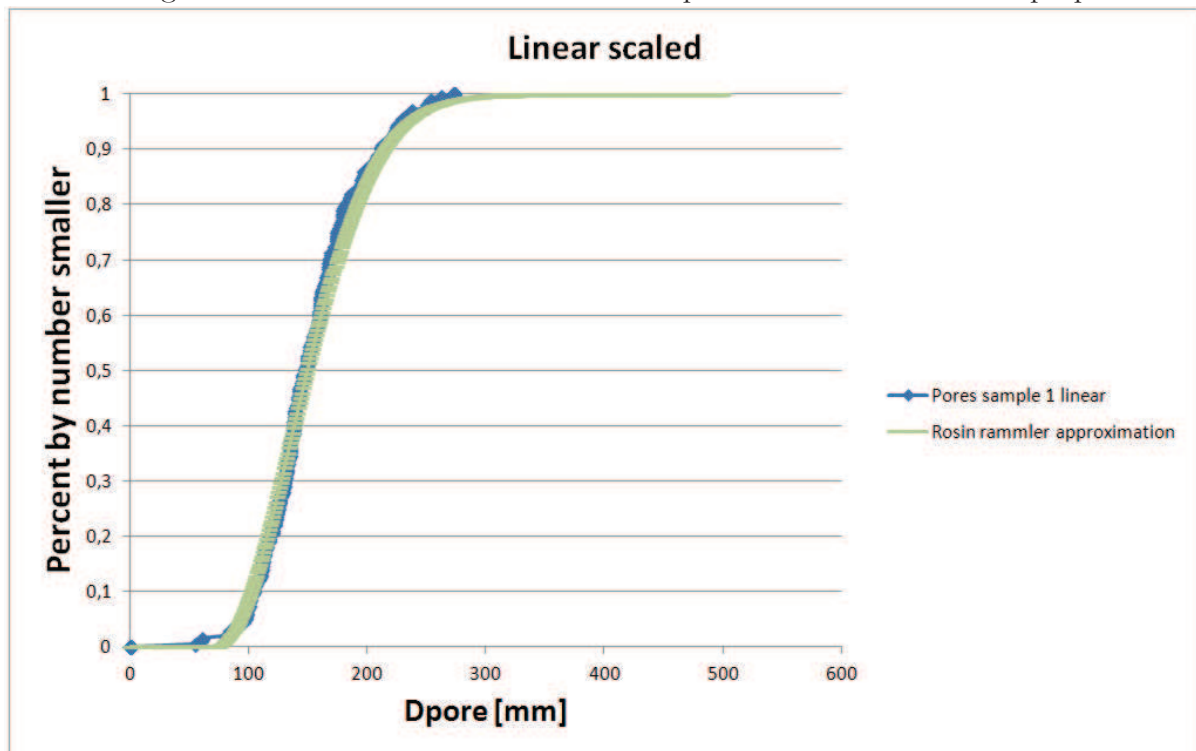
Figure 6-44: Linear scaled pores size distribution of sample 1 with factor 10 and D50 of sample 1 also scaled with factor 10.

A remark has to be made about the validity of the formula. The formula is valid if x>F. Furthermore, the formula includes the porosity of the bed protection, but the porosity differences obtained during the experiment were small (between 35% and 38%). So the accuracy of the formula for much higher/lower porosities is arguable.

The accuracy of the formula which describes the number of pores (equation 6.14) is elaborated in Table 6-13. The number of pores calculated with equation 6.14 and the number of pores obtain by scanning are presented next to each other. The error between these values are presented in the last column of this table.

Table 6-13: Determining of the accuracy of equation 6.14.

	Number of pores calculated with equation 6.14	Number of pores obtained by scanning	Error
Sample 1	181	199	10 %
Sample 2	203	208	2 %
Sample 3	210	205	2 %
Sample 4	234	230	2 %
Sample 6	69	107	55 %
Sample 7	33	53	61 %
Sample 8	198	188	5 %
Sample 9	201	184	9 %
Linear scaled	20269	18400	10 %

The error is within 10% accuracy of the scanned pores. Only if the number of pores decreases to a low value, the error increases significantly. Furthermore, the volume and the number of pores of sample 9 is linearly scaled by a factor 100. This means when 100 buckets are stacked on top of each other, the number of pores is assumed also multiplied by a factor 100. Also in this case the formula describes the number of pores with a 10% accuracy. The validity of formula 6.14 is therefore assumed accurate with a margin of 10% if the number of pores are more than 200.

To determine the accuracy of the other formula, which describes the number of pores (equation 6.16), Table 6-14 is included. The number of pores is calculated with equation 6.16, and the number of pores is obtained by the scanning, and both are presented next to each other. The error between these values are presented in the last column of this table.

Table 6-14: Determining of the accuracy of equation 6.16.

	Number of pores calculated with equation 6.16	Number of pores obtained by scanning	Error
Sample 1	175	199	13 %
Sample 2	211	208	1 %
Sample 3	220	205	8 %
Sample 4	364	230	58 %
Sample 6	87	107	23 %
Sample 7	41	53	28 %
Sample 8	187	188	0 %
Sample 9	197	184	7 %
Linear scaled	19681	18400	7 %

In some of the cases the number of pores are better estimated than equation 6.14 and in some cases the estimation of the number of pores are worse. The nice feature of formula 6.16 is that it can be compared with the analytical model. The factor between the number of pores and the number of stones is 0.7371 in equation 6.16.

In comparison with the analytical model:
- For an infinite number of cubic packed glass balls, the relation between glass balls and pores is 1:1 (proof: porosity is 0.476 and if the volume of the glass ball is $0.524m^3$, the pore volume is $0.476m^3$).
- For an infinite number of rhombohedral-hexagonal packed glass balls, the relation between glass balls and pores is 1:2 (proof: porosity is 0.25952 and if the volume of the glass ball is $0.740m^3$, the pore volume is $0.130m^3$).

The disadvantage of equation 6.16 is that the number of stones has to be calculated first. This calculation is based on the number distribution of stones, see equation 4.6.
- The percentage of mass between two values (sieve sizes) can be derived from the stone-size distribution.
- The total weight of stones in this class can be calculated (percentage * total volume of installed stones * (1-ϕ) * density): m_i.
- The weight of one stone in this class can be calculated based on equation 4.4, see equation 6.17.

$$Weight\ of\ one\ stone = \left(0.84 * \frac{(Dsieve1 - Dsieve2)}{2}\right)^3 \qquad (6.17)$$

- The total weight divided by the weight of one stone results in the number of stones in this class.
- The number of stones divided by the associated percentage of the number distribution results in the total number of stones, see equation 6.18.

$$Number\ of\ stones = \frac{\dfrac{m_i}{(0.84 * d_i)^3}}{Percentage\ of\ number\ distribution} \qquad (6.18)$$

The stones in the bucket are counted and compared with the estimated number of stones, see Table 6-15. For higher gradings the error increase, but the error is not more than 15%. The error is probably caused by the shape factor 0.84 or due to a large difference between the sieve sizes.

Table 6-15: Validation number of stones calculated.

	Stones count	Stones estimated	Error
Sample 1	309	328	6%
Sample 2	417	460	10%
Sample 3	358	358	0%
Sample 4	901	1031	14%
Sample 6	141	133	6%
Sample 7	65	64	2%

Therefore if equation 6.16 is used to describe the number of pores, the inaccuracy of this formula and the accuracy of the number of stones has to be taken into account.

Underneath all lies the error of the CT scanner. The CT scanner is validated with the glass ball experiment. But the error of every sample can be estimated by counting the number of stones in the bucket and checking the number of stones which are obtained by imaging analysis, see Table 6-16.

Table 6-16: Validation of CT scanner.

	Number of stones CT scanner	Stones counted	Error
Sample 1	**310**	309	0%
Sample 2	**410**	417	2%
Sample 3	**361**	358	1%
Sample 4	**784**	901	13%
Sample 6	**147**	141	4%
Sample 7	**69**	65	6%
Sample 8	**318**	309	3%
Sample 9	**314**	309	2%

The number of stones 'seen' by the CT scanner are very close to the actually count number of stones. Only for sample 4 the error is slightly higher. This is probably because some stones in sample 4 are too small (to low scanning resolution) to separate the stones with Avizo Fire. This can therefore also influence the number of pores. The number of pores of sample 4 are probably slightly underestimated.

The influence of the boundaries of the cylinder are also investigated. The volume of the cylinder is stepwise reduced and the number of pores, the number of stones, and porosity of this cylinder is measured. Figure 6-45 is the expected outcome of this analysis.
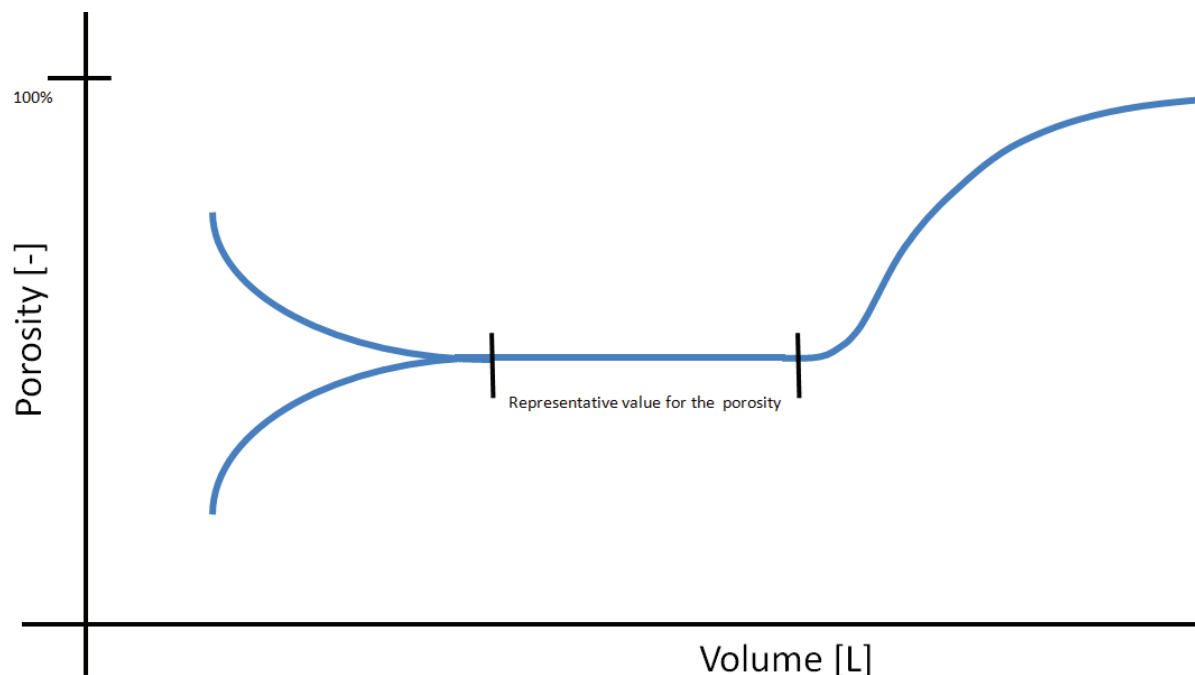
Figure 6-45: Expected influence of volume of cylinder on the porosity.

The results of this analysis is presented in Table 6-17. If the cylinder is too big (larger than 2.3L), the porosity is not representative because the boundary layer is included. The porosity is constant for volumes between 0.7L and 2.3L. If the volume is smaller than 0.7L, the porosity increases again. A volume smaller volume is therefore not representative because in this case the place of the cylinder would determine the porosity. It is assumed that the porosity also can decreases if the volume is smaller than 0.7L if a larger volume of stones is selected inside the small cylinder.

Table 6-17: Number of stones, number of pores, and porosity versus the volume of the cylinder.

	Volume 1	Volume 2	Volume 3	Volume 4	Volume 5	Volume 6	Volume 7	Volume 8	Volume 9
Number of pores [-]	253	199	192	162	106	109	67	27	1
Number of stones [-]	311	238	232	227	164	145	94	34	2
Pore volume [mm3]	7.99E+06	8.72E+05	8.44E+05	8.09E+05	5.73E+05	4.85E+05	2.61E+05	8.79E+04	1.08E+03
total volume [mm3]	1.07E+07	2.29E+06	2.21E+06	2.20E+06	1.55E+06	1.26E+06	6.98E+05	2.21E+05	1.93E+03
Porosity [-]	75%	38%	38%	37%	37%	38%	37%	40%	56%

Number of pores / Number of stones	0.81	0.84	0.83	0.71	0.65	0.75	0.71	0.79	0.50

Not only representative porosities can be investigated with this test, also the error of the number of pores due to the boundary layer. The ratio of the number of pores divided by the number of stones fluctuates between the 0.65 and the 0.85, but there is not a strong correlation visible between the volume and this ratio.

6.6   CONSTRICTION-SIZE DISTRIBUTION RESULTS

The analysis of the constriction-size distribution is difficult with the experimental model. The constriction-sizes of the glass balls gave good results as presented in 6.2. Of the 104 constriction-sizes calculated with the analytical model, 102 were found. After analyzing the individual constriction-sizes, the missing 2 constriction-size were found. The missing 2 were connected to other constriction-sizes. Because of four connected constriction-sizes the area3D was doubled. The constriction-sizes for stones gave a lot of connected constriction-sizes, see Figure 6-46. A very detailed zoom is presented in Figure 6-47.
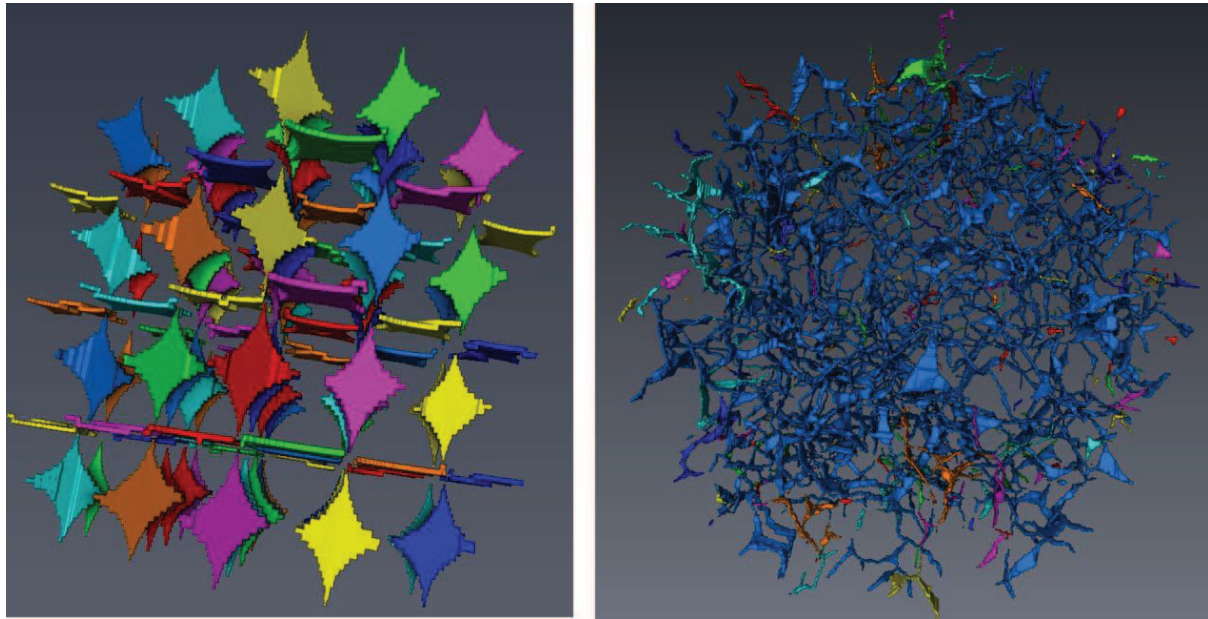
Figure 6-46: Constriction-sizes for glass balls (left) and stones (right).
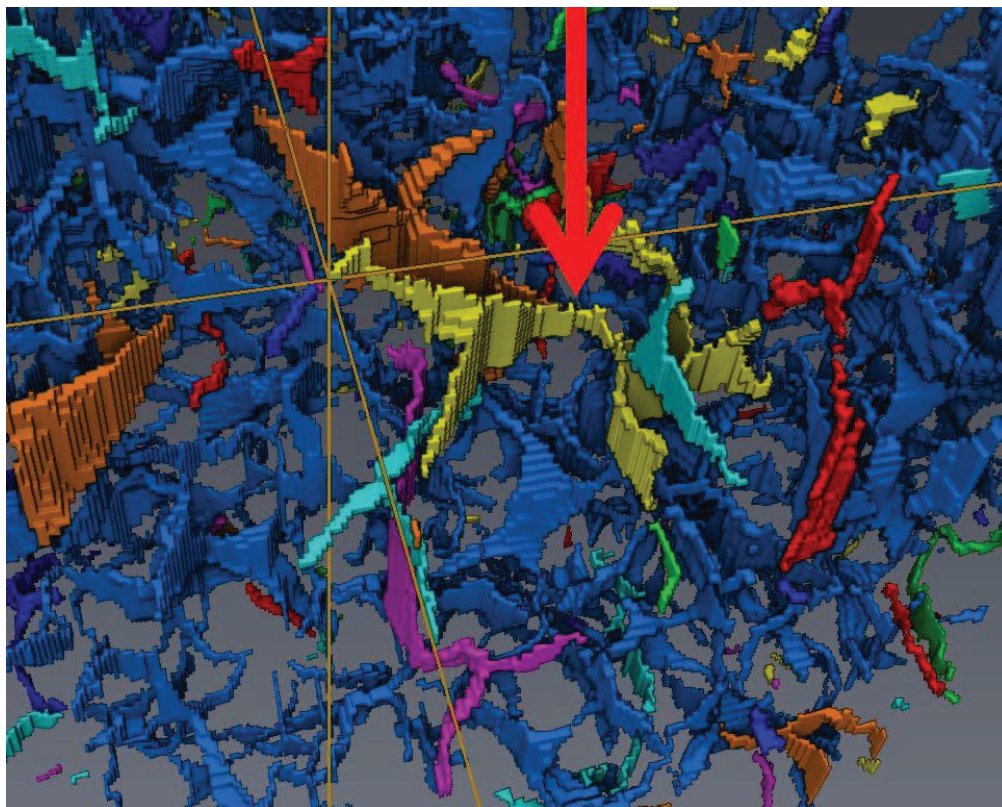
Figure 6-47: Example of connected constriction-sizes.

The second drawback of the experimental model with respect to the constriction-size distribution is the output. As discussed in 6.1.4 the constriction-size is a volume. The output of the constriction-size distribution is:

- Feret diameter
- Area3D
- Volume

The volume is unusable because it depends on the constriction orientation, see Figure 6-13. The feret diameter is not representative for the constriction-size, and therefore the area3D of constriction-sizes is analyzed. The constriction is one voxel wide and therefore the constriction-size is assumed as equation 6.19. This is a small overestimate of the real constriction-size.

$$Constriction\ size = \frac{Area3D}{2} \quad [mm^2] \qquad (6.19)$$

The constriction-size is in mm^2. To describe it in the same units as the analytical model, equation 6.20 is proposed. The constriction is described as the diameter of a circle.

$$Constriction\ size = \sqrt{\left(\frac{4 * \frac{Area3D}{2}}{\pi}\right)} \quad [mm] \qquad (6.20)$$

Because of the first problem mentioned (the constrictions are interconnected), a manual solution is proposed. All the constrictions are individual analyzed. When the constriction is not interconnected, the constriction is registered, see Figure 6-48.
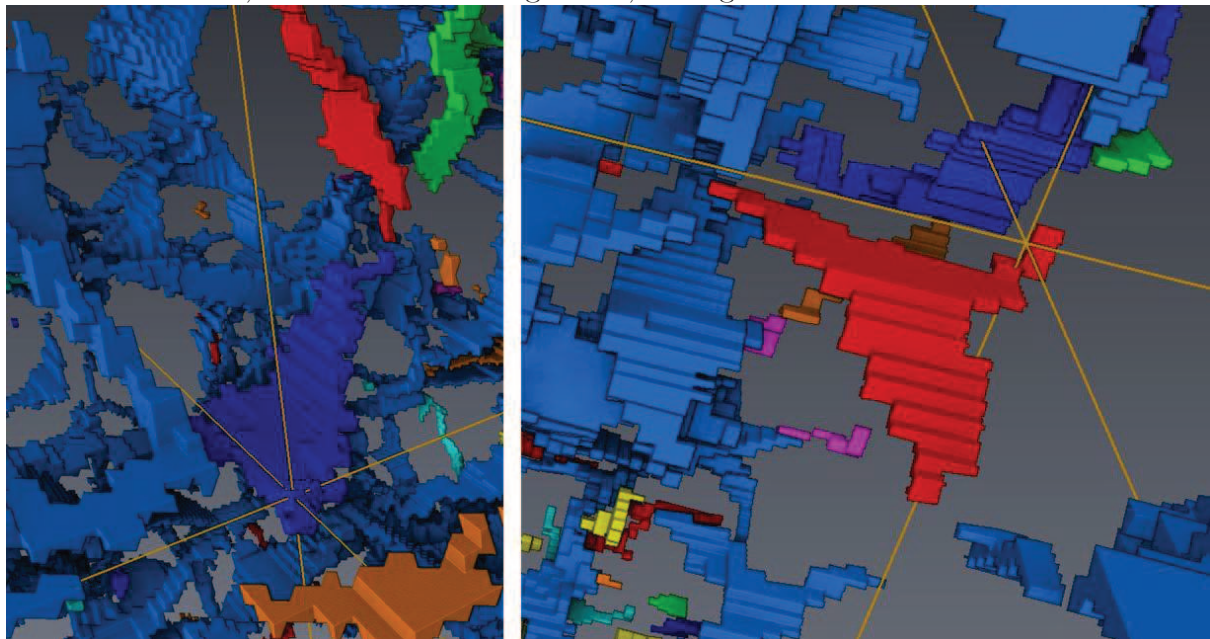
Figure 6-48: Two non interconnected constrictions.

A total of 10 constrictions is registered. The data of these individual registrations is presented in Table 6-18. The constrictions, described as equation 6.20, are presented in column 'D opening'. The mean of this column and the standard deviation of this column forms the mu and the sigma for the approximation by a normal distribution. This approximation is presented in Figure 6-49.

Table 6-18: 10 individual measured constrictions.

Area3d (mm^2)	Volume3d (mm^3)	Length3d (mm)		p	P		D opening			D opening
37,3384	13,5899	7,50396		10%	10%		4,88		Mean opening	7,62
39,8042	10,4904	12,0487		10%	20%		5,03		STD opening	1,68
56,9208	16,2125	11,248		10%	30%		6,02			
94,1876	26,226	12,2813		10%	40%		7,74			
102,756	29,8023	13,4901		10%	50%		8,09			
111,34	34,3323	12,0053		10%	60%		8,42			
123,724	42,4385	14,6415		10%	70%		8,87			
124,319	33,8554	15,4028		10%	80%		8,90			
127,424	40,7696	14,9031		10%	90%		9,01			
135,052	46,9685	15,9671		10%	100%		9,27			
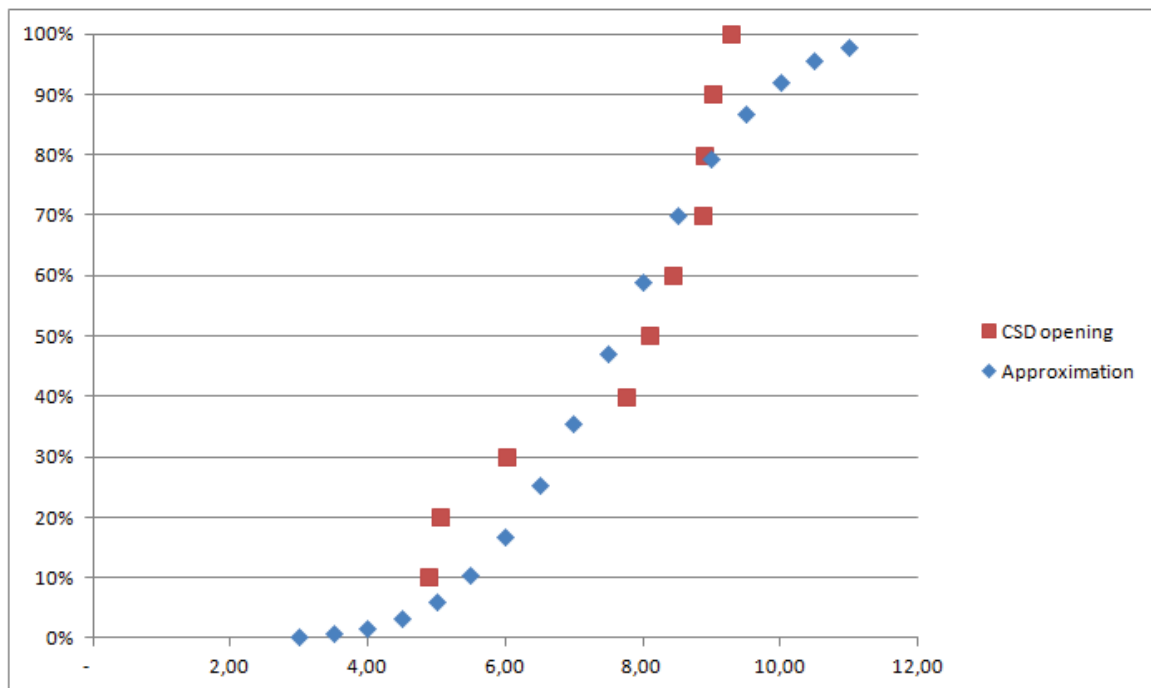
Figure 6-49: 10 individual constrictions and the approximation of these constrictions.

To place this constriction-size distribution in perspective, this distribution is plotted in the same graph as the outcome of the analytical approach, see Figure 6-50. The input is the mass distribution of sample 1 (D50=25mm, D85/D15=1.5). The output of the analytical model (spheres!) is the red line for the most dense arrangement (ϕ=25.95%) and the purple line for the most loose arrangement (ϕ=47.64%).

The light blue line is the constriction-size distribution of stones (ϕ=38%) for sample 1 with:
- Mu   =7.62
- Sigma =1.7
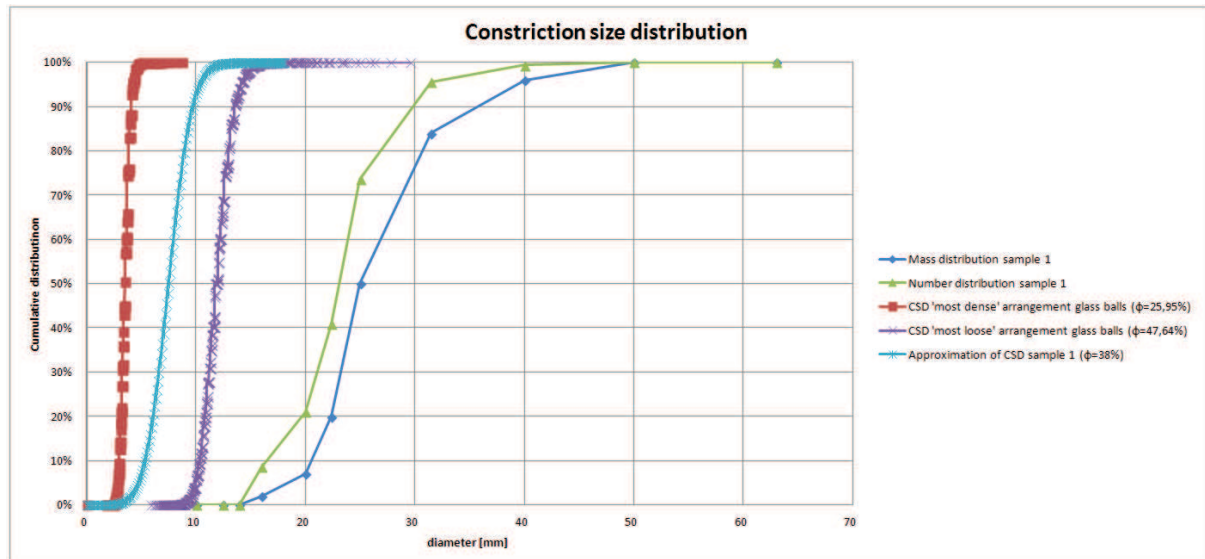
Figure 6-50: Constriction-size distribution of sample 1.

To investigate the light blue line of Figure 6-50 in even more detail, equation 5.14 and equation 5.15 are used to describe the constriction-size distribution for spheres. This results in:

- Mu   =8.24
- Sigma =0.9

These values are graphically presented in Figure 6-51. The slope of this line is a bit less steep in comparison with the analytical distribution. The mean of this line 'seems' to correspond very well with the analytical model of spheres.
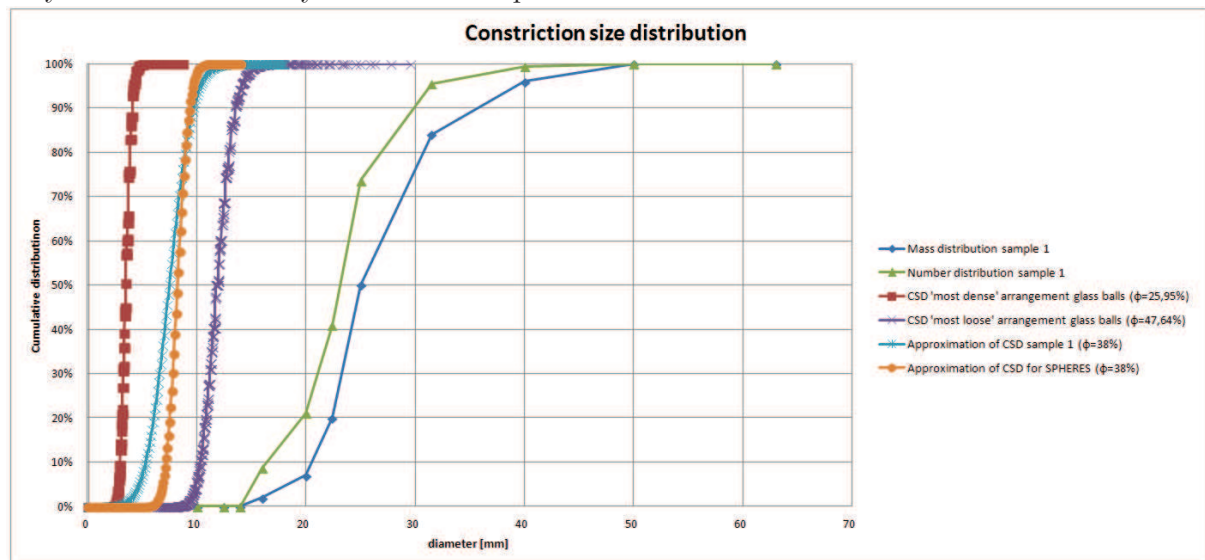
Figure 6-51: Constriction-size distribution of sample 1 including CSD for spheres.

A hard conclusion is not statistical justifiable, because the constriction-size distribution of stones is based on 10 values of one sample. However, it gives confidence that the analytical approach that describes the constriction-size distribution is reasonable. It could not be falsified with the experimental model. The constriction-size distribution for stones lies in the same range as the constriction-size distribution for spheres.

6.7   ADDITIONAL FINDINGS

By selecting another range of gray patterns (threshold between 617 – 3071) the air is 'removed' and the only object left are the stones. After separating the stones the stones are labeled. The label includes the volume of each stone. With the volume of the stone known, the Dn of the stone can be obtained by using equation 6.21.

$$D_n = Volume_{stone}^{\frac{1}{3}} \qquad [m] \qquad\qquad (6.21)$$

The result for sample 9 is presented in Figure 6-52. The blue line is the mass distribution of the stones in the bucket, which is established by sieving. The red line is the scanned mass distribution of the stones. There is quite a difference. This error is because the sieved mass distribution is based on the sieve size (D) and the scanned distribution is based on the Dn value.
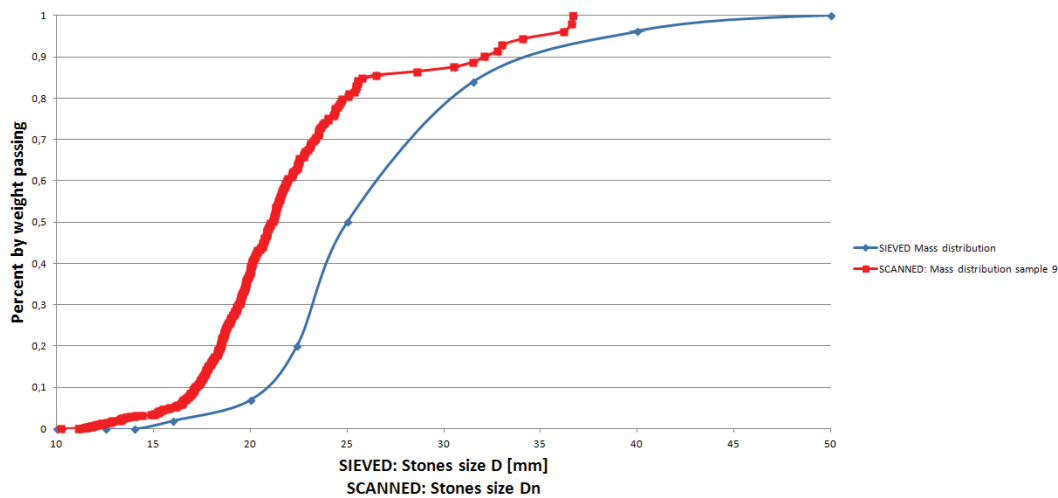
Figure 6-52: Sieved and scanned mass distribution of stones.

The relation between Dn and D is discussed in chapter 4, but repeated in equation 6.22.

$$D_n = 0.84 * D \qquad\qquad (6.22)$$

By dividing the red line in Figure 6-52 by the factor 0.84 Figure 6-53 is obtained.
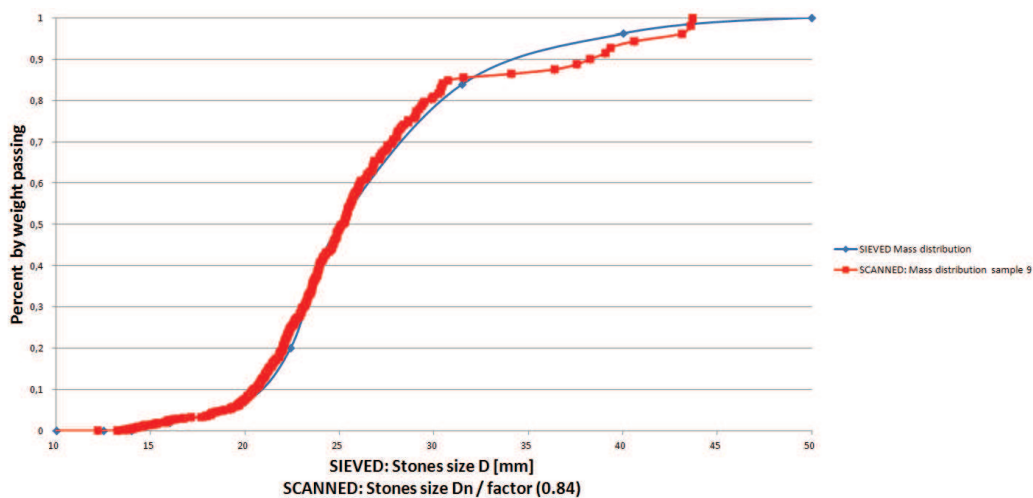
Figure 6-53: Scanned mass distribution of stones divided by factor 0.84.

It seems that the factor 0.84 represents the shape factor quite well. The small error above 85% can be explained as follows:

- It is a mass distribution so less stones determine the top part of the shape of curve
- The sieve sizes are more coarse at the top part of the curve. The mass distribution is based on sieves of 14mm, 16mm, 20 mm, 22.4mm, 25mm, 31.5mm, 40mm, 50 mm.

This principal can also be applied to the number distribution. The number distribution of stones is derived from the mass distribution of stones as also explained in chapter 4. The derivation looks sound if it is compared with the scanned curved, see Figure 6-54 and Figure 6-55. In Figure 6-55 the scanned values (Dn) are again divided by 0.84.
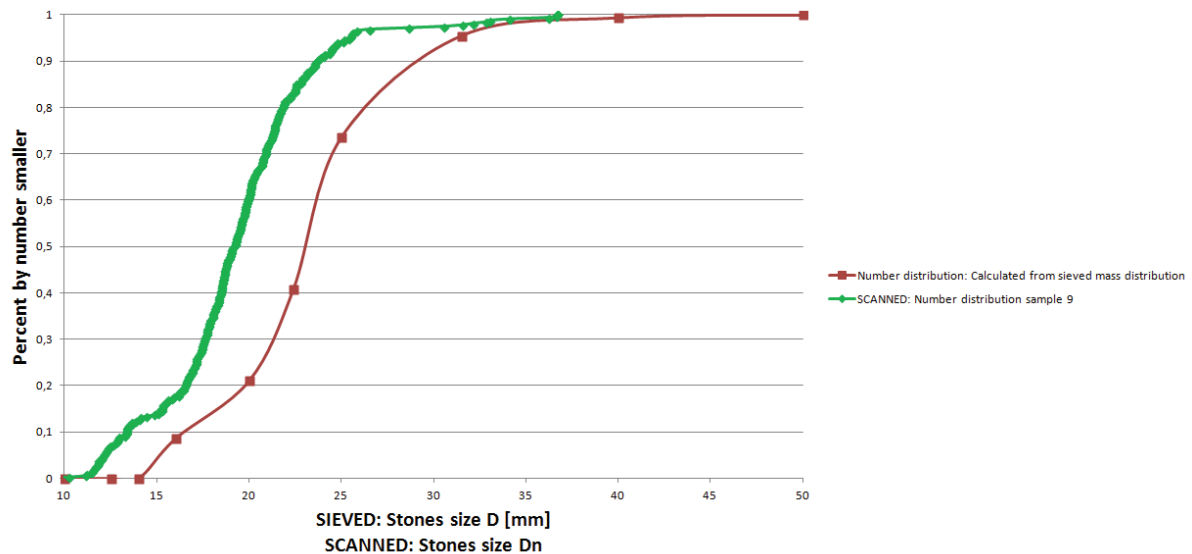
Figure 6-54: Sieved and scanned number distribution of stones.
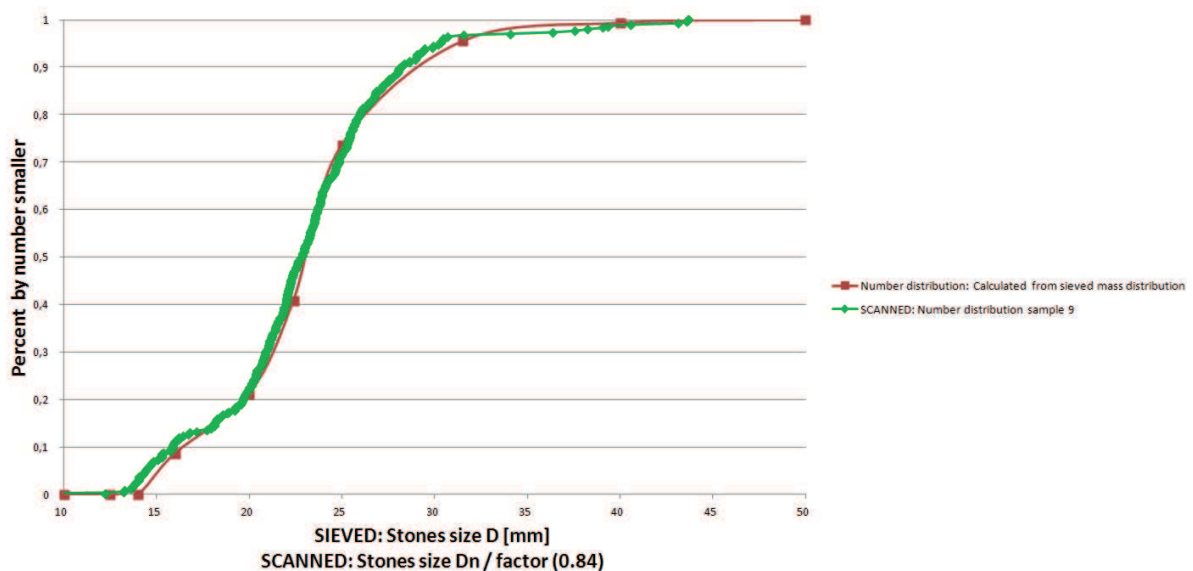
Figure 6-55: Scanned number distribution of stones divided by factor 0.84.

7. INTERPRETATION OF RESULTS

Now we are faced with the challenge of how to interpret the results of the models in chapter 5 and chapter 6 for ecology. In section 7.1 the suitable cavities for the lobsters are discussed, based on the literature review in chapter 2. In section 7.2 a practical example is elaborated to describe the application of this research. In appendix C an additional case is presented.

7.1 CAVITIES FOR LOBSTERS

As described in the literature review in chapter 2, lobsters live and find shelter in cavities. Unfortunately, the preferred cavity sizes for the lobster are not found in literature. However, the author found a paper about the carapace length (CL) distribution of wild lobsters, see Figure 7-1 (Schmalenbach, Janke, & Buchholz, 2009).
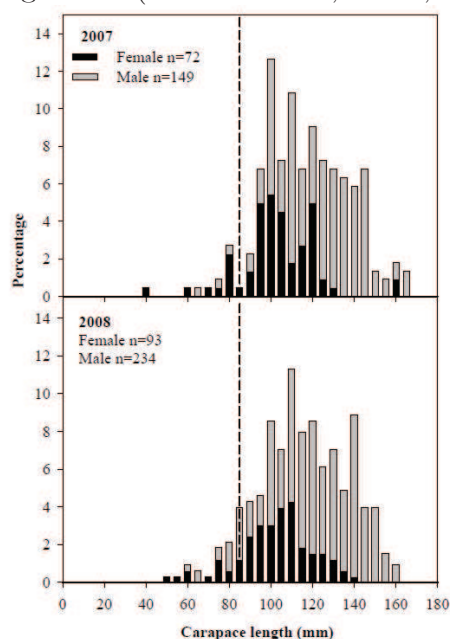
Figure 7-1: Size distribution of wild captured lobsters at Helgoland per 5 mm size group. The dashed vertical line represent the legal size for landing lobsters.

In 2007, 221 wild lobsters were captured, and in 2008, 327 wild lobsters were captured at Helgoland in the North Sea. The range of the CL was between 37 and 165 mm with a mean of 110 ± 22 mm (114 ± 22 mm CL in 2007 and 110 ± 23 mm CL in 2008). The CL of the 149 wild captured females (carrying eggs) ranged from 85 to 140mm with a mean of 108 ± 11 mm.

In the same report was found that the rostrum length is about 30% of the carapace length. The total length is almost three times the carapace length, see Figure 7-2.
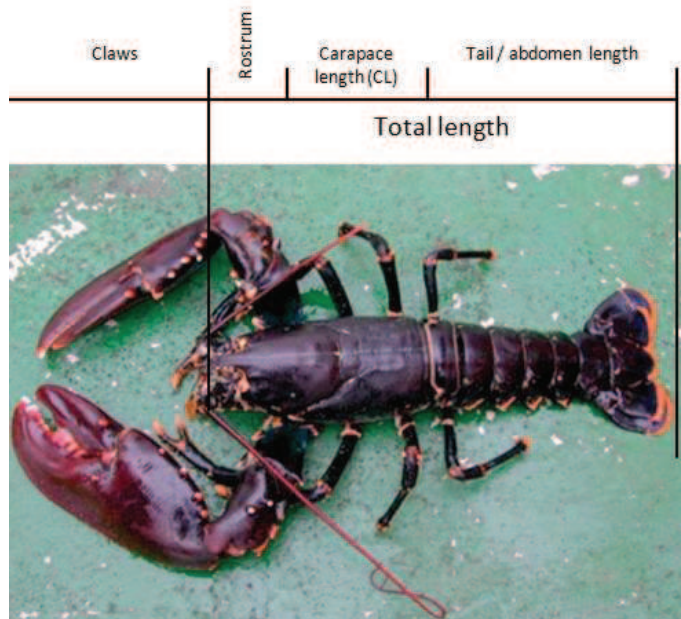
Figure 7-2: Lobsters and length measurements.

This data forms the basis for deriving the preferred cavity sizes for the lobsters. The lobsters have to be able to pass through opening of the cavity and have to be able to fit inside the cavity. Therefore two assumptions are made.

Assumption 1: cavity opening
The opening of a cavity must not be too large for the lobster because of the predators. The opening must not be too small because the lobsters has to go through the opening to get inside the cavity. The preferred opening is probably determined by the width of the claws and legs of the lobster. The width of the claws are assumed in the same order as twice the carapace length. Therefore the assumption is made that the opening for a lobster should be about twice the carapace length, see equation 7.1.

$$D_{cavity\ opening} \approx 2 * Carapace\ Length \qquad [m] \qquad\qquad (7.1)$$

Assumption 2: cavity volume
The lobster does not have to fit perfectly in the cavity. Sometimes the claws can protrude outside the cavity. The assumption is made that the volume of cavity has to be the total length to the third power, see equation 7.2. The total length is assumed 3 times the carapace length.

$$V_{cavity} \approx (Total\ Length)^3 \approx (3 * CL)^3 \qquad [m^3] \qquad\qquad (7.2)$$

Remarks:
The validity of the assumptions described above needs to be tested via ecological research. The preferred openings and cavities are here determined just from length indications. Furthermore, there are factors besides the opening and the cavity volume that are relevant, such as:
- Shape of the opening and the cavity
- Max length of the opening and the cavity
- The orientation of the opening and the cavity

All these assumptions are made insightful in the practical example in the next section.

7.2   PRACTICAL EXAMPLE

In this section a practical example is discussed which falls within the scope of this research. The number of cavities and their sizes are discussed for an offshore wind turbine. During this research a question is received from the dredging industry which shows the generic applicability of this research. This question is presented in appendix C.

7.2.1   Case: offshore wind turbine

The wind turbines of offshore wind farm 'Meerwind' in Germany are protected with a scour protections which consists of rock. The data is summarized and depicted below.
- $D50 = 0.6$ m
- $V=575$ m^3
- $D85/D15 = 1.5$ (assumed)
- Porosity $= 38\%$ (assumed)
- Dimensions are sketched in Figure 7-3
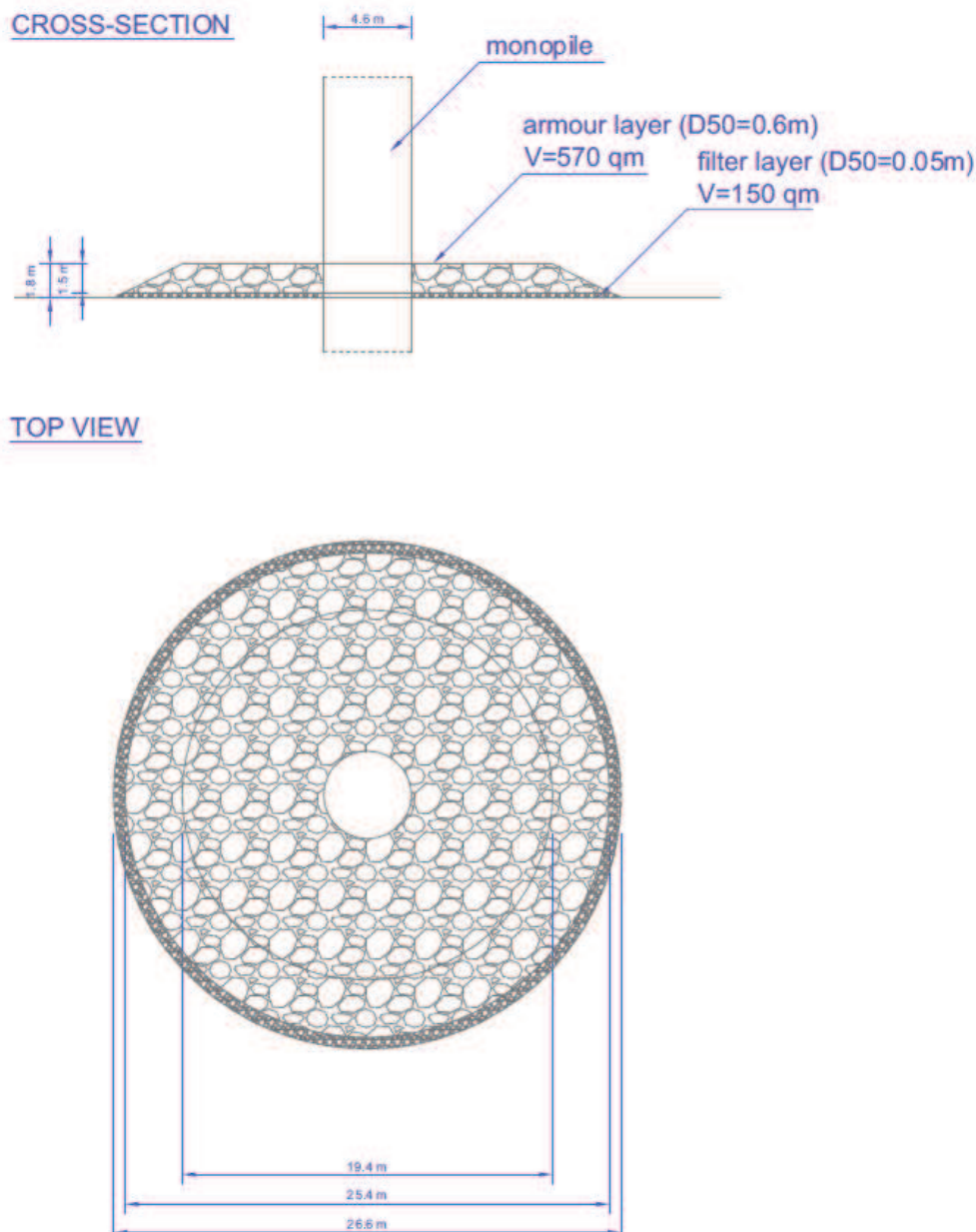
Figure 7-3: Bed protection of a monopile of offshore wind farm 'Meerwind'.

Figure 7-4 is the result if the above mentioned values are filled in equation 6.10 and equation 6.14. The total number of cavities is almost 3300.
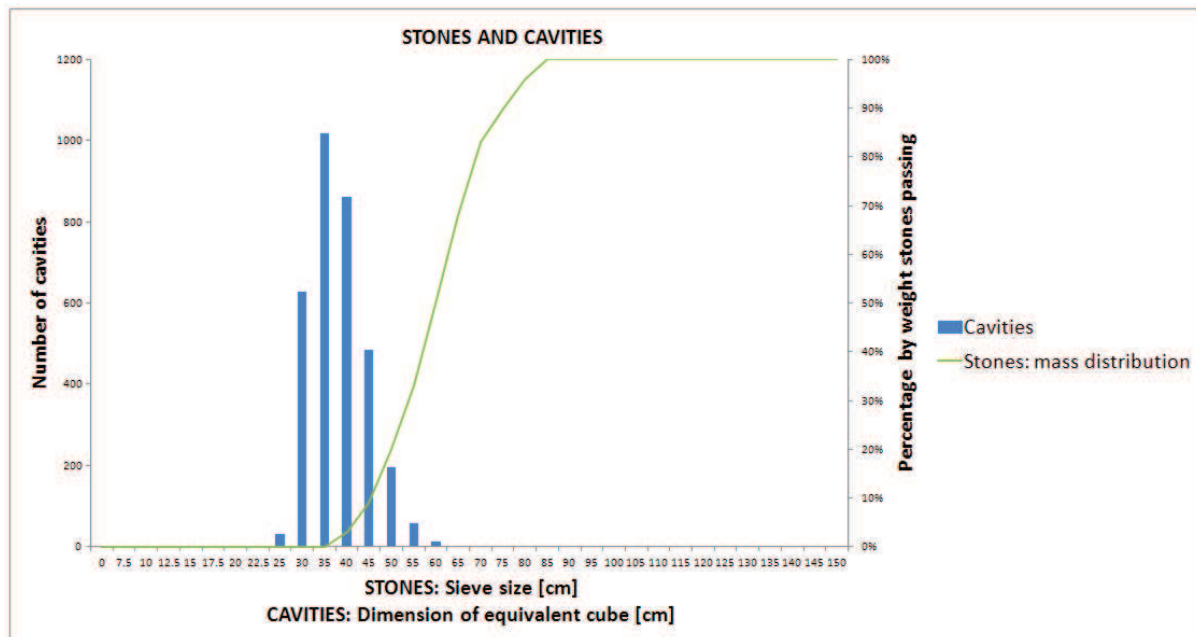
Figure 7-4: Stone-size distribution and cavities of a bed protection of a wind turbine.

Not all of these cavities can function as a lobster habitat due to:
- Location of the cavity
  The bed protection of the offshore wind turbine is 1.5 meter in height. Lobsters prefer shelter at surface level.
- Orientation/shape of the cavity
  The cavities which have the shape a 'horizontal column' are less attractive for shelter.
- Opening of the cavity
  The lobsters has to fit through the opening of the cavity.

These three points have to be taken into account. For these aspects assumptions have to be made, because these points are not included in the model.

Assumption location:
The cavities which are attractive for the lobsters are assumed not 'deeper' than one D50. So in this case the interesting area is the first 60cm. The rest of the height of the bed protection is not suitable as a lobster habitat. The maximum number of potential lobster habitats is therefore $40\% \left(\frac{0.6}{1.5}\right)$ of the total number of cavities.

Assumption shape/orientation:
The assumption is made that orientation of the cavities is uniform in all directions. Based on this assumption a new assumption is made that 75% of the total number of cavities are not suitable as a lobster habitat, see Figure 7-5. Also the shape of the cavities are not taken into account, but because of the derivation of the cavities and the assumption that the lobsters like to squeeze in, the shape effect is ignored.
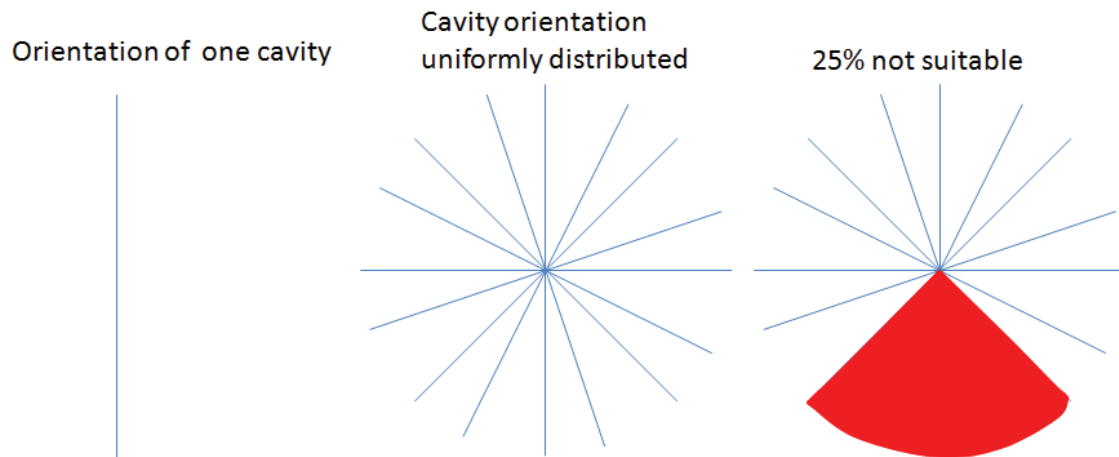
Figure 7-5: Cavity orientation.

Assumption opening:
What is the chance that the cavity size is suitable for the lobsters, but the lobster cannot go through the opening? This is a difficult assumption, because the opening distribution is not related to the cavity size distribution. This means that it is not known if large cavities can have small openings and vice versa. This relation is not researched.

The most elegant way is to relate the openings and the cavities, but with the gained knowledge this is not possible. To make an assumption about the reduction factor due to cavity openings that are too small, the openings are related to the lobsters. The openings in the bed protection and the openings needed for the lobsters are presented in Figure 7-6.
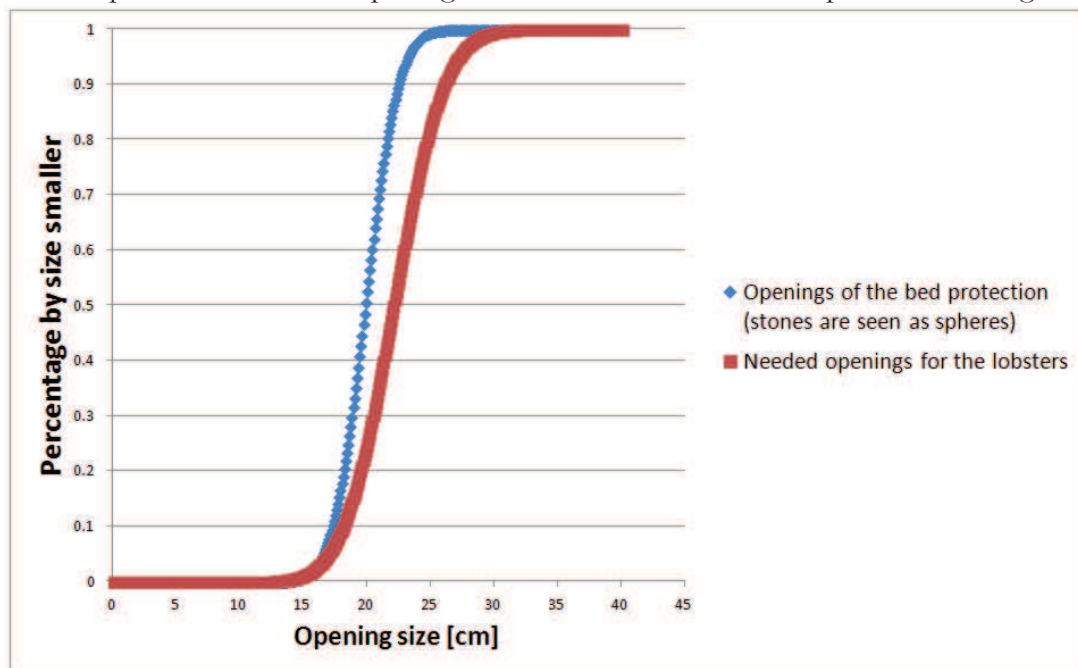
Figure 7-6: Assumed openings in bed protection and the needed openings for the lobsters.

It is difficult to draw any conclusions from this figure, because the lines are so close together. Both lines are based on significant assumptions. The stones are modeled as spheres and the real opening needed for the lobster is also an assumption. Furthermore, the shape of the opening is not taken into account. The surface of the openings in the bed protection are translated and presented as disks with diameter D. The assumption is made that the lobster needs diameter D (width between the claws).

So if Figure 7-6 is close to reality, then it can be conclude that the openings are too small for the largest lobsters. About 50% of the wild lobster population needs a opening larger than 22 cm and about 90% of all the openings are smaller than 22 cm. However, the author cannot draw this conclusion with any certainty. In this practical calculation example the reduction factor due to too small openings (the cavity size is suitable for the lobsters, but the lobster cannot go through the opening) is set to 50% to continue this calculation example.

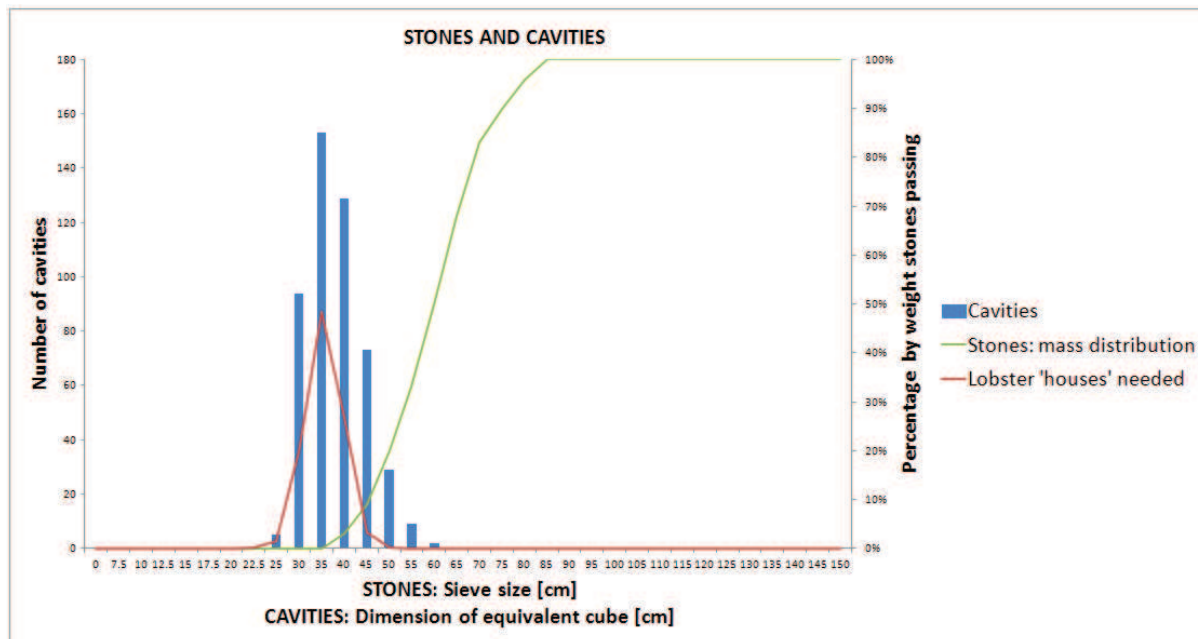Al these factor together lead to the summarizing graph below, see Figure 7-7.
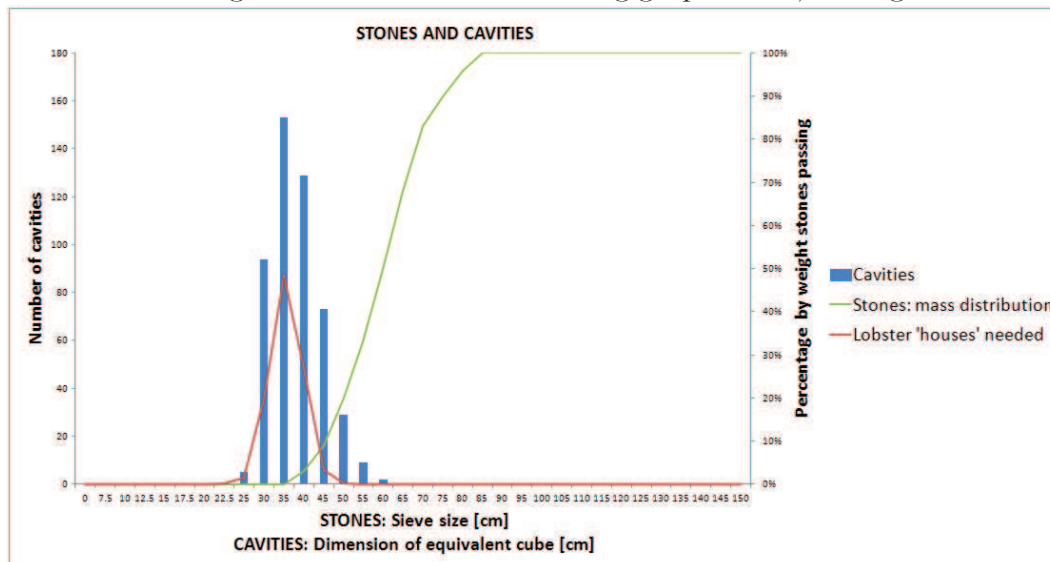
Figure 7-7: Stone-size distribution, number and size of suitable cavities, and the needed cavities for the wild European lobster.

Conclusions:
- The cavity sizes in the bed protection have already very suitable sizes in comparison with the required cavities for the lobster.
- There are almost 500 suitable cavities in a bed protection of an offshore wind turbine with a surface of almost 500 m².
- The cavities are related to the wild lobster population. It provides good shelter for lobsters bigger than the legal landing size and also for females carrying eggs. However, for the small juvenile lobsters the cavities are too big. Lobster with an age of 3 years have a carapace length of 60 mm. This means, following the assumption in equation 7.2, that this lobster need a cavity of 180mm. In Figure 7-7 it is visible that the cavities are bigger than 18cm. Therefore this bed protection is not suitable for juvenile lobsters.
- By adapting the design (smaller D50 or wider grading) also favorable ecological conditions can be provided for juvenile lobsters. The stability of the bed protection is no longer sufficient for equation 2.26. Whether the bed protection really fails is not investigated. Additional spots can be installed to provide cavities for juvenile lobsters.

This case is only explicated for lobsters, which is a good starting point for eco engineering. The lobsters were selected because of their declining rate and their economical value. However, more realistic ecological results can be achieved if more species are included. The limiting conditions of all the species have to be obtained and then this model would really work. The lobster is just a positive indicator. Based on more limiting conditions of species and further technical development of the model (especially the openings), future bed protections can really be designed to be ecologically friendly.

8. CONCLUSIONS & RECOMMENDATIONS

The conclusions about ecology-based bed protections of offshore wind farms are presented in section 8.1, followed by the main recommendations in section 8.2.

8.1 CONCLUSIONS

The conclusions are presented in the same order as the research question in section 1.4. First, the conclusions from the literature review are elaborated. Secondly, the conclusions about the pore-size distribution and the constriction-size distribution are drawn. In subsection 8.1.3 the main research question is answered. In the last subsection a reflection on the results is presented.

8.1.1   Literature review and parameter conclusions (part I)

"Which species can be selected to provide favorable ecological conditions near offshore wind turbines and what are the parameters to describe these conditions?"

- At Offshore Wind Farm Egmond aan Zee no short-term effects on the benthos are found, while the new hard substratum of the scour protection led to the establishment of new species and new fauna communities (Lindeboom, Kouwenhoven, Bergman, & Bouma, 2011).

- In the past a significant part of the North Sea floor consisted of hard substrate, but due to trawling activities by humans this hard substrate is removed. Nowadays the North Sea floor consists of sand. By placing stones for the bed protection of offshore wind farms hard substrate will be added which was present in the past. So, the hard substrate balance will more or less be restored.

- The Cod and the European lobster are examples of the species found around offshore wind turbines. These species find shelter between the hard substrate (Winter, Aarts, & van Keeken, 2010).

- The Cod and the European lobster are selected because they are economically attractive and their stock is decreasing.

- The Habitat Suitability Index is not used, but all the abiotic influencing parameters for these species are described.

- The main influencing parameters are the physical conditions, the design of the bed protection, the material properties of rock, the water quality, and the external effects.

"What are the determining parameters for the technical requirements of a bed protection design of an offshore wind turbine?"

- Bed protections are installed to prevent scour around the monopile. Without scour protection the scour can be almost two times the pile diameter for slender piles, which influences the pile foundation.

- The bed shear stress is induced by the waves, the currents, and their interaction together with monopile. The pile diameter is an important parameter.

- The bed shear stress, the Shields parameter, the relative density, the density of water and the acceleration of gravity are the main parameters that determine the median stone size for the bed protection.

- Furthermore, the material properties of the stones, the filter layer, and the dimensions of the bed protections are important for the technical requirements.

"What are the matching and controllable parameters between the favorable ecological conditions and the technical requirements?"

- The list of parameters to provide favorable ecological conditions and the list of parameters that determine technical requirements results in six matching and controllable parameters.

- These six parameters are:
  o Waves
  o Currents
  o Dimension of the bed protection
  o Pore size distribution
  o Turbidity
  o Properties of rock

- One of these six main parameters, which combine favorable ecological conditions and the technical requirements, is elaborated in further detail. Due to the authors interest and the authors background, the pore-size distribution is chosen for further detailed investigation.

8.1.2   Model and interpretation conclusions (Part II)

"What are the relations between the stone-size distribution, the pore-size distribution, and the constriction-size distribution?"

Two models are developed to derive the pore-size distribution from the stone-size distribution. With the same models it is attempted to derive the constriction-size distribution from stone-size distribution.

The first model is based on spheres. The pore-sizes and the pore-openings are determined geometrically. The second model is based on an experiment. In this experiment stones are measured and put in a bucket. This bucket is scanned with a medical CT scanner and the results are analyzed with an imaging technique.

The results are as follows:

Pore-size distribution
- The pore-size distribution can be derived with medical CT scanner and an imaging software tool. The slices made by the CT scanner must be smaller than 1 mm for stones of 25 mm to get sufficient resolution. The resolution of great importance for the imaging operations with the imaging software tool.

- The pore-size distribution cannot be derived with the analytical model. The pore-size can only be determined for uniform spheres.

- The pore-size distribution based on experimental results is formulated below:

$$f\left(x, P_{80}, m, F\right) = 1 - e^{\ln(0.2)*\left(\frac{x-F}{P_{80}}\right)^{m}} \qquad [m] \qquad for\ x > F$$

With
$$P_{80} = \left(-2.13 * \phi * \frac{D85}{D15} + 13.2\right) * \frac{D50}{25}$$
$$m = \left(-0.533 * \phi * \frac{D85}{D15} + 2.29\right)$$
$$F = (27.5 * \phi - 3.35) * \frac{D50}{25}$$

- The formula that describes the pore-size distribution corresponds well with the pore-size distribution found using the CT scanner and imaging software. However, this formula is not fully validated. The analytical model with spheres is not sufficient to validate the results.

- To validate the model a scan is made with glass balls. The output of this scan was exactly the same as the input. Furthermore, the number of stones of the samples was counted by hand and compared with the number of stones counted using the imaging software tool. The results have less accuracy than the glass ball scan (probably due to the stone shape and the random packing of the stones), but the errors are not significant.

Number of pores

- The number of pores can be described using the analytical model and is related to the number of spheres. The number of spheres versus the number of pores is 1:1 for an infinite number of cubic packed glass balls (most loose arrangement) and 1:2 for an infinite number of rhombohedral-hexagonal packed glass balls (most dense arrangement). The number of pores for a random packing is not derived.

- Two formulas are derived to describe the number of pores for the experimental model. The first formula is based on all the input parameters of the stone-size dsitribution. The second formula is based on the number of stones which have to be calculated first. Both formulas are described below:

$$Number\ of\ pores = 1.81 * \left(\frac{D85}{D15}stone\right)^{0.25} * \frac{V * (1 - \phi)}{D50^3} \qquad [-]$$

$$Number\ of\ pores = 0.737 * number\ of\ stones \qquad [-]$$

- The formulas for the number of pores are not validated. The validation scan with spheres gives confidence that the obtained results are a good indication.

- The last mentioned formula for the number of pores can be compared with the analytically determined number of pores. The relation between the number of stones and the number of pores is 1:0.74. This is lower than the analytical model, which is assumed due to the stone shape and the random packing of the stones.

- The formulas that describe the number of pores have an error margin of 10% compared with the number of pores found using the CT scanner. However, the error increases when the number of pores is very low.

Constriction-size distribution

- The formula to describe the pore openings is derived geometrically with spheres.

- The curve fit (normal distribution) that represents the constriction-size distribution is formulated below.

$$\mu = (1.57 * \phi - 0.267\ ) * D50 * \left(-0.152 * \frac{D85}{D15} + 1.23\right) \qquad [m]$$

$$\sigma = (0.148 * \phi - 0.0223) * D50 \qquad [m]$$

- This curve fit brings some marginal but non-significant errors.

- The constriction-size distribution is not derived using the experimental model. Most of the constrictions are connected using this model. Therefore, a few constrictions are manually investigated and the results could not falsify the analytical results.

The model can be applied to other areas of research than bed protections of an offshore wind turbines. It can also be applied to revetments, breakwaters, or other civil engineering structures made of rock.

> *"What cavity-sizes and opening-sizes are suitable to provide favorable ecological conditions?"*

- The measured size distribution of a lobster population is found in literature (Schmalenbach, Janke, & Buchholz, 2009). Based on these finding the preferred cavity sizes and openings are derived, because the preferred cavities for the lobsters are not found in literature.

- The assumption is made that the minimum opening is determined by the width of the claws. This comes down on twice the carapace length.

$$D_{cavity\ opening} \approx 2 * Carapace\ Length \qquad [m]$$

- The assumption is made that the volume of cavity is determined by the total length of the lobster (without the claws). This comes down on 3 times the carapace length to the third power.

$$V_{cavity} \approx (Total\ Length)^3 \approx (3 * CL)^3 \qquad [m^3]$$

- Note: the bed protection provide potential lobster habitat. The real effect of providing favorable ecological conditions in this way is still uncertain. Whether holes will be occupied depends on multiple factors.

- Second note: The derived formulas of the pore-size distribution and the constriction-size distribution can also be compared with suitable cavities and/or openings for other species than lobsters. For these species the limiting conditions would have to be established as input for the model.

> *"How can cavities, which provide favorable ecological conditions for lobsters, be included in the technical design of a bed protection?"*

The ecological interpretation of the derived formulas of the pore-size distribution and the constriction-size distribution is concluded here. The example of the offshore wind turbine (chapter 7) shows that the number of cavities and the cavity sizes can be estimated, see Figure 8-1.

Targeted cavities can be include in bed protection design. In this example the cavities were already suitable for the lobster population. The cavities are not suitable for juvenile lobster. By adapting the design (smaller D50 or wider grading) also favorable ecological conditions can be provided for juvenile lobsters. The stability of the bed protection is no longer sufficient following the stability requirements of bed protection designs. Whether the bed protection could fail is not investigated. Additional spots on or around bed protections can be installed to provide cavities for juvenile lobsters.

Figure 8-1: Stone size distribution, number and size of suitable cavities, and the needed cavities for the wild European lobster.

8.1.3 General conclusion

> *Research question: "How can technical aspects of bed protection designs of offshore wind turbines be altered to provide favorable ecological conditions for marine life?"*

This research question is answered within the scope of this research: the *pore-size distribution* is one of the technical aspects found, which can be included and altered in bed protection designs to provide favorable ecological conditions for marine life. The pore-size distribution has until now not been included in bed protection designs, while, in fact, it is always installed. This distribution can be derived, and future bed protections can be designed based on favorable cavity sizes for species, as well as technical stability. This holds for the *constriction-size distribution*.

8.1.4 Reflection on results & research

The answer of this research question is influenced by the scope of this research. The answer of this thesis is given within the defined framework and scope. If the research question says the same, but the scope was set differently, the outcome of this thesis would have been different. For instance by looking at an offshore wind farm in totality (instead of looking at one offshore wind turbine), wave patterns could be investigated, which can stimulate larval transport. Another possibility, which is ignored due to the scope, is looking at other types of scour protection designs. For instance, a cylindrically plate around the monopile to reduce the scour. The cylindrically plate could be designed in such a way that it could provide favorable ecological conditions for species.

Furthermore, even within the scope a certain direction is chosen which influences the conclusions of this research. Another parameter, described in chapter 3, could be chosen to provide favorable ecological conditions for lobsters. Also other species could be selected to provide favorable ecological conditions for.

These choices are the main influencing choices made in this thesis which influences the results and this research.

8.2   RECOMMENDATIONS

The outcome of this research results in the following recommendations:
- To increase the statistical significance of the derived formula, the dataset has to be increased. A larger dataset can be generated by repeating the experimental tests. Repeat not only the test for the same samples, but create a wider diversity in samples (wider grading, lower/higher porosities etc.).

- Explore alternative methods to find the pore-size distribution and the number of pores. Other methods mentioned in chapter 4 could validate the found results. The experiment of 'dropping glass balls' shows the most potential.

- Find a alternative way of determining the pore openings with a CT scanner. All the openings can be evaluated individually or the algorithm can be rewritten to disconnect the openings. The mathematical operations possible in Avizo Fire are expected non suitable to disconnect the openings. Scanning with a higher resolution will reduce the connectedness of the openings, but will not completely reduce this phenomenon.

- An ecological research is needed to establish the favorable ecological conditions of the lobster in detail. Especially, the behavior of the lobster in hard substrate (suitable holes and suitable openings) is most interesting. The made assumptions in chapter 7 can be validated.

- This thesis provides a formula that estimates the number of pores, the pore openings, and the pore-size distribution, but it is not known if the pores will be occupied. Therefore field measurements have to be conducted or a pilot has to be set up.
  - First of all, a lobster field needs to be surveyed.
  - Secondly, natural recruitment needs to be observed at the bed protection of an offshore wind turbine.
  - Furthermore, a number of tagged lobsters have to be released after installation of bed protection around a monopile. The behavior and patterns of the lobsters have to be monitored in and around the bed protection with divers and a ROV. The behavior of lobsters have to be monitored also around a monopile in the same offshore wind farm where the tagged lobsters are not released.
  These field measurements can establish the type of suitable cavities and the number of suitable cavities. Another interesting question is if the number of lobster 'houses' can determine the population size of lobsters.

- More insight has to be gained in the stability of a bed protection if wider grading is applied. More knowledge can create more freedom in designing the optimal bed protection (in terms of ecology, stability, and cost effective).

The following recommendation are made for the extension of this research:
- Study the properties of pores and openings. The properties of interest are the shape, the orientation, and the length. These properties can give more insight in the suitability of a cavity. This study can be based on the obtained data.

- Investigate the local variability of the top layer of the bed protection with respect to the rest of the bed protection. Most ecological activities take place at the surface.

TUDelft Delft University of Technology   Boskalis

- Search for a method to relate the pore openings to the cavities.

- There is an apparent need to study more species and establish their favorable ecological conditions. A matrix with limiting conditions of species has to be derived. Furthermore, the chosen species are 'positive', but there will be species which are negatively affected by the presence of the bed protection.

The following recommendations are made for additional research:
- A Joint Industry Project (JIP) is started to make a handbook for scour protection. One of the ideas is to make a single layer system. The single layer system consists of a very wide grading. The technical feasibility of this idea can be investigated by determining the maximum constriction-sizes. The method used in this thesis can form the basis of the determination of these constriction-sizes. Furthermore, this proposed solution should be tested in ecological context. Are the created cavities preferred?

- The design rules for geometrically closed filters are based on the openings between the grains. The method applied in this research to establish the openings can confirm these design rules or optimize these design rules.

- The openings between the grains and the pore sizes are of large influence for the permeability of a stone class. The applied methods in this thesis can also be linked to porous flow or wave damping studies.

- Porosity is a parameter of influence for the pore-size distribution and constriction-size distribution. Can the porosity be related to the installation method? Additional research can lead to new insights about the relation between the installation of rock and corresponding porosity.

- The relation between the sieve size (D) and the diameter of a equivalent cube (Dn) is mentioned in section 6.7 of this thesis. The applied method in this thesis can lead to a more substantiated determination of this factor.

The following recommendations are made for Boskalis and the industry:
- There is an overlap between technical designs of civil structures and ecological preferences of native species. Future civil rock works can be designed in a way, which is also beneficial for its surrounding ecological situation.

- The presented formula in this thesis gives a good estimation of the pore-size distribution for civil rock works. Civil rock works include not only the bed protection of offshore wind turbines, but also revetments, breakwaters, and other bed protections. The pore-size distribution can be included in future designs to estimate the impact of the structure on the species. Moreover, the civil rock work design can be based on the preferred pore sizes for native species. This fits perfectly in the philosophy of Building with Nature. For Boskalis this could be an unique selling point to win tenders to build offshore wind farms (starting point of this thesis).

9. REFERENCES

Aber, J. (2012). *Offshore Wind Farms in Europe.* Retrieved from http://studentaccess.emporia.edu/~lgerber1/Intro%20to%20GSA%20project.html

Albers, L. J. (2005). *Initial porosity of random packings.* Delft: TU Delft.

Al-Kharusi, A. S., & Blunt, M. J. (2006). *Network extraction from sandstone and carbonate pore space images.*

Alternative Energy in New York. (2014). Retrieved from http://macaulay.cuny.edu/eportfolios/alternativeenergyinnewyork/wind-energy-in-nyc/

Andersson, M. (2011). *Offshore wind farms – ecological effects of noise.*

Baptist, M., van der Meer, J., & de Vries, M. (2007). *De Rijke Dijk.* Port Research Center.

Belwind. (2014). *Belwind offshore energy Facts an Figures.* Retrieved from http://www.belwind.eu/en/facts-and-figures/

Beurskens, J., & van Kuik, G. (2004). *Alles in de wind.* Maastricht: Daedalus.

Bijker, E. W., & de Bruyn, C. A. (1988). *Erosion around a pile due to current and breaking waves.*

Birdlife. (2009). Retrieved from http://www.birdlife.org/datazone/sowb/casestudy/289

Bolier, G. (2006). *Onderzoek naar fysiotopen in de Rotterdamse haven.* Port Research Centre Rotterdam-Delft.

Bouma, S., & Lengkeek, W. (2012). *Benthic communities on hard substrates of the offshore wind farm OWEZ.* Bureau Waardenburg.

Breve, N. W. (2013). *Kennisdocument Atlantische kabeljauw.*

Bruijs, M. C. (2010). *Survey of marine fouling on turbine support structures of the Offshore Windfarm Egmond aan Zee.*

Bult, T. P., Stikvoort, E. C., & Willemse, B. S. (1999). *Mogelijkheden en beperkingen van omgevingsclassificaties en habitatgeschiktheidsmodellen voor het inschatten van effecten op bodemdieren.*

Busch, K.-F., Luckner, L., & Tiemer, K. (1993). *Geohydraulik.*

Coastal energy and environment. (2014). Retrieved from http://coastalenergyandenvironment.web.unc.edu/environmental-stressors/physical-dynamic-presence/habitat-enhancement-and-loss/

Compendium. (2014). Retrieved from http://www.compendiumvoordeleefomgeving.nl/indicatoren/nl0073-Visbestanden-in-de-Noordzee.html?i=4-32

Coolen, J., & van der Weide, B. (2014, december 4). Ecology-based bed protection of offshore wind turbines interview at Imares. (W. Buijs, & A. Hermans, Interviewers)

de Vos, L. (2011). *Empirical design of scour protections around monopile foundations*.

Dekkers, J. (2007). *Rapportage Proces Vergunningverlening OWEZ*.

Deltares Mytilus edulis. (2014). Retrieved from https://publicwiki.deltares.nl/display/HBTDB/Mossel+-+Mytilus+edulis

Deltares, WINN, & RWS. (2010). *Construction of Ecobasins along dikes to improve biodiversity and bio-productivity - BwN manual*.

DNV. (2014). *Design of Offshore Wind Turbine Structures*.

DTU-Aqua. (2012). *Technical University of Denmark*. Retrieved from Fish thriving around wind farms: http://www.aqua.dtu.dk/english/News/2012/04/120410_Fish-thriving-around-wind-farms

Ecomare. (2014). Retrieved from http://www.ecomare.nl/en/encyclopedia/man-and-the-environment/water-management/hydraulic-engineering/artificial-reefs/

Ecomare; common lobsters. (2014). Retrieved from http://www.ecomare.nl/en/encyclopedia/organisms/animals/invertebrates/arthropods/crustaceans/decapods/lobsters/common-lobster/

Ecoshape. (2014). Retrieved from http://www.ecoshape.nl/

EcoShape. (2014). *Multifunctional coastal protection scheme East Coast Park Area, Singapore*. Retrieved from http://www.ecoshape.nl/multifunctional-coastal-protection-singapore.html

Enbaia, A. E. (2014). *Pore size and geometry of reservoir rocks used as key factor for drilling and completion fluid design of oils wells*.

Etzer, T., Aufleger, M., & Muckenthaler, P. (2012). *A Software Tool to evaluate the Internal Stability of Grain Structures*.

EWEA. (2014). *Key trends and statistics 1st half 2014*.

EWEA. (2013). *Positive environmental impacts of offshore wind farms*.

Fabi, G. (2011). *Overview on artificial reefs in Europe*.

Global Offshore Wind Farms Database. (2014). Retrieved from http://www.4coffshore.com/offshorewind/

Haddorp, R. (2005). *Predictability of Scour at Large Piles due to Waves and Currents.*

Hales, T. C. (2005). *A proof of the Kepler conjecture.*

Havforskningsinstituttet. (2007). *Institute of marine research.* Retrieved from http://www.imr.no/temasider/skalldyr/hummer/europeisk_hummer/en

Holthuijsen, L. H. (2007). *Waves in oceanic and coastal waters.*

Island-Institute. (2012). *Interactions with Offshore Wind Energy: Marine Species.*

Jensen, A., Wickings, J., & Bannister, C. (2000). *The potential use of artificial reefs to enhanve lobster habitat.*

Jong, S. d. (n.d.). *Cover page from Rijkswaterstaat.* Retrieved from https://beeldbank.rws.nl/(S(211rjbtbwyrw50zrwyesba4j))/MediaObject/Details/Noordzee_Windpark_windturbine_Offshore_windpark_Egmond_aan_Zee__OWEZ_333870

Kamerik, H. (2014). *Design and Placement of Artificial Coral Reefs.* Boskalis internship report.

Kamp, H., & Schultz van Haegen, M. (26 september 2014). *Windenergie op zee.* Den Haag.

KED-Ingenieure-GmbH. (2011). *OWP Meerwind WindMW.*

Kleinhans, M. G. (2008). *Magnetic Resonance Imaging of coarse sediment.*

Krone, R., & Schmalenbach, I. (2011). *Secondary use of offshore wind farms - Settlement of juvenile European lobsters (Homarus gammarus).*

Krone, R., & Schroder, A. (2010). *Wrecks as artificial lobster habitats in the German Bight.*

Langhamer, O., & Wilhelmsson, D. (2009). *Colonisation of fish and crabs of wave energy foundations and the effects of manufactured holes – A field experiment.*

Lavies, H. (2014). *Damping of wind waves in the IJmuiden breakwaters (Master Thesis).* Delft University of Technology.

Lawson, J. (2013). *Windpower international.* Retrieved from http://www.windpower-international.com/features/featuregood-foundations-the-pros-and-cons-of-monopiles-4158694/

Leewis, R. J., Dankers, N., & de Jong, D. J. (1998). *Naar een ecotopensysteem zoute wateren Nederland.*

Lindeboom, H. J., Kouwenhoven, H. J., Bergman, M. J., & Bouma, S. (2011). *Short-term ecological effects of an offshore wind farm in the Dutch coastal zone; a compilation.* IP Publishing.

Lindner, B. (2015). *natuurkunde.nl.* Retrieved from http://www.natuurkunde.nl/artikelen/view.do?supportId=764277

Linley, E., Wilding, T., Black, K., Hawkins, A., & Mangi, S. (2007). *Review of the reef effects of offshore wind farm structures and their potential for enhancement and mitigation.*

Loosveldt, L., & Vannieuwenhuyse, K. (2012). *Experimental validation of empirical design of a scour protection around monopiles under combined wave and current loading.*

Louwersheimer, W. F. (2007). *Scour around an offshore wind turbine.*

Maritime Journal. (2014, March 17). Retrieved from http://www.maritimejournal.com/news101/marine-renewable-energy/car-tyres-protecting-turbines-from-scour

MER. (2014). Retrieved from http://www.eia.nl/en/environmental-assessment/eia

Mermaid. (2012). Retrieved from http://www.imbaenergyclub.gr/2012/12/06/research-on-innovative-multi-purpose-offshore-platforms-in-greece/

Moraci, N., Mandaglio, M., & Ielo, D. (2012). *A new theoretical method to evaluate the internal stabilty of granular soils.*

Moraci, N., Mandaglio, M., & Ielo, D. (2012). *Reply to the discussion by Dallo and Wang on 'A new theoretical method to evaluate the internal stability of granular soils'.*

Natuur & Milieu. (2014). Retrieved from http://nos.nl/artikel/722443-wind-op-zee-is-slimme-verzekering.html

Nederlandse Wind Energie Associatie. (2015). Retrieved from http://www.nwea.nl/hoeveel-elektriciteit-levert-een-windmolen-op

Nimmo, J. R. (2004). *Porosity and Pore Size Distribution.*

Noordzeeloket. (2015). *Sediment North Continental Plate.* Retrieved from http://www.noordzeeloket.nl/en/spatial-management/north-sea-atlas/watersysteem/sediment.aspx

Omroep Zeeland. (2014). Retrieved from http://www.omroepzeeland.nl/nieuws/2014-06-26/701111/staalslakken-oosterschelde-voortaan-afgedekt#.VJQjzsDC

Omroep Zeeland. (2014). Retrieved 2014, from http://www.omroepzeeland.nl/nieuws/2014-11-26/773291/rijkswaterstaat-brengt-kreeften-gevaar#.VJQj0sDB http://www.omroepzeeland.nl/nieuws/2014-09-13/737641/reddingsactie-voor-kreeften-oosterschelde#.VJQj2sDB

Prodöhl, P. A., Jørstad, K. E., Triantafyllidis, A., Katsares, V., & Triantaphyllidis, C. (2006). *European lobster.*

Raaijmakers, T. (2014, december 9). Ecology-based bed protection of offshore wind turbines interview. (W. Buijs, Interviewer)

Raaijmakers, T. (2015). Handbook offshore scour protection methods. *Joint Industry project.*

Raaijmakers, T. (Performer). (2009). *Offshore scour and scour protection lecture.* Delft University of Technology.

Raaijmakers, T., Joon, T., Segeren, M., & Meijers, P. (2014). *Feasibility of omitting scour protection.* Deltares & TU Delft.

Reboul, N., Vincens, E., & Cambou, B. (2009). *A computational procedure to assess the distribution of constriction sizes for an assembly of spheres.*

Redwave. (2014). Retrieved from http://www.redwave.nl/doelpagina/2743893/2743879/De-monopile.html

Rijksoverheid. (2014). Retrieved from http://www.rijksoverheid.nl/onderwerpen/duurzame-energie/windenergie

Rijksoverheid. (2014). Retrieved from http://www.rvo.nl/subsidies-regelingen/windparken

Rijksoverheid. (2014). *Noordzeeloket.* Retrieved from http://www.noordzeeloket.nl/functies-en-gebruik/windenergie/

Rockmanual. (2007). *Chapter III Materials.*

Royal-HaskoningDHV. (2014). *Milieueffectrapport Rijksstructuurvisie Windenergie op Zee.*

Schaumann & Keindorf Ingenieurges. (2014). Retrieved from http://www.ski-consult.de/1/offshore/offshore-wind-energy/monopile.html?T=5

Schiereck, G. J. (2001). *Introduction to bed, bank and shore protection.* Delft: Delft University Press.

Schmalenbach, I., Janke, M., & Buchholz, F. (2009). *Growth, reproduction, movement and abundance of the European Lobster, Homarus Gammarus, at the rock Island of Helgoland, North Sea.* Hamburg.

Scientist plan to settle lobsters in wind farms. (2013). Retrieved from http://www.spiegel.de/international/germany/researchers-are-hoping-to-boost-lobster-populations-in-the-north-sea-a-895477.html

Shah, A. (2014). *Globalissues.* Retrieved from http://www.globalissues.org/issue/169/biodiversity

Silin, D. B., & Patzek, T. W. (2003). *Robust Determination of the Pore Space Morphology in Sedimentary Rocks.*

Sumer, B. M., & Fredsøe, J. (2002). *Hydrodynamics around cylindrical structures.*

Sustainable Energy Technology. (2006). Msc course TU Delft.

TO, H. D., Scheuermann, A., & Williams, D. J. (2012). *A new simple model for the determination of the pore constriction size distribution.*

van Breukelen, S. (1992). *Habitat geschiktheidsindex model - de blankvoorn.*

van de Sande, S. A. (2013). *Stability of open filter structures.*

Van den Bos, J. P. (2006). *Design of granular near-bed structures in waves and currents.*

van der Tempel, J., Zaaijer, M. B., & Subroto, H. (2004). *The effects of Scour on the design of Offshore Wind Turbines.*

Verhagen, H. J., d'Angremond, K., & Roode, F. v. (2001). *Breakwaters and closure dams* (second ed.). Delft: VSSD.

Vincens, E., Witt, K. J., & Homberg, U. (2014). *Approaches to Determine the Constriction Size Distribution for Understanding Filtration Phenomena in Granular Materials.*

Wesseling, M. (2012). Mussels, Oysters and skate thrive well on wind farms. *Trouw* .

Wind energy the facts. (2011). Retrieved from http://www.wind-energy-the-facts.org/offshore-support-structures.html

Windenenergie-nieuws. (2014). Retrieved from http://www.windenergie-nieuws.nl/24/onvoldoende-voor-milieu-effectrapport-wind-op-zee/

Winter, H. V., Aarts, G., & van Keeken, O. A. (2010). *Residence time and behaviour of sole and cod in the Offshore Wind farm Egmond aan Zee (OWEZ).*

Zettler, M. L., & Pollehne, F. (2006). *The impact of wind engine construction on benthic growth patterns in the western baltic.*

Zucco, C., Wende, W., Merck, T., Kochling, I., & Koppel, J. (2006). *Literature Review of the Ecological Impacts of Offshore Wind Farms.*

LIST OF FIGURES

LIST OF TABLES

Appendices

A. CT SCANS RESULTS

In this appendix the results of all the CT scans are graphical presented. In total 8 scans are performed. Sample 5 and sample 10 are ignored, because the resolution of the scans was too low to get representative results.

The stone-size distribution and the porosity is varied per sample. The aim is to find a formula that describes the derivation of the pore-size distribution if only the stone-size distribution is known.

The mass distribution as well as the number distribution of the stone-size distribution is presented. The pore-size distribution is presented as a number distribution.
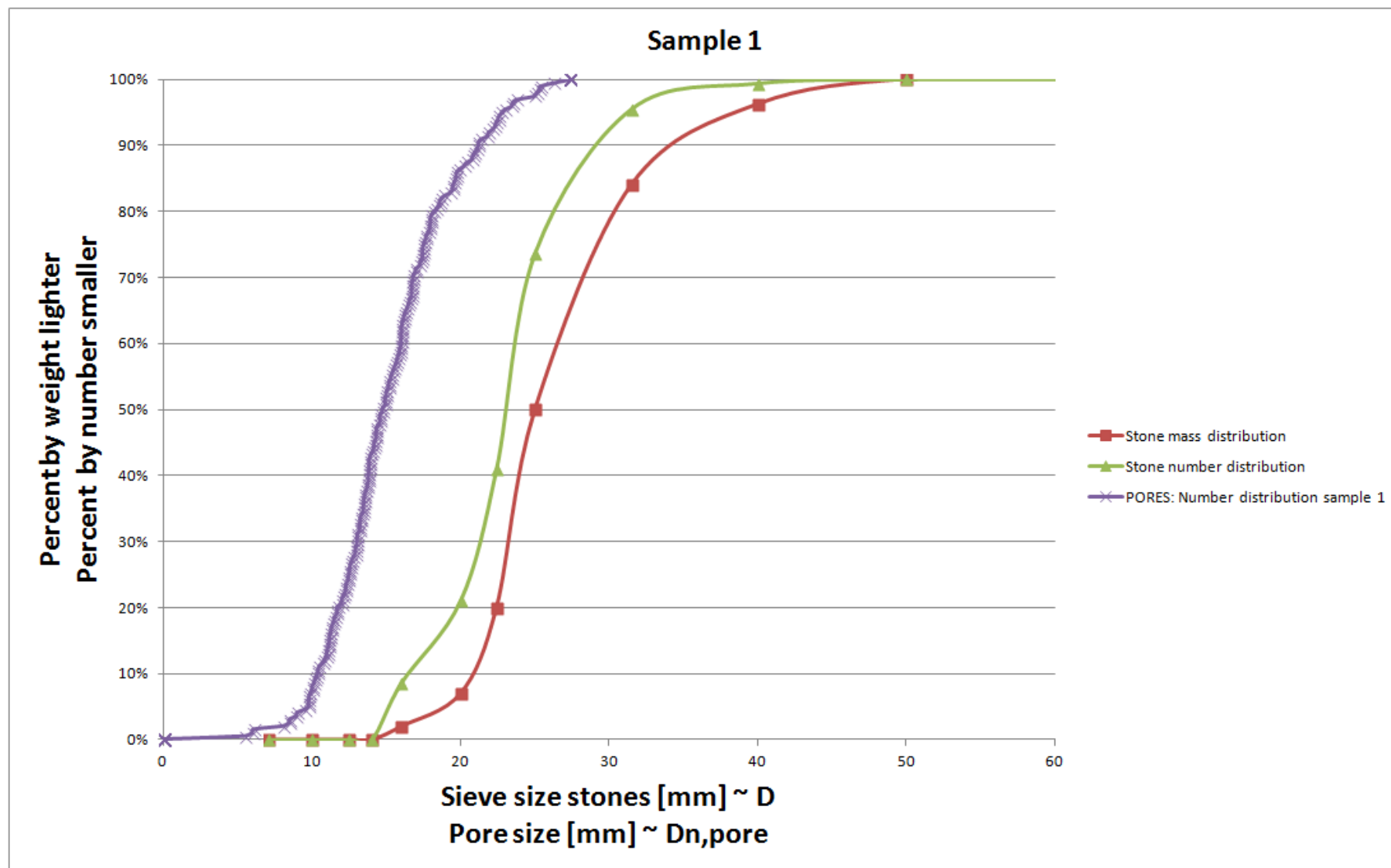
Figure A-1: Stone and pore-size distribution of sample 1.
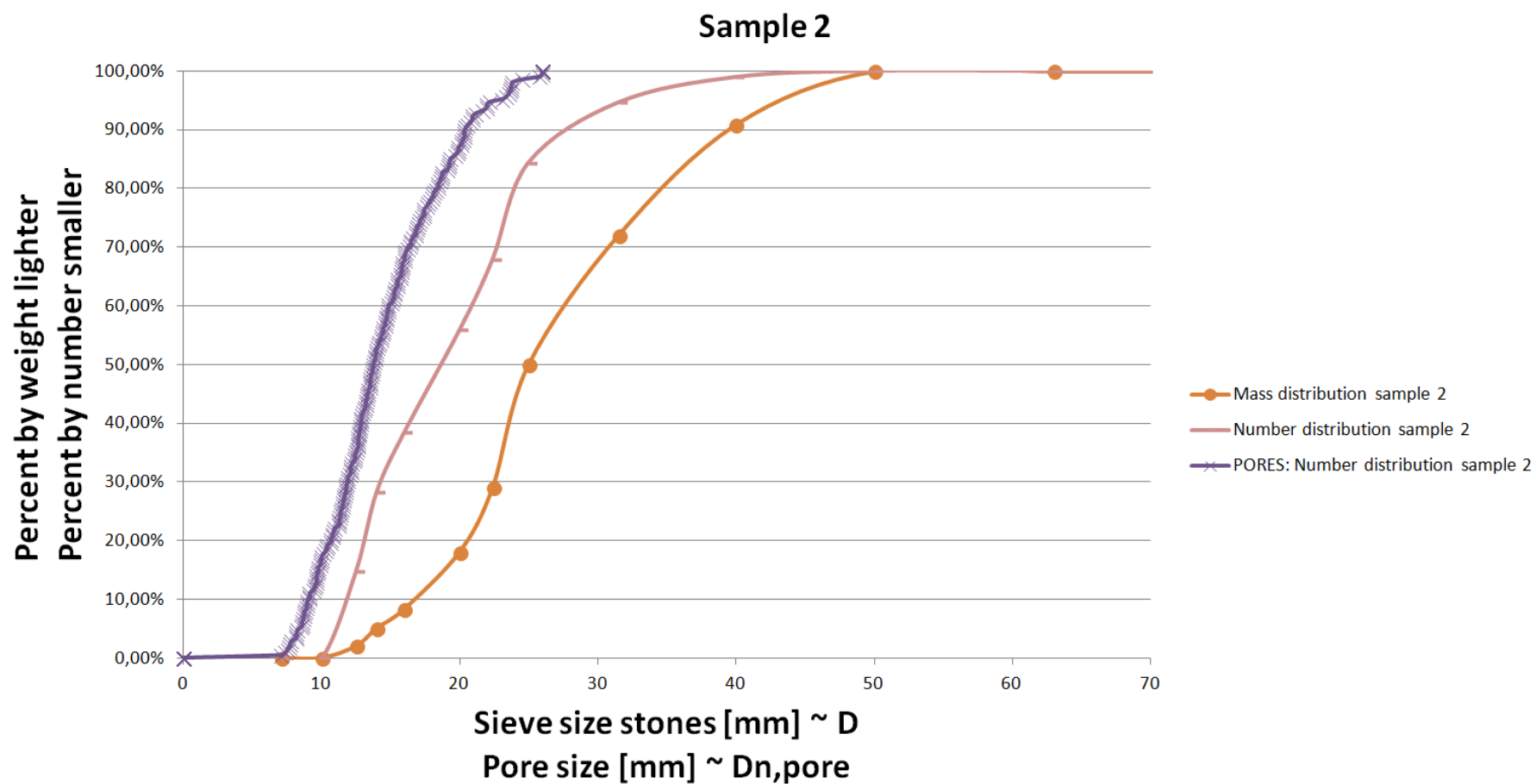
Figure A-2: Stone and pore-size distribution of sample 2.
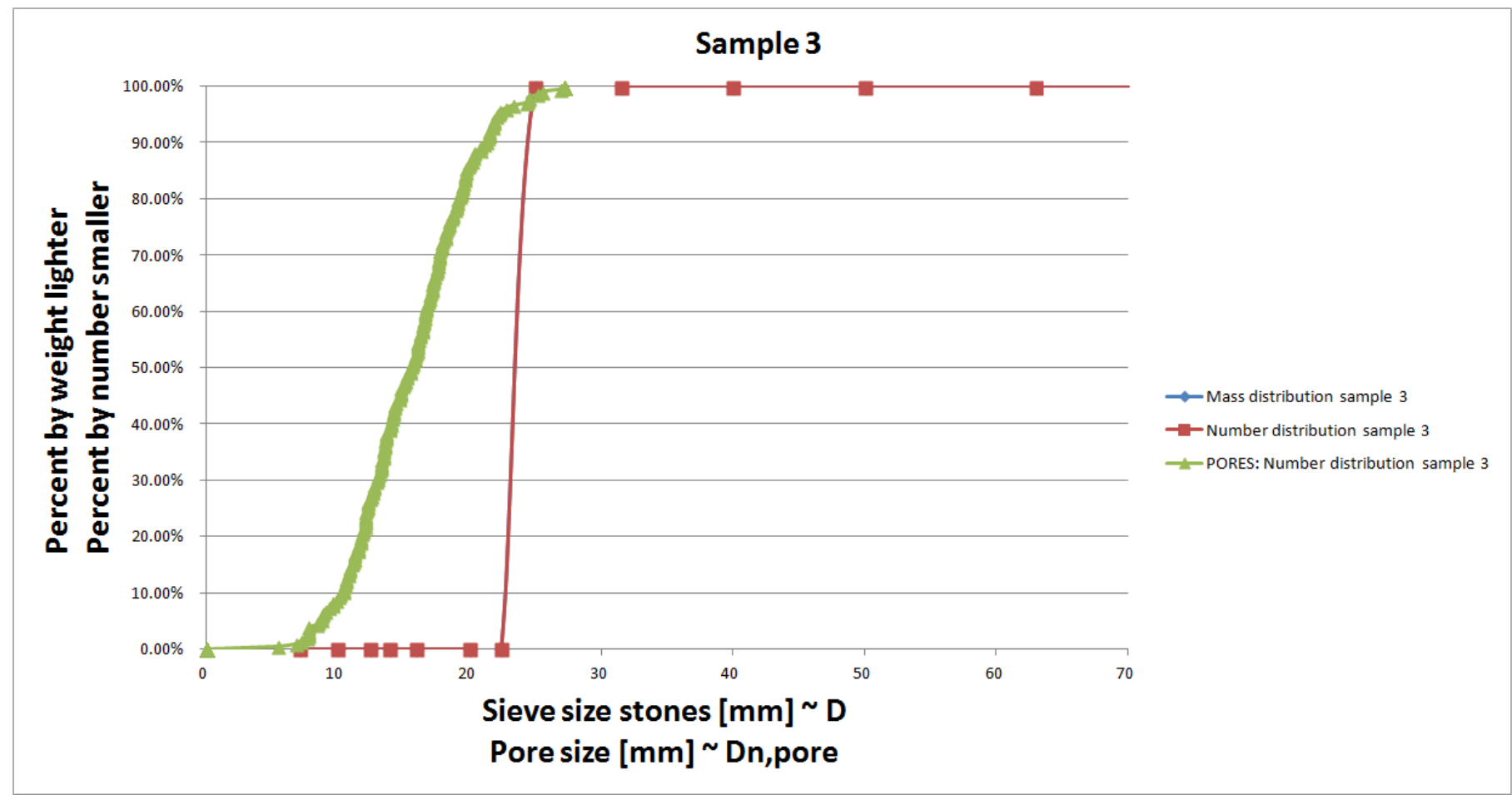
Figure A-3: Stone and pore-size distribution of sample 3.
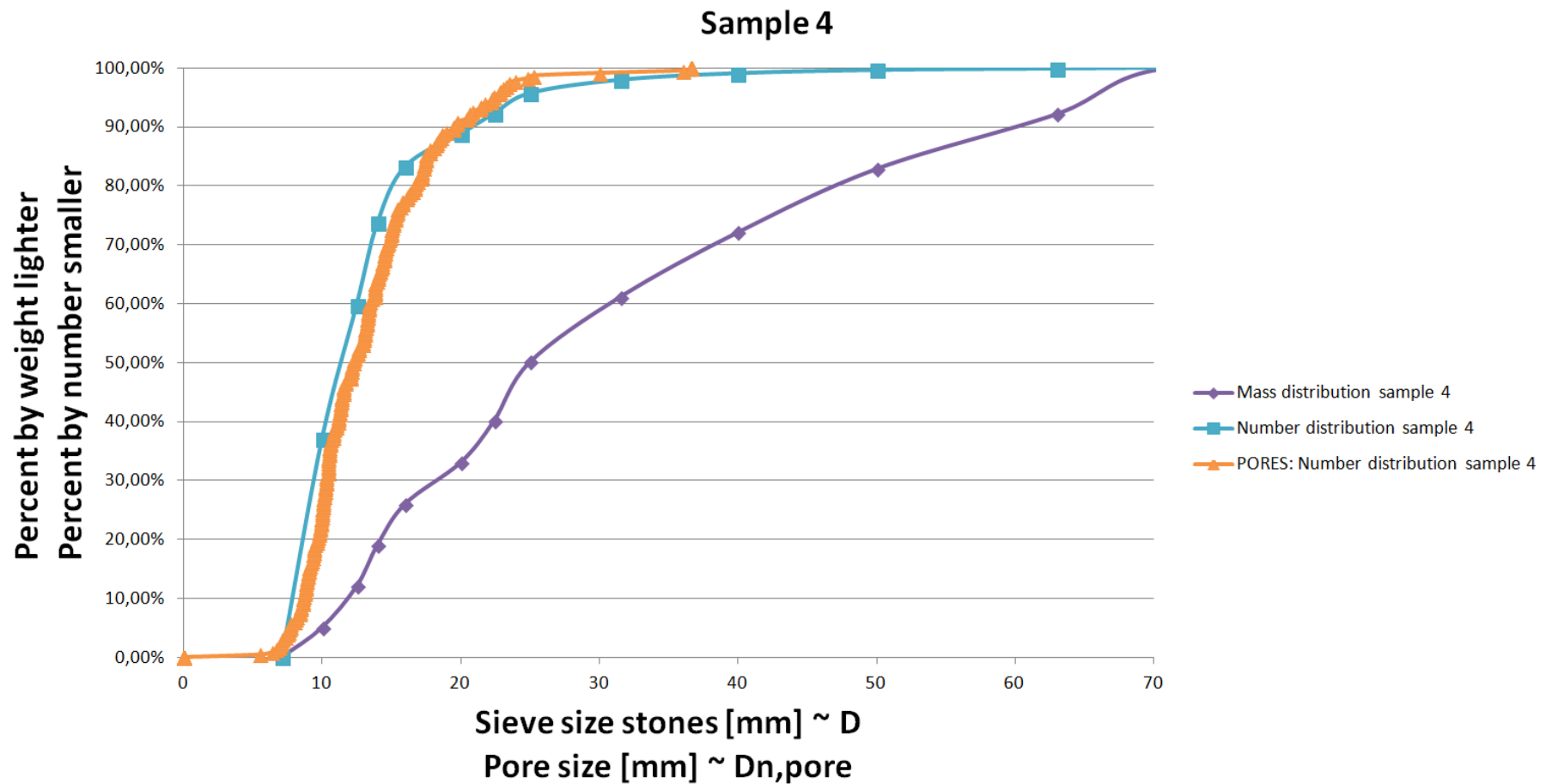
Figure A-4: Stone and pore-size distribution of sample 4.
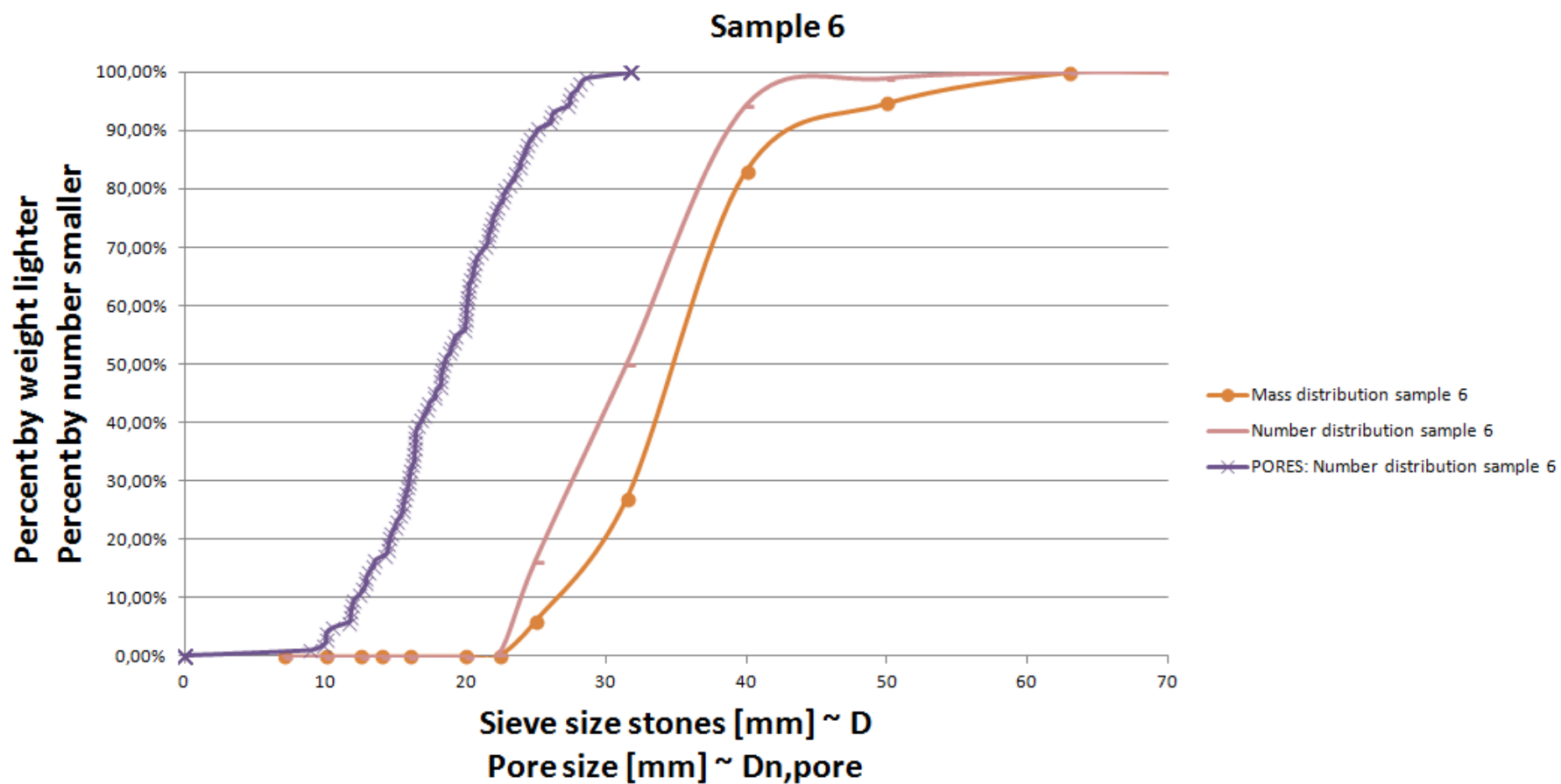
Figure A-5: Stone and pore-size distribution of sample 6.
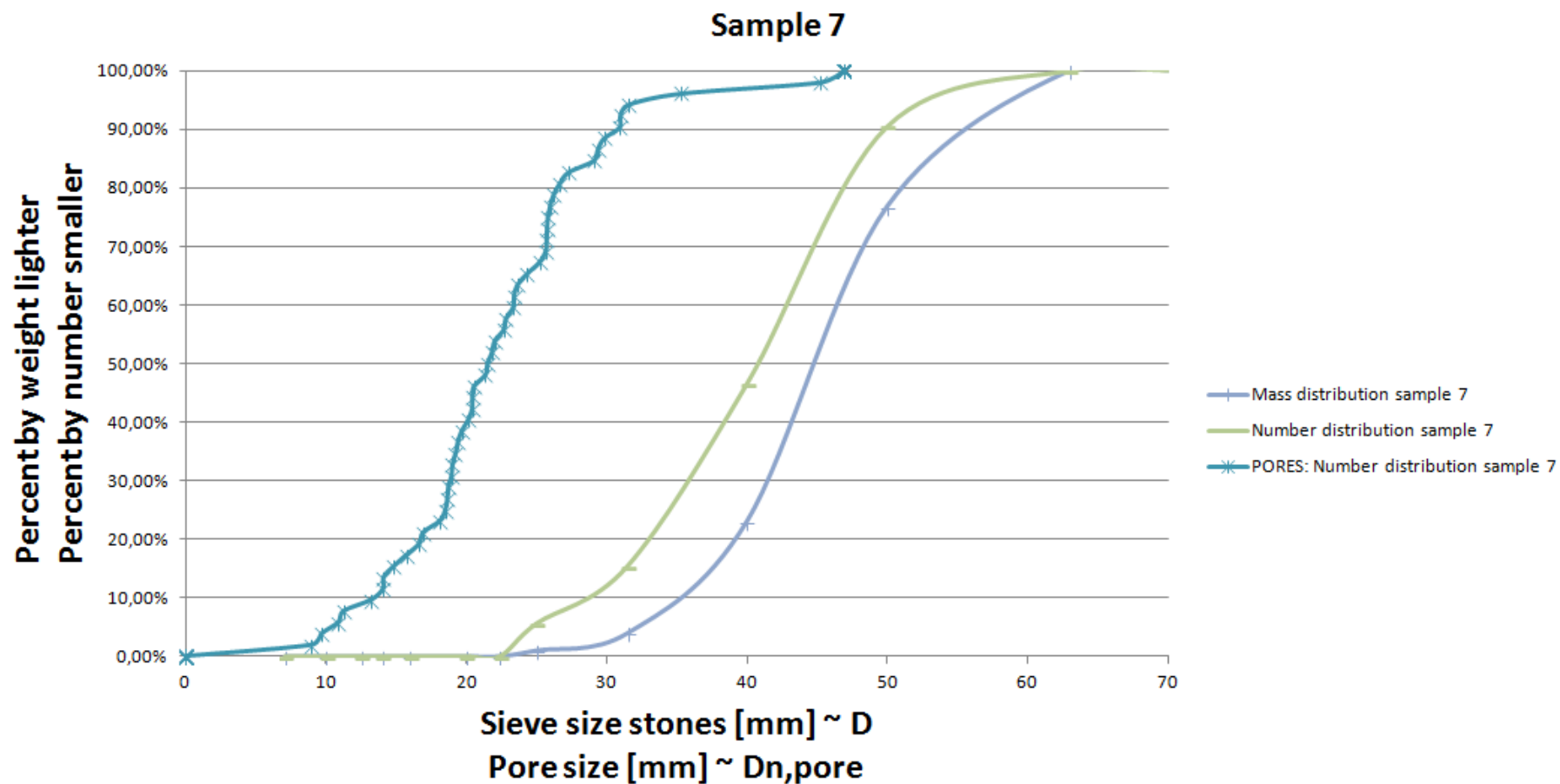
Figure A-6: Stone and pore-size distribution of sample 7.
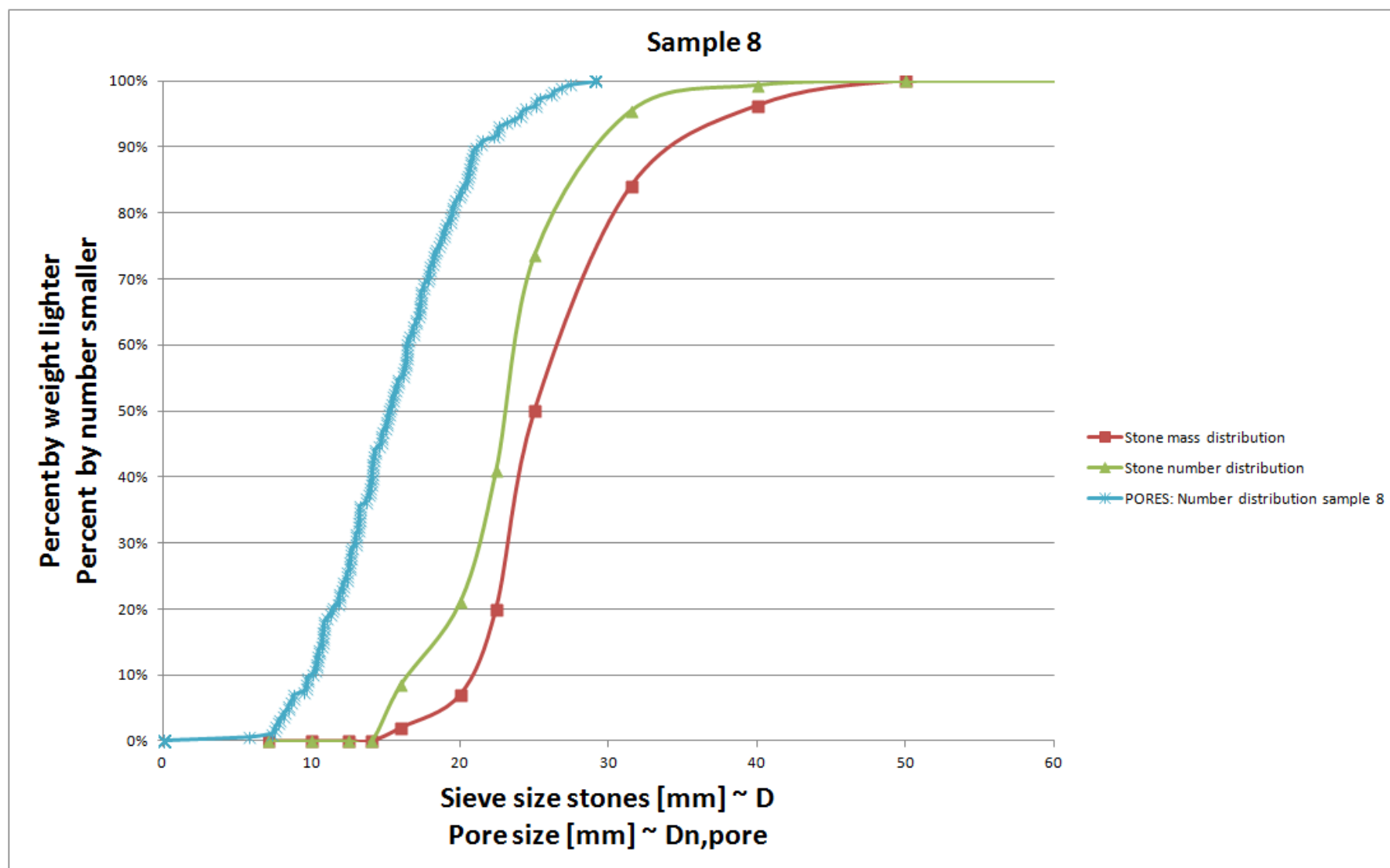
Figure A-7: Stone and pore-size distribution of sample 8.
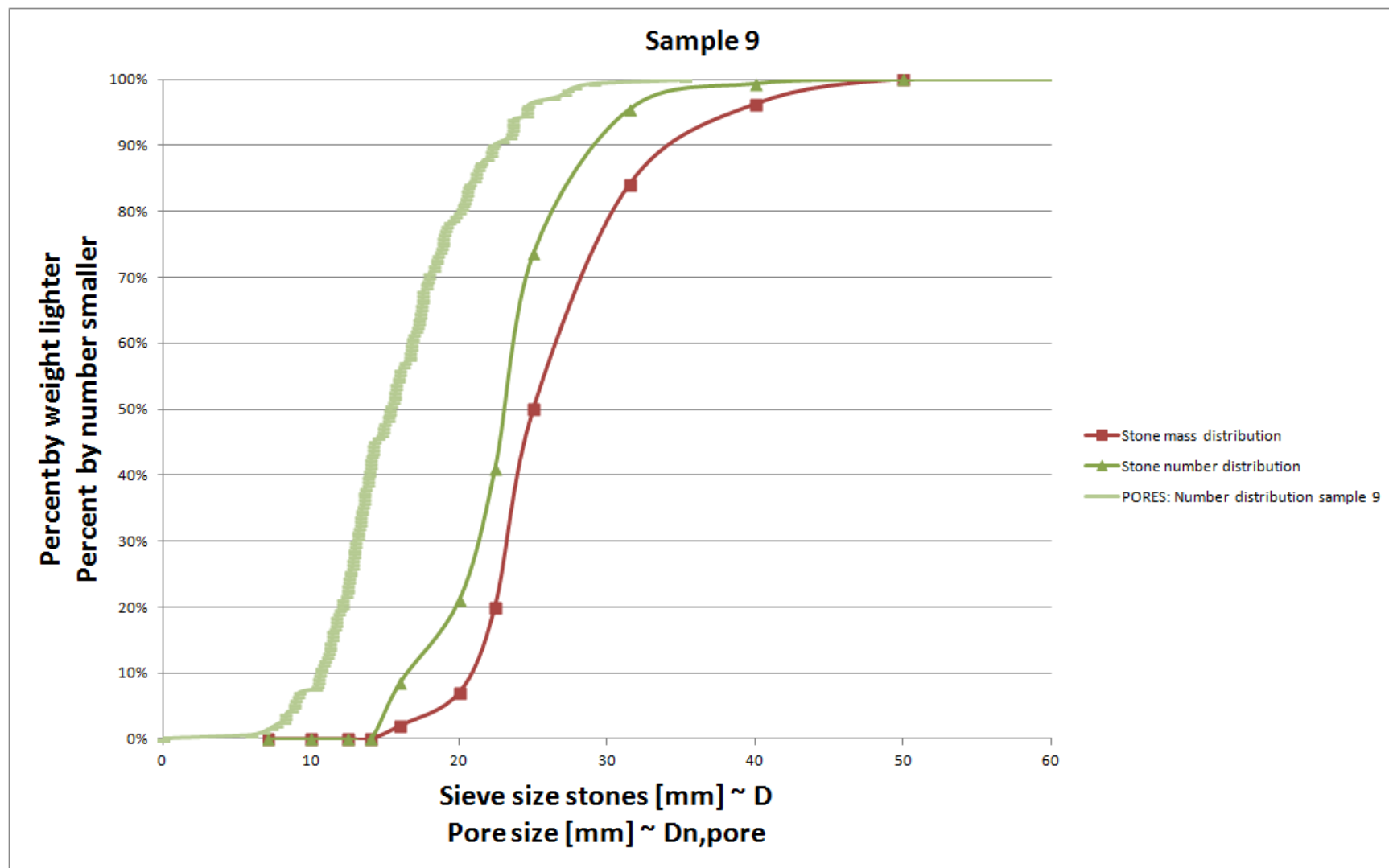
Figure A-8: Stone and pore-size distribution of sample 9.

B. ANALYSIS OF RESULTS

In the previous appendix (A) the results of the CT-scans are presented. In this appendix the analysis and method to find a relation between stone-size distribution and the pore-size distribution is discussed. Two approaches are elaborated to find the formula for the pore-size distribution.

- The first approach is based on an approximation function that approximates the pore-size distribution. This method works fast and accurate, and is this approach is therefore presented in section 6.5.1 of the main report.
- The second approach is based on finding the D50 of the pore-number distribution and the slope of the pore number distribution. A nice curve fit formula is not derived for this method, but this method is suitable for a quick estimation of $D50_{pore}$. This approach is therefore elaborated in this appendix.

The steps to derive a general formula for the pore-size distribution are listed below and visual presented in Figure B-1.

1. The relation that describes the $D50_{pore}$ see section B.1
2. The relation that describes the $D85/D15_{pore}$ see section B.2
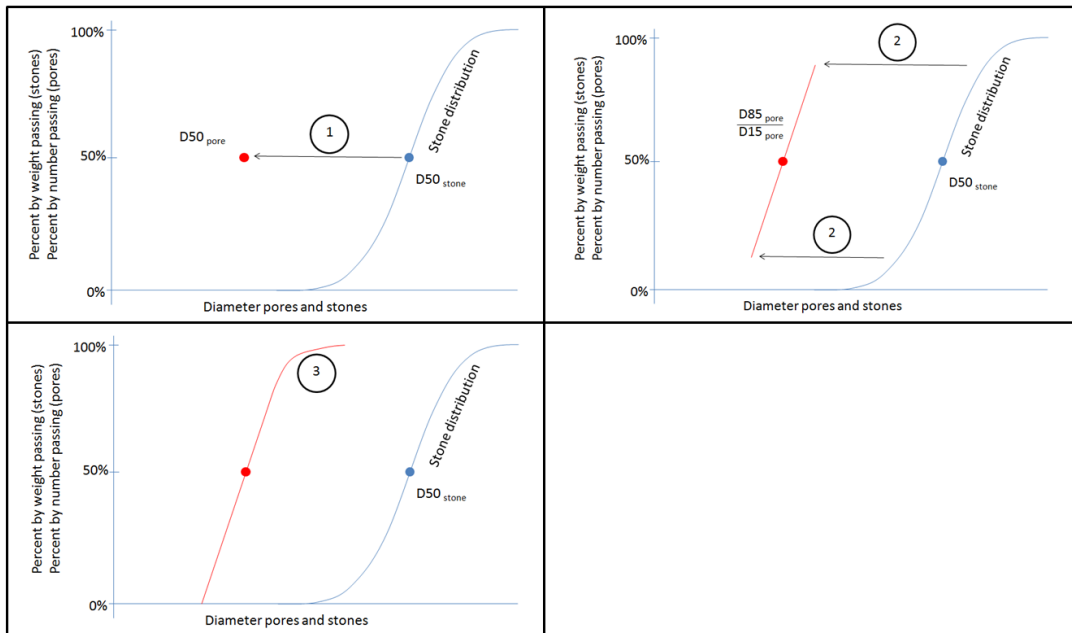3. The relation that makes a curve fit of the above to parameters   see section B.3

Figure B-1: Steps to describe the relation between stone-size distribution and pore-size distribution.

B.1 D50_{PORE} CORRELATION

The assumption is made the D50 $_{pore}$ depends on the following parameters:
* D50 $_{stone}$
* D85/D15 $_{stone}$
* Porosity (ϕ)

The formula to describe the relation is based on dimensionless parameters and is stated in equation B.1.

$$\frac{D50_{stone}}{D50_{pore}} = \left\{ \left[\frac{D85}{D15} stone \right]^{a}, [\phi]^{b} \right\} \tag{B.1}$$

As mentioned in chapter 4, the D50 $_{stone}$ can be described with the D50 of the mass distribution of stones and the number distribution of stones. This holds for the D50 $_{pore}$. There are already 20 possibilities if the parameters a and b are 0 or 1.

The hypothesis is made that if D85/D15 $_{stone}$ mass distribution gets larger, the number of small stones increases and so the number of small pores. The number distribution of pores will shift a little to the left (smaller D50 $_{pore}$). This is also visible in Figure 6-35. Therefore, the a-value is assumed positive. Secondly, the hypothesis is made that if the porosity decreases, the pore-size decreases and so the D50 $_{pore}$ of the pore-size number distribution. This means that the b value is assumed negative.

To test these hypotheses two plots are presented in Figure B-2:
* Left plot: a=0, b=1, D50 $_{stone}$ mass distribution, D50 $_{pore}$ number distribution
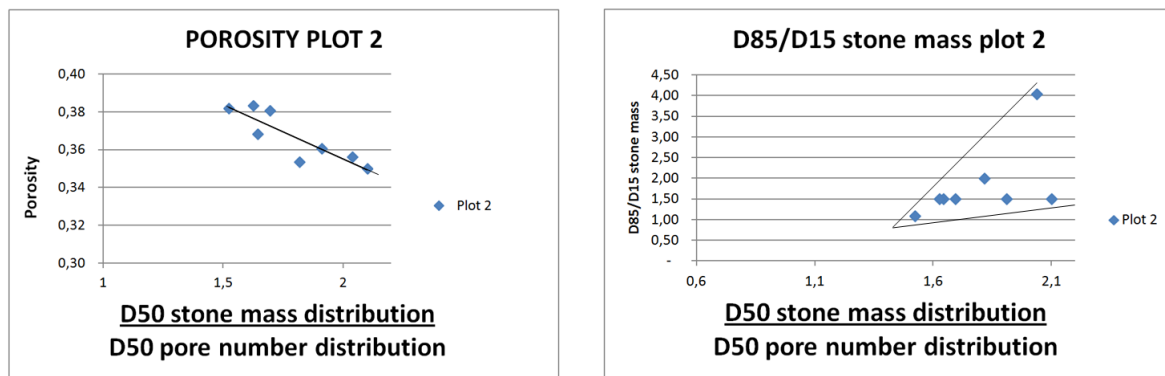* Right plot: a=1 and b=0, D50 $_{stone}$ mass distribution, D50 $_{pore}$ number distribution

Figure B-2: D50 $_{pore}$ - porosity relation (left) and D50 $_{pore}$ - D85/D15 $_{stone}$ relation (right).
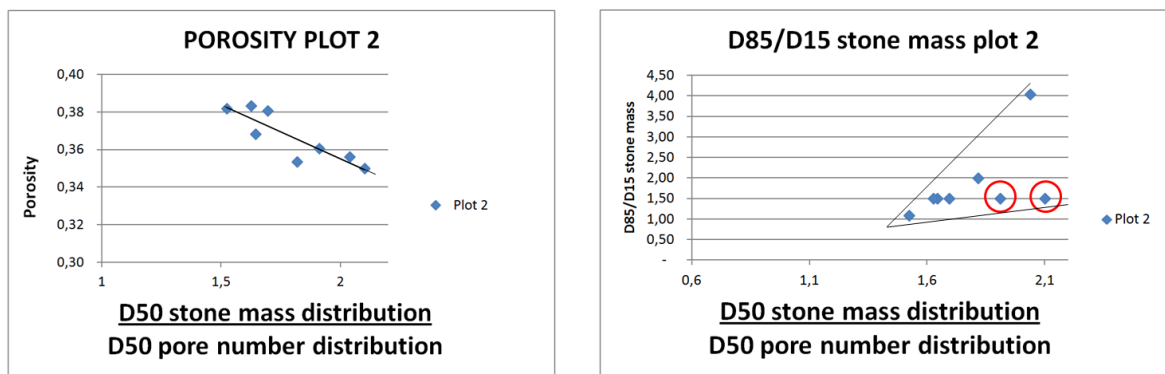

Figure B-3: Two labeled outliers.

The porosity seems to have negative correlation if b=1 is plotted. This is just as expected. The relation in the right figure of Figure B-2 is less obvious. This is mainly because there are two outliers, see Figure B-3.

These outliers are also visible if the porosity and the $D85/D15_{stone}$ are plotted together, see red circles in Figure B-4.
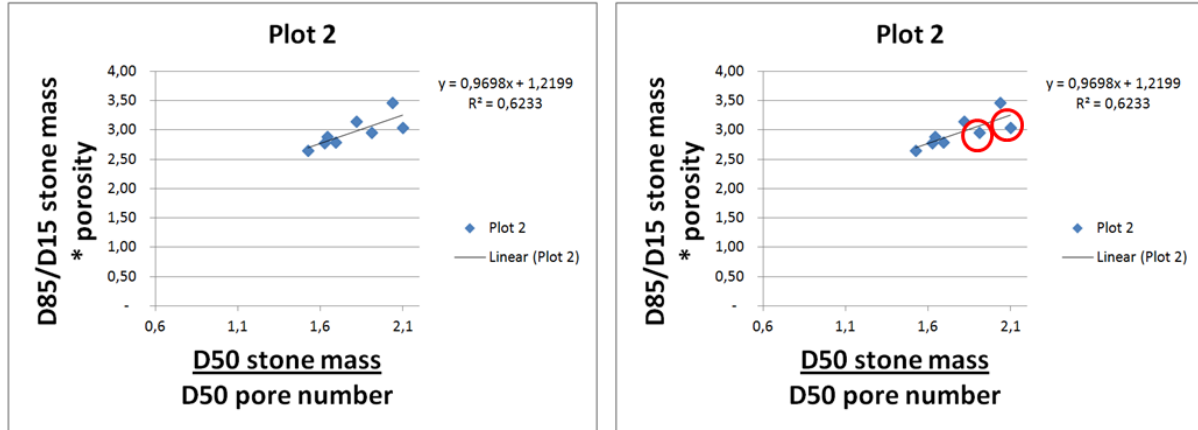

Figure B-4: Plot of equation B.3 for a=0.15 and b=-1.

The two outliers are sample 6 and sample 7. The reason of these two outliers is explained in Figure B-5. The stones of sample 6 are big and the stones of sample 7 are even bigger. Because the stones in the bucket are bigger, less stones and less pores are present (in the same-sized bucket). The created edge effects have more influence if the number of pores are less. By applying a small threshold and ignore the very small pores (assumed only present due to the edge effects), the right graph is obtained instead of the left graph, see Figure B-5.
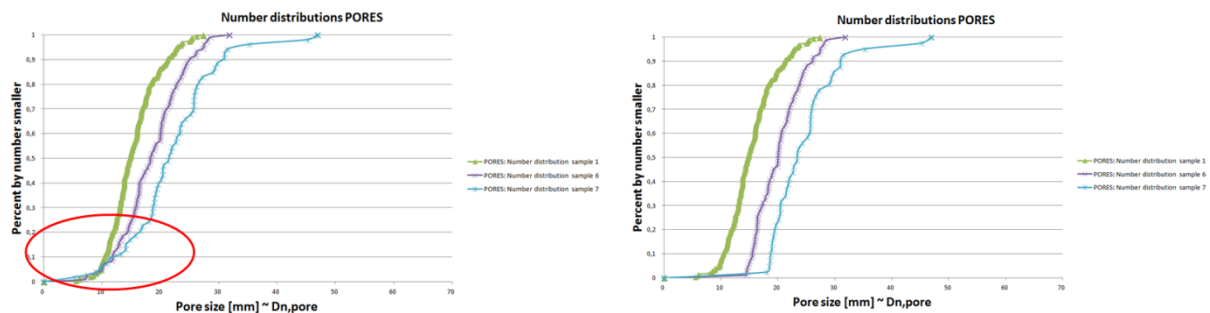

Figure B-5: 'Error' in sample 6 and 7.

If sample 6 and sample 7 are adapted (by applying a small threshold of the small pores), the left graph of Figure B-6 is obtained. By deleting the points of sample 6 and sample 7 the right graph of Figure B-6 is obtained.
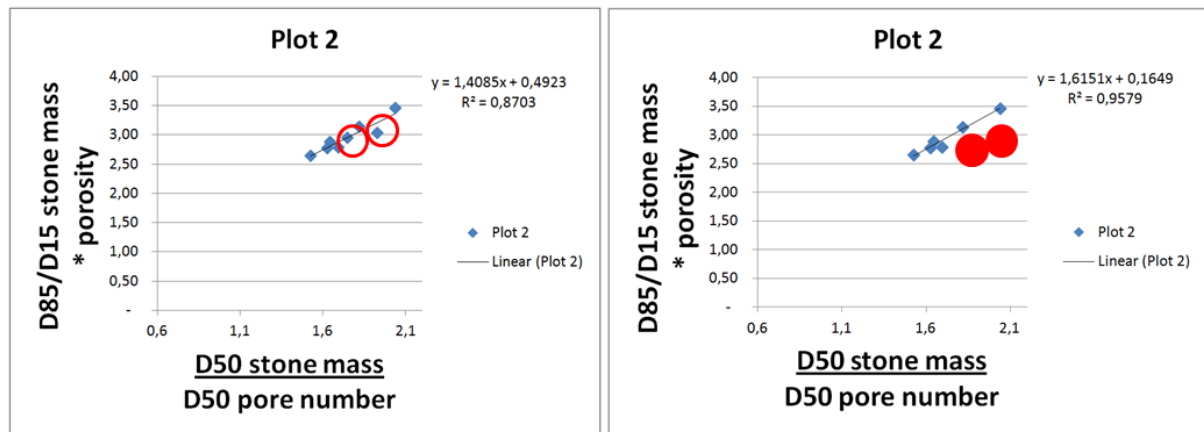
Figure B-6: Plot of equation B.3 for a=0.15 and b=-1 by adapting sample 6 and 7.

The points will are not ignored. The adapted plot shows a quite good correlation.

After tweaking the optimum fit and re-writing the formula, equation B.2 is the end result to describe the D50 pore number. This fit is presented in Figure B-7.

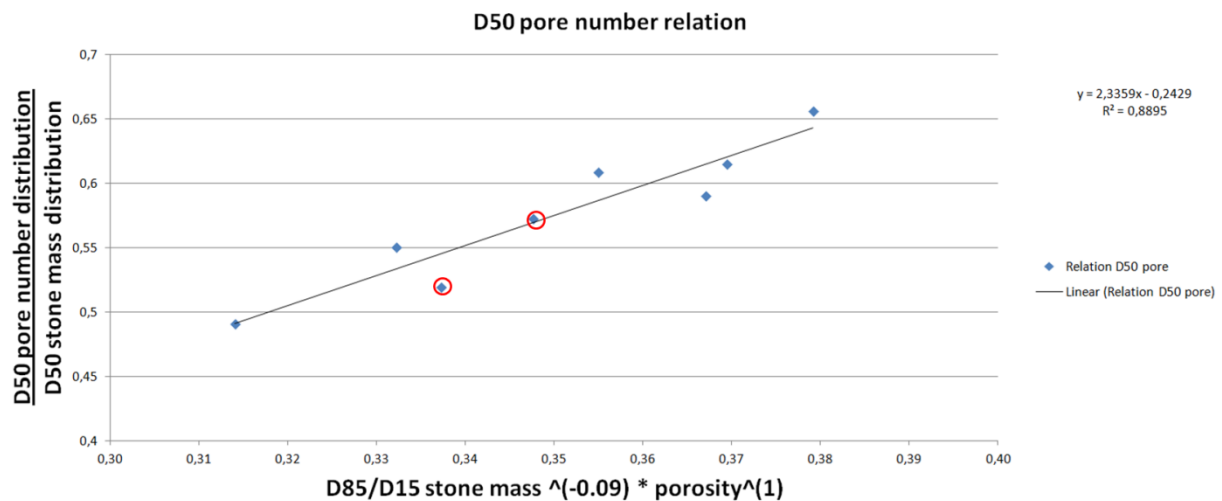$$\frac{D50_{pore}}{D50_{stone}} = 2.3359 * \left(\frac{D85}{D15} \; stone\right)^{-0.09} * \phi^1 - 0.2429 \hspace{2cm} (B.2)$$

Figure B-7: Relation of D50 _pore_ number distribution.

B.2 D85/D15$_{PORE}$ CORRELATION

The assumption is made the D85/D15 $_{pore}$ depends on the following parameters:
- D85/D15$_{stone}$
- Porosity (ɸ)

The formula to describe the relation is based on dimensionless parameters and is stated in equation B.3.

$$\frac{D85}{D85}pore = \left\{ \left[\frac{D85}{D15}stone\right]^a , [ɸ]^b \right\} \tag{B.3}$$

The hypothesis is made that if D85/D15$_{stone}$ mass distribution gets larger, the number of small stones increases and so the number of small pores. Due to this increase in small stones, the number distribution start steeper. However, a wider distribution of stones results also in a few big pores. But in a number distribution this effects only the pore curve above D85$_{pore}$. Secondly, the hypothesis is made that if the porosity decreases, the pore-size decreases and so the D85/D15$_{pore}$ of the pore-size number distribution gets steeper. This means that the b value of equation B.5 is assumed negative.

To test these hypotheses two plots are presented in Figure B-8:
- Left plot: a=0, b=1, D85/15 $_{pore}$ number distribution
- Right plot: a=1 and b=0, D85/D15$_{stone}$ mass distribution, D85/D15$_{pore}$ number distribution
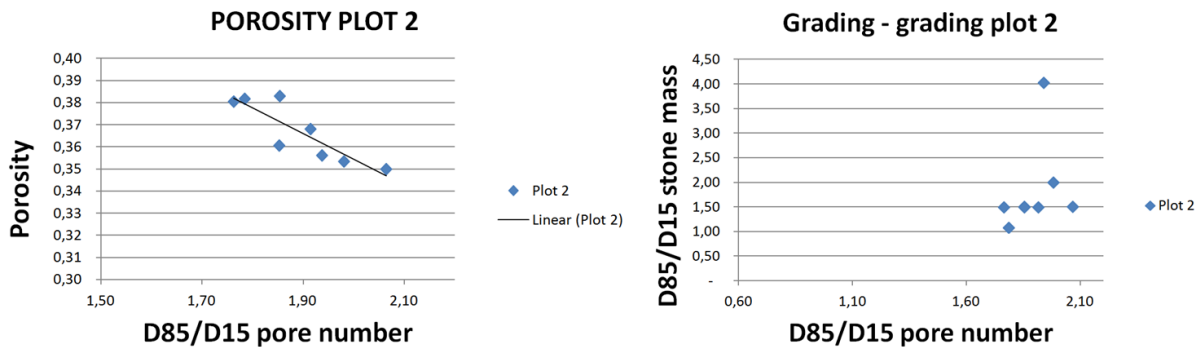

Figure B-8: D85/D15 $_{pore}$ - porosity relation (left) and D85/D15 $_{pore}$ - D85/D15 $_{stone}$ relation (right).

The porosity seems to have negative correlation if b=1 is plotted. This is just as expected. A relation in the right figure of Figure B-8 is hardly noticeable. However, some information can be extracted from it, see Figure B-9.

The D85/D15$_{stone}$ cannot be smaller than 1. Further it can be noticed that the D85/D15$_{pore}$ of the number distribution is always between 1.76 and 2.06, while the grading varies from 1 to 4. The point 2.06 is from sample 7, so due to the small number of pores this value is also a bit arbitrary (probably it has to be smaller). The conclusion can be made that the stone grading of the mass distribution has not a large influence on the slope of the number distribution of pores.
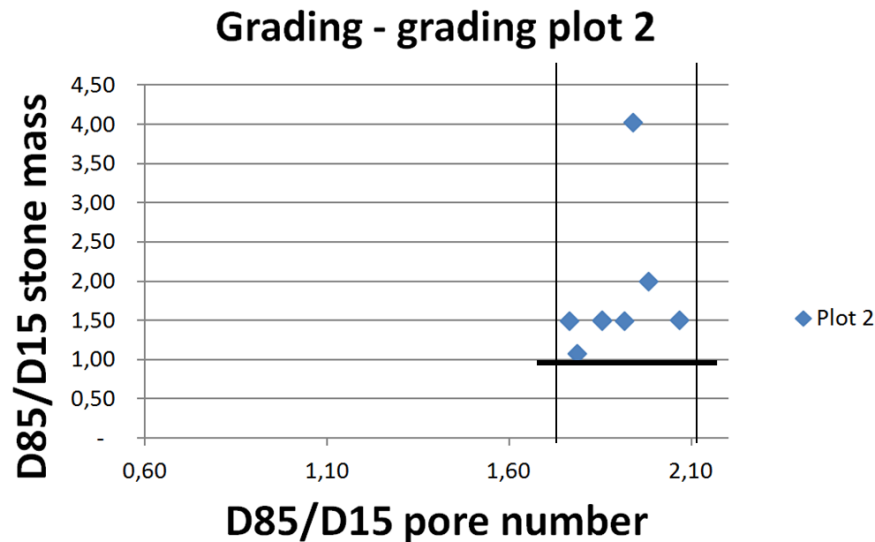
Figure B-9: Relation D85/D15 stone - D85/D15 pore.

The D85/D15 pore depends on the porosity but not on the D85/D15 of the mass distribution of stones. Therefore the easy relation in equation B.4 is found to describe the slope of the number distribution of pores, see Figure B-10.

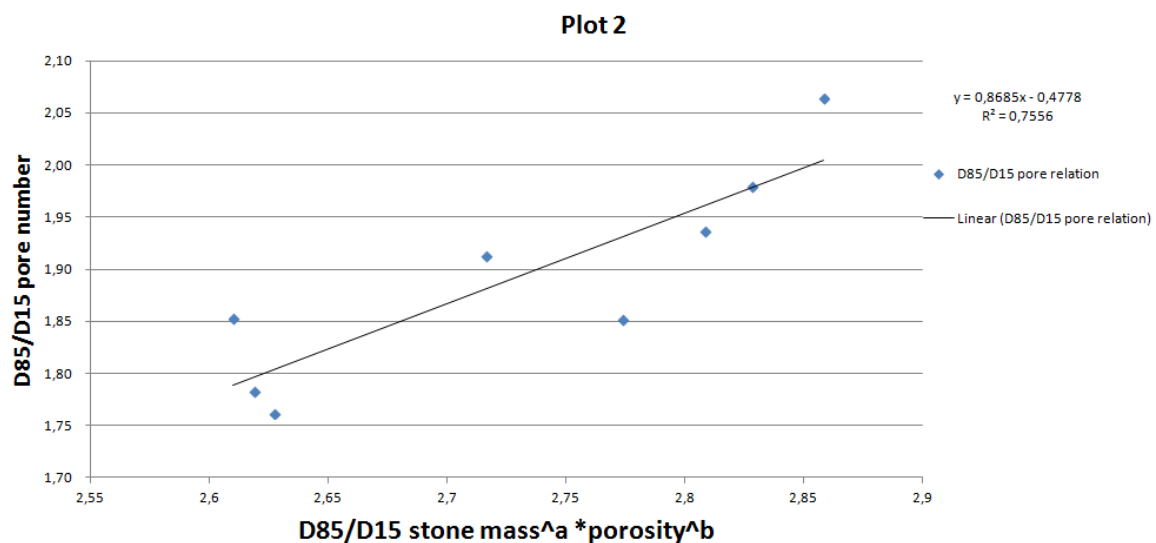$$\frac{D85}{D85}pore = 0.8685\,\phi - 0.4778 \tag{B.4}$$

Figure B-10: Relation of D85/D15 pore number distribution.

B.3 CURVE FITTING LINE

In the previous sections the relation is explained for the $D50_{pore}$ and the $D85/D15_{pore}$. This section focuses on a curve fit formula, based on the two discovered relations.

The $D85/D15_{stone}$ does not influence the $D85/D15_{pore}$, as described in the previous section. However, the $D85/D15_{stone}$ does probably influence the part between the $D85_{pore}$ and the $D100_{pore}$, see Figure B-11.

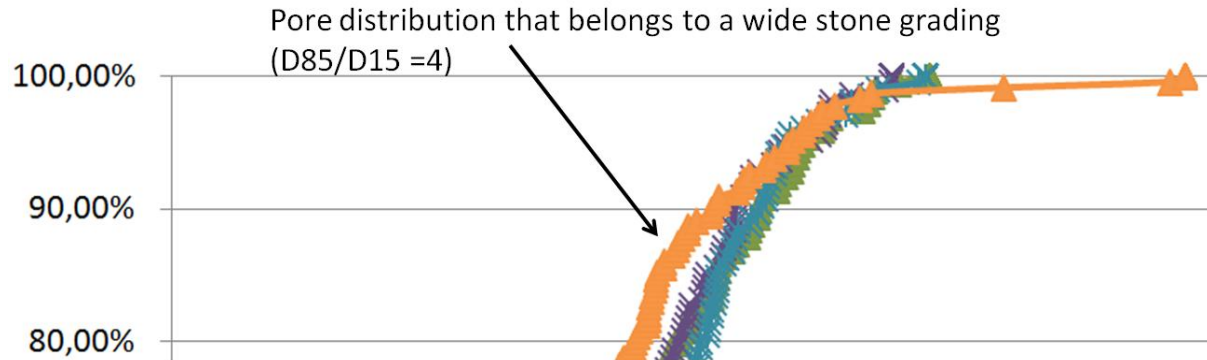**Figure B-11: Number distribution of pores of sample 1, 2, 3, and 4.**

A trend is found for the relation between $D100_{pore}/D85_{pore}$ and $D85/D15_{stone}$, but there is a wide spreading visible, see Figure B-12.

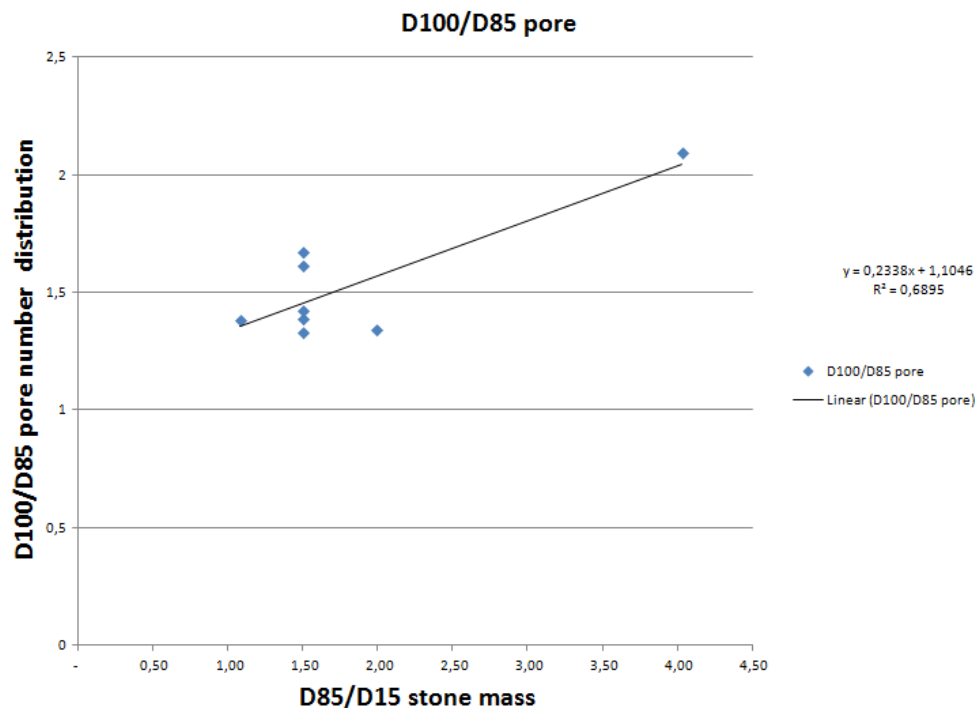**Figure B-12: Trend between D100/D15pore and D85/D15pore.**

It is tried to find a formula that includes the found relations of section B.1, section B.2, and this section. The formula is not found. Therefore, this method will only provides a quick estimate to determine the $D50_{pore}$ and the slope of the pore-number distribution. To come up with a formula that includes all these factors, another method is proposed, as mentioned in the introduction of this appendix. In this method the pore-size distribution is directly approximated with the Rosin Rammler distribution. This is method works better and is elaborated in section 6.5.1.

C. GENERIC APPLICABILITY

During this research a question came up from the dredging industry. Although this question falls outside the scope of this research, it is included in this appendix as it is an example of the generic applicability of the results of this research. This case also supports the motivation of this thesis. Therefore this question is included as an additional case. This case is elaborated in this appendix. The project information is classified. Therefore the species and the location are not specified.

The posed question from the industry was about a revetment. To make this revetment suitable for native species X, the openings should have a sufficient size. On the other hand, the openings should be not too large, otherwise the openings are also suitable for exotic species Y (non-desirable situation). The species are pictured in Figure C-1.

Figure C-1: Native species X and exotic species Y.

The openings must have a maximum of circa 15 centimeters. About 30% of the openings should fit species X, and therefore should have openings of maximal 15 centimeters. About 70% of the openings should fit juvenile natives and should be smaller than 15 centimeters. The stone class applied as armour layer is 60-300kg.

First, the situation is evaluated by determining the D50, the grading width (D85/D15) and the porosity, see Table C-1.

Table C-1: Stone class of the revetment.

Stone class	rho [kg/m^3]	kg	V [m^3]	Dn [m]	D [m]
D$_0$	2800	60	0.02	0.28	0.33
D$_{100}$	2800	300	0.11	0.47	0.57

The D50 is estimated by taking the mean of the extreme values which lead to a D50 of 0.45m. $D_{100}/D_0 = 1.71$, so D85/D15 is assumed 1.5. The porosity is assumed 38%, because most of the rock works have a porosity of 38%. Figure C-2 is the result when these values are used in equation 5.15.
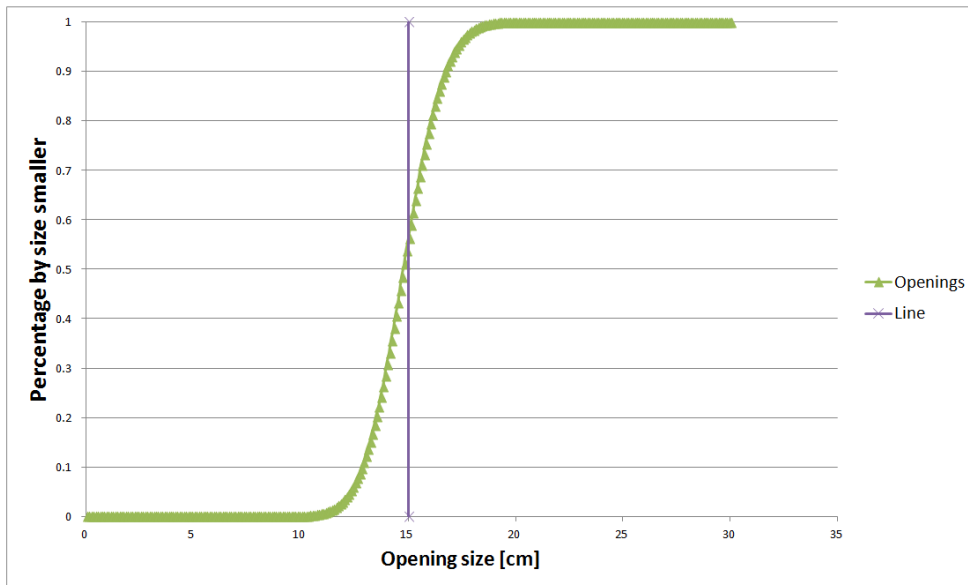
Figure C-2: Result of the openings in the revetment.

The stones in this example are still modeled as spheres. But as mentioned in section 6.6, this is not falsified for the stone openings.

The openings are not matching the requirements as posed in the introduction of this appendix. 30% of the openings is larger than the requested 15cm. Figure C-3 is the result when the stone class is adapted to 30-300 kg stones (changing the parameters D50 and the stone grading). The D50 decreases (from 0.45m to 0.41cm) and the grading wide is increased (from 1.5 to 2). The maximum opening size of 15 centimeter (requirement of the ecologist) is hardly exceeded anymore.
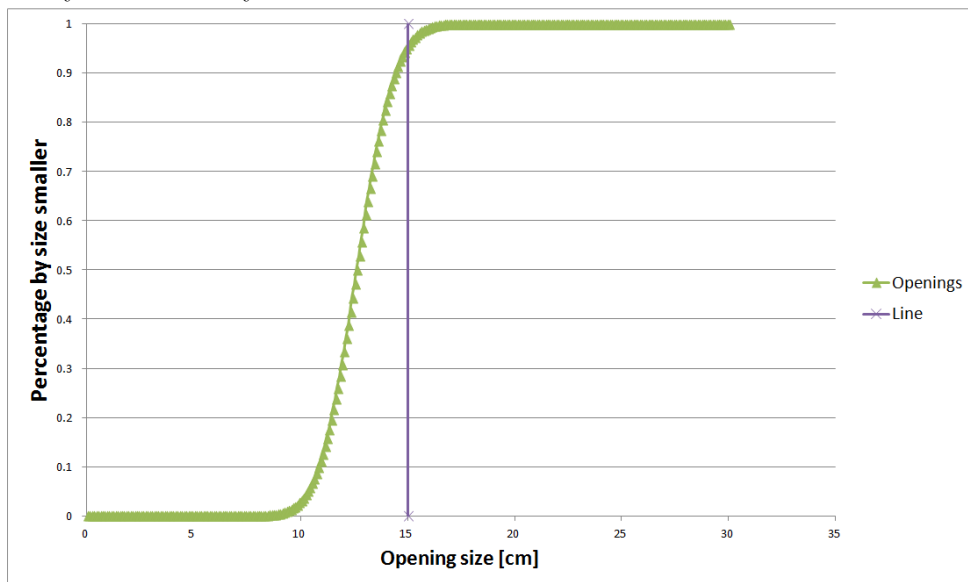

Figure C-3: Result of the openings in the revetment if the stone class is adapted.

This is just one of the solutions to adapt the design in a more eco-friendly way.